OCRWM	MODEL COVER SHEET	1. QA: QA Page 1 of 158

2. Type of Mathematical Model

DOC.20030916.0010

☒ Process Model ☐ Abstraction Model ☐ System Model

Describe Intended Use of Model

This model report documents the analyses and models for general and localized corrosion of the waste package outer barrier (WPOB). The models are used to analyze degradation of the Alloy 22 outer barrier by general and localized corrosion processes under the expected repository exposure conditions over the repository performance period.

3. Title

General Corrosion and Localized Corrosion of Waste Package Outer Barrier

4. DI (including Rev. No. and Change No., if applicable):

ANL-EBS-MD-000003 REV 01

5. Total Attachments	6. Attachment Numbers - No. of Pages in Each
7	I - 5 pages, II - 4 pages, III - 4 pages, IV - 10 pages, V - 3 pages, VI - 4 pages, VII - 2 pages

	Printed Name	Signature	Date
7. Originator	Joon H. Lee	SIGNATURE ON FILE	09/09/2003
8. CSO	David Stahl	SIGNATURE ON FILE	09/09/03
9. Checker	Gopal De	SIGNATURE ON FILE	09/09/2003
10. QER	Charlie Warren	SIGNATURE ON FILE	09/10/03
11. Responsible Manager/Lead	Tammy S. Summers	SIGNATURE ON FILE	09/10/03
12. Responsible Manager	Curtis Clower	SIGNATURE ON FILE	~~9/15/03~~ 9/15/03* VP 9/15/03

13. Remarks

Project staff and contractors who made contribution to this model report include Raul Rebak, Tammy Summers, Hatem Elayat, Kevin Mon, Gerry Gordon, Fed Hua, Bryan Bullard, Lana Wong, John Estil, Joe Farmer, Digby Macdonald, David Shoesmith, and Young Kim. Review comments by Fred Hua and Gabriel Ilevbare improved the report. Direct management and oversight included Tammy Summers, Venkataraman Pasupathi and Curtis Clower. Katherine Scott provided administrative support.

Model validation activities (Section 7) address TER-02-0022 and part of TER-02-0072.

This model report also addresses CIRS Item #002235.

For TSPA-LA.

* Originally signed on 9/10/03 on a fax copy of the cover sheet VP 9/15/03

2. Model Title:

General Corrosion and Localized Corrosion of Waste Package Outer Barrier

3. Document Identifier (including Rev. No. and Change No., if applicable):

ANL-EBS-MD-000003 REV 01

4. Revision/Change No.	5. Description of Revision/Change
00	Initial Issue
01	The purpose of this revision is to include new information, data, and results pertinent to general corrosion and localized corrosion of the waste package outer barrier. Most of the sections in this model report have been rewritten with new information, and as a result, the changes were too extensive to use Revision Bars per Section 5.9d)1) of AP-SIII.10Q.

TABLE OF CONTENTS

Page

LIST OF FIGURES

Page

LIST OF TABLES

Page

ACRONYMS AND ABBREVIATIONS

ACM	alternative conceptual model
AR	as-received
ASTM	American Society for Testing and Materials
ASW	as-welded
BSC	Bechtel SAIC Company
BSW	basic saturated water
CCT	critical crevice-corrosion temperature
CDF	cumulative distribution function
CFR	Code of Federal Regulations
CNWRA	Center for Nuclear Waste Regulatory Analyses
CPP	cyclic potentiodynamic polarization
CPT	critical pitting temperature
CRWMS	Civilian Radioactive Waste Management System
CSNF	commercial spent nuclear fuel
DHLW	defense high level waste
DIRS	Document Input Reference System
DOE	U.S. Department of Energy
DS	drip shield
DTN	data tracking number
EBS	engineered barrier system
ECDF	empirical cumulative distribution function
FEPs	features events and processes
FIB	focused ion beam system
HLW	high level waste
KTI	key technical issue
LA	license application
LLNL	Lawrence Livermore National Laboratory
LTCTF	Long Term Corrosion Test Facility
MCA	multiple crevice assembly
MIC	microbially influenced corrosion
NRC	Nuclear Regulatory Commission
OCP	open circuit potential
OCRWM	Office of Civilian Radioactive Waste Management

PDF	probability density function
PDM	Point Defect Model
PRD	Project Requirements Document
PSP	potentiostatic polarization
RH	relative humidity
SAW	Simulated Acidified Water
SCW	Simulated Concentrated Water
SDW	Simulated Dilute Water
SCC	stress corrosion cracking
SCE	saturated calomel reference electrode scale
sd	standard deviation
SEM	scanning electron microscope
SHE	standard hydrogen reference electrode scale
SN	Scientific Notebook
SNF	spent nuclear fuel
SSC	silver-silver chloride reference electrode scale
TDMS	Technical Data Management System
TEM	transmission electron microscopy
TSPA	total system performance assessment
TWP	Technical Work Plan
UNS	Unified Numbering System
WP	waste package
WPOB	waste package outer barrier
XPS	x-ray photoelectron spectroscopy
YMP	Yucca Mountain Project

1 PURPOSE

The current waste package design for the License Application is a double-wall waste package (WP) underneath a protective drip shield (DS) (BSC 2002c; BSC 2003b). The purpose and scope of this model report is to document the analyses and models for general and localized corrosion of the waste package outer barrier (WPOB), which is constructed of Alloy 22 (UNS N06022). The Alloy 22 outer barrier is considered as the corrosion barrier of the WP. The stainless steel inner shell is not considered as a corrosion barrier; therefore, the inner shell is not considered in the WP corrosion degradation analysis. The purpose of the general corrosion model is to analyze degradation of the Alloy 22 outer barrier by general corrosion under the expected repository environmental conditions over the repository performance period. The general corrosion model includes several sub-models, which account for dry oxidation, aqueous general corrosion, effect of aging and phase stability, and microbially influenced corrosion (MIC). The purpose of the localized corrosion model is to analyze degradation of the Alloy 22 outer barrier by crevice corrosion under the expected repository environmental conditions over the repository performance period. The sub-models included in the localized corrosion model are the crevice repassivation potential model, long-term corrosion potential model, and crevice corrosion propagation model. This model report serves as a feed to the waste package degradation analyses and TSPA-LA.

Lists of Data Tracking Numbers (DTNs) and their Q-status are included in the Document Input Reference System (DIRS) database and are also included in the Technical Data Management System (TDMS) report.

1.1 BACKGROUND ON ALLOY 22

Alloy 22 (UNS N06022) is the current reference material for construction of the outer barrier of the WP. This alloy consists, by weight, of 20.0-22.5% Cr, 12.5-14.5% Mo, 2.0-6.0% Fe, 2.5-3.5% W, 2.5% (max.) Co, and balance Ni (ASTM B 575 1994). Other impurity elements include P, Si, S, Mn, and V (CRWMS M&O 1999a; Treseder et al. 1991). Alloy 22 is less susceptible to localized corrosion in environments that contain halide ions such as Cl^- than Alloys 825 and 625, materials of choice in earlier designs (Gdowski 1991, Section 3.0; Gruss et al. 1998; Haynes 1997a, 1997b). The unusual localized corrosion resistance of Alloy 22 is mainly due to the additions of Mo and W. Addition of these alloying elements to nickel alloys has been proven to significantly improve the resistance to localized corrosion of nickel alloys (Hack 1983; ASM International 1987, pages 641 to 657). The oxides of these elements are very insoluble at low pH. Consequently, Alloy 22 exhibits relatively high thresholds for localized corrosion attack. Very high repassivation potentials have been observed by some investigators (Gruss et al. 1998; Rebak et al. 2002), while others have found very low corrosion rates in simulated crevice solutions containing 10 weight percent $FeCl_3$ (Gdowski 1991, Section 3.0; Haynes 1997a, 1997b). Furthermore, no significant localized corrosion attack of Alloy 22 has been seen in crevices exposed to the waters with mixed ions that are relevant to those expected in the repository. Such tests have been conducted in the Yucca Mountain Project's (YMP's) Long Term Corrosion Test Facility (LTCTF) at Lawrence Livermore National Laboratory (LLNL) (Estill 1998). Test media used in this facility include simulated acidic concentrated water (SAW), simulated dilute water (SDW), and simulated concentrated water (SCW). See Table 6-2 for the solution definitions and compositions.

1.2 RANGES OF MODEL APPLICATION

The purpose and scope of this report is to document the analyses and models for general and localized corrosion of the waste package outer barrier (WPOB). The purpose of the general corrosion model is to quantitatively analyze degradation of the Alloy 22 outer barrier by general corrosion under the expected repository environmental conditions over the repository performance period. The purpose of the localized corrosion model is to quantitatively analyze degradation of the Alloy 22 outer barrier by crevice corrosion under the expected repository exposure conditions over the repository performance period. The general and localized corrosion models include several sub-models, which account for dry oxidation, general corrosion, microbially influenced corrosion (MIC), crevice corrosion initiation, and crevice corrosion propagation. Because dry-oxidation of the WPOB has insignificant impact on the waste package performance (see Section 6.4.2), this mode is not included in the waste package degradation analysis. Thermal aging and phase stability is not included in the waste package degradation analysis because waste packages are not expected to be subject to the thermal aging and phase instability processes for the thermal conditions expected in the repository (see BSC 2003a, Sections 6.6.5.3 and 8.0). Furthermore, although highly unlikely, the thermal aging of the WPOB, subjected to the extent that may occur during the waste package fabrication, has insignificant effect on its corrosion performance under the environmental conditions expected in the repository (see Section 6.4.6).

The general corrosion model is applied to the conditions in which a stable aqueous water film can exist on the waste package surface (see Section 6.4.3.4). The MIC model is applied when the relative humidity at the waste package surface is greater than 90 % (see Section 6.4.5).

The waste package will experience a wide range of conditions during its service life in the repository. Crevices will be formed on the waste package surface, such places as between the waste package and supports. Crevices may also form beneath mineral scales that form from interaction of the in-drift materials with water, corrosion products, dust, rocks, and biofilms; and between the layers of the containers when the outer layer is breached. The crevice environment may be more severe than the near field environment. The hydrolysis of dissolved metal can lead to the accumulation of H^+ inside the crevice and a corresponding decrease in pH. Electromigration of Cl^- (and other anions) into the crevice must occur to balance the cationic charge associated with H^+ ions and dissolved metal ions (Jones 1996, pages 220-222). Accordingly, crevice corrosion is assumed to be representative of localized corrosion of the WPOB under the exposure conditions expected in the post-closure repository (see Assumption 5.3).

The empirical correlations of the two model components, corrosion potential model (E_{corr}) and crevice repassivation potential model (E_{rcrev}), of the localized corrosion initiation model are expressed as a function of temperature, pH, chloride concentration and nitrate concentration (see Sections 6.4.4.3 and 6.4.4.5). The localized corrosion model is applicable to the following conditions.

- Temperature from 20 °C up to boiling temperature of $CaCl_2$–containing brines.
- Solution pH from 2 to 12.

- Chloride concentration from a very low non-zero value to 25 molal (*m*, moles/kg water). A value of 0.001 *m* is recommended for the chloride concentration for solutions with no chloride.
- Nitrate concentration from a very low non-zero value to 6 molal (*m*, moles/kg water). A value of 0.001 *m* is recommended for the nitrate concentration for solutions with no nitrate.
- The nitrate to chloride concentration ratio from zero to 1.0 for the crevice repassivation potential model. For solutions with the ratio greater than 1.0, the ratio is limited to 1.0. This ratio range is not applied to the corrosion potential model.

Note that no localized corrosion of the WPOB is expected for any water chemistries with the nitrate concentration greater than the upper bound (6 *m*). Because only nitrate ions are accounted for in the localized corrosion model for the inhibitive effect, the model results for solutions with significant amounts of other potentially inhibitive ions such as carbonate and sulfate (in addition to nitrate ions) are conservative. The model results for the beneficial effects of the inhibitive ions combined with alkaline pH conditions of the typical carbonate-containing waters in the repository are consistent with the experimental observations on the immunity of Alloy 22 to localized corrosion in those waters (see Section 7.3).

1.3 BARRIER CAPABILITIES

10 CFR 63 defines a barrier as "any material, structure, or feature that, for a period to be determined by NRC, prevents or substantially reduces the rate of movement of water or radionuclides from the Yucca Mountain repository to the accessible environment, or prevents the release or substantially reduces the release rate of radionuclides from the waste." 10 CFR 63.102 (h) and 10 CFR 63.113 (a) require that the repository system must include multiple barriers, both natural and engineered. The capability of a barrier is defined by its ability to achieve one or more of the functions described above: *i.e.*, the extent to which it can prevent or delay the movement of water or radionuclides, or prevent or reduce the release rate from the waste.

In this document, the barrier considered is the waste package outer barrier. The barrier contributes to waste isolation by keeping water away from the waste for its lifetime and, when breached, by reducing the contact of water with the waste and radionuclide release rate from the waste.

1.4 INCLUDED FEPS RELEVANT TO THIS MODEL REPORT

A list of Features, Events, and Processes (FEPs) that are included in the analyses and models documented in this model report is provided in Table 1-1 (DTN MO0306SEPFEPS3.000). More details of the included FEPs and their disposition in this model report are described in Section 6.2 of this model report.

Table 1-1. List of Included FEPs Relevant to This Model Report.

FEP Number	FEP Name	FEP Description	Section(s) Where Disposition is Described
2.1.03.01.0A	General corrosion of waste packages	General corrosion may contribute to waste package failure.	6.4.3, 6.4.5
2.1.03.03.0A	Localized corrosion of waste packages	Localized corrosion (pitting or crevice corrosion) leads to failure of the waste packages.	6.4.4
2.1.03.05.0A	Microbially influenced corrosion (MIC) of waste packages	Microbial activity may catalyze waste package corrosion by otherwise kinetically hindered oxidizing agents. The most likely process is microbial reduction of groundwater sulfates to sulfides and reaction of iron with dissolved sulfides.	6.4.5
2.1.06.07.0A	Chemical effects at EBS component interfaces	Chemical effects that occur at the interfaces between materials in the drift may affect the performance of the system.	6.4.3, 6.4.4, 6.4.5
2.1.11.06.0A	Thermal sensitization of waste packages	Phase changes in waste package materials can result from long-term storage at moderately hot temperatures in the repository. Stress-corrosion cracking, inter-granular corrosion, or mechanical degradation may ensue.	6.4.6
Note:	Upon further consideration, FEP 2.1.10.01.0A, “Biological activity in waste and EBS, is now assigned only to Waste Form and Engineered Barrier System, not to Waste Package. FEP 2.1.03.05.0A addresses the microbiological effects on the waste package corrosion.		

Source: DTN MO0306SEPFEPS3.000

2 QUALITY ASSURANCE

The Office of Civilian Radioactive Waste Management (OCRWM) Quality Assurance (QA) program applies to this model report and the analyses contained therein. All types of waste packages were classified per QAP-2-3 as Quality Level-1. The classification has been documented in a number of Project's documents such as in *Classification of the MGR Uncanistered Spent Nuclear Fuel Disposal Container System* (CRWMS M&O 1999a, p. 7). This classification is still in effect.

The technical work plan *Waste Package Materials Data Analyses and Modeling* (BSC 2002a), associated with this activity was prepared per AP-2.27Q, *Planning for Science Activities*. This analysis was prepared under the activity evaluation conducted for work package number AWPM01. The results of this evaluation indicate that the activity is subject to the *Quality Assurance Requirements and Description* (QARD) DOE/RW-0333P (DOE 2003) requirements. The methods used to control the electronic management of data as required by AP-SV.1Q, *Control of the Electronic Management of Information*, were accomplished in accordance with the technical work plan. Inputs and transfers of data were checked to assure completeness and accuracy in accordance with Supplement V requirements. Data were also protected from damage and were also password protected.

This document was prepared in accordance with AP-SIII.10Q, *Models,* and reviewed in accordance with AP-2.14Q, *Review of Technical Products and Data.*

3 COMPUTER SOFTWARE AND MODEL USAGE

3.1 COMPUTER SOFTWARE

Microsoft Excel 2000, bundled with Microsoft Office 2000, is a commercial off-the-shelf software program used in this report. The computations performed in this report using Excel use only standard built-in functions and are documented in sufficient detail to allow an independent technical reviewer to reproduce or verify the results by visual inspection or hand calculation without recourse to the originator (see Sections 6.4.3 to 6.4.6, and the Excel files included in the output DTNs SN0308T0506303.003 and SN0308T0506303.004). Therefore this software is exempt from the AP-SI.1Q, *Software Management,* procedure. Microsoft Excel 2000, in accordance with AP-SI.1Q, *Software Management*, is appropriate for this application as it offers all of the mathematical and graphical functionality necessary to perform and document the numerical manipulations used in this model report. Microsoft Excel 2000 was executed on a DELL Latitude C640 laptop equipped with a Pentium 4 processor (CRWMS M&O Bar Code 501216) in the Windows 2000 operating system.

Mathcad 2000 Professional is a commercial off-the-shelf software program used in this model report. The computations performed in this report using MathCad use only standard functions and are documented in sufficient detail to allow an independent technical reviewer to reproduce or verify the results by visual inspection or hand calculation without recourse to the originator (see Sections 6.4.3 and 6.4.4, and the Mathcad worksheet files included in the output DTNs SN0308T0506303.003 and SN0308T0506303.004). Therefore this software is exempt from the AP-SI.1Q, *Software Management,* procedure. This software, in accordance with AP-SI.1Q, *Software Management*, is appropriate for this application as it offers all of the mathematical and graphical functionality necessary to perform and document the numerical manipulations used in this model report. Mathcad 2000 Professional was executed on a DELL Latitude C640 laptop equipped with a Pentium 4 processor (CRWMS M&O Bar Code 501216) in the Windows 2000 operating system.

3.2 MODELS USED

No pre-existing models were used in this model report.

4 INPUTS

This section documents input data and parameters used in the models and analyses in this model report. This section also documents inputs from other models and/or analyses used in this model report. Criteria that are directly applicable to the analyses and models in this model report are identified, and a list of the applicable codes and standards used in the analyses and models in this model report is also provided.

4.1 DATA, PARAMETERS, AND OTHER MODEL/ANALYSES INPUTS

This section identifies and documents input data and parameters that are used in the analyses and models in this model report. It also documents inputs from other analyses and models. Inputs are handled as per OCRWM procedures AP-SIII.10Q and AP-3.15Q. Data are submitted to the Technical Data Management System (TDMS) and are listed in the associated Document Input Reference System (DIRS) report.

4.1.1 Data

This section identifies and documents input data that were used in the analyses and models documented in this model report. Table 4-1 lists all the input data used in the analyses and models documented in this model report. The numerical values of most of the input data used in the analyses documented in Section 6 are listed in the attachments of this report. Table 4-1 identifies the DTNs and specific subsections where the data were used. Additional details of the input data are described in the individual sub-sections that follow. The test procedures for the various electrochemical corrosion tests that were employed to generate the input data documented in this section are summarized in Attachment I, along with a summary for the test conditions and parameters. The electrochemical corrosion tests that are summarized in Attachment I include polarization resistance tests and cyclic potentiodynamic polarization (CPP) tests. The long-term open circuit potential tests are summarized in Section 6.4.4.4. A summary of the test procedures for the weight loss measurements of the 5-year samples from the Long-Term Corrosion Test Facility (LTCTF) is given in Section 6.4.3.1. The electrochemical corrosion test data for the electrolytes containing NaF and oxalic acid were not included in the quantitative model analysis in this model report because these chemical environments are not expected to be relevant to the repository conditions. Details of those tests are provided in the corresponding Scientific Notebooks cited in the individual Data Tracking Numbers (DTNs) of the input data listed in the table. The treatment of input data uncertainty is addressed in the data analysis and model development throughout Section 6.4.

Table 4-1. Summary of All Input Data Used in the Analyses and Models in This Model Report.

Data Name	Data Source	DTN	Data Use in This report
Oxide Layer on Alloy 22 Formed in Air	Waste Package Materials Testing	LL030406412251.045	Section 6.4.2
Oxide Layer on Alloy 22 Formed in Mixed Salt Environment	Andresen et al. 2002, Section 3.0, DIRS	LL021105312251.023, Table 3-2, Figures 3-6 to	Section 6.4.1

Data Name	Data Source	DTN	Data Use in This report
	161253	3-11.	
Target Composition of Aged SDW Solutions from LTCTF Employed in Long-Term Open Circuit Potential Tests	Waste Package Materials Testing	LL000320405924.146	Sections 6.4.3, 6.4.4
Measured pH of Solutions from Long-Term Open Circuit Potential Measurements	Waste Package Materials Testing	LL030201212251.033	Section 6.4.4
Molal Concentrations of Simple Salt Solutions Used in Various Electrochemical Tests	Waste Package Materials Testing	LL030703723121.031	Section 6.4.4
Molal Concentrations of Complex Salt Solutions Used in Various Electrochemical Tests	Waste Package Materials Testing	LL030706223121.032	Section 6.4.4
Molal Concentrations of BSW Solution Used in Long-Term Open Circuit Potential Tests	Waste Package Materials Testing	LL030709812251.067	Section 6.4.4, and Attachment V
Alloy 22 Weight Loss Data of Crevice and Weight-Loss Specimens After Five Year Exposure in the LTCTF	Waste Package Materials Testing	LL030412512251.057	Section 6.4.3
Linear Polarization Resistance Data for Temperature Effect	Waste Package Materials Testing	LL030309512251.042, LL030502212251.063, LL030409812251.054	Section 6.4.3, and Attachment IV
Linear Polarization Resistance Data for Weld Effect	Waste Package Materials Testing	LL030309512251.042, LL030502212251.063, LL030409812251.054	Sections 6.4.3 and 6.4.6, and Attachment IV
Linear Polarization Resistance Data for Aging Effect	Waste Package Materials Testing	LL030309512251.042, LL030502212251.063, LL030409812251.054	Sections 6.4.3 and 6.4.6, and Attachment IV
Long-Term Open Circuit Potential Measurement Data in “Aged” LTCTF Solutions at Different Temperatures	Waste Package Materials Testing	LL020711612251.017	Section 6.4.4
Long-Term Open Circuit Potential Measurement Data in “Fresh” LTCTF Solutions at Different Temperatures	Waste Package Materials Testing	LL020711612251.017	Section 6.4.4
Long-Term Open Circuit Potential Measurement Data in BSW at Different Temperatures	Waste Package Materials Testing	LL020711612251.017	Section 6.4.4
Long-Term Open Circuit Potential Measurement Data in $CaCl_2$ + $Ca(NO_3)_2$ Solution with Varying Chloride and Nitrate Concentration Ratios at Different Temperatures	Waste Package Materials Testing	LL020711612251.017	Section 6.4.4
Cyclic Potentiodynamic Polarization Measurement Data in Fresh Chloride-	Waste Package Materials Testing	LL030409512251.051, LL030309512251.042,	Section 6.4.4

Data Name	Data Source	DTN	Data Use in This report
containing Solutions with Varying Nitrate Ion Concentrations at Different Temperatures		LL030502212251.063, LL030409812251.054, LL021105112251.022, LL030400112251.043, LL030406212251.044	
Alteration of Corrosion Rates Associated with Microbial Activity	Waste Package Materials Testing	LL991203505924.094	Section 6.4.5
Density of Alloy 22	Reference Information Base	MO0003RIB00071.000	Section 6.4.3

4.1.1.1 Passive Film Characterization

The characterization of the passive film formed on Alloy 22 in various exposure environments will be used to provide a technical basis for constructing the conceptual model of the structure and composition of the film. The input information will be also used as an aid to interpreting corrosion data and their implication to developing corrosion models. Table 4-2 lists the names of the passive film characterization data, their sources and associated DTNs. Because these input data are used in a qualitative manner, no quantitative analysis for the input data uncertainty will be performed. Where available, alternative conceptual models and/or other relevant data from the literature will be considered and analyzed in the analyses and models to the extent possible.

Table 4-2. Alloy 22 Passive Film Characterization Data.

Data Name	Data Source	DTN	Data Use in This report
Oxide Layer on Alloy 22 Formed in Air	Waste Package Materials Testing	LL030406412251.045	Section 6.4.2
Oxide Layer on Alloy 22 Formed in Mixed Salt Environment	Andresen et al. 2002, Section 3.0, DIRS 161253	LL021105312251.023, Table 3-2, Figures 3-6 to 3-11.	Section 6.4.1

4.1.1.2 Corrosion Test Solution Composition

Models and analyses of Alloy 22 corrosion consider the exposure conditions, in addition to material conditions (i.e., base metal vs. weld, aged vs. non-aged, etc.). The exposure condition parameters that are important to corrosion of metal are temperature and composition of the solution contacting the metal. The key species that significantly affect metal corrosion are hydrogen ion (e.g., pH), halide ions (such as chloride), corrosion inhibiting ions (such as nitrate and sulfate ions), and dissolved oxygen. The compositions of the solutions employed in various corrosion tests for Alloy 22 are therefore key input to the Alloy 22 corrosion analyses and models. Table 4-3 lists the data names of the corrosion test solution compositions, their sources and associated DTNs. The solution composition data include concentrations of major cations and anions including those stated above. Because a single concentration measurement for each

species for each solution condition (or each test condition) was reported and little uncertainty was expected in the measurement, no discussion or analysis were considered for the input data uncertainty.

Table 4-3. Compositions of Solutions Employed in Various Corrosion Tests of Alloy 22.

Data Name	Data Source	DTN	Data Use in This report
Target Composition of Aged SDW Solutions from LTCTF Employed in Long-Term Open Circuit Potential Tests	Waste Package Materials Testing	LL000320405924.146	Sections 6.4.3, 6.4.4
pH of Solutions from Long-Term Open Circuit Potential Measurements	Waste Package Materials Testing	LL030201212251.033	Section 6.4.4
Molal Concentrations of Simple Salt Solutions Used in Various Electrochemical Tests	Waste Package Materials Testing	LL030703723121.031	Section 6.4.4
Molal Concentrations of Complex Salt Solutions Used in Various Electrochemical Tests	Waste Package Materials Testing	LL030706223121.032	Section 6.4.4
Molal Concentrations of BSW Solution Used in Long-Term Open Circuit Potential Tests	Waste Package Materials Testing	LL030709812251.067	Section 6.4.4

4.1.1.3 Long-Term Corrosion Weight Loss Data

Alloy 22 specimens with differing configurations and material conditions have been under testing in the Long-Term Corrosion Testing Facility (LTCTF) at the Lawrence Livermore National Laboratory (LLNL). The longest exposure to date is over 5 years. The shorter exposure-time data were used in the previous corrosion modeling exercise and documented in the earlier version of this model report. The 5-year data were used as input to the Alloy 22 general corrosion model documented in this model report. The inputs from DTN LL030412512251.057 used in the model analysis were the weight loss measurements and characteristics of the sample and exposure conditions. The corrosion rates were calculated from the weight loss measurement data in this model report. The input data and the calculated rates are listed in Attachments II and III. The calculated corrosion rates are slightly different from those in the input DTN due to round-off errors. Uncertainty in the data will be described in detail in Section 6.4.3.3. The data uncertainty will be analyzed, quantified, and propagated into the general corrosion model. These will be documented in Section 6.4.3.3. Listed in Table 4-4 are the data names of the Alloy 22 weight loss data for four different exposure periods, their sources and associated DTNs.

Table 4-4. Long-Term Corrosion Weight Loss Data for Alloy 22.

Data Name	Data Source	DTN	Data Use in This report
Alloy 22 Weight Loss Data of Crevice and Weight-Loss Specimens After Five Year Exposure in the LTCTF	Waste Package Materials Testing	LL030412512251.057	Section 6.4.3

4.1.1.4 Linear Polarizarion Resistance Data

The linear polarization resistance technique was used to measure the corrosion rate of Alloy 22 in varying testing conditions. The corrosion rates measured by the technique are for comparative analysis of corrosion behaviors of the alloy under a wide range of test conditions. They are not intended to be used to obtain the absolute values of the corrosion rates. The linear polarization resistance data were used to determine the temperature dependence of the general corrosion rate (see Section 6.4.3) and to evaluate the effect of welds and aging on Alloy 22 corrosion (see Section 6.4.6). The test conditions included in the tests are exposure condition (e.g., temperature and water chemistry), sample configuration (e.g., crevice, rod, prism and disc), and material conditions (e.g., mill-annealed, as-welded, and as-welded plus thermally aged). Table 4-5 lists the sources of the linear polarization resistance data of Alloy 22, which were used to analyze and quantify the effect of the exposure and materials conditions on the WPOB corrosion performance in the proposed repository. The sources of the data and associated DTNs are also listed in the table. The input data are listed in Attachment IV of this report. Each of the DTNs listed in the table also contains the 24-hour open-circuit corrosion potential (or 24-hour corrosion potential) data and the cyclic potentiodynamic polarization (CPP) data. Details of the electrochemical testing techniques to measure the above corrosion properties of Alloy 22 are described in Attachment I. Uncertainty in the data was analyzed, quantified, and propagated into the model. These are documented in Section 6.4.3.4.

The linear polarization resistance data for the electrolytes containing NaF and oxalic acid were not included in the quantitative model analysis because these chemical environments are not expected to be relevant to the repository conditions. The data for the multiple crevice assembly (MCA) samples with the surface condition labeled as “As Received (AR)”were not included in the model analysis in this model report. This was because the surface of the edges of those MCA samples may have been damaged and contaminated with some “active” materials during the sample preparation. The MCA samples with their edges not properly polished appeared to have caused abnormal signals in the electrochemical corrosion tests. Details of the conditions of those MCA samples are provided in the individual Scientific Notebooks noted in the associated DTN.

Table 4-5. Linear Polarization Resistance Measurement Data for Alloy 22.

Data Name	Data Source	DTN	Data Use in This report
Linear Polarization Resistance Data for Temperature Effect	Waste Package Materials Testing	LL030309512251.042, LL030502212251.063, LL030409812251.054	Section 6.4.3
Linear Polarization Resistance Data for Weld Effect	Waste Package Materials Testing	LL030309512251.042, LL030502212251.063, LL030409812251.054	Sections 6.4.3 and 6.4.6
Linear Polarization Resistance Data for Aging Effect	Waste Package Materials Testing	LL030309512251.042, LL030502212251.063, LL030409812251.054	Sections 6.4.3 and 6.4.6

4.1.1.5 Long-Term Open Circuit Corrosion Potential Data

The open-circuit corrosion potential (referred to as corrosion potential (E_{corr}) hereafter) is an important corrosion property of a metal/alloy. The corrosion potential of a metal or alloy may be affected by the sample configuration (e.g., boldly exposed and crevice), metallurgical condition (e.g., mill-annealed, welded and aged), and exposure condition. For a given exposure condition, it can change over time depending mostly on the kinetics of electrochemical reactions involved. In this model report, the corrosion potentials, along with the critical potentials for localized corrosion discussed in Section 6.4.4.3, was used for the localized corrosion initiation model. See Section 6.4.4.3 for details of the localized corrosion initiation model.

As stated above, because the corrosion potential may change over time and the changes can be significant initially (see Section 6.4.4.4), the long-term steady-state corrosion potentials were used for the corrosion potential model of Alloy 22. The test conditions employed in the long-term corrosion potential measurement are exposure conditions (temperature and water chemistry), sample configuration (crevice or non-crevice), and metallurgical conditions (mill annealed, as-welded, or aged). Table 4-6 lists the long-term open circuit corrosion potential data of Alloy 22 for a range of exposure and materials conditions that the waste packages could experience in the proposed repository. The sources of the data and associated DTNs are also listed in the table. Because of the measurement noises of the long-term corrosion potentials, an average of the readings for the final week of each sample was used for the model analysis. The data that were obtained accordingly are listed in Attachment V of this report. Uncertainty in the data was analyzed, quantified, and propagated into the corrosion potential model. Details of the uncertainty analysis are documented in Section 6.4.4.5. The long-term open circuit potential tests continue to obtain longer term behaviors of the corrosion potentials of Alloy 22. The data reported in DTN LL020711612251.017 capture the data that were available for this model report.

The long-term corrosion potential data for the electrolytes containing NaF and oxalic acid reported in DTN LL020711612251.017 were not included in the quantitative model analysis because these chemical environments are not expected to be relevant to the repository conditions.

Table 4-6. Long-Term Open Circuit Corrosion Potential Measurement Data for Alloy 22.

Data Name	Data Source	DTN	Data Use in This report
Long-Term Open Circuit Potential Measurement Data in “Aged” LTCTF Solutions at Different Temperatures	Waste Package Materials Testing	LL020711612251.017	Section 6.4.4
Long-Term Open Circuit Potential Measurement Data in “Fresh” LTCTF Solutions at Different Temperatures	Waste Package Materials Testing	LL020711612251.017	Section 6.4.4
Long-Term Open Circuit Potential Measurement Data in BSW at Different Temperatures	Waste Package Materials Testing	LL020711612251.017	Section 6.4.4
Long-Term Open Circuit Potential Measurement Data in $CaCl_2$ + $Ca(NO_3)_2$ Solution with Varying Chloride and Nitrate Concentration Ratios at Different Temperatures	Waste Package Materials Testing	LL020711612251.017	Section 6.4.4

4.1.1.6 Cyclic Potentiodynamic Polarization Data

The cyclic potentiodynamic polarization (CPP) technique was used to measure a critical potential ($E_{critical}$) for localized corrosion (pitting and crevice corrosion) of Alloy 22 for a range of exposure conditions that are relevant to the repository. Localized corrosion (crevice corrosion in this model report) is a type of corrosion in which the attack progresses at discrete sites or in a non-uniform manner. The rate of localized corrosion is generally much greater than the rate of general corrosion.

The test conditions that were considered in the CPP tests are exposure conditions (temperature and water chemistry), sample configuration (crevice or boldly exposed), and metallurgical conditions (mill-annealed, as-weld, or aged). Table 4-7 lists the sources of the CPP data of Alloy 22 for a wide range of exposure and material conditions that the waste packages could experience in the proposed repository. The test conditions also included a set of extreme bounding conditions such as concentrated $CaCl_2$-containing brines.

The input DTNs listed in the table also contain other electrochemical measurement data such as 24-hour open-circuit corrosion potentials (or 24-hour corrosion potentials) and linear polarization resistance measurements (see Section 4.1.1.4). Details of the electrochemical testing techniques used to measure the above corrosion properties of Alloy 22 are described in Attachment I. The sources of the data and associated DTNs are also listed in the table.

The CPP data for the electrolytes containing NaF and oxalic acid reported in some of the input DTNs were not included in the quantitative model analysis because these chemical environments are not expected to be relevant to the repository conditions. The data for the multiple crevice assembly (MCA) samples with the surface condition labeled as "As Received (AR)"or as "Edges Not Polished" were not included in the quantitative model analysis of this model report. This was because the surface of the edges of those MCA samples may have been damaged and/or contaminated with some "active" materials during the sample preparation. The MCA samples labeled "AR" did not have the edges properly polished, and this caused abnormal signals in the electrochemical corrosion tests. Details of the conditions of those MCA samples are found in the individual Scientific Notebooks noted in the associated DTN.

Table 4-7. Cyclic Potentiodynamic Polarization Measurement Data for Alloy 22.

Data Name	Data Source	DTN	Data Use in This report
Cyclic Potentiodynamic Polarization Measurement Data in Fresh Chloride-containing Solutions with Varying Nitrate Ion Concentrations at Different Temperatures	Waste Package Materials Testing	LL030309512251.042, LL030502212251.063, LL030409812251.054, LL021105112251.022, LL030400112251.043, LL030406212251.044	Section 6.4.4

4.1.1.7 Crevice Repassivation Potential Data

The localized corrosion conceptual model assumes that crevices may form on the waste package surface in the repository (see Assumption 5.3 and Section 6.3). Thus, crevice corrosion was

conservatively taken as the representative form of localized corrosion on the WPOB (see Assumption 5.3). The crevice repassivation potentials (E_{rcrev}) from the CPP curves described in Section 4.1.1.6 were selected as the critical potentials for localized corrosion, which is considered a highly conservative measure. Input DTN LL030409512251.051 documents the analyses for obtaining the crevice repassivation potentials from the CPP curves. The final set of data developed from the analyses are listed in the tables contained in the files with the file name beginning with "TSES" under the "LL030409512251.051 TDMS" directory of the DTN data package.

The data for non-creviced samples (prisms and discs) were not included in the crevice repassivation potential model analysis. Only the crevice (i.e., MCA) sample data were used for the model analysis. In addition, the MCA corrosion data that did not show occurrence of localized corrosion were conservatively excluded from the analysis. The test environments of those excluded data include the LTCTF-type solutions (SDW, SAW, and SCW (see Table 6-2 for the solution definitions and compositions)) as well as the subset of results in NaCl or $CaCl_2$ solutions that did not show the occurrence of localized corrosion. See Section 6.4.4.2 for details on the data screening analysis, and additional details are documented in DTN LL030409512251.051. The crevice repassivation potential data used in the analyses are listed in Attachment VI. Further details of the tests and data are provided in the individual Scientific Notebooks noted in the associated DTN.

Table 4-8 lists the sources of the crevice repassivation potential data of Alloy 22 used in the critical potential model analysis. Uncertainty in the data was analyzed, quantified, and propagated into the critical potential model. Details of the uncertainty analysis are documented in Section 6.4.4.3.

Table 4-8. Crevice Repassivation Potential Data for Alloy 22.

Data Name	Data Source	DTN	Data Use in This report
Crevice Repassivation Potentials of Alloy 22 in NaCl and $CaCl_2$ Solutions with Varying Nitrate Concentrations at Different Temperatures	Waste Package Materials Testing	LL030409512251.051	Section 6.4.4

4.1.1.8 Microbially Influenced Corrosion

Microbially influenced corrosion (MIC) is the contribution to the corrosion of a metal or alloy due to the presence or activity, or both, of microorganisms. It has been observed that nickel-based alloys such as Alloy 22 are relatively resistant to microbially influenced corrosion (Lian et al. 1999).

The effect of MIC on the WPOB corrosion is represented with a general corrosion enhancement factor. Table 4-9 lists the source of the input data used to evaluate the MIC effect on the WPOB general corrosion rate. DTN LL991203505924.094 contains measurements for the corrosion potentials and corrosion rates of several engineering alloys, including Alloy 22, in the presence and absence of microbes that are relevant to the proposed repository. The corrosion rates were obtained from the short-term polarization resistance tests. The MIC enhancement factor was

determined from the comparative analysis of the corrosion rates of Alloy 22 samples in abiotic and biotic conditions. Uncertainty associated with the MIC enhancement factor is discussed in Section 6.4.5.

Table 4-9. Input Data for Microbially Influenced Corrosion of Alloy 22.

Data Name	Data Source	DTN	Data Use in This report
Alteration of Corrosion Rates Associated with Microbial Activity	Waste Package Materials Testing	LL991203505924.094	Section 6.4.5

4.1.1.9 Density of Alloy 22

The density of Alloy 22 was used to calculate the general corrosion rates of Alloy 22 from the weight loss measurements of the 5-year samples from the LTCTF. Table 4-10 lists the source of the density data.

Table 4-10. Density of Alloy 22.

Data Name	Data Source	DTN	Data Use in This report
Density of Alloy 22	Reference Information Base	MO0003RIB00071.000	Section 6.4.3

4.1.2 Parameters and Parameter Uncertainty

There is no input parameter used in the analyses and models documented in this model report.

4.1.3 Other Model/Analyses Inputs

An approach similar to that used for the Alloy 22 crevice repassivation potentials described in Section 4.1.1.7 was also used by the investigators at the Center for Nuclear Waste Regulatory Analyses (CNWRA) for the Nuclear Regulatory Commission (NRC) to obtain the crevice repassivation potentials for Alloy 22. The data were generated under the QA procedures and reported in Brossia et al. (2001, Table A-1). The test environments for the reported data set are 0.005 M to 4 M chloride concentration and 80 to 150 °C. These data were also included in the critical potential model analysis, and are listed in Attachment VII. Table 4-11 lists the source of the CNWRA crevice repassivation potential data of Alloy 22 used in the critical potential model analysis. Uncertainty in the data was analyzed, quantified, and propagated into the critical potential model. Details of the uncertainty analysis are documented in Section 6.4.4.3.

Table 4-11. Crevice Repassivation Potentials for Alloy 22 from Other Source.

Data Name	Data Source	DTN	Data Use in This report
Crevice Repassivation Potentials of Alloy 22 in NaCl Solutions at Varying Temperatures	Brossia et al. 2001, Table A-1	Technical Information	Section 6.4.4

Faraday constant was used to calculate the corrosion rates from the corrosion current measurements, and its value used in this model report is 96,486 coulombs/mol (Lide, Table 1, page I-1). This constant is used in Attachment I.

4.2 CRITERIA

The Waste Package Technical Work Plan (TWP) (BSC 2002a, Table C5) has identified the following acceptance criteria (AC) based on the requirements mentioned in the Project Requirements Document (Canori and Leitner 2003) and the Yucca Mountain Review Plan (NRC 2003):

1. System Description and Demonstration of Multiple Barriers (NRC 2003, Section 2.2.1.1.3; Canori and Leitner 2003, PRD-002/T-014, PRD-002/T-016)

Specific requirements involve identification of multiple barriers (natural and engineered), describing the capabilities of these barriers to isolate waste, and providing technical bases for capabilities descriptions consistent with the post-closure performance objectives. To comply with these requirements, the following acceptance criteria are identified in the Waste Package TWP (BSC 2002a, Table C5):

- AC1: Identification of Barriers is Adequate
- AC2: Description of the Capability of Identified Barriers is Acceptable
- AC3: Technical Basis for Barrier Capability is Adequately Presented

2. Degradation of Engineered Barriers (NRC 2003, Section 2.2.1.3.1.3; Canori and Leitner 2003, PRD-002/T-015)

Specific requirements include describing deterioration or degradation of engineered barriers and modeling degradation processes using data for performance assessment, including total system performance assessment (TSPA). Consideration of uncertainties and variabilities in model parameters and alternative conceptual models are also required. To fulfill these requirements, the following acceptance criteria are identified in the Waste Package TWP (BSC 2002a, Table C5):

- AC1: System Description and Model Integration are Adequate
- AC2: Data are Sufficient for Model Justification

- AC3: Data Uncertainty is Characterized and Propagated Through the Model Abstraction
- AC4: Model Uncertainty is Characterized and Propagated Through the Model Abstraction
- AC5: Model Abstraction Output is Supported by Objective Comparisons

The above TWP (BSC 2002a, Table C5) also identifies criteria for the Quantity and Chemistry of Water Contacting Waste Package and Waste Forms as being applicable to this model report. These criteria are not applicable to this model report because no analyses of the Quantity and Chemistry of Water Contacting Waste Package and Waste Forms was undertaken in this report. These criteria were improperly identified in the above TWP (BSC 2002a, Table C5) as being applicable to this report.

4.3 CODES AND STANDARDS

This section lists the codes and standards used in the model analyses documented in this report.

4.3.1 Corrosion Degradation Analyses and Models

Standard Practice for Prediction of the Long-Term Behavior of Materials, Including Waste Forms, Used in Engineered Barrier Systems (EBS) for Geological Disposal of High-Level Radioactive Waste. ASTM C 1174-97. 1998. West Conshohocken, Pennsylvania: American Society for Testing and Materials. TIC: 246015.

4.3.2 Cyclic Polarization Measurements

Standard Reference Test Method for Making Potentiostatic and Potentiodynamic Anodic Polarization Measurements. ASTM G 5 - 94. 1997. Philadelphia, Pennsylvania: American Society for Testing and Materials. TIC: 231902.

Standard Test Method for Conducting Cyclic Potentiodynamic Polarization Measurements for Localized Corrosion Susceptibility of Iron-, Nickel-, or Cobalt-Based Alloys. ASTM G 61-86 (Reapproved 1998). 1987. West Conshohocken, Pennsylvania: American Society for Testing and Materials. TIC: 246716.

Standard Practice for Making and Using U-Bend Stress-Corrosion Test Specimens. ASTM G 30-94. 1994. Philadelphia, Pennsylvania: American Society for Testing and Materials. TIC: 246890.

4.3.3 General Corrosion Measurements

Standard Practice for Preparing, Cleaning, and Evaluating Corrosion Test Specimens. ASTM G 1-90 (Reapproved 1999). 1990. West Conshohocken, Pennsylvania: American Society for Testing and Materials. TIC: 238771.

Standard Test Method for Conducting Potentiodynamic Polarization Resistance Measurements. ASTM G 59-97. 1997. West Conshohocken, Pennsylvania: American Society for Testing and Materials.

Standard Practice for Conventions Applicable to Electrochemical Measurements in Corrosion Testing. ASTM G 3-89 (Reapproved 1999). 1989. West Conshohocken, Pennsylvania: American Society for Testing and Materials. TIC: 247076.

Standard Practice for Calculation of Corrosion Rates and Related Information from Electrochemical Measurements. ASTM G 102-89 (Reapproved 1999). 1989. West Conshohocken, Pennsylvania: American Society for Testing and Materials.

4.3.4 Comparative Density of Alloy 22

Standard Specification for Low-Carbon Nickel-Molybdenum-Chromium and Low-Carbon Nickel-Chromium-Molybdenum Steel Alloy Plate, Sheet, and Strip. ASTM B 575-94. 1994. Philadelphia, Pennsylvania: American Society for Testing and Materials. TIC: 237683.

5 ASSUMPTIONS

This Section documents the assumptions that were used to perform analyses and model development and, if necessary, their abstractions for general corrosion and localized corrosion of the waste package outer barrier (WPOB) for the exposure conditions expected in the post-closure repository. Where necessary, additional details of the assumptions are described in the section(s) in which the analyses and models are documented.

5.1 The localized corrosion data of the WPOB material (Alloy 22) that were generated in a fully immersed condition are assumed to be applicable to the localized corrosion processes of the waste package under a thin water film that has the same water chemistry as the fully immersed condition. A thin water film condition is expected to form on the waste package surface in the nominal-case post-closure repository. This assumption is considered conservative because, for the same water chemistry, a fully immersed condition is generally more aggressive than a thin water film condition. Kinetics of the cathodic and anodic reactions involved in localized corrosion under discontinued tortuous thin water films is expected to be slower than a fully immersed condition.

This assumption is based on the experimental observations and analyses for significantly suppressed anodic currents (corrosion rates) from the inside of a crevice, which was caused by the limited cathodic currents (i.e., limited "throwing power") over the insulated metal surface outside the crevice mouth (Manahan et al. 1995; Zhou et al. 1998). The experiments were to simulate the conditions for limited electrical conduction between the inside and outside of a crevice and to evaluate the importance of the electrical coupling between the anodic reactions (occurring inside a pit or crevice) and cathodic reactions (occurring outside the pit or crevice mouth) to the initiation and growth of localized corrosion. The electrical conductivity in discontinued tortuous thin water films that form on the waste package surface would be much lower than a fully immersed condition, therefore the kinetics of the electrochemical reactions involved in localized corrosion would be slower than a fully immersed condition. This is a conservative assumption and does not need confirmation. This assumption is used throughout this model report.

5.2 General corrosion is assumed to occur at relative humidity (RH) above a threshold RH ($RH_{threshold}$) and progress uniformly over a large surface. The general corrosion rate is temperature dependent, and for a given temperature, it is assumed to be constant (i.e., time-independent). Therefore, for a given temperature, the depth of penetration or thinning of the WPOB by general corrosion is equal to the general corrosion rate at that temperature, multiplied by the time duration that the waste package surface is at that temperature. This assumption is considered conservative because the general corrosion rate of metals and alloys tend to decrease with time. This assumption does not need confirmation and is used throughout this model report.

5.3 Crevice corrosion is assumed to be representative of localized corrosion of the WPOB under the exposure conditions expected in the post-closure repository. This is a conservative bounding assumption because the initiation threshold for crevice corrosion in terms of water chemistry and temperature is lower than that for pitting corrosion, which is another form of localized corrosion attacking boldly exposed surface (Gdowski 1991, Section 3.7; Agarwal 2000,

pages 845 to 847). No additional confirmation of this assumption is necessary. This assumption is used throughout this model report.

5.4 When localized corrosion occurs, the localized corrosion of the WPOB is assumed to propagate at a (time-independent) constant rate. This assumption is highly conservative because it is known that the localized corrosion rate decreases with time (CRWMS M&O 1998, Table 3-2; Hunkeler and Boehni 1983; McGuire et al. 1998, Section 5.2.8, EPRI 2002, Section 5.3.1; Frankel 1998; Newman and Franz 1984). Decrease of the localized corrosion rate with the penetration depth is particularly more likely under the condition of discontinued tortuous thin water films that is expected to form on the waste package surface in the post-closure repository. As discussed in Assumption 5.1, in the presence of such discontinued tortuous thin water films on the waste package surface, the cathodic currents from the interior of the corroding crevice to the outside surrounding the crevice mouth would be limited and not be able to support a sustained penetration rate as the crevice grows deeper. No additional confirmation of this assumption is necessary. This assumption is used throughout this model report.

5.5 It is assumed that the WPOB base metal and all fabrication welds (except the welds for the closure lids) are fully annealed before the waste packages are loaded with waste. This assumption is based on the waste package design and fabrication specification (Plinski 2001, Section 8.0). No additional confirmation of this assumption is necessary. This assumption is used throughout this model report.

6 MODEL DISCUSSION

6.1 ANALYSIS AND MODELING OBJECTIVES

The purpose and scope of this model report are to document the analyses and models for general and localized corrosion of the waste package outer barrier (WPOB). The purpose of the general corrosion model is to analyze degradation of the Alloy 22 outer barrier by general corrosion under the range of expected repository exposure conditions over the repository performance period. The purpose of the localized corrosion model is to analyze degradation of the Alloy 22 outer barrier by crevice corrosion under the range of expected repository exposure conditions over the repository performance period. The general and localized corrosion models include several sub-models, which account for dry oxidation, aqueous general corrosion, crevice corrosion initiation, crevice corrosion growth, microbially influenced corrosion (MIC), and effect of aging and phase stability. This model report serves as a feed to the waste package degradation analyses. The corroborating/supporting data and information used to develop the models in this model report can be found in the DIRS report of this report. Those are identified in the report as "reference only" and listed as used in Section 6.

6.2 FEATURES, EVENTS, AND PROCESSES INCLUDED IN THIS MODEL REPORT

The development of a comprehensive list of features, events, and processes (FEPs) potentially relevant to post-closure performance of the proposed Yucca Mountain repository is an ongoing, iterative process based on site-specific information, design, and regulations. The approach for developing an initial list of FEPs, in support of TSPA-SR (CRWMS M&O 2000a), was documented in Freeze et al. (2001). The initial FEP list contained 328 FEPs, of which 176 were included in TSPA-SR models (CRWMS M&O 2000a, Tables B-9 through B-17). To support TSPA-LA, the FEP list was re-evaluated in accordance with the Enhanced FEP Plan (BSC 2002b; Section 3.2). Table 6-1 provides a list of FEPs that are included in TSPA-LA models described in this model document, summarizes the details of their implementation in TSPA-LA, and provides specific references to Sections within this document. See also Table 1-1 for the description of these included FEPs.

Table 6-1. Included FEPs for This Model Report and Their Disposition in TSPA-LA.

FEP No.	FEP Name	Section Where Disposition is Described	Summary of Disposition in TSPA-LA
2.1.03.01.0A	General corrosion of waste packages	Sections 6.4.3 and 6.4.5	General corrosion of the WPOB occurs when the RH at the waste package surface is equal to or greater than the RH threshold for corrosion initiation ($RH_{threshold}$). Because general corrosion is likely to be operative for most of the repository operation period, it is one of the key corrosion degradation processes for waste packages in the repository. Because the repository atmosphere interacts with the air outside the mountain through the fractures, the general corrosion in oxidizing condition is considered for the waste package degradation.

FEP No.	FEP Name	Section Where Disposition is Described	Summary of Disposition in TSPA-LA
			The general corrosion model for the WPOB is based on a temperature dependence of the corrosion process, represented by an activation energy using a modified Arrhenius relation (see Equation 6-28). The activation energy term is normally distributed with a mean of -3116.47 and a standard deviation of 296.47. The activation energy was estimated to be 25.9 ± 2.5 kJ/mol. R_o is a Weibull distribution (α = 8.88, β = 1.62, and θ = 0) fitted to the general corrosion rate distribution derived from the weight loss data of the 5-year crevice specimens. The model and parameters feed to the waste package degradation analysis. Effect of water chemistry on general corrosion is not considered because it is insignificantly small for the range of water chemistry expected in the repository (see Sections 6.4.3.2 and 6.4.3.4). The WPOB is subject to MIC when the RH at the WPOB surface is above 90 %. The effect of MIC on general corrosion of the WPOB is represented by a multiplication factor (or MIC factor) to the abiotic general corrosion rate. The MIC factor is uniformly distributed between 1 and 2, and the entire variance of the distribution is due to uncertainty (see Section 6.4.5). Thermal aging and phase stability is not included in the waste package degradation analysis. Effect of the thermal aging of the WPOB, subjected to the extent that may occur (although highly unlikely) during the waste package fabrication, is insignificantly small on its corrosion performance under the environmental conditions expected in the repository (see Section 6.4.6). Furthermore, an extrapolation of the aging and phase stability data does not indicate that the phase stability of Alloy 22 base metal, annealed welds, and un-annealed welds (i.e., as-welded) will be a problem for temperatures near and below 200°C (BSC 2003a, Sections 6.6.5.3 and 8.0). Accordingly the corrosion performance of the WPOB is not expected to be affected significantly by the aging and phase stability under the thermal conditions expected in the repository. Because it is not a performance limiting process of the WPOB under the exposure conditions expected in the repository, dry oxidation is not considered for the waste package performance analysis in the repository (see Section 6.4.2). The general corrosion is modeled in TSPA. The general corrosion model and its associated parameters feed to the waste package degradation model. The waste package degradation analysis generates as output waste package degradation profiles consisting of the fraction of waste packages failed versus time and the average number of

FEP No.	FEP Name	Section Where Disposition is Described	Summary of Disposition in TSPA-LA
			penetration openings (per failed waste package) by general corrosion versus time. The degradation profiles are used as input into the TSPA model.
2.1.03.03.0A	Localized corrosion of waste packages	Section 6.4.4	Localized corrosion (pitting and crevice corrosion) is a type of corrosion in which the attack progresses at discrete sites or in a non-uniform manner. The penetration rate of localized corrosion is relatively higher than that of general corrosion because the attack is generally on small discrete areas (Jones 1996, page 198), and, if it occurs, could lead to rapid failure of the waste packages. The localized corrosion model consists of two components: initiation and propagation. The model considers that localized corrosion of the WPOB occurs when the open circuit corrosion potential (E_{corr}) is equal to or greater than the crevice repassivation potential (E_{rcrev}) (see Section 6.4.4.1). The model assumes that, once initiated, localized corrosion of the WPOB propagates at a (time-independent) constant rate (see Assumption 5.4 and Section 6.4.4.7). This is highly conservative because it is known that the localized corrosion rate generally decreases with time (see Section 6.4.4.8). The localized corrosion model and its associated parameters feed to the waste package degradation model. While the drip shield performs its design function and prevents seepage water from directly contacting the underlying waste package, solutions that form on the waste package surface from evaporative concentration of the leachate from the dust have neutral to alkaline pH and contain significant concentrations of inhibitive ions such as nitrate. Localized corrosion of the WPOB in such environments is expected to be a very low probability process (see Section 6.4.4.6). A possible scenario for the WPOB to be potentially subjected to localized corrosion in the repository is the *concurrent occurrence* of drip shield failure and direct contact of the waste package with the seepage water while the waste package is at elevated temperatures (i.e., during the first few hundred years of active thermal perturbation). Some seepage waters with a characteristic chemistry could evolve to the type of water that could lead to crevice corrosion of waste package at elevated temperatures. These waters are concentrated chloride-containing acidic brines with relatively lower concentrations of inhibitive ions such as nitrate (see Section 6.4.4.6). After peaked during the active thermal perturbation period, the waste package temperature slowly decreases with time. Once it cools to the temperatures that are lower than the minimum threshold temperature for crevice corrosion initiation

FEP No.	FEP Name	Section Where Disposition is Described	Summary of Disposition in TSPA-LA
			in such concentrated chloride-containing brines, the waste packages are completely immune to localized corrosion. Therefore the main technical issue associated with the waste package localized corrosion susceptibility is the probability of having seepage waters with the characteristic chemistry directly contacting the waste packages while the surface temperature is above the threshold temperature.
2.1.03.05.0A	Microbially influenced corrosion (MIC) of waste packages	Section 6.4.5	In the post-closure environments of the repository, the waste package is subject to MIC when the relative humidity at the waste package surface is above 90 % (CRWMS M&O 2000b, Sections 6.3.1.6 and 6.5.2). Effect of MIC on general corrosion of the WPOB is represented by a general corrosion enhancement factor. The enhancement factor was determined from the comparative analysis of the corrosion rates from the short-term polarization resistance test of samples in abiotic and biotic conditions. The enhancement factor is uniformly distributed between 1 and 2. In the MIC model, the abiotic general corrosion rate is multiplied by the enhancement factor when the exposure conditions on the waste package surface warrant MIC of the WPOB. See Section 6.4.5 for more details. MIC of the WPOB is included in TSPA as part of the waste package degradation analysis. The WPOB MIC is modeled in TSPA with the waste package degradation model. The model generates as output waste package degradation profiles consisting of the fraction of waste packages failed versus time and the average number of penetration openings (per failed waste package) versus time. The degradation profiles are used as input to the TSPA model.
2.1.06.07.0A	Chemical effects at EBS component interfaces	Sections 6.4.3, 6.4.4, and 6.4.5	The waste package corrosion analysis includes the effects of material interfaces in the repository. The thermal-hydrologic-geochemical analyses at the waste package surface include effects of materials present in the emplacement drift, including waste package and drip shield. A threshold RH ($RH_{threshold}$) is used for corrosion initiation of the WPOB. The $RH_{threshold}$ at a given temperature is defined as the lowest humidity condition necessary for aqueous electrochemical corrosion processes of a metal, and this is determined by the deliquescence points of the salts or salt assemblage at that temperature that form on the waste package surface. For the waste packages that are not subject to dripping water, hygroscopic salts may be deposited on the waste package surface by aerosols and dust introduced into the emplacement drift. They could also form from the evaporative concentration of the leachate from the dust and aerosols in contact with humid

FEP No.	FEP Name	Section Where Disposition is Described	Summary of Disposition in TSPA-LA
			air. For the waste packages that are subject to dripping water (i.e., placed at the locations where seepage occurs and under the drip shield that has failed to the extent that it no longer provides the seepage-diversion function), hygroscopic salts could form on the waste package surface from the evaporative concentration of the seepage water that contacts the waste package. Such hygroscopic salts enable aqueous solutions to exist as thin water films at relative humidity (RH) below 100%. The deliquescence points of the salts or salt assemblages, are determined as a function of temperature, considering the thermal-hydrologic-geochemical constituents at the waste package surface. The thermal-hydrologic-geochemical processes can leave mineral deposits and scales on the waste package surface, and these could act as crevice. Also the contacts of the WPOB with the emplacement pallets on which the waste package is placed can create metal-metal crevices. When the pallets degrade to the extent that they no longer support the waste package, the waste package settles on the invert, and the contacts of the waste package bottom with the invert can also create crevices. The waste package corrosion analyses in the TSPA model consider those conditions as the potential crevice formation sites on the waste package surface, and take a conservative approach such that crevices potentially form over the entire surface of the waste package. For the nominal-case post-closure condition of the proposed repository, a thin water film condition is expected to form on the waste package surface when the RH at the waste package surface is above the $RH_{threshold}$ for corrosion initiation. The water films on the waste package would be discontinued and tortuous. The WPOB corrosion models and analyses in the TSPA model are based on the data for a fully immersed condition, and these models are applied to a thin film water condition for the same water chemistry as the fully immersed condition. This is a conservative approach because, for the same water chemistry, a fully immersed condition is generally more aggressive for localized corrosion than a condition of discontinued tortuous thin water film. Kinetics of the electrochemical reactions involved in corrosion under a condition of discontinued tortuous thin water film would be slower than a fully immersed condition because of low electrical conductivity in such water films. In the waste package degradation analysis, no performance credit is taken for the waste package inner shell (316NG stainless steel), thus the material interface between the WPOB and the inner shell is not explicitly modeled. However, upon first

FEP No.	FEP Name	Section Where Disposition is Described	Summary of Disposition in TSPA-LA
			penetration of the WPOB, inside-out corrosion of the WPOB is modeled using the in-package chemistry. As for the outside-in corrosion, general and localized corrosion of the WPOB are included for the inside-out corrosion. The in-package chemistry considers the degradation of the waste package inner shell and the waste package internals including the waste form itself. Therefore, the waste package degradation analysis includes the effects of the WPOB and inner-shell interface indirectly.
2.1.11.06.0A	Thermal sensitization of waste packages	Section 6.4.6	Alloy 22 is known to be subject to "aging" and phase instability when exposed to elevated temperatures. The processes involve precipitation of various secondary phases. The affected material exhibits increased brittleness and decreased resistance to localized corrosion (BSC 2003a). The waste package design and fabrication specification (Plinski 2001, Section 8.0) specifies the WPOB body and all fabrication welds (except the welds for the closure lids) are fully annealed before the waste packages are loaded with waste. According to the analysis documented in the aging and phase stability model report (BSC 2003a, Sections 6.6.5.3 and 8.0), phase instabilities are not expected in Alloy 22 base metal and welded material so long as the temperature remains below about 200°C. Non-thermal stress mitigation processes, currently planned for the closure weld, however, may introduce cold work into the material. Although this cold work might accelerated phase transformation kinetics, it would have to do so by at least a couple of orders of magnitude before it would be expected to be observed at low temperatures in 10,000 years. In addition, project data (see Section 6.4.6) show that the corrosion properties of aged welds are comparable to those of un-aged welds. Therefore, because phase instabilities are not expected and because, even if they do occur, they are not expected to have a significant effect on the corrosion properties, the effects of aging and phase instability of the WPOB were not modeled in TSPA.

6.3 BASE-CASE CONCEPTUAL MODEL

This Section describes the base-case conceptual model that was developed for the analyses and models and, if necessary, their abstractions for the general corrosion and localized corrosion of the waste package outer barrier (WPOB) for the exposure conditions expected for the nominal-case post-closure repository. In general, the ASTM C 1174-97 procedures (ASTM C 1174-97 1998) were followed for development of the models for general and localized corrosion of the WPOB documented in this model report. Because the data and analyses for the above degradation processes were not sufficient for the mechanistic models, semi-empirical modeling

approaches were adopted by incorporating, to the extent available, mechanical understanding of the degradation mechanisms into the modeling process.

A schematic representation of the base-case conceptual model is shown in Figure 6-1. Where necessary, additional details are described in the section(s) in which the analyses and models are documented.

The design functions of the drip shield are to prevent the water seeping into the emplacement drifts from dripping directly onto the waste package and to provide protection from rock-fall damage to the waste package. While the drip shield performs these design functions, the major source that determines the evolution pathway of the chemistry of liquid water contacting the waste package would be the chemistry of the leachate from the dust that has settled on the waste package. In conjunction with the dynamically changing thermal-hydrologic conditions in the emplacement drift as the thermal heat output from the radioactive waste decays with time, concentrated brines could form on the waste package surface from evaporative concentration of the leachate, and the chemical evolution of the brines would be dependent on the humidity and temperature conditions. When the drip shield fails and no longer performs the seepage-diversion design function, and the waste package underneath the failed drip shield is contacted by the seepage water, the major source that determines the evolution pathway of the chemistry of liquid water contacting the waste package would be the chemistry of the seepage water. In conjunction with the dynamically changing thermal-hydrologic conditions in the emplacement drift, concentrated brines could form on the waste package surface from evaporative concentration of the seepage water, and the humidity and temperature conditions at the waste package surface would affect the evolution of the brines.

Hygroscopic salts may be deposited on the waste package surface by aerosols and dust introduced into the emplacement drift. They could form from the evaporative concentration of the leachate from the dust and aerosols in contact with humid air. For the waste packages that are subject to dripping water (i.e., those at the locations where seepage occurs and under the drip shield that has failed to the extent that it no longer provides the seepage-diversion function), hygroscopic salts could form on the waste package surface from the evaporative concentration of the seepage water that contacts the waste package. Such hygroscopic salts enable aqueous solutions to exist as thin water films at relative humidity (RH) below 100%. The RH threshold ($RH_{threshold}$) at a given temperature, at which an aqueous solution can exist, is defined as the deliquescence point at that temperature. This threshold defines the lowest humidity condition necessary for aqueous electrochemical corrosion processes of a metal to occur at a given temperature, and is considered as the corrosion initiation threshold at that temperature. The deliquescence points are a function of temperature of the salts that form on the waste package surface.

Dry oxidation of the WPOB occurs at any RH below the corrosion initiation RH threshold ($RH_{threshold}$). This process results in the formation of an adherent, protective oxide film of uniform thickness. The rate of dry oxidation is generally limited by mass transport through the growing metal oxide film. As discussed in Section 6.4.2 of this model report, dry oxidation is not a performance limiting process of the WPOB under the thermal conditions expected in the repository, therefore it is not considered for any further analysis in this model report.

General corrosion (or passive corrosion) is the uniform thinning of the WPOB at its open-circuit corrosion potential (E_{corr}). At a given surface temperature, the existence of liquid water on the waste package surface depends upon the hygroscopic nature of the salts and minerals deposited on the surface. In the presence of such a deposit, a liquid-phase can be established at a higher temperature and lower RH than otherwise possible. As stated in Assumption 5.2, general corrosion of the WPOB is assumed to occur at any RH above the corrosion initiation RH threshold ($RH_{threshold}$). General corrosion is assumed to progress uniformly over a large surface. The general corrosion rate is temperature dependent, and for a given temperature, the rate is assumed to be constant (i.e., time-independent). Therefore, at a given temperature, the depth of penetration or thinning of the WPOB by general corrosion is equal to the general corrosion rate at that temperature, multiplied by the time duration that the waste package surface is at that temperature. This assumption is considered conservative because the general corrosion rate of metals and alloys tend to decrease with time (see Assumption 5.3 and Section 6.4.3.5).

The general corrosion model analyses in this model report consider that the corrosion rate distribution obtained from the weight loss measurements of the Alloy 22 crevice specimens that were exposed over 5 years in a wide range of mixed salts, multi-ionic solutions at the Long Term Corrosion Testing Facility (LTCTF) represents the distribution of long-term general corrosion rate of the WPOB in the post-closure repository. As discussed in Section 6.4.3.2, this is reasonably bounding because the general corrosion rates for the crevice specimens are generally higher than those of the plain weight-loss specimens (i.e., with no crevice).

As discussed in detail in Section 6.4.3.2, the sample configuration (crevice, disk or rod), metallurgical conditions (mill annealed or as-welded), and water chemistry within the range expected in the repository do not show significant effect on the general corrosion behavior of Alloy 22. The temperature dependence of the general corrosion rate is represented with an activation energy following an Arrhenius relation. The activation energy was determined from the corrosion rates calculated from the short-term polarization resistance measurements of Alloy 22 specimens with varying sample configurations and metallurgical conditions, tested for a range of exposure conditions (temperature and water chemistry). As with the general corrosion rate from the long-term weight loss measurements discussed above, the sample configuration (crevice, disk or rod), metallurgical conditions (mill annealed or as-welded), and water chemistry within the range expected in the repository do not have significant effect on temperature dependence of the general corrosion rate of the alloy (see Section 6.4.3.4). A similar conceptual description was presented in a recent report by the Electric Power Research Institute (EPRI 2002, Section 5.3.2), using the literature data for corrosion resistant Ni-Cr-Mo alloys.

Localized corrosion is a type of corrosion in which the attack progresses at discrete sites or in a non-uniform manner. The rate of localized corrosion is generally much higher than the rate of general corrosion. As stated in Assumption 5.3, the current analysis considers crevice corrosion is representative of localized corrosion of the WPOB under the exposure conditions expected in the post-closure repository. This is a conservative bounding assumption because the initiation threshold for crevice corrosion of Alloy 22 in terms of water chemistry and temperature is lower than pitting corrosion, which is another form of localized corrosion attacking boldly exposed surface (Gdowski 1991, Section 3.0; Haynes 1997a and 1997b).

Localized corrosion of the WPOB is modeled with two model components: initiation model and propagation model. The initiation model considers that localized corrosion of the WPOB occurs when the open circuit corrosion potential (E_{corr}) is equal to or greater than a certain critical potential ($E_{critical}$), that is, ΔE (= $E_{critical}$ - E_{corr}) ≤ 0. This conceptual model of localized corrosion initiation is widely accepted by the corrosion community (Bohni 2000, Section B; Dunn et al. 2000 and 2003; Frankel 1998; Frankel 2002; Frankel and Kelly 2002; Beavers et al. 2002, Section 8.1). Both the crevice corrosion initiation model components (i.e., E_{corr} and $E_{critical}$) are represented as a function of temperature, pH, chloride ion concentration, nitrate ion concentration.

When localized corrosion occurs, the localized corrosion of the WPOB is assumed to propagate at a (time-independent) constant rate (Assumption 5.4). This assumption is highly conservative because it is known that the localized corrosion rate decreases with time, and this is particularly more likely under a condition of discontinued tortuous thin water films that is expected to form on the waste package surface in the post-closure repository. See Section 6.4.4.8 for detailed discussion.

The WPOB is subject to microbially influenced corrosion (MIC) when the relative humidity at the WPOB surface is above 90 %. This MIC initiation threshold RH is based on the analysis documented in the model report titled *In-Drift Microbial Communities* (CRWMS M&O 2000b, Sections 6.3.1.6 and 6.5.2, Table 23). The effect of MIC on general corrosion of the WPOB is represented by a general corrosion enhancement factor. The enhancement factor was determined from the comparative analysis of the corrosion rates measured from the short-term polarization resistance measurements of Alloy 22 specimens tested in abiotic and biotic conditions.

The waste package design and fabrication specification specifies that the WPOB base metal and all fabrication welds (except the closure lid welds) are fully annealed before the waste packages are loaded with waste (Plinski 2001, Section 8.1) (Assumption 5.5).

According to the analysis documented in the aging and phase stability model report (BSC 2003a, Sections 6.6.5.3 and 8.0), phase instabilities are not expected in Alloy 22 base metal and welded material so long as the temperature remains below about 200°C. Non-thermal stress mitigation processes, currently planned for the closure weld, however, may introduce cold work into the material. Although this cold work might accelerated phase transformation kinetics, it would have to do so by at least a couple of orders of magnitude before it would be expected to be observed at low temperatures in 10,000 years. In addition, project data (see Section 6.4.6) show that the corrosion properties of aged welds are comparable to those of un-aged welds. Therefore, because phase instabilities are not expected and because, even if they do occur, they are not expected to have a significant effect on the corrosion properties, the effects of aging and phase instability of the WPOB are not modeled in TSPA.

Effects of oxidant on corrosion such as hydrogen peroxide generated from gamma radiolysis may be accounted for through the open circuit corrosion potential (E_{corr}). However, the radiolysis-enhanced corrosion has been screened out in the analysis report titled *FEPs Screening of Processes and Issues in Drip Shield and Waste Package Degradation* (CRWMS M&O 2001, Section 6.2.27). Therefore the radiolysis-enhanced corrosion of the WPOB is not considered in the waste package degradation analysis.

In the current waste package corrosion analysis, all corrosion performance is allocated to the WPOB, even though the waste package is a double-wall container and the stainless steel 316 NG inner cylinder can potentially provide significant corrosion performance. The inner cylinder is to provide structural integrity for the waste package (Plinski 2001, Sections 1.0 and 4.0). No performance credit is claimed for the corrosion resistance of this stainless steel shell. This model approach is used throughout the analysis and is conservative because the inner barrier is expected to be a barrier for water ingress and radionuclide release.

After penetration of the WPOB, a crevice can form in the interfacial region between the Alloy 22 outer cylinder and 316NG inner cylinder. The formation of a low-pH crevice environment in this interfacial region is possible. Local acidic water chemistry could be developed through hydrolysis of dissolved metal ions in the crevice regions between the two barriers, however the availability of oxygen (dominant oxidizer for this condition) to such an occluded area may be limited. The analyses in this model report show that Alloy 22 is highly resistant to the expected crevice corrosion conditions, especially in solutions with mixed ions. Such inside-out attack of the WPOB is accounted for in the present waste package performance analysis.

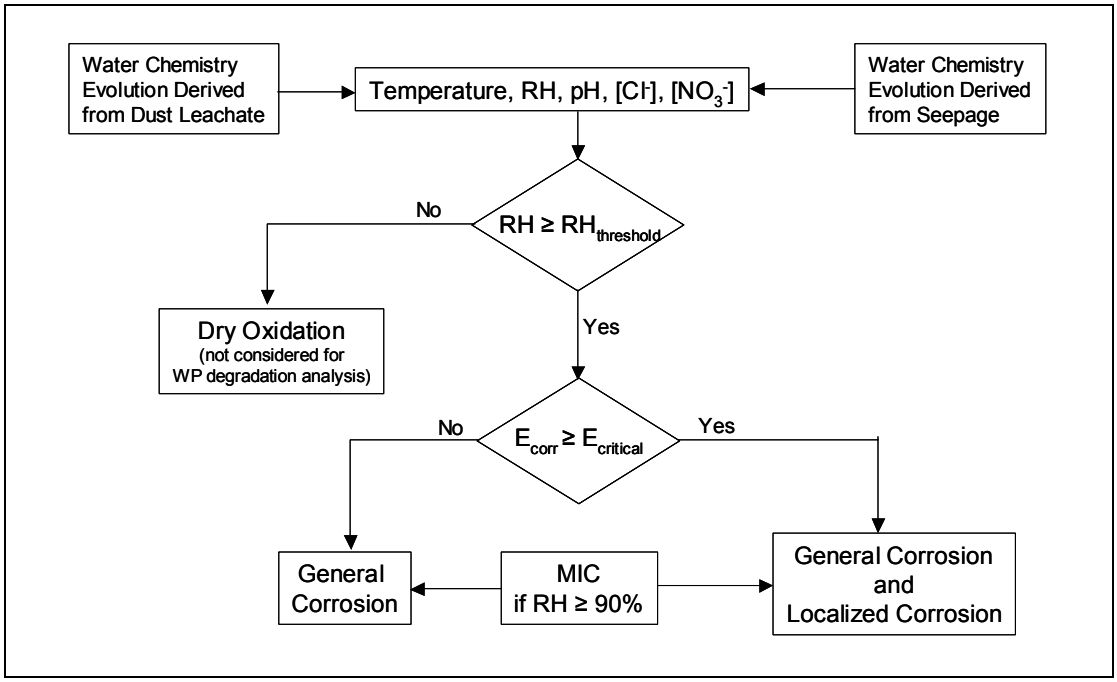

Figure 6-1. Schematic Representation of the Base-Case Conceptual Model for the General And Localized Corrosion Model of the Waste Package Outer Barrier Developed in This Model Report.

6.4 MODEL FORMULATION FOR BASE-CASE MODEL

This section documents the analyses and models development for the base case models for general and localized corrosion of the WPOB for the conditions expected in the proposed

repository. The analyses and models also consider effects of microbiological processes (see Section 6.4.5) and aging and phase stability (see Section 6.4.6) of the barrier for the conditions expected in the proposed repository.

6.4.1 Stability of Passive Film in Repository Relevant Environments

Corrosion performance of the WPOB depends on the integrity of the thin, compact, adherent passive film formed on the alloy surface in contact with the exposure environments in the repository. The extremely low general corrosion rates and excellent resistance to localized corrosion of the WPOB in the repository intimately depend on the long-term stability of the passive film on the surface of the barrier. This section discusses the conceptual understanding of passivity and passive film stability of Ni-Cr-Mo alloys summarizing the data and information from the literature. Also discussed in this section is a summary of the experimental results to characterize the passive film of Alloy 22 tested in environments relevant to the conditions expected in the repository.

6.4.1.1 Conceptual Description of Passivity and Passive Film Stability

Long-term stability of the passive film on the surface of the Alloy 22 waste package outer barrier is one of the key issues that determines the long-term performance of the waste packages in the proposed repository. Corrosion performance of highly corrosion-resistant alloys like Alloy 22 depends on the integrity of the thin, compact, adherent passive film formed on the alloy surface in contact with the corrosive environment. Extrapolation of the measured short-term corrosion rates over a repository time frame is based on that the integrity of this passive film remains stable over very long times. This section provides a brief description of the conceptual understanding of passivity and the passive film formation and growth on highly corrosion-resistant alloys relevant to Alloy 22.

Passivity can be defined as a phenomenon concerned with the formation of a thin, compact, and adherent oxide or oxyhydroxide film that protects a metal or alloy from corrosive degradation. It has now been accepted that the passive film formed under aqueous condition is not a single layer, but rather has a stratified structure (Macdonald 1992; Marcus and Maurice 2000, page 138). According to this bilayer model, the passive film consists of an inner layer of oxide and an outer layer of hydroxide or oxyhydroxide. The inner oxide layer plays the role of a barrier layer against corrosion, and the outer layer plays the role of an exchange layer (Marcus and Maurice 2000, page 138).

6.4.1.1.1 Passive Film Formed on Metals

In general, the chemical composition and thickness of passive films depend on the nature of the metal, the pH of the electrolyte in which the metal is passivated, and the electrochemical potential (Macdonald 1992; Macdonald 1999; Marcus and Maurice 2000, page 138). For example, for nickel that can passivate in solutions over a wide range of pH, the passive film is generally composed of nickel(II) cations with an inner layer of NiO and an outer layer of $Ni(OH)_2$ (Marcus and Maurice 2000, page 140).

The passive films formed on metal surfaces are generally not electronic conductors, but rather semiconductors or insulators. The electronic structures of passive films can be determined by photoelectrochemical measurements. However, the structural analyses are rather difficult, inherent to the nanometer thickness of passive films and the roughness of the surfaces because of dissolution. The passive film formed on nickel (in 0.05 M H_2SO_4) has shown crystallites, the size of which are reduced with increasing potential. The shape of crystallites also changes with potential (Marcus and Maurice 2000, Table 3-1). Another factor that should be considered is active dissolution, which occurs as long as the surface is not completely passivated. The dissolution rate increases exponentially with increasing potential (Tafel relationship) ; dissolution may create new sites for oxide nucleation and can, thus, favor a higher density of oxide nuclei (Marcus and Maurice 2000, page 147). The passive film formed on nickel has revealed crystallinity, with the surface exhibiting terraces and steps. On the other hand, the passive oxide film formed on chromium can have a nanocrystalline structure. These oxide nanocrystals are cemented together by the chromium hydroxide outer layer, making the passive film extremely protective against corrosion-induced damage.

6.4.1.1.2 Passive Film Growth Mechanisms

As summarized in the literature (Macdonald 1992; Macdonald 1999), the barrier oxide layer (inner layer) forms by the generation of oxygen vacancies (and hence new film) at the metal/film interface, balanced in the steady state by dissolution of the barrier layer at the barrier layer/outer layer interface. The outer layer forms via the hydrolysis and precipitation of cations transmitted through the barrier layer or by hydrolytic restructuring of the barrier layer/outer layer interface. The distinctly different origins of the barrier and outer layers are amply demonstrated by the fact that both layers may incorporate alloying elements from the alloy substrate, but only the outer layer incorporates species from the solution. Furthermore, with respect to the laboratory frame of reference, the barrier layer grows into the substrate metal, whereas the outer layer grows outwards into the solution (Macdonald 1992; Macdonald 1999). Thus, while the growth of the barrier layer is exclusively due to the generation of oxygen vacancies at the metal/barrier layer interface, the growth of the outer layer is commonly (but not exclusively) due to the transmission of cations through the barrier layer, either through cation vacancies or as cation interstitials, and their eventual emission at the barrier layer/outer layer interface. The origin of the outer layer is not exclusively due to cation transmission, because it may also form via hydrolytic restructuring of the barrier layer at the barrier layer/outer layer interface (Macdonald 1992; Macdonald 1999).

Current is carried by all charged species in the barrier layer, including cation vacancies, cation interstitials, and oxygen vacancies, which are generated and annihilated at the interfaces and by dissolution of the barrier layer, depending on whether a change in oxidation state occurs (Macdonald 1992; Macdonald 1999). The principal mode of transport of the defects is migration under the influence of a strong electric field, the magnitude of which is postulated to be established by the potential differences across the film and interfaces and by buffering due to Esaki (band-to-band) tunneling within the barrier layer (Macdonald 1992; Macdonald 1999). Because a barrier layer exists on all passive metals, all barrier layers are oxygen vacancy conductors to an extent that, in the steady-state, is determined by the dissolution rate of the film. However, other defects may dominate the structural and electronic defect structures of the barrier layer. For example, the defect structure of the barrier layer on nickel is dominated by cation

vacancies, while that on zinc is dominated by cation interstitials, even though oxygen vacancies exist in both cases.

6.4.1.1.3 Chromium Enrichment in Passivated Nickel-Base Alloys

Chromium concentration plays a significant role in the passivation of austenitic nickel-base alloys, such as Alloy 600 and Alloy 690. The passive films in these alloys can be described by the bilayer model (Macdonald 1992; Macdonald 1999). The concentration of Cr^{+3} in the inner oxide layer is higher than the nominal chromium content of the alloy (Marcus and Maurice 2000, p. 153; Lorang et al. 1990, Figures 1 and 2). The mechanism of surface enrichment of chromium in the barrier layer has been developed within the framework of the PDM (Zhang and Macdonald 1998a and 1998b) and is based on the selective oxidation of the elements at the alloy/barrier layer interface, differences in transport properties of the species in the barrier layer, and selective oxidation of the elements at the barrier layer/outer layer interface. In the specific case of the passive film on iron-chromium alloys, enrichment of the barrier layer in chromium appears to entail the dissolution of iron and the oxidative segregation of chromium (Marcus and Maurice 2000, p. 153). Iron atoms are detached from the surface and go into solution as ions, whereas chromium atoms are rapidly oxidized and the passive film forms by the nucleation and growth of a Cr_2O_3-like phase (Marcus and Maurice 2000, p. 153). However, the barrier layers on iron-chromium and nickel-chromium alloys are not pure chromium oxide (Cr_2O_3), and they still contain significant amounts of other metal species, such as nickel, ferrous, and ferric ions (Lorang et al. 1990). Finally, it is important to note that the accurate description of alloy segregation phenomena requires solving the "moving boundary" problem, because the interfaces at which the segregation reactions occur and the phases bounded by these interfaces move differently with respect to the laboratory frame of reference. This is the approach adopted in the PDM (Zhang and Macdonald 1998a and 1998b).

6.4.1.1.4 Role of Molybdenum

The exact mechanism of the effect of molybdenum on the corrosion resistance of nickel-chromium-molybdenum alloys is not fully understood. However, there is a consensus that molybdenum reduces the rate of anodic dissolution in the active state (Marcus and Maurice 2000, pp. 155 to 158), but it is not clear whether this observation is relevant to the corrosion of a passive alloy. Molybdenum is postulated to be located preferentially at local defects on the surface, which normally act as dissolution sites. The slowing down of the dissolution rate could be due to the increased metal-metal bond strength where molybdenum is present (Marcus and Maurice 2000, pp. 155 to 158). Further, the presence of molybdenum counteracts the deleterious effect of species such as sulfur which can cause grain-boundary attack, in that it bonds to sulfur and then dissolves, thus eliminating the detrimental effect of sulfur (Marcus and Maurice 2000, p. 158).

An analytical prediction of the role played by molybdenum (or any alloying element) in inhibiting passivity breakdown on alloys is provided by the point defect model (Urquidi and Macdonald 1985), which is found to account quantitatively (within the accuracy of the experimental data) for the impact of molybdenum on the pitting resistance of 18 chromium-8 nickel stainless steels (e.g., AISI Type 304 versus Type 316). In this model, highly oxidized

alloy elements that are present substitutionally in the barrier layer lattice form immobile, positively charged centers. For example, recognizing that the barrier layer on chromium containing stainless steels and nickel-base alloys is essentially Cr_2O_3, substitution of Mo^{6+} into a chromium cation vacancy would produce the immobile species ($Mo_{Cr}^{3\bullet}$). This species may interact electrostatically with the mobile, negatively charged cation vacancies ($V_{Cr}^{3'}$) that are responsible for passivity breakdown via condensation at the metal/film interface under supra breakdown conditions (Macdonald 1992; Macdonald 1999). Thus, the solute-vacancy interaction reduces the free cation vacancy concentration and diffusivity, which results in a positive shift in the breakdown voltage and a lengthening of the induction time (i.e., the alloy becomes more resistant to passivity breakdown). The electrostatic interaction is described rigorously in terms of ion-pairing theory that is commonly employed to describe ionic interaction in solutions. This solute-vacancy interaction model (Urquidi and Macdonald 1985) successfully accounts for the positive shift in the breakdown voltage upon adding molybdenum to the alloy without the need for arbitrary, adjustable parameters. Most importantly, the solute-vacancy interaction model accounts for why molybdenum must be present in the barrier layer at concentrations greater than about 2 percent for significant protection to be achieved.

Finally, complexing between $Mo_{Cr}^{3\bullet}$ and a defect will only occur if the defect is negatively charged (i.e., if the defect is a cation vacancy). However, the Cr_2O_3 passive film on chromium containing alloys is normally n-type in electronic character; hence, the dominant defect is either a cation interstitial or an oxygen vacancy, both of which are formally positively charged. Consequently, there should be little solute ($Mo_{Cr}^{3\bullet}$) – vacancy ($V_O^{\bullet\bullet}$ or $M_i^{\chi+}$) interaction and pairing, and molybdenum should have little consistent impact on the passive current density, as observed.

6.4.1.2 Characterization of Alloy 22 Passive Film

The passivity behavior of Alloy 22 has been studied at 95 °C in a high pH salt environment characteristic of concentrated Yucca Mountain groundwater. Measurements of corrosion potential (CP) versus time, potentiostatic polarization (PSP) and cyclic potentiodynamic polarization (CPP) behavior were conducted to evaluate the passivity of these alloys. The characterization of passive films was also analyzed by x-ray photoelectron spectroscopy (XPS) and transmission electron microscopy (TEM) to obtain the chemical composition and cross-sectional view of the metal, interface, and oxide layers. Details of the study are described by Andresen et al. (2002, Section 3).

6.4.1.2.1 Summary of Experimental Procedures

All materials were tested in the as-received condition. Specimens (0.3 cm in diameter by 6 cm in length for CP, PSP, and CPP measurements, and 1 cm x 1 cm x 0.08 cm for the oxide analysis) were cut by electrodischarging machining and then wet-ground using a 600 grit SiC paper before test. Specimens for electrochemical measurements were spot welded to a polytetrafluoroethylene (PTFE)-insulated Alloy 600 wire and mounted in an insulated fitting. The solution used represents a less concentrated version of so-called Basic Saturated Water (BSW) which is simulated Yucca Mountain ground water (J-13 well water) evaporatively concentrated approximately 50,000-fold. The less concentrated solution used in these tests is

BSW diluted to yield approximately 2800-fold J-13 and has a pH of approximately 12.4 at 95 °C.

The chemicals were mixed with water that had been heated to the boiling point in an autoclave. All testing was performed in either a Hastelloy C-276 autoclave body or a commercial-purity titanium autoclave. However, some stainless steel was present in all test autoclaves, and there was no evidence of its corrosion indicating the solution was not extremely aggressive. Solution was sampled from the autoclaves during the test.

To prevent evaporative loss of water, a four foot long tube-in-tube heat exchanger was used, with cooling water on the outside. The solution level in the test autoclave was monitored periodically by checking for continuity between the autoclave and an insulated stainless steel feed-through bar. No water addition was needed.

All potentials were measured with respect to a saturated calomel electrode (SCE). A Luggin probe with a porous zirconia membrane filled with the test solution was used to maintain a SCE at room temperature. A platinum flag electrode was employed as a counter electrode. All tests were performed at 95 °C ± 1 °C. CPP scans at 0.17 mV/second were started at 50 mV below the corrosion potential obtained 1 hour after immersion in solution and reversed when a current density of 5 mA/cm^2 was reached. After the completion of each test, specimens were cleaned ultrasonically in deionized water, dried, and the specimen surface was examined with a scanning electron microscope (SEM). In addition, potentiostatic polarization (PSP) tests were conducted by applying various anodic potentials for 24 hours to measure the passive current and to characterize the oxide properties; both, oxide composition and thickness were analyzed by XPS. The XPS data are quantitative for film composition, but the depth is considered qualitative because precise calibrations of sputtering rate on an oxide of this composition was not performed (although very good estimates exist). No visual evidence of localized corrosion attack was observed after CPP or PSP measurements.

The cross-sectional TEM sample was prepared using a focused ion beam (FIB) system. The bulk sample was placed into the FIB system, and the region of interest was coated with a 1 μm thick platinum layer using the in-situ metal deposition facilities of the FIB system. The platinum layer was used to protect the underlying material. Staircase shaped cuts were milled on either side of the region of interest using a gallium ion source. The ion current was reduced as the thickness of the section approached the desired dimension. The dimension of the final TEM cross-section was 10 μm long, 4 μm deep and 150 nm thick. The sample was then removed from the FIB chamber, and the TEM cross-section was picked out of the bulk sample and placed on a porous carbon grid using a micro-manipulator. The TEM data are considered quantitative for composition, but qualitative dimensionally.

6.4.1.2.2 Passive Film Characterization Under Potentiostatic Polarization

The passive current transition behavior and oxide thickness formed on Alloy 22 at various anodic potentials is shown in Figure 6-2. The passive current density increases with the applied potential, and the oxide film becomes slightly thicker. Figure 6-3 shows the elemental distribution on the outermost oxide layer formed on Alloy 22 at various anodic potentials. Applied anodic potentials in Figures 6-2 and 6-3 were chosen from the CPP curves (see Figures

3-6 and 3-7 in Andresen et al. (2002)). Steady-state currents were normally achieved within a 5-10 hour period of polarization at applied potentials. In addition to anodic dissolution, there may be contributions to the measured current due to redox reactions occurring in the mixed-salt environment. No evidence of localized corrosion attack on test specimens after polarization was observed.

Note that the current density increased after the applied anodic potential was increased to 200 mV and a slight increase in oxide thickness was also observed. However, no evidence was observed to conclude the current increase and a slightly thicker oxide at high anodic potentials were due to localized passive film breakdown. The primary cause of the high current density may be due to changes in surface chemistry and oxidation states of Mo and W in the passive film (Pourbaix 1974, Sections 10.2 and 10.3).

6.4.1.2.3 Passive Film Oxide Analysis

The chemical composition and structure of oxide films play very important roles in the corrosion process and protection. The mechanisms and kinetics of the corrosion processes can be altered by the chemical and physical properties of oxide films. Figure 6-4 shows the TEM cross-section micrograph of the oxide film formed on Alloy 22 after 2-month immersion in open circuit potential in the mixed-salt solution at 95°C. An oxide approximately 5-8 nm thick, enriched with Cr, was formed. Electron diffraction patterns showed a thermodynamically stable Cr_2O_3 rich oxide film containing NiO.

XPS analysis was performed to get quantitative chemical profile data regarding the oxide thickness and elemental distribution through the oxide film. Figure 6-5 show the elemental concentrations of the outermost oxide layer formed on Alloy 22 in a mixed-salt solution at 95°C as a function of immersion time. The oxide film on Alloy 22 was enriched with Cr and Ni, and no significant amounts of Mo and W were measured. This is consistent with the findings by other investigators (Lorang et al. 1990; Macdonald 1999; Marcus and Maurice 2000, page 153). However, a large amount of SiO_2 with various salts on the outer oxide film was detected, but no evidence of penetration of SiO_2 to the underlying substrate was observed. Figure 6-6 shows the oxide thickness formed on Alloy 22 as a function of immersion time. Approximately 5–6 nm thick oxides were formed on Alloy 22. The long-term immersion test is still in progress to generate more oxide characteristics to shed light on understanding the relation between corrosion potential and oxide nature.

6.4.1.3 Summary

The conceptual understanding of the passive film growth and stability of Alloy 22 was described summarizing data and information from the literature. The passivity of Alloy 22 was examined by measuring the corrosion potential and polarization behavior in a mixed-salt environment at 95 °C. Steady-state corrosion potentials of Alloy 22 were measured. The surface analysis data indicated that the oxide layers responsible for passivity of Alloy 22 consist of chromium oxide (Cr_2O_3) containing NiO. After two months' exposure to the mixed-salt solution at 95 °C, oxide films about 5 –6 nm-thick were formed. In addition, the passive films formed on Alloy 22 at high anodic potentials (> 0 mV vs. SCE) contained more Mo and W than ones formed at lower anodic potentials (< 0 mV vs. SCE). However, no evidence of localized corrosion attack on

Alloy 22 after potentiostatic polarization measurements was observed. No significant change in the open circuit potential (OCP, or corrosion potential) of the test electrodes was measured. These data indicate that (1) the passive films become very protective and stable, (2) contributions from metal corrosion become extremely small, and (3) redox reactions from the species in solution are stable.

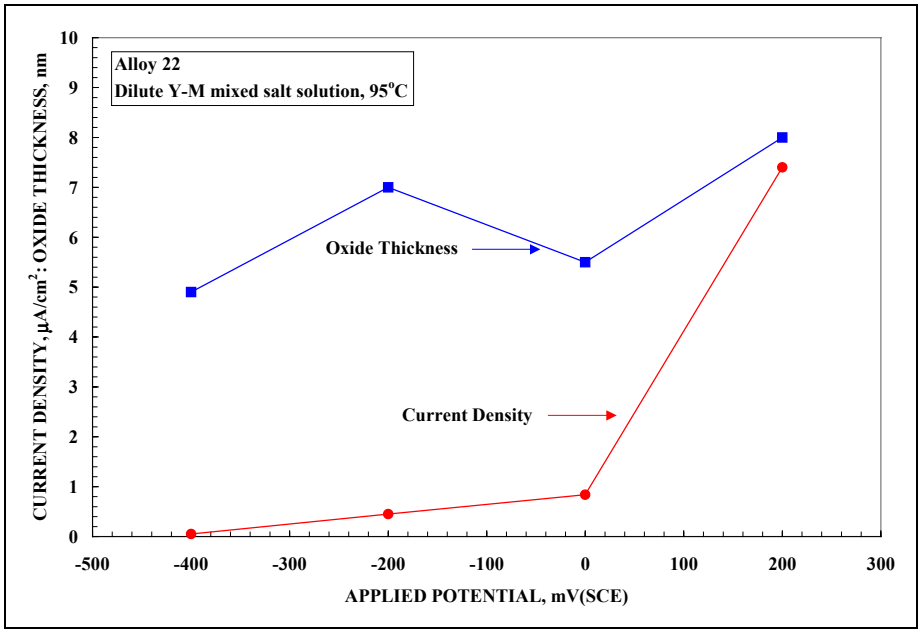

Source DTN LL021105312251.023

Figure 6-2. Passive Current Densities and Oxide Thickness as a Function of Applied Potential for Alloy 22.

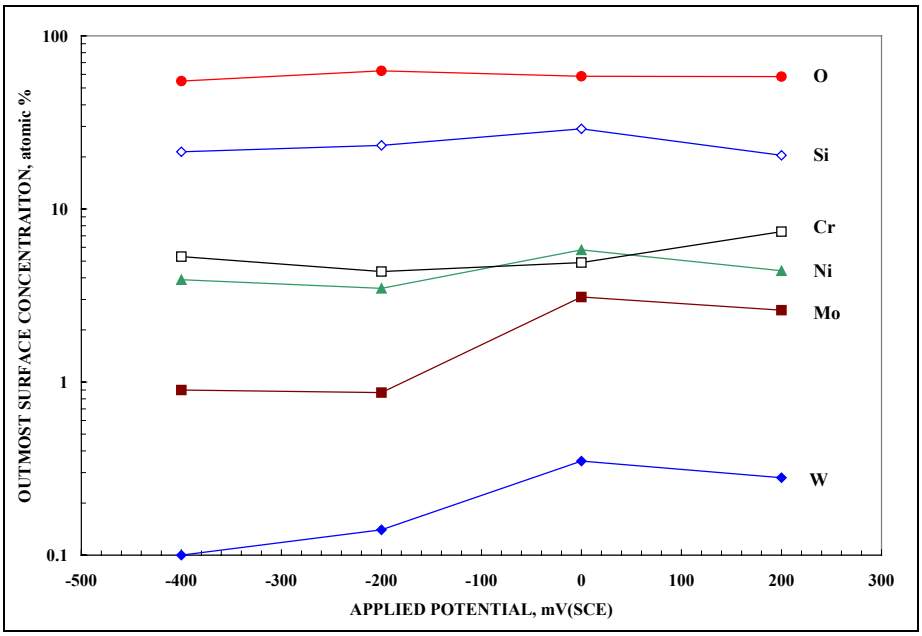

Source DTN LL021105312251.023

Figure 6-3. Elemental Concentration on the Outermost Oxide Layer as a Function of Applied Potential for Alloy 22.

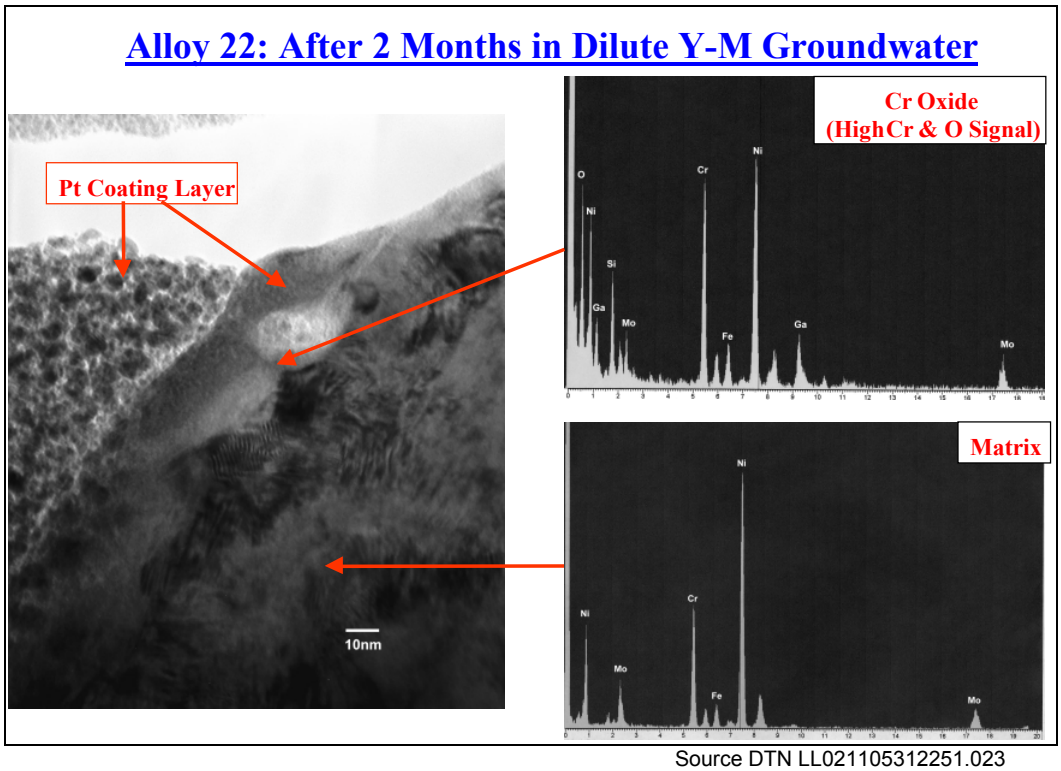

Source DTN LL021105312251.023

Figure 6-4. TEM Micrograph Showing the Cross-Section Views and Oxide Chemistry Formed on Alloy 22 After 2-Month Immersion in a Mixed-Salt Environment at 95 °C.

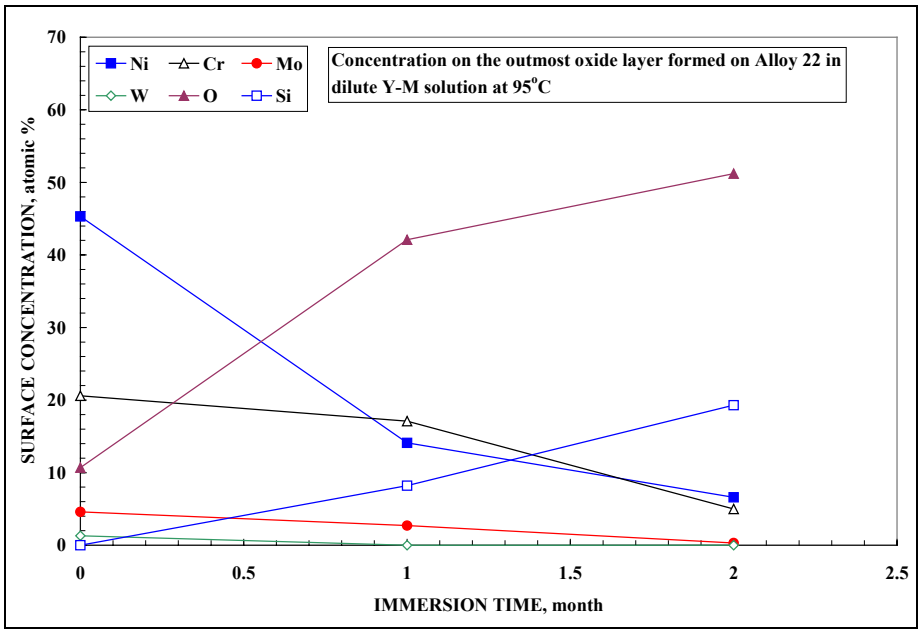

Source DTN LL021105312251.023

Figure 6-5. Elemental Concentration on the Outermost Oxide Layer Formed on Alloy 22 in a Mixed-Salt Environment at 95 °C as a Function of Immersion Time.

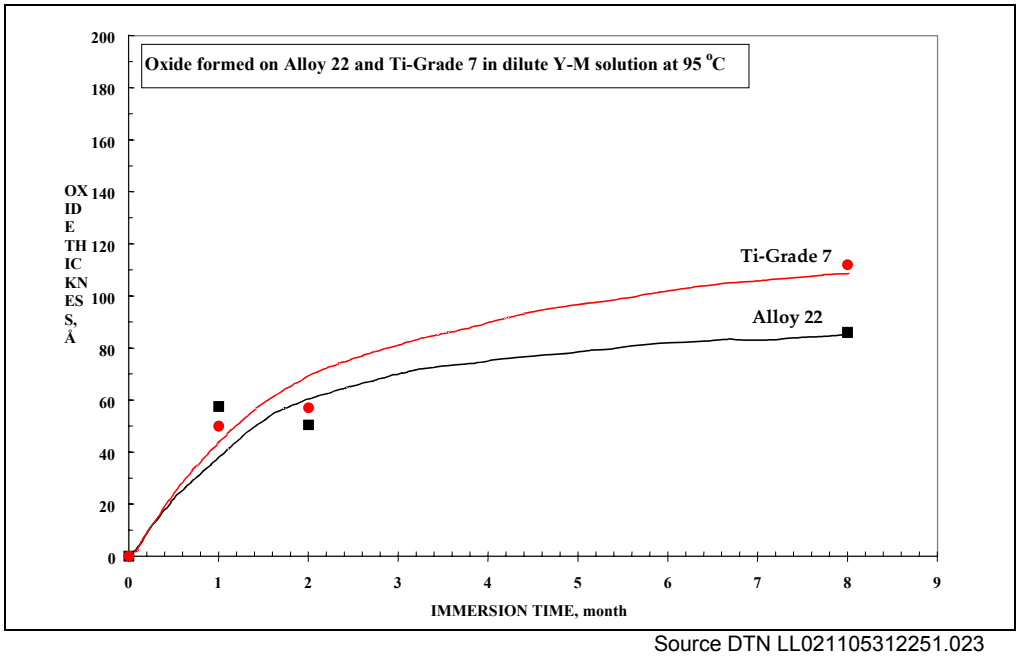

Source DTN LL021105312251.023

Figure 6-6. Oxide Thickness Formed on Alloy 22 and Ti Grade 7 as a Function of Immersion Time at 95 °C in a Mixed-Salt Environment.

6.4.2 Dry Oxidation

Dry oxidation of Alloy 22 occurs at any $RH < RH_{threshold}$, thereby forming an adherent, protective oxide film of uniform thickness. The dry oxidation model presented here considers uniform oxidation of the WPOB surface. The current analysis considers that the protective oxide film is primarily Cr_2O_3. The oxidation reaction is given as (Welsch et al. 1996):

$$4/3\,Cr + O_2 \longrightarrow 2/3\,Cr_2O_3 \qquad \text{(Equation 6-1)}$$

The rate of dry oxidation is considered to be limited by mass transport through this growing metal oxide film. Fick's first law is applied, considering a linear concentration gradient across the oxide film of thickness x:

$$J_{oxide} = -D_{oxide}\frac{\partial C}{\partial x} \approx -D_{oxde}\frac{\Delta C}{x} \qquad \text{(Equation 6-2)}$$

where J_{oxide} is the molar flux of the reacting species in the oxide, D_{oxide} is the diffusivity of the reacting species in the oxide, ΔC is the corresponding differential molar concentration. Oxide growth is related to the flux by:

$$\frac{dx}{dt} = \frac{\zeta_{oxide} \times w_{oxide} \times J_{oxide}}{\rho_{oxide}} \qquad \text{(Equation 6-3)}$$

where ζ_{oxide} is the stoichiometric coefficient (moles of oxide per mole of diffusing species), w_{oxide} is the formula weight of the oxide, and ρ_{oxide} is the density of the oxide. Integration shows that the oxide thickness should obey the following parabolic growth law (Wagner's Law [Welsch et al. 1996]), where the film thickness is proportional to the square root of time. This is represented by Equation 6-4.

$$x = \sqrt{x_0^2 + k \times t} \qquad \text{(Equation 6-4)}$$

where x_0 is the initial oxide thickness, x is the oxide thickness at time t, and k is a temperature-dependent parabolic rate constant. More specifically, k is defined as follows:

$$k = \frac{2 \times \zeta_{oxide} \times w_{oxide} \times D_{oxide} \times \Delta C}{\rho_{oxide}} \qquad \text{(Equation 6-5)}$$

To facilitate an approximate calculation, published values of k can be used (Welsch et al. 1996). The data in Figure 18 of this reference were fitted to an Arrhenius relation such that all observed values of k fall below a line defined by:

$$\log\left[k\left(\frac{m^2}{\text{sec}}\right)\right] = -3.5 - \left(\frac{12500}{T(K)}\right) \qquad \text{(Equation 6-6)}$$

where T is defined as the absolute temperature. Recent measurements of the thickness of the Alloy 22 oxide film exposed to air at 550 °C showed that the oxide film approaches a limiting thickness of about 0.025 to 0.050 μm after about 333 days exposure (DTN LL030406412251.045), which corresponds to a penetration rate of 0.027 to 0.054 μm/year. For that temperature, the value of k corresponding to the upper limit from Equation 6-6 is 2.06×10^{-19} m^2/sec (6.51 $\mu m^2/year$). Ignoring the initial oxide thickness in Equation 6-4, after one year, this corresponds to a growth of 2.55 μm (about 2.55 $\mu m/year$). This shows that the model estimates are about 100 times greater than the measured thickness, and the above expression represents a conservative upper bound.

Logarithmic growth laws may be more appropriate at lower temperatures than parabolic laws. However, such logarithmic expressions predict that the oxide thickness (penetration) asymptotically approaches a small maximum level. In contrast, the parabolic law predicts continuous growth of the oxide, which is much more conservative. Since such conservative estimates of the rate of dry oxidation do not appear to be life limiting and since reliable data for determining the maximum oxide thickness for Alloy 22 do not appear to be available, the parabolic growth law were used for the WPOB.

For a high temperature of 350 °C for the waste package, the value of k corresponding to the upper limit is 2.73×10^{-24} m^2/sec (8.61×10^{-5} $\mu m^2/year$). After one year, this corresponds to a growth of 0.0093 μm (about 9.3 $nm/year$). As discussed in Section 6.4.3, this estimated dry-oxidation rate is comparable to the mean value of the general corrosion rate of Alloy 22 at lower temperatures. Assuming a constant rate of the upper bound conservative estimate of 0.0093 μm/year (i.e., exposure to the constant temperature of 350 °C), a total penetration depth in the WPOB by dry oxidation for 10,000 years is only 93 μm, which is negligibly small (less than 1 percent of the total thickness of the WPOB (20 mm)).

On the basis of the above analysis, dry oxidation is not expected to be a performance limiting process of the WPOB under the exposure condition expected in the repository. Therefore dry oxidation will not be discussed any further in this model report. It is recommended that dry oxidation not be included in the waste package performance analysis.

6.4.3 General Corrosion

General corrosion (or passive corrosion) is the uniform thinning of the WPOB at its open-circuit corrosion potential (E_{corr}). General corrosion can occur under immersed conditions or when a liquid film exists on the surface. At a given surface temperature, the existence of liquid water on the waste package surface depends upon the hygroscopic nature of salts and/or minerals deposited on the surface. In the presence of such a deposit, a liquid-phase can be established at a higher temperature and lower RH than otherwise possible. General corrosion of the WPOB is assumed to occur at any RH above the corrosion initiation RH threshold ($RH_{threshold}$) and progress uniformly over a large surface (Assumption 5.2). The general corrosion rate is temperature dependent, and for a given temperature, it is assumed to be constant (i.e., time-independent)

(Assumption 5.2). Therefore, for a given temperature, the depth of penetration or thinning of the WPOB by general corrosion is equal to the general corrosion rate at that temperature, multiplied by the time duration that the waste package surface is at that temperature. This assumption is considered conservative because the general corrosion rate of metals and alloys tend to decrease with time (see Section 6.4.3.5 for an additional discussion).

As will be discussed in the following sections, general corrosion rates of the WPOB have been estimated from the weight-loss data of Alloy 22 samples after 5-year exposure in the Long Term Corrosion Testing Facility (LTCTF) (Estill 1998, Section 2.2). The LTCTF provides a comprehensive source of corrosion data for Alloy 22 in environments relevant to the proposed repository. The LTCTF facility is described in detail in a previous publication by Estill (1998, Section 2.2). The 5-year weight loss measurement data is documented in DTN LL030412512251.057.

6.4.3.1 Long-Term Weight Loss Measurements

The LTCTF is equipped with an array of fiberglass tanks. Each tank has a total volume of approximately 2000 L and is filled with approximately 1000 L of aqueous test solution. The solution in a particular tank is controlled at either 60 or 90 °C, covered with a blanket of air flowing at approximately 150 cm^3/min, and agitated. Four generic types of samples, U-bends, creviced samples, weight loss samples, and galvanic couples, are mounted on insulating racks and placed in the tanks. Approximately half of the samples are submersed, half are in the saturated vapor above the aqueous phase, and a limited number are at the water line. It is important to note that condensed water is present on specimens located in the saturated vapor. Details of the facility are described in Estill (1998, Section 2.2).

The weight loss measurement testing includes a wide range of plausible generic test media, including SDW, SCW, Simulated Cement-Modified Water, and SAW. The compositions of three of these solutions are summarized in Table 6-2. The SCW test medium is three orders-of-magnitude (1000×) more concentrated than J-13 well water and is slightly alkaline (pH approximately 8). The SAW test medium is three orders-of-magnitude (1000×) more concentrated than J-13 well water and is acidic (pH approximately 2.7). Concentrated solutions are intended to mimic the evaporative concentration of the electrolytes on the hot waste package surface. Two temperature levels (60 and 90°C) are included. See Estill (1998, Section 2.2) for additional details.

The corrosion rate of Alloy 22 was determined using immersion tests according to ASTM G 1 (ASTM G 1-90 1990). Two types of coupons were used. These were labeled weight loss coupons and crevice coupons. The nominal dimensions were 2 inch x 1 inch x 1/8 inch (approximately 50 mm x 25 mm x 3 mm) and 2 inch x 2 inch x 1/8 inch (50 mm x 50 mm x 3 mm), respectively. The coupons have a 0.312 inch (7.9 mm) diameter hole in the center for sample mounting. For each coupon type, there were two variants, wrought (only base metal) and welded. The coupons were fabricated from Alloy 22 plate stock. All weight loss coupons were affixed using an insulating ½-inch (12.7 mm) diameter PTFE or ceramic washer while all crevice coupons were affixed using a ¾-inch (19.1 mm) diameter PTFE or ceramic crevice former. The purpose of the crevice former was to create an environment that might induce corrosion at the

contact interface, or under occluded conditions. Details of the sample configuration are given elsewhere (Estill 1998, Section 2.2.5; DTN LL030412512251.057).

Table 6-2. Target Chemical Compositions of the Electrolyte Solutions (mg/L) Employed in the Long-Term Weight Loss Measurement.

	Concentration (mg/L)			
Ion	**Simulated Dilute Water (SDW)**	**Simulated Concentrated Water (SCW)**	**Simulated Acidified Water (SAW)**	**Basic Saturated Water (BSW)**
	60 & 90 °C	60 & 90 °C	60 & 90 °C	--
K	34	3400	3400	91100
Na	409	40,900	37,690	230400
Mg	1	<1	1000	0
Ca	0.5	<1	1000	0
F	14	1400	0	1800
Cl	67	6700	24,250	178600
NO_3	64	6400	23,000	176800
SO_4	167	16,700	38,600	16100
HCO_3	947	70,000	0	214300
Si (aq)	27 (60 °C) 49 (90 °C)	27 (60 °C) 49 (90 °C)	27 (60 °C) 49 (90 °C)	7100
pH	9.8 – 10.2	9.8 – 10.2	2.7	>12

Source: DTN LL000320405924.146

Approximately half of the specimens were exposed to the liquid phase of the solution (complete immersion) and the other half were exposed to the vapor phase (suspended over the liquid surface). The reported test temperature corresponded to the liquid phase temperature. Thus, welded and non-welded (wrought) coupons were tested in twelve different conditions (3 electrolytes x 2 temperatures x 2 phases). The exposure time for each specimen was approximately 5 years. The actual testing time for each vessel is shown in Table 6-3 along with the specimen label, and vessel number. Each sample was designated with 3 letters and 3 characteristic numbers. The letter D represents Alloy 22, the letter C represents crevice coupon, the letter W represents weight loss coupon, the letter A indicates that the coupon does not contain a weld seam and the letter B indicates that the coupon does contain a weld seam along the middle of the specimen. Table 6-3 shows that 122 test specimens were examined for the results reported here. Twelve welded crevice samples, representing each of the different test conditions, have been set aside for surface analyses and will be characterized later. Galvanic samples contained in DTN LL030412512251.057 were not included in the current analysis because they are not representative of the current waste package design. The weight-loss samples tested in the water-line condition were included in the liquid phase samples for the model analysis.

The simulated electrolyte solutions were naturally aerated, i.e. the solutions were not purged and the ingress of air above the solution was not restricted. All tests were carried out under ambient pressure. After an approximate five years exposure to each solution/environmental condition, the specimens were removed from their respective test vessel to determine the corrosion rate by mass loss. In all of the tested conditions, the coupons were covered with deposits. Therefore, the coupons were cleaned prior to final weighing. Cleaning was carried out using ASTM standard G 1 (ASTM G 1-90 1999). Details of the cleaning processes are found in DTN LL030412512251.057 and the Scientific Notebook referenced therein.

6.4.3.2 Weight Loss Data Analysis

The general corrosion rate measurements are based upon ASTM G 1 (ASTM G 1-90 1999). The general corrosion (or penetration) rate of an alloy was calculated from weight loss data as follows with the following general formula:

$$Corrosion\ Rate = \frac{87.6 \times 10^9 \cdot \Delta w}{\rho \cdot A \cdot t} \qquad \text{(Equation 6-7)}$$

where 87.6 x 10^9 is the proportionality constant ($nm \cdot hour \cdot year^{-1} \cdot cm^{-1}$), Δw is the mass loss in *grams* after 5+ years, ρ is the density of Alloy 22 (8.69 g/cm^3) (DTN MO0003RIB00071.000), A is the exposed surface area of each coupon (cm^2), and t is the exposure time (*hours*). The exposed surface area A is calculated as follows

$$A = 2ab + 2bc + 2ac - \left(\frac{\pi d^2}{2}\right) + \pi dc \qquad \text{(Equation 6-8)}$$

where a is the length of the specimen in cm, b is the width of the specimen in cm, c is the thickness of the specimen in cm, and d is diameter of the hole in cm. See Figure 6-9 for a schematic of the sample coupon. For a given temperature, the general corrosion rate is assumed to be constant and does not decay with time (Assumption 5.2). Less conservative corrosion models consider that the rate decays with time.

Note that calculation of the exposed surface area of the weight-loss and crevice samples using Equation (6-8) included the area directly under the crevice former for the crevice samples and the area directly under the sample spacer for the weight-loss samples. These areas were included because the test solutions can penetrate and wet the areas under the crevice former or sample spacer. The inputs from DTN LL030412512251.057 used in the model analysis were the weight loss measurements and characteristics of the sample and exposure conditions. The corrosion rates were calculated from the weight loss measurement data in this model report. The calculated corrosion rates of the weight-loss and crevice coupons are listed in Attachments II and III respectively of this model report. The calculated corrosion rates are slightly different from those in the input DTN due to round-off errors.

Table 6-3. List of Examined Weight-Loss and Crevice Alloy 22 Coupons.

	SAW 60°C	SAW 90°C	SCW 60°C	SCW 90°C	SDW 60°C	SDW 90°C
Vessel No.	**25**	**26**	**27**	**28**	**29**	**30**
Weight Loss - Vapor Phase	DWA019 DWA020 DWA021	DWA059 DWA060 DWA061	DWA089 DWA090 DWA091	DWA129 DWA130 DWA131	DWA147	DWA174
Crevice – Vapor Phase	DCA019 DCA020 DCA021	DCA049 DCA050 DCA051	DCA079 DCA080 DCA081	DCA109 DCA110 DCA111	DCA139 DCA140 DCA141	DCA175 DCA176 DCA177
Weight Loss - Liquid Phase	DWA022 DWA023 DWA024	DWA062 DWA063 DWA064	DWA092 DWA093 DWA094	DWA132 DWA133 DWA134	DWA148	DWA175
Crevice – Liquid Phase	DCA022 DCA023 DCA024	DCA052 DCA053 DCA054	DCA082 DCA083 DCA084	DCA112 DCA113 DCA114	DCA142 DCA143 DCA144	DCA178 DCA179 DCA180
Weight Loss - Waterline	DWA034	DWA039	DWA104	DWA109	DWA154	DWA167
Welded Weight Loss - Vapor Phase	DWB019 DWB020 DWB021	DWB059 DWB060 DWB061	DWB089 DWB090 DWB091	DWB129 DWB130 DWB131	DWB147	DWB174
Welded Crevice - Vapor Phase	DCB019 DCB020 DCB021 (SA)	DCB049 DCB050 DCB051 (SA)	DCB079 DCB080 DCB081 (SA)	DCB109 DCB110 DCB111 (SA)	DCB139 DCB140 DCB141 (SA)	DCB175 DCB176 DCB177 (SA)
Welded Weight Loss- Liquid Phase	DWB022 DWB023 DWB024	DWB062 DWB063 DWB064	DWB092 DWB093 DWB094	DWB132 DWB133 DWB134	DWB148	DWB175
Welded Crevice - Liquid Phase	DCB022 DCB023 DCB024 (SA)	DCB052 DCB053 DCB054 (SA)	DCB082 DCB083 DCB084 (SA)	DCB112 DCB113 DCB114 (SA)	DCB142 DCB143 DCB144 (SA)	DCB178 DCB179 DCB180 (SA)

Source DTN LL030412512251.057

Note: SA = Reserved for surface analyses (not subject to cleaning for weight loss measurement).

As noted in Attachment II, Sample DCA177 is an outlier and was not included in the weight-loss data analysis and the WPOB general corrosion model analysis. The mean and standard deviation of all the 5-year crevice sample data including Sample DCA177 are 7.90 nm/year and 7.09 nm/year respectively (see output DTN SN0306T0506303.002). Therefore the measured corrosion rate (46.68 nm/year) of Sample DCA177 is beyond five standard deviations from the mean. In addition, the sample was tested in the vapor phase over the SDW solution, which is the least corrosive condition among the test conditions of the long-term weight loss tests. The above arguments provide sufficient justification for exclusion of the outlier. Sample DWA089 from the

weight loss samples yielded a negative corrosion rate. This sample is an outlier and was not included in the weight loss analysis of the 5-year samples.

Figure 6-7 summarizes the calculated corrosion rates for the Alloy 22 weight loss coupons exposed to the SAW, SCW and SDW solutions at 60°C and 90°C for over 5 years. Similarly, Figure 6-8 summarizes the corrosion rates for the Alloy 22 crevice coupons exposed to the same multi-ionic solutions and test conditions. The mill annealed (MA) and as-welded (ASW) samples were lumped together for the analyses. The average corrosion rates and 2 standard deviation ranges were calculated considering a normal distribution and are presented in the figures. The 2 standard deviation range represents a 95% confidence level. Although the appearance and amount of deposits on the coupons exposed to different solutions were different, the calculated corrosion rates were not significantly different. The individual corrosion rates for the weight loss coupons ranged from 0-12 nm/yr with the lowest rates observed for the coupons in the SDW solution. The individual corrosion rates for the crevice coupons ranged from 0-23 nm/yr with the highest rates observed in the SAW solution vessels and, again, the lowest rates observed in the SDW solution vessels. In most cases, the crevice coupons exhibited corrosion rates 2-5 times higher than the weight loss coupons in the same solutions. Stereomicroscopic and scanning electron microscopic (SEM) observations of both weight loss and crevice specimens indicated little or no corrosion for Alloy 22. The machining grooves remained uniform and sharp throughout each coupon. It is not yet clear why the corrosion rates of the crevice coupons were higher than those of the weight loss coupons because crevice corrosion was not observed in any of the tested coupons. It is possible that a different surface finish treatment used for the crevice samples may have caused the different (i.e., higher) measured corrosion rates. However, it is noteworthy that among all test specimens, a maximum corrosion rate of only 23 nm/yr was observed.

For both the weight loss and crevice coupons, the corrosion rates were generally lower for those specimens exposed to vapor than those immersed in liquid, regardless of the test temperature or electrolyte solution. For the weight loss coupons exposed to liquid, the corrosion rates were generally slightly lower at 90°C than at 60°C. For the weight loss coupons exposed to vapor, the corrosion rates were generally higher at 90°C than at 60°C. Overall, coupons in the SAW solution vessels exhibited slightly lower corrosion rates at the higher temperature.

Similar to the weight loss coupons, the corrosion rates for the crevice coupons exposed to liquid were lower at 90°C than at 60°C, while the corrosion rates were generally higher at 90°C than at 60°C for the crevice coupons exposed to vapor. In general, for corrosion processes, the corrosion rate increases with temperature. However, since in this study the corrosion rates were so low and the temperature range studied (60 to 90 °C) is small, a clear dependence with the temperature cannot be established for any set of coupons. Finally, for the weight loss coupons, there appeared to be no weld effect on the corrosion rate, however, the non-welded crevice coupons exhibited slightly higher rates than their welded counterparts.

The general corrosion rates of the coupons were analyzed with “empirical” cumulative distribution functions (ECDFs) of the calculated rates. In constructing the ECDFs, the cumulative probability values of the general corrosion rate (except the upper and lower bounds) were calculated by the following plotting positions (Cleveland 1993, Section 2.1), i.e.,

$$q_i = \frac{i - 0.5}{n} \qquad \text{(Equation 6-9)}$$

where q_i is the cumulative probability of the i^{th} smallest event (e.g., general corrosion rate) and n is the total number of events. The above plotting position formula was originally developed by Hazen and has been considered a traditional choice for probability plotting (Stedinger et al., 1993, Section 18.3.2). The ECDFs developed using the above plotting position formula for the 5-year weight loss analysis are to present the data trends and comparative analysis of different sets of data for varying sample geometry and exposure conditions. The ECDFs presented in this section were not intended for detailed quantitative analysis for the weight loss data.

The ECDFs for the general corrosion rates of the weight-loss specimens are shown in Figure 6-10 to Figure 6-14 for comparative analyses of the effect of various experimental factors on the general corrosion rate, such as for the solution chemistry, temperature, and metallurgical condition. The ECDFs for the general corrosion rates of the crevice coupons are shown in Figure 6-15 to Figure 6-19 for comparative analyses of the effect of various experimental factors on the general corrosion rate.

The ECDFs for the general corrosion rates of all the weight-loss and crevice samples, regardless of the test medium or temperature, are shown in Figure 6-20. For the crevice samples the mean corrosion rate is 7.24 nm/year, and the standard deviation is 4.98 nm/year. For the weight-loss samples the mean corrosion rate is 2.75 nm/year and the standard deviation is 2.74 nm/year. These are discussed in detail in Section 6.4.3.3 and summarized in Table 6-5. The corrosion rate distribution for the crevice coupons were used as the base case general corrosion rate of the WPOB. See Section 6.4.3.4 for details of the of the base case general corrosion model.

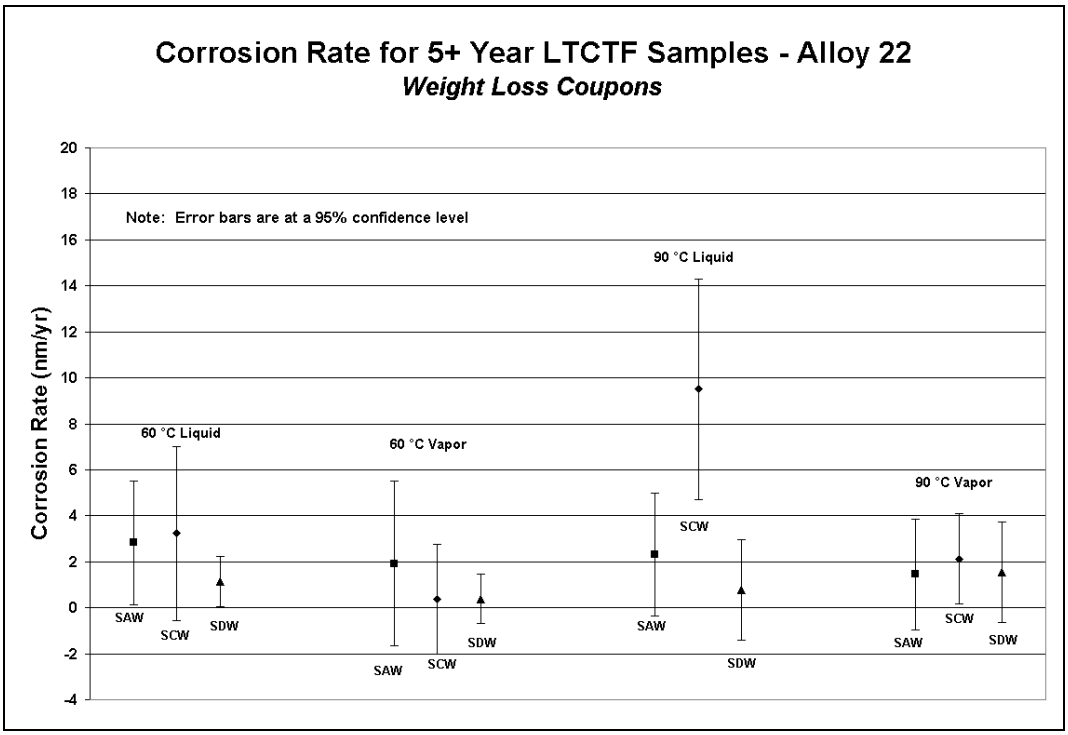

Output DTN: SN0308T0506303.004

Figure 6-7. Corrosion Rates for Alloy 22 Weight Loss Coupons in SAW, SCW and SDW.

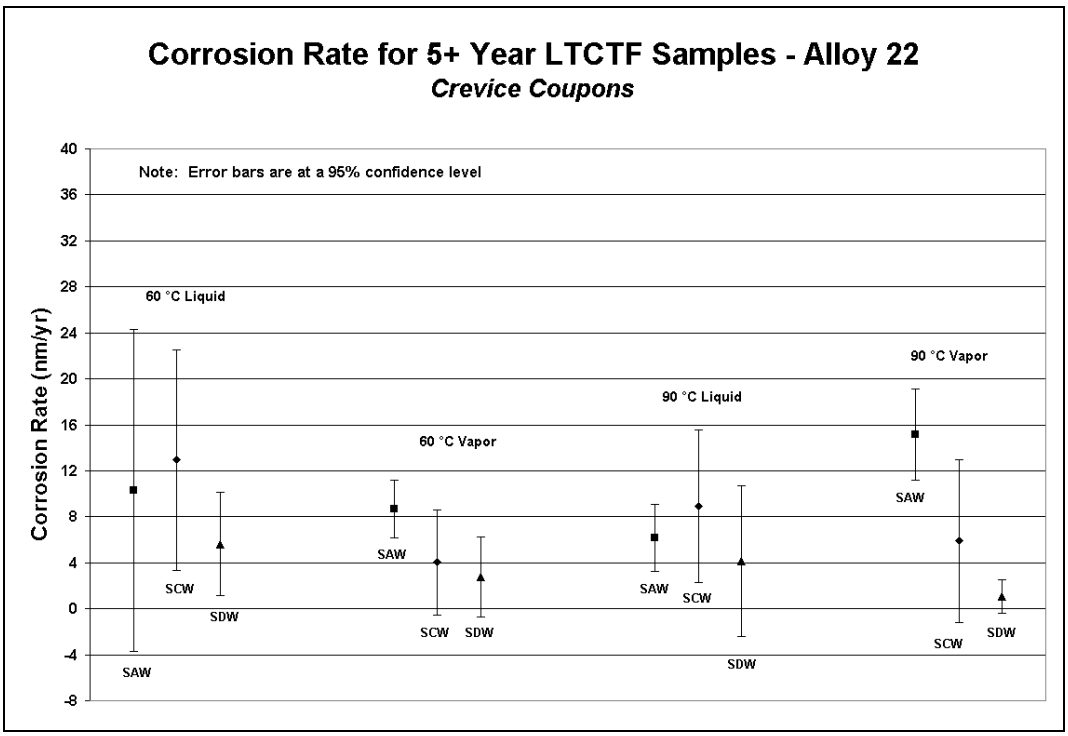

Output DTN SN0308T0506303.004

Figure 6-8. Corrosion Rates for Alloy 22 Crevice Coupons in SAW, SCW and SDW.

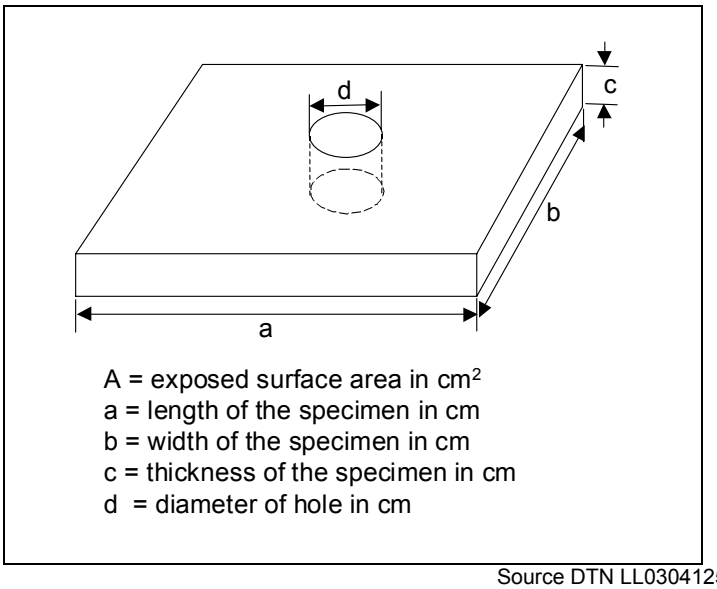

Source DTN LL030412512251.057

Figure 6-9. Schematic of Specimen Used in the Weight-Loss Measurements of Alloy 22 Samples in LTCTF.

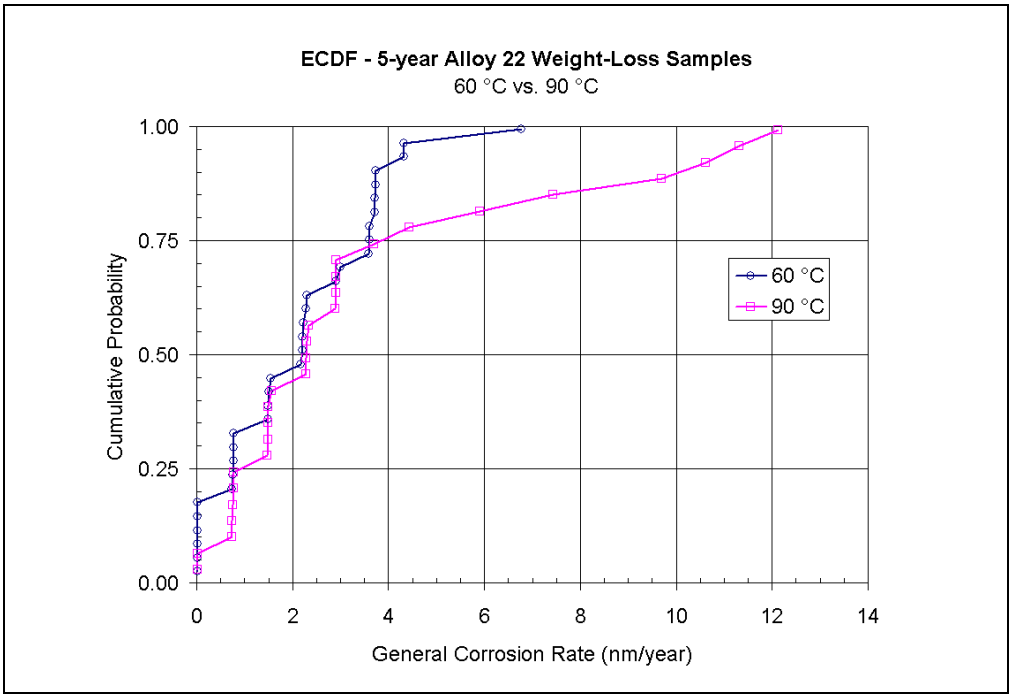

Output DTN: SN0308T0506303.004

Figure 6-10. Empirical Cumulative Distributions for General Corrosion Rate of Alloy 22 Weight-Loss Samples at 60 and 90 °C after 5-Years Exposure in the LTCTF.

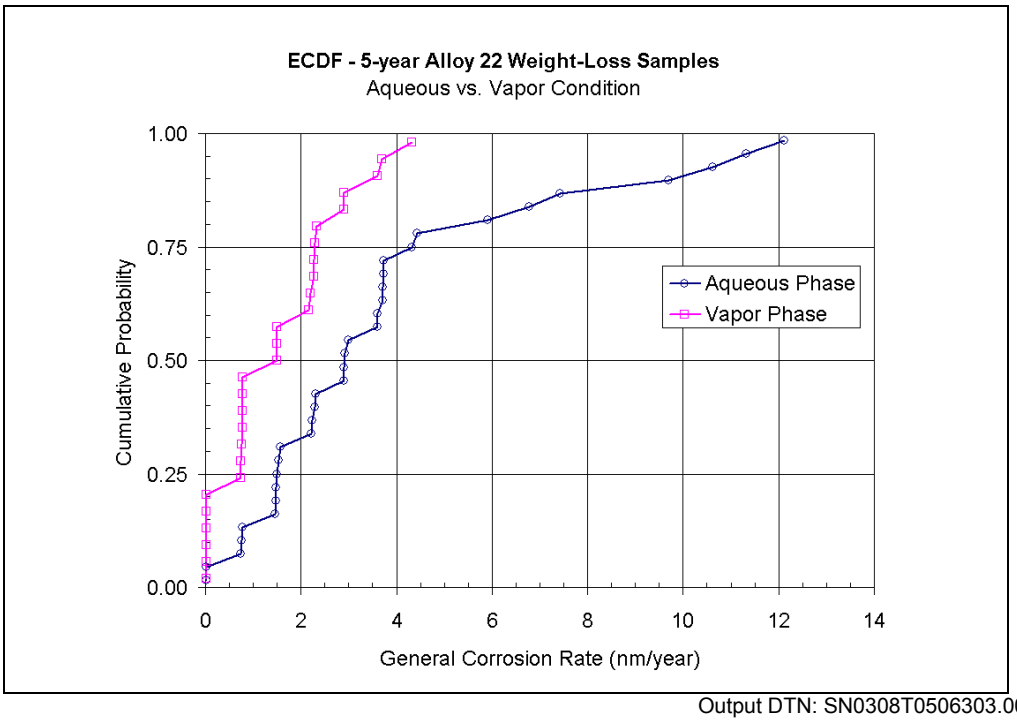

Output DTN: SN0308T0506303.004

Figure 6-11. Empirical Cumulative Distributions for General Corrosion Rate of Alloy 22 Weight-Loss Samples Exposed in the Vapor Phase and Aqueous Phase after 5-Years Exposure in the LTCTF.

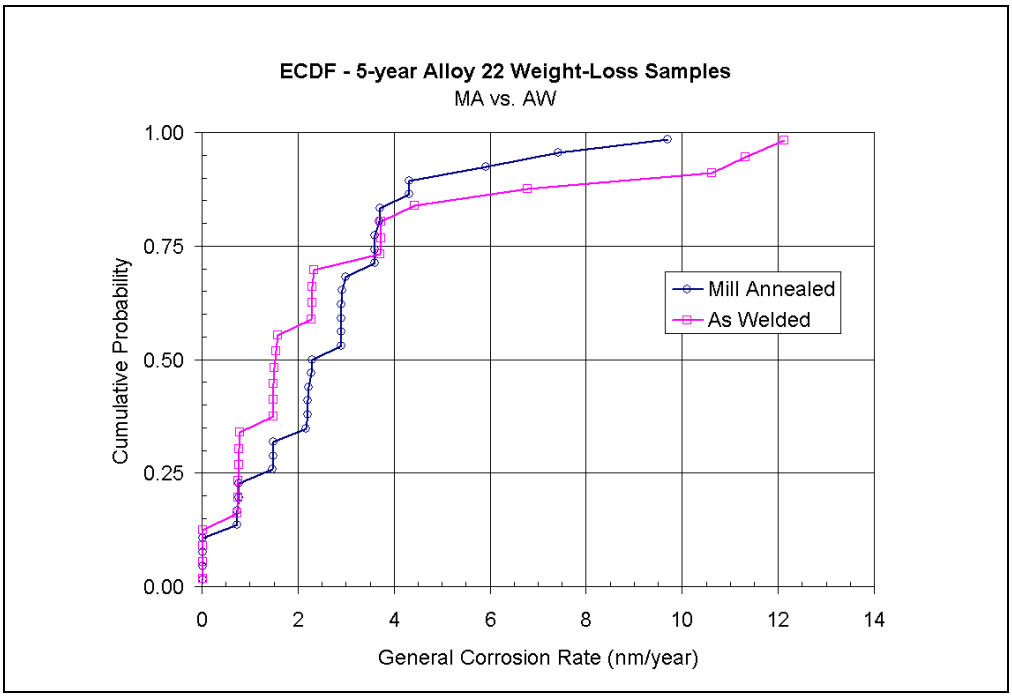

Output DTN: SN0308T0506303.004

Figure 6-12. Empirical Cumulative Distributions for General Corrosion Rate of Mill Annealed and As-Welded Alloy 22 Weight-Loss Samples after 5-Years Exposure in the LTCTF.

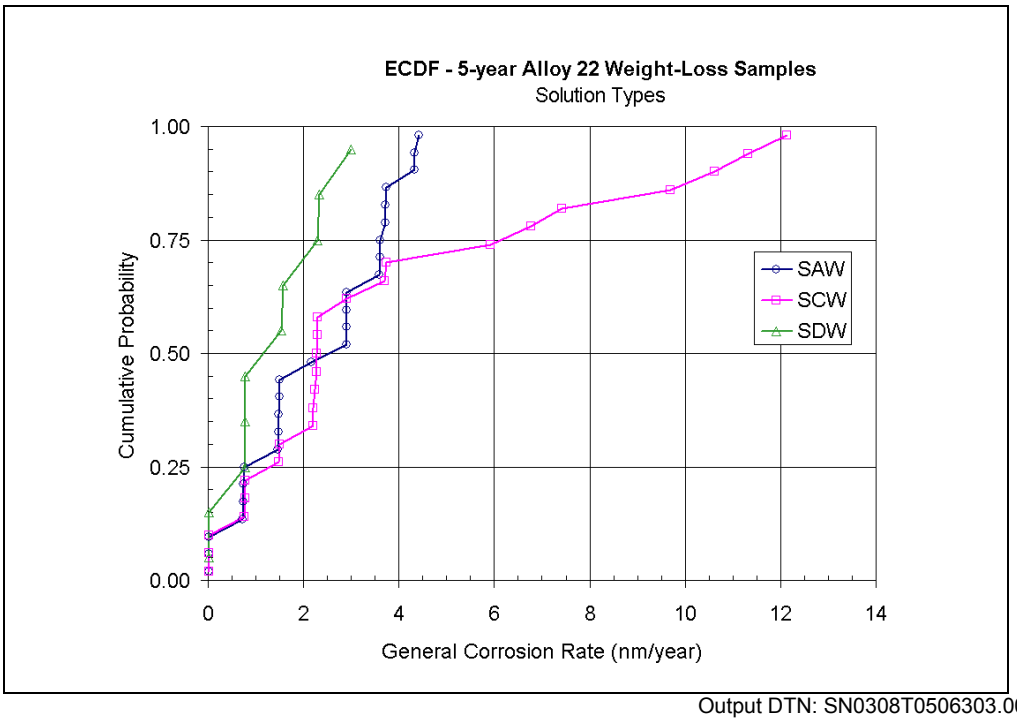

Output DTN: SN0308T0506303.004

Figure 6-13. Empirical Cumulative Distributions for General Corrosion Rate of Alloy 22 Weight-Loss Samples Tested in Three Different Solution Types After 5-Years Exposure in the LTCTF.

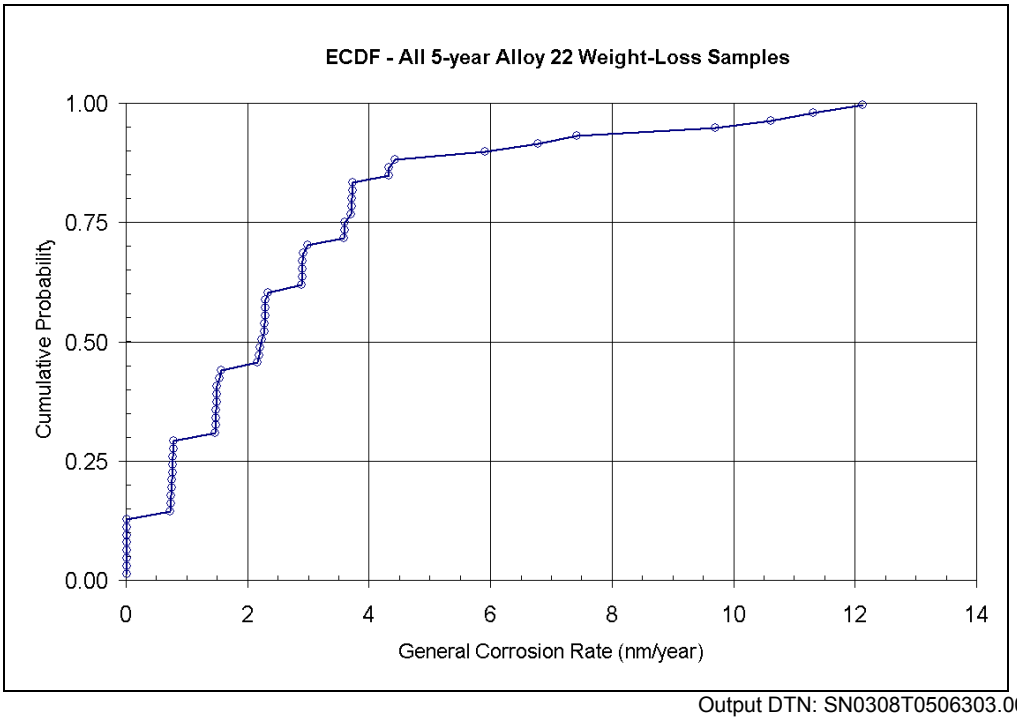

Output DTN: SN0308T0506303.004

Figure 6-14. Empirical Cumulative Distributions for General Corrosion Rate of All Alloy 22 Weight-Loss Samples after 5-Years Exposure in the LTCTF.

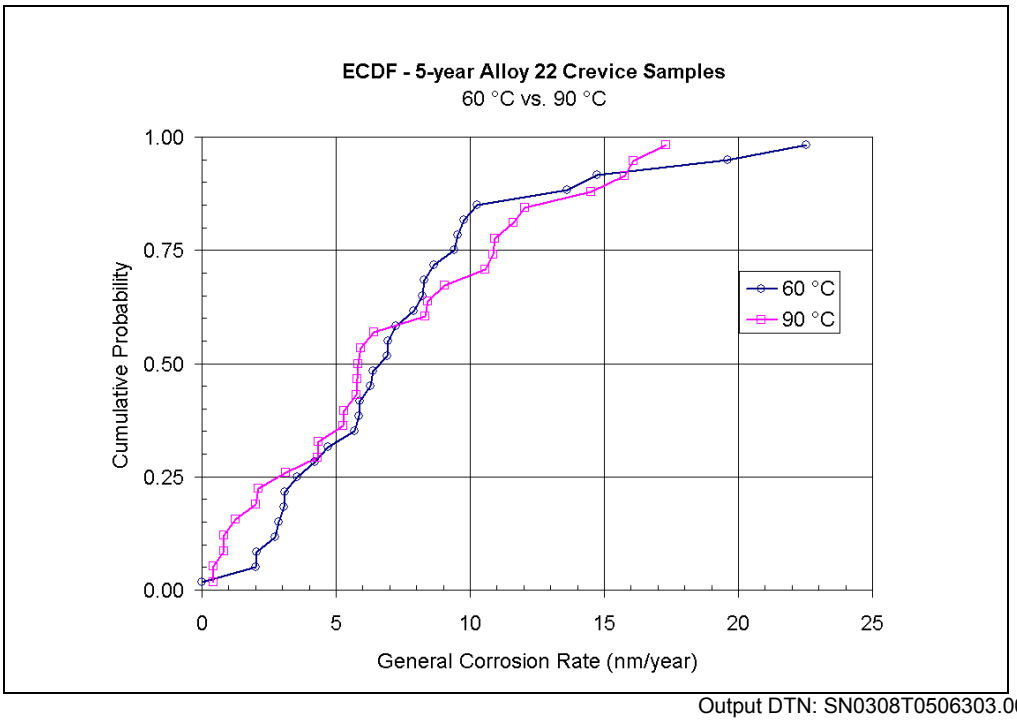

Output DTN: SN0308T0506303.004

Figure 6-15. Empirical Cumulative Distributions for General Corrosion Rate of Alloy 22 Crevice Samples at 60 and 90 °C after 5-Years Exposure in the LTCTF.

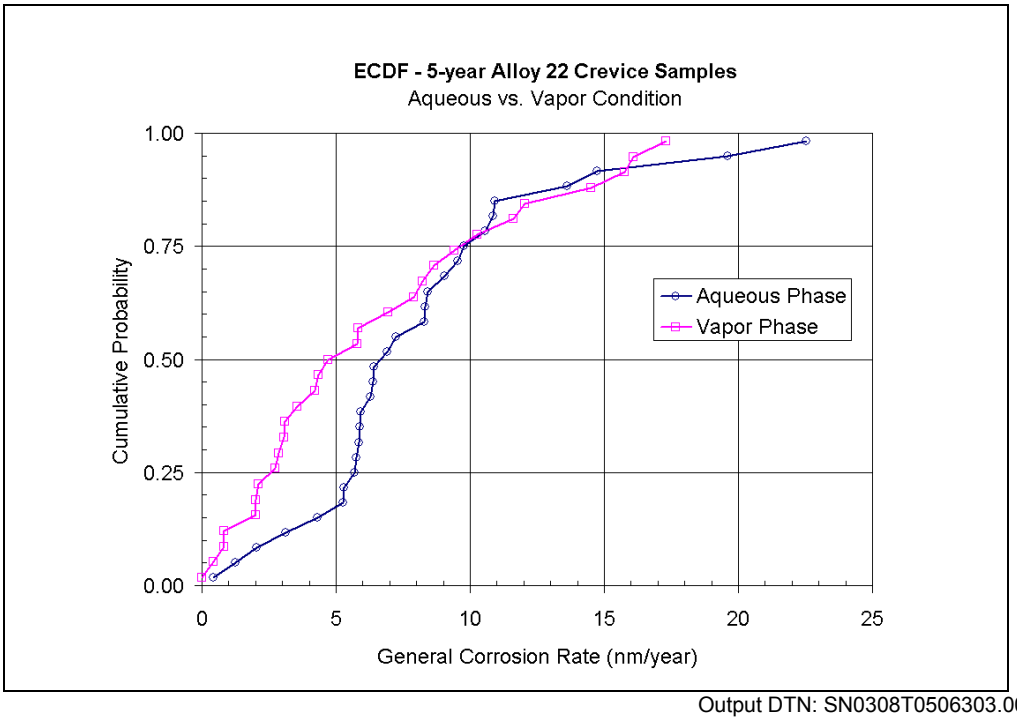

Output DTN: SN0308T0506303.004

Figure 6-16. Empirical Cumulative Distributions for General Corrosion Rate of Alloy 22 Crevice Samples Exposed in the Vapor Phase and Aqueous Phase after 5-Years Exposure in the LTCTF.

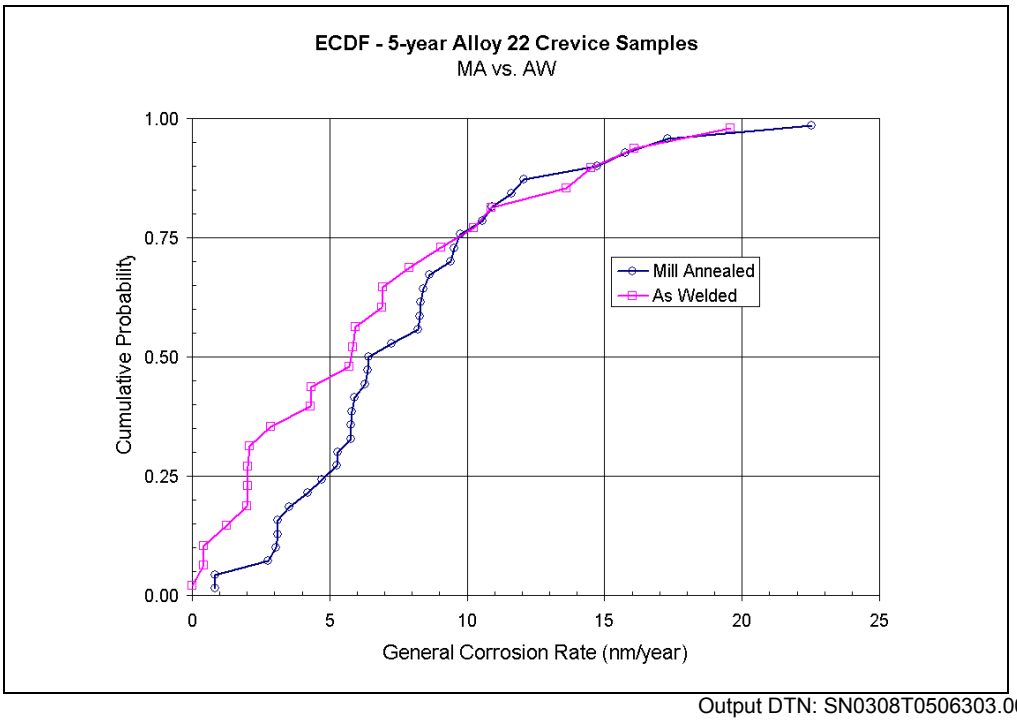

Output DTN: SN0308T0506303.004

Figure 6-17. Empirical Cumulative Distributions for General Corrosion Rate of Mill Annealed and As-Welded Alloy 22 Crevice Samples after 5-Years Exposure in the LTCTF.

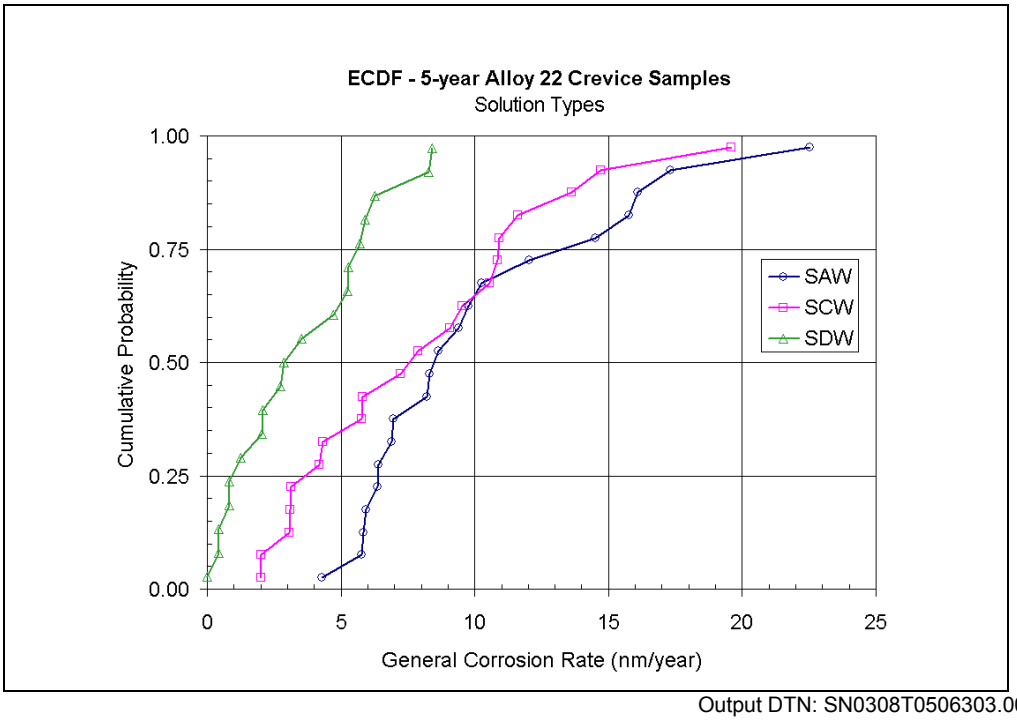

Output DTN: SN0308T0506303.004

Figure 6-18. Empirical Cumulative Distributions for General Corrosion Rate of Alloy 22 Crevice Samples Tested in Three Different Solution Types After 5-Years Exposure in the LTCTF.

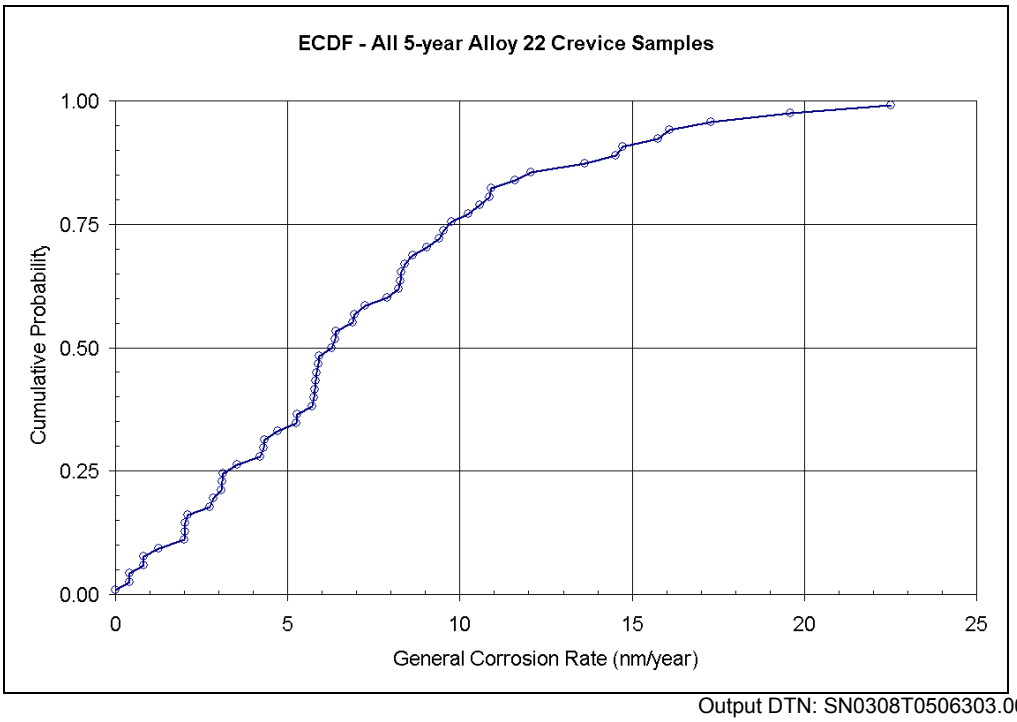

Output DTN: SN0308T0506303.004

Figure 6-19. Empirical Cumulative Distributions for General Corrosion Rate of All Alloy 22 Crevice Samples after 5-Years Exposure in the LTCTF.

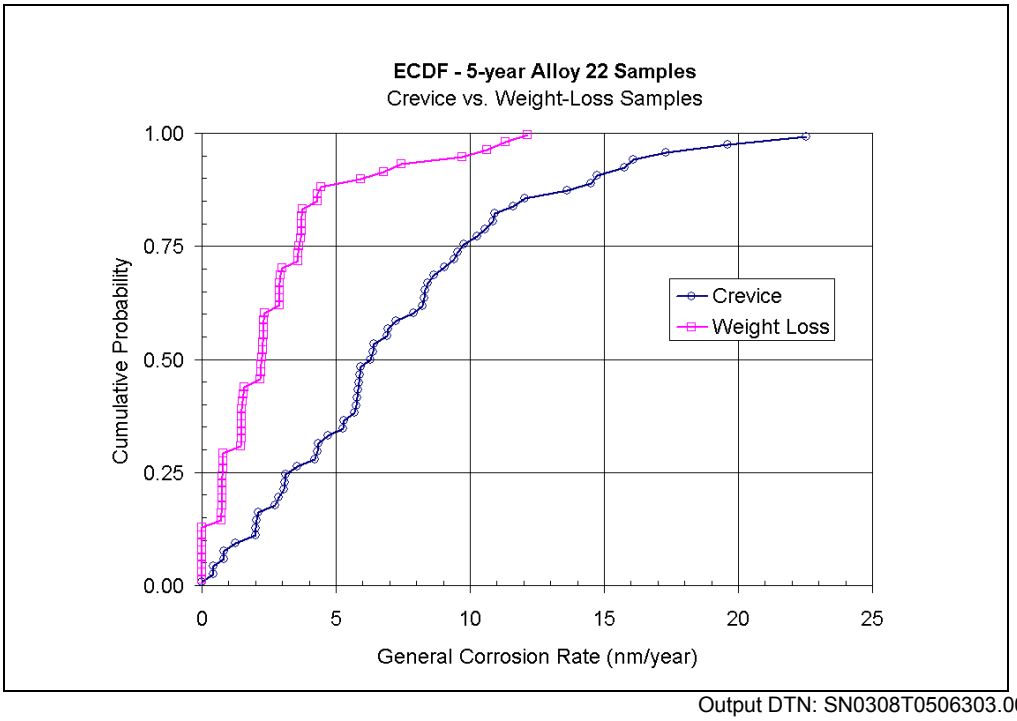

Output DTN: SN0308T0506303.004

Figure 6-20. Empirical Cumulative Distributions for General Corrosion Rate of Alloy 22 Weight-Loss and Crevice Samples after 5-Years Exposure in the LTCTF.

6.4.3.3 Uncertainty Analysis of General Corrosion Rate Data

This section documents the analyses performed to quantify the uncertainties of the general corrosion rates of Alloy 22 measured from the 5-year weight loss measurements of Alloy 22 samples from the LTCTF. As discussed in Section 6.4.3.4, the 5-year data were used for the base-case general corrosion model for the WPOB, therefore it is important to adequately quantify the uncertainty associated with the data and propagate it into the general corrosion model.

The previous analysis for the shorter term data has shown the general corrosion rate of Alloy 22 based on the weight-loss measurements has large uncertainties. Most of the uncertainties were from insufficient resolution of the weight-loss measurements of the samples due to the extremely low corrosion rates of the alloy in the test media. Measurement uncertainty was the main source of uncertainty. The method used in measurement uncertainty analysis is presented in this section, and this is important because it enables sound interpretation of the general corrosion data shown in Figure 6-20 (also in Attachments II and III) and its use in the waste package degradation analysis in the repository.

Consider a measurand Y is not measured directly, but is determined from N other quantities $X_1, X_2, ..., X_N$ through a functional relationship f defined as follows:

$$Y = f(X_1, X_2, \cdots X_N) \qquad \text{(Equation 6-10)}$$

An estimate of the measurand Y, denoted by y, is obtained using input estimates $x_1, x_2, ..., x_N$ for the values of N input quantities $X_1, X_2, \cdots X_N$. The output estimate y, is given by

$$y = f(x_1, x_2, \cdots x_N) \qquad \text{(Equation 6-11)}$$

The combined uncertainty of the measurement result y, designated by Δy, is given by Equation (6-12), the law of propagation of uncertainty (Taylor et al. 1994, Appendix A).

$$\Delta y = \sqrt{\sum_{i=1}^{N}\left(\frac{\partial f}{\partial x_i}\right)^2 \Delta x_i^2 + 2\sum_{i=1}^{N-1}\sum_{j=i+1}^{N}\frac{\partial f}{\partial x_i}\frac{\partial f}{\partial x_j}\Delta x_i x_j} \qquad \text{(Equation 6-12)}$$

In Equation (6-12), the partial derivatives $\frac{\partial f}{\partial x_i}$ are the sensitivity coefficients, Δx_i is the standard uncertainty associated with the input estimate x_i, and $\Delta x_i x_j$ is the estimated covariance associated with x_i and x_j.

Now refer to Figure 6-9 for a schematic of the Alloy 22 sample used in the weight-loss measurement in LTCTF. Therefore the exposed surface area of the sample is

$$A = 2ab + 2bc + 2ac - \left(\frac{\pi d^2}{2}\right) + \pi dc \qquad \text{(Equation 6-13)}$$

Referring to Equation 6-7 and letting the dependent variable y be the 5-year general corrosion rate measured in the LTCTF, the equation for the general corrosion rate is expressed as follows:

$$y = \frac{dp}{dt} = \frac{w}{\rho \times t\left(2ab + 2bc + 2ac - \left(\frac{\pi d^2}{2}\right) + \pi dc\right)} \quad \text{(Equation 6-14)}$$

where y = corrosion rate in cm per hour, w = total weight loss for 5 years in grams, ρ= density in grams per cubic centimeter, and t = time of exposure in hours. The combined uncertainty of the measurement result y, the corrosion rate, is calculated using the law of propagation of uncertainty (Taylor et al. 1994, Appendix A):

$$\Delta y = \sqrt{\left(\frac{\partial y}{\partial w}\right)^2 \Delta w^2 + \left(\frac{\partial y}{\partial \rho}\right)^2 \Delta \rho^2 + \left(\frac{\partial y}{\partial t}\right)^2 \Delta t^2 + \left(\frac{\partial y}{\partial a}\right)^2 \Delta a^2 + \left(\frac{\partial y}{\partial b}\right)^2 \Delta b^2 + \left(\frac{\partial y}{\partial c}\right)^2 \Delta c^2 + \left(\frac{\partial y}{\partial d}\right)^2 \Delta d^2} \quad \text{(Equation 6-15)}$$

where we consider that w, ρ, t, a, b, c, and d are independent, hence the covariance terms disappear.

The partial derivatives are:

$$\frac{\partial y}{\partial w} = \frac{1}{\rho \times t\left(2ab + 2bc + 2ac - \left(\frac{\pi d^2}{2}\right) + \pi dc\right)} \quad \text{(Equation 6-16)}$$

$$\frac{\partial y}{\partial \rho} = -\frac{w}{\rho^2 \times t\left(2ab + 2bc + 2ac - \left(\frac{\pi d^2}{2}\right) + \pi dc\right)} \quad \text{(Equation 6-17)}$$

$$\frac{\partial y}{\partial t} = -\frac{w}{\rho \times t^2\left(2ab + 2bc + 2ac - \left(\frac{\pi d^2}{2}\right) + \pi dc\right)} \quad \text{(Equation 6-18)}$$

$$\frac{\partial y}{\partial a} = -\frac{2w(b + c)}{\rho \times t\left(2ab + 2bc + 2ac - \left(\frac{\pi d^2}{2}\right) + \pi dc\right)^2} \quad \text{(Equation 6-19)}$$

$$\frac{\partial y}{\partial b} = -\frac{2w(a+c)}{\rho \times t\left(2ab+2bc+2ac-\left(\frac{\pi d^2}{2}\right)+\pi dc\right)^2} \quad \text{(Equation 6-20)}$$

$$\frac{\partial y}{\partial c} = -\frac{w[2(a+b)+\pi d]}{\rho \times t\left(2ab+2bc+2ac-\left(\frac{\pi d^2}{2}\right)+\pi dc\right)^2} \quad \text{(Equation 6-21)}$$

$$\frac{\partial y}{\partial d} = -\frac{w\pi(c-d)}{\rho \times t\left(2ab+2bc+2ac-\left(\frac{\pi d^2}{2}\right)+\pi dc\right)^2} \quad \text{(Equation 6-22)}$$

The maximum error in the corrosion rate is estimated by calculating numeric values of the partial derivatives from expected values of the independent variables, multiplying each partial derivative by the corresponding error (i.e., standard uncertainty) associated in the independent variables (Δw, $\Delta\rho$, Δt, Δa, Δb, and Δc), and summing the resulting products.

The combined standard uncertainty in the corrosion rate is estimated with Equation (6-15) by calculating numeric values of the partial derivatives from expected values of the input variables and their estimated standard uncertainties. Those values and intermediate calculation steps are summarized in Table 6-4.

Upon examining the sensitivity coefficients in Equation (6-15), it was found that Δy was most sensitive to the estimate of Δw. Because it is important, a detailed description of how Δw was calculated is given below. The Mettler AT200 balance was used to measure the weight of the specimens. The balance displays mass measurements to four decimal places. For instance a four-digit readout might indicate a mass of 60.2675 g for the weight of a specimen. The balance probably employs the standard round-off practice, and we know that the displayed number is derived from a value that lies between 60.26745 g and 60.26755 g. We can ascertain that the mass has an equal probability of lying between those two numbers. This would indicate that the error term has a uniform distribution. If we let w_1 = original weight of specimen and w_2 = final weight of specimen, then $w_1 = \mu_1 + 10^{-4}\varepsilon_1$ and $w_2 = \mu_2 + 10^{-4}\varepsilon_2$. That is, the mass = true mass + error term, and $\varepsilon_1 \sim U(-0.5, 0.5)$, and $\varepsilon_2 \sim U(-0.5, 0.5)$. The weight loss due to corrosion is

$$w = w_1 - w_2 = (\mu_1 - \mu_2) + 10^{-4}(\varepsilon_1 - \varepsilon_2), \quad \text{(Equation 6-23)}$$

where $(\mu_1 - \mu_2)$ is the true difference in mass and $10^{-4}(\varepsilon_1 - \varepsilon_2)$ is the error term. The error term $(\varepsilon_1 - \varepsilon_2)$ has a triangular distribution (Papoulis 1965, pages 189-192) between –1 and 1, i.e., $(\varepsilon_1 - \varepsilon_2) \sim$ Triangular (-1, 1, 0). For this distribution the standard deviation is

$$s = \frac{1}{\sqrt{6}} = 0.41. \qquad \text{(Equation 6-24)}$$

Therefore $\Delta w = 0.41 \times 10^{-4}$ g. The summary of the measurement uncertainty analysis for the 5-year data based upon this method is shown in Table 6-5.

Table 6-4. Summary of Measurement Uncertainty Analysis for Corrosion Rates Based Upon Weight Loss Measurements After 5-Year Exposure in LTCTF.

Uncertainty Analysis of 5-Year Weight-Loss Measurement Data			
Parameters	**Units**	**Crevice Samples**	**Weight-Loss Samples**
w	g	0.00187	0.00036
ρ	g/cm^3	8.69	8.69
t	hour	43800	43800
a	cm	5.08	5.08
b	cm	5.08	2.54
c	cm	0.3048	0.3048
d	cm	0.7925	0.7925
Δw	g	4.100E-05	4.100E-05
Δρ	g/cm^3	0.1	0.1
Δt	hour	24	24
Δa	cm	0.00254	0.00254
Δb	cm	0.00254	0.00254
Δc	cm	0.00254	0.00254
Δd	cm	0.00254	0.00254
Surface Area	cm^2	57.5787	30.2239
∂y/∂w		4.563E-08	8.693E-08
∂y/∂ρ		-9.819E-12	-3.601E-12
∂y/∂t		-1.948E-15	-7.145E-16
∂y/∂a		-1.596E-11	-5.891E-12
∂y/∂b		-1.596E-11	-1.115E-11
∂y/∂c		-3.380E-11	-1.836E-11
∂y/∂d		2.271E-12	1.586E-12
$(\partial y/\partial w)^2 \Delta w^2$		3.500E-24	1.270E-23
$(\partial y/\partial \rho)^2 \Delta \rho^2$		9.641E-25	1.297E-25

Uncertainty Analysis of 5-Year Weight-Loss Measurement Data			
Parameters	**Units**	**Crevice Samples**	**Weight-Loss Samples**
$(\partial y/\partial t)^2\Delta t^2$		2.186E-27	2.940E-28
$(\partial y/\partial a)^2\Delta a^2$		1.643E-27	2.239E-28
$(\partial y/\partial b)^2\Delta b^2$		1.643E-27	8.022E-28
$(\partial y/\partial c)^2\Delta c^2$		7.372E-27	2.174E-27
$(\partial y/\partial d)^2\Delta d^2$		3.326E-29	1.624E-29
Δy	cm/hour	2.116E-12	3.583E-12
Δy	μm/year	1.853E-04	3.138E-04
Δy	nm/year	**0.185**	**0.314**

Output DTN: SN0308T0506303.004

Table 6-5. Summary of Measurement Uncertainty Analysis for Corrosion Rates Based Upon Weight Loss Measurements After 5-Year Exposure in LTCTF.

	Sample Configuration	**Avg. Weight Loss (g)**	**Δy (nm/year)**	**Mean Corrosion Rate (nm/year)**	**Standard Deviation (nm/year)**
	Weight Loss Samples	0.00036	0.314	2.75	2.74
	Crevice Samples	0.00187	0.185	7.24	4.98

Output DTN: SN0308T0506303.004

The combined standard uncertainty is estimated to be approximately 0.185 nm/year in the case of crevice samples and 0.314 nm/year in the case of weight loss samples. These estimates correspond to one standard deviation (1σ). Therefore, for the crevice samples, about 3 percent of the variation in the measured general corrosion rate is due to the measurement uncertainty, and 97 percent of it is from the variations of the corrosion rate among the specimens. For the weight loss samples, most of the variation (about 89 percent) in the measured corrosion rate is due to variations among the specimens, and the rest is from measurement uncertainty.

As discussed in the base-case conceptual model in Section 6.3, crevices could form on the waste package surface from evaporative concentration of the constituents that are present on the surface such as dust and salts. Therefore the corrosion rate distribution of the crevice samples was used for the base-case general corrosion rate of the WPOB. Because only about 3 percent of the total variation in the measured general corrosion rate of the crevice samples is due to the measurement uncertainty, all (100 percent) of the measured variation is considered to be due to the variability in the general corrosion processes. It is recommended that the general corrosion rate variability be applied among waste packages to be modeled and local areas on a single waste package.

6.4.3.4 Base-Case Temperature-Dependent General Corrosion Model

The passive dissolution (general corrosion) of highly corrosion-resistant alloys such as Alloy 22 is governed by the transport properties of reacting species (e.g., metal ions, oxygen ions, vacancies and interstitials) in the very thin (typically a few nanometers), compact, adherent passive film that forms on the alloy surface in contact with the corrosive environment and the dissolution rate of the passive film. These processes are influenced by the characteristics of the passive film, electrochemical potential across the film, and the chemistry of solution contacting the film (BSC 2001, Section 7.3.5.1). Chromium and nickel oxides, which are the major constituents of the passive film of nickel-chromium-molybdenum alloys like Alloy 22 (Lorang et al. 1990), are stable and exhibit extremely low dissolution rates over a wide range of solution chemistry. The transport properties of the reacting species and reaction rates in the passive film are considered thermally activated processes, so the general corrosion rate of the Alloy 22 waste package outer barrier is expected to have a certain level of temperature dependency (BSC 2001, Section 7.3.5.1). The literature data summarized in a recent report by the Electric Power Research Institute (EPRI 2002, Section 5.3.2) show such a temperature-dependency of Alloy 22 general corrosion in a wide range of test solution chemistries.

The temperature dependence of general corrosion rate is represented with an activation energy according to the Arrhenius relation.

$$\ln(R_T) = C_o + \frac{C_1}{T} \qquad \text{(Equation 6-25)}$$

R_T is temperature-dependent general corrosion rate in nm/year, T is temperature in Kelvin, and C_0 and C_1 are constants.

The temperature-dependence term (C_1) is determined from the corrosion rates obtained from the short-term polarization resistance data for Alloy 22 specimens tested for a range of sample configurations, metallurgical conditions, and exposure conditions (temperature and water chemistry). Figure 6-21 shows the temperature dependence of corrosion rates of mill annealed (MA) Alloy 22 samples measured by the polarization resistance technique over the temperature range from 45 to 130 °C. The corrosion rates for the as-welded (ASW) samples and as-welded plus thermally aged samples are shown in Figure 6-22. The "aged" samples were treated for 173 hours at 700 °C prior to the electrochemical testing. The corrosion rate data are listed in Attachment IV. The polarization resistance of the samples was measured after 24-hour exposure of the samples in open-circuit potential in the test environments (see Section 4.1.1.4 and Attachment I). This model approach is justified because, as discussed in detail in Section 7.1, the activation energies of general corrosion rate of highly corrosion resistant Ni-Cr-Mo alloys are similar regardless of the exposure time in the test environments. That is, the literature data presented in Section 7.1 demonstrate that the temperature dependence of general corrosion rate of Alloy 22 does not change significantly as the general corrosion rate decreases with the exposure time.

Although there is a spread of the data for a given temperature, Figure 6-21 and Figure 6-22 clearly show a consistent trend of the temperature dependence of the corrosion rates measured by the polarization resistance. It is also shown that the corrosion rates of the ASW and ASW plus

thermally aged samples (Figure 6-22) are comparable to those of the MA samples (Figure 6-21). There are no significant differences in the 24-hour corrosion rates for the samples with different metallurgical conditions (i.e., MA, ASW, and ASW plus thermally aged). See Section 6.4.6 for detailed discussion on the effect of aging on the WPOB corrosion.

The corrosion rate data for all the samples with the three different metallurgical conditions were used together for the analysis to estimate the temperature dependence of the WPOB general corrosion because their corrosion rates are all comparable. Note that the corrosion rates from the polarization resistance measurements were for a comparative analysis to extract the temperature dependence of the corrosion rates. The measurements were not intended for obtaining the absolute values of the corrosion rate. From fitting the data (listed in Attachment IV) to the Arrhenius relation of Equation (6-25), the temperature-dependence term (C_1) was determined to have a mean of –3116.47 and a standard deviation of 296.47. Normal distribution was considered for the parameter in the regression analysis. According to the Arrhenius relation, $C_1 = -E_a/R$, where E_a is the activation energy (J/mol), and R is the universal gas constant (8.314 $J \cdot mol^{-1} \cdot K^{-1}$). This temperature dependence corresponds to an activation energy of 25.91 ± 2.46 kJ/mol. Note that the data for the MCA samples with their edges not polished were not included in the regression analysis for the temperature dependence (see Section 4.1.1.4).

Now, let the general corrosion rate distribution measured from the weight loss data of the 5-year crevice specimens (see Figure 6-20) represent the distribution of long-term general corrosion rate of the WPOB at 60 °C. This model approach is reasonably bounding because the general corrosion rates for crevice specimens are generally higher than those of plain weight-loss specimens (i.e., with no crevice). Therefore,

$$\ln(R_o) = C_o + \frac{C_1}{T_0 \ (=333.15K)} \qquad \text{(Equation 6-26)}$$

$$C_0 = \ln(R_o) - \frac{C_1}{333.15} \qquad \text{(Equation 6-27)}$$

where R_o is a distribution to represent the general corrosion rate distribution from the weight loss of the 5-year crevice samples (see Figure 6-20) at T_o = 333.15 K (60 °C). Substituting for C_0 in Equation (6-26), we get

$$\ln(R_T) = \ln(R_o) + C_1\left(\frac{1}{T} - \frac{1}{333.15}\right) \qquad \text{(Equation 6-28)}$$

As discussed above, C_1 is normally distributed, $N(\mu = -3116.47, \sigma = 296.47)$. Further analysis of the residuals showed that the errors are normally distributed. The activation energy was estimated to be 25.91 ± 2.46 kJ/mol.

The 5-year corrosion rate data for Alloy 22 were analyzed to determine the theoretical distribution that best fits the data. The following three goodness of fit tests were performed for the data analysis: the Chi-Square test, the Kolmogorov-Smirnov test, and the Anderson-Darling

test. All the statistical tests indicated that the Weibull distribution best fits the 5-year corrosion rate data. Therefore it was decided to use a Weibull distribution. To estimate the parameters of the Weibull distribution, the method of Maximum Likelihood Estimator (MLE) was used. A Weibull distribution, with scale factor s = 8.88, shape factor b = 1.62, and location factor l = 0, best fits the corrosion rate distribution. Therefore R_o is expressed as follows (Evans et al. 1993, page 154).

$$R_o = s[\ln(\frac{1}{1-p})]^{1/b} \quad \text{(Equation 6-29)}$$

where p is the cumulative probability, and s and b were defined and their values were given above. The cumulative distribution function of R_o is given in Figure 6-23.

The model outputs (R_T) at temperatures of 25, 50, 75, 100, 125 and 150 °C are shown in Figure 6-24. The model results shown in the figure are for the mean value of the temperature dependence term (C_1) and having the entire variance of R_o due to the variability in the general corrosion process (see Table 6-5 and associated discussions above for additional details on the basis for the corrosion rate variability). Therefore the cumulative distribution functions of the model calculated general corrosion rates in the figure represent the range of the variable general corrosion rates of the WPOB at each exposure temperature of interest, with the C_1 value sampled at the mean.

For a constant waste package surface temperature of 150 ºC, the median penetration depth by general corrosion over 10,000 years, using the median general corrosion rate of 51.8 nm/year, is about 518 µm, which is less than 3 percent of the total thickness of the WPOB (20 mm). For the upper bound value of the general corrosion rate of 256 nm/year (99.99^{th} percentile rate at 150 °C), the total penetration depth by general corrosion is about 2560 µm, which is less than 13 percent of the total thickness of the WPOB. This bounding analysis demonstrates that the waste package performance in the repository is not limited by general corrosion.

Equation 6-28 is the base-case general corrosion model for the WPOB. As stated above, the entire variance of R_o represents the variability of the general corrosion process. It is recommended that the general corrosion rate variability represented by the parameter be applied among the waste packages to be modeled and also to local areas on an individual waste package. The entire variance of the temperature dependence term (C_1) is due to uncertainty, and the uncertainty is limited to ± 3 standard deviations.

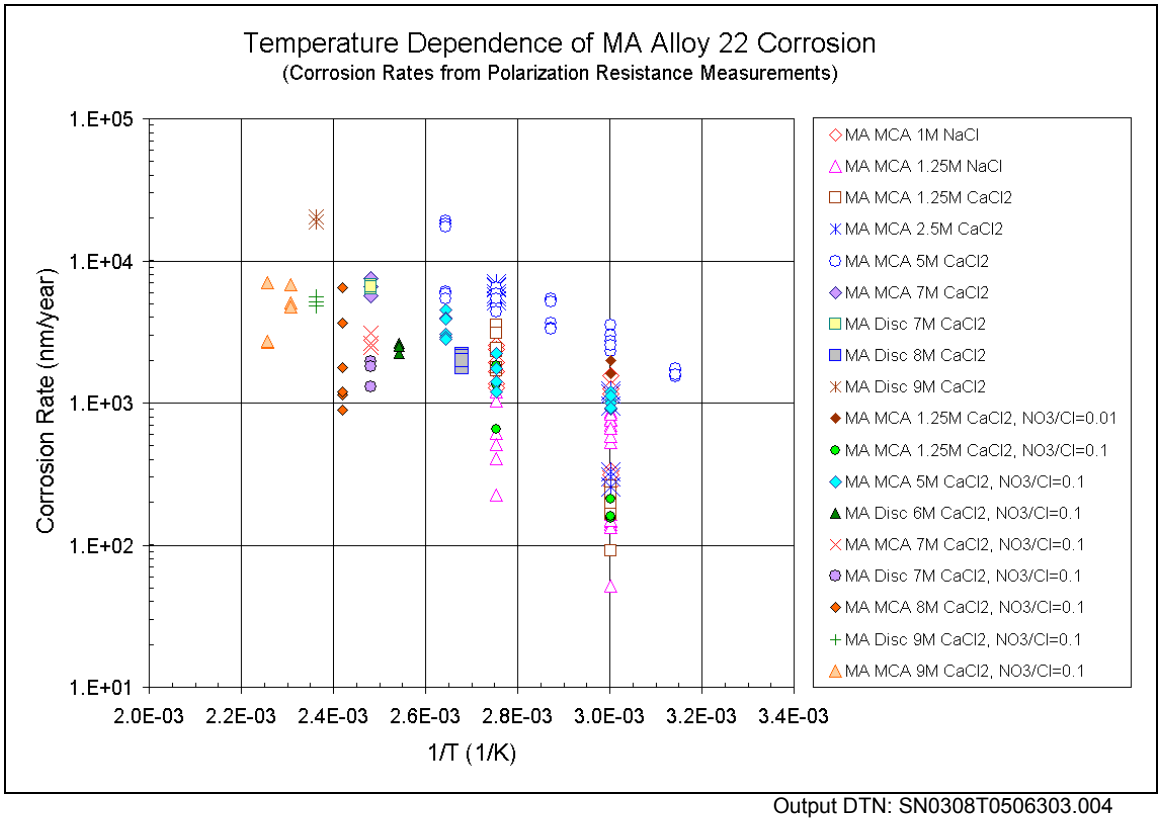

Output DTN: SN0308T0506303.004

Figure 6-21. Temperature Dependency of Corrosion Rates of Mill Annealed Alloy 22 Samples Obtained from the Polarization Resistance Measurements for Varying Sample Configurations in a Wide Range of Solution Chemistries.

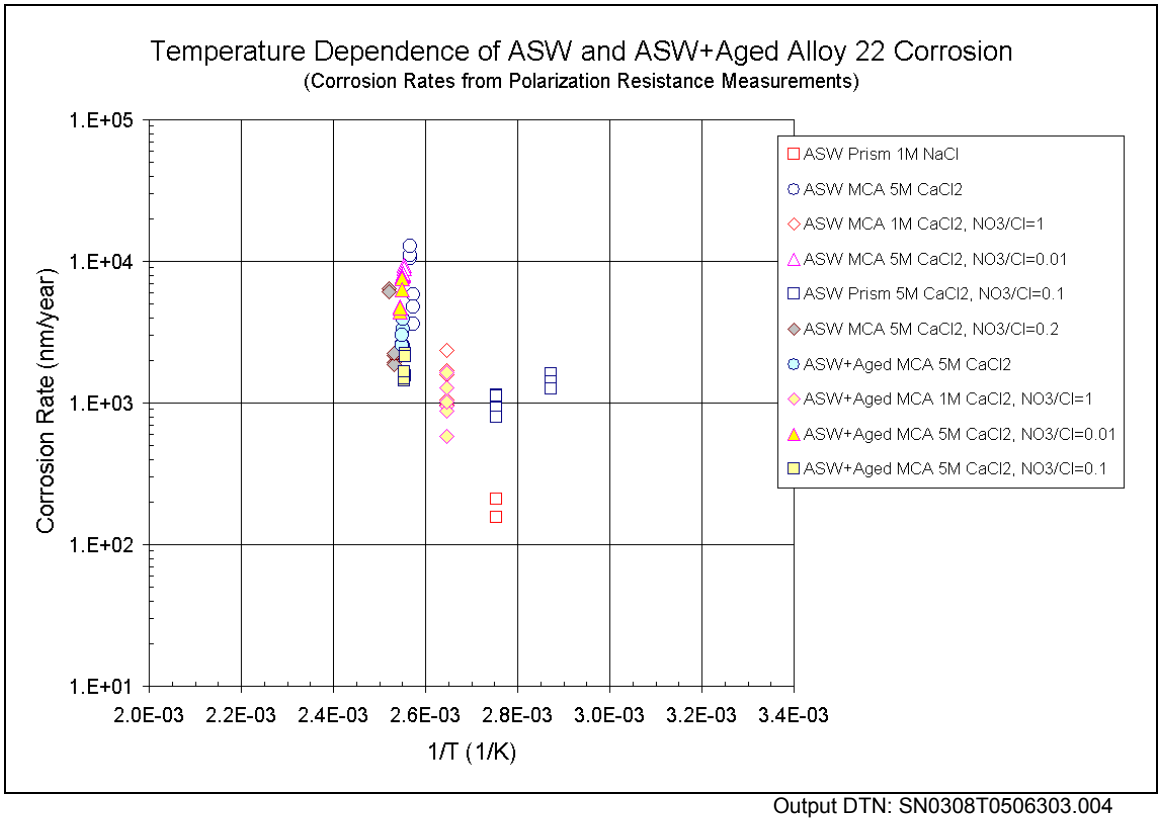

Output DTN: SN0308T0506303.004

Figure 6-22. Temperature Dependency of Corrosion Rates of As-welded and As-welded Plus Thermally Aged Alloy 22 Samples Obtained from the Polarization Resistance Measurements for Varying Sample Configurations in a Wide Range of Solution Chemistries.

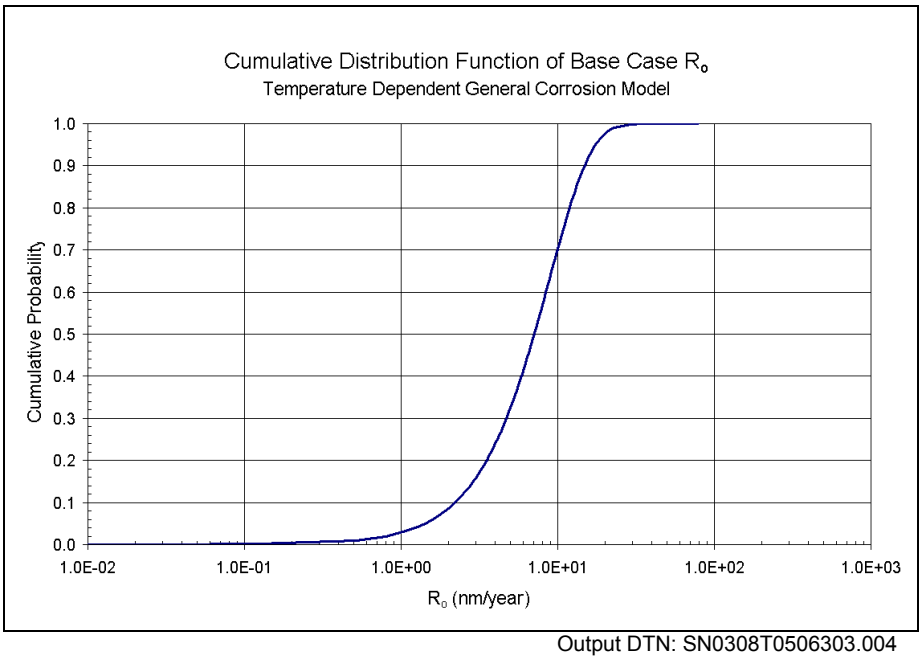

Output DTN: SN0308T0506303.004

Figure 6-23. Cumulative Distribution Function (CDF) of R_o of the Base-Case Temperature Dependent General Corrosion Model of the WPOB.

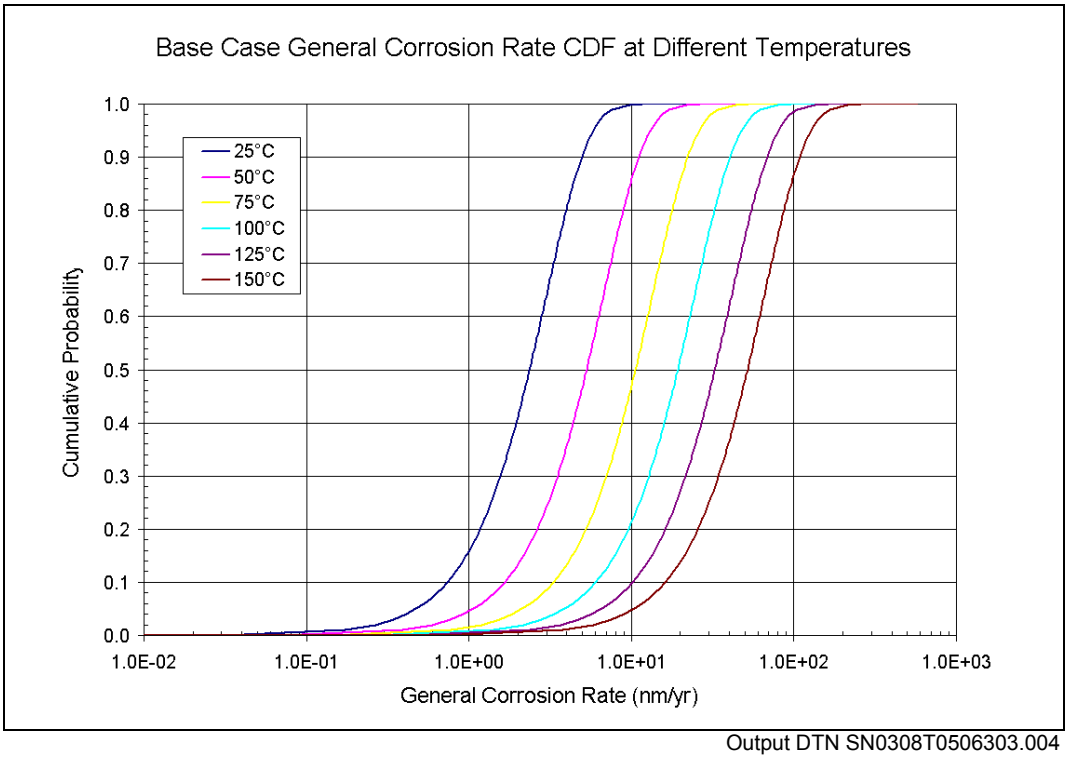

Output DTN SN0308T0506303.004

Note: The calculations were performed using the mean value (-3116.47) of the temperature-dependency term (C_1), and the calculated general corrosion rate ranges represent the variability of the rate.

Figure 6-24. Calculated Model Outputs of the Base Case Temperature Dependent General Corrosion Model Based on the Crevice Sample Data at Temperatures of 25, 50, 75, 100, 125 and 150 °C.

6.4.3.5 Alternative Conceptual Model for General Corrosion

Alternative conceptual models (ACMs) are based on assumptions and simplifications that are different from those employed in the base-case model. An important reason for considering ACMs is to help build confidence that changes in modeling assumptions or simplifications will not change conclusions regarding subsystem and total system performance. Conceptual model uncertainty results from sparse observational data and a lack of available information to corroborate or refute plausible alternative interpretations of the subsystem and the processes occurring within the subsystem. This section discusses the ACMs for the general corrosion models of the waste package outer barrier (WPOB). None of the general corrosion ACMs discussed in this section is recommend for inclusion in the TSPA.

6.4.3.5.1 Time-Dependent General Corrosion Behavior of the WPOB

As discussed in detail in Section 6.4.3.4, the base-case general corrosion model for the WPOB is based on the five-year weight-loss measurements of Alloy 22 crevice samples from the LTCTF. The general corrosion model implemented in the TSPA assumes that general corrosion of the WPOB progresses uniformly over a large surface (Assumption 5.2). The general corrosion rate is temperature dependent, and for a given temperature, it is assumed to be constant (i.e., time-independent) (Assumption 5.2). Therefore, for a given temperature, the depth of penetration or thinning of the WPOB by general corrosion is equal to the general corrosion rate at that temperature, multiplied by the time duration that the waste package surface is at that temperature. However, general corrosion rates of metals and alloys tend to decrease with time. This is shown in Figure 6-25 for the mean general corrosion rates of Alloy 22 at 90 °C, measured by different techniques. The exposure time ranges from one day to 5-plus years exposure at the LTCTF. Each data point for the 6-month, 1-year, and 2-year weight loss measurements in the figure is the mean of at least 144 samples (CRWMS M&O 2000c, page 3-39). The 5-year general corrosion rate is the mean of the weight-loss measurements of 59 crevice samples from the LTCTF (see Table 6-5 and Section 6.4.3.4). These data shown in the figure are summarized in Table 6-6. A trend line was drawn for the data for a better visualization of the data trend. The trend of decreasing general corrosion rate with time is consistent with the expected corrosion behavior of passive alloys such as Alloy 22 under repository-type aqueous conditions.

The time-dependent general corrosion behavior of the WPOB was not included in the TSPA because the constant (time-independent) rate model (for a given temperature) is more conservative and should bound the general corrosion behavior of the WPOB over the repository time period. The 5-year corrosion rates were conservatively selected for extrapolation over the repository time scale.

Table 6-6. Summary of Mean General Corrosion Rates of Alloy 22 at 90 °C vs. Exposure Time.

Exposure Time		Mean Rate (μm/year)	Remarks
(years)	(days)		
0.0027	1	0.460	Lian et al. 2002, Table 3, potentiostatic polarization technique at 100 mV vs. SSC applied potential in SAW, 90 °C, N_2 purge.
0.0027	1	1.250	Lian et al. 2002, Table 3, potentiostatic polarization technique at 100 mV vs. SSC applied potential in SCW, 90 °C, N_2 purge.
0.019	7	0.100	Evans and Rebak 2002, Figure 2, linear polarization resistance technique, after 1 week in open circuit potential in SAW, 90 °C, air purge.
0.154	56	0.182	Hua 2002, page 97, calculated from regression fit for 56-day weight loss in BSW, CR (MPY) = 31.3*exp(-25300/RT).
0.50	183	0.050	CRWMS M&O 2000c (Page 3-39), LTCTF weight loss data
1.00	365	0.030	CRWMS M&O 2000c (Page 3-39), LTCTF weight loss data
2.30	840	0.010	CRWMS M&O 2000c (Page 3-39), LTCTF weight loss data
5.06	1846	0.007	This model report, Section 6.4.3.2, Table 6-5

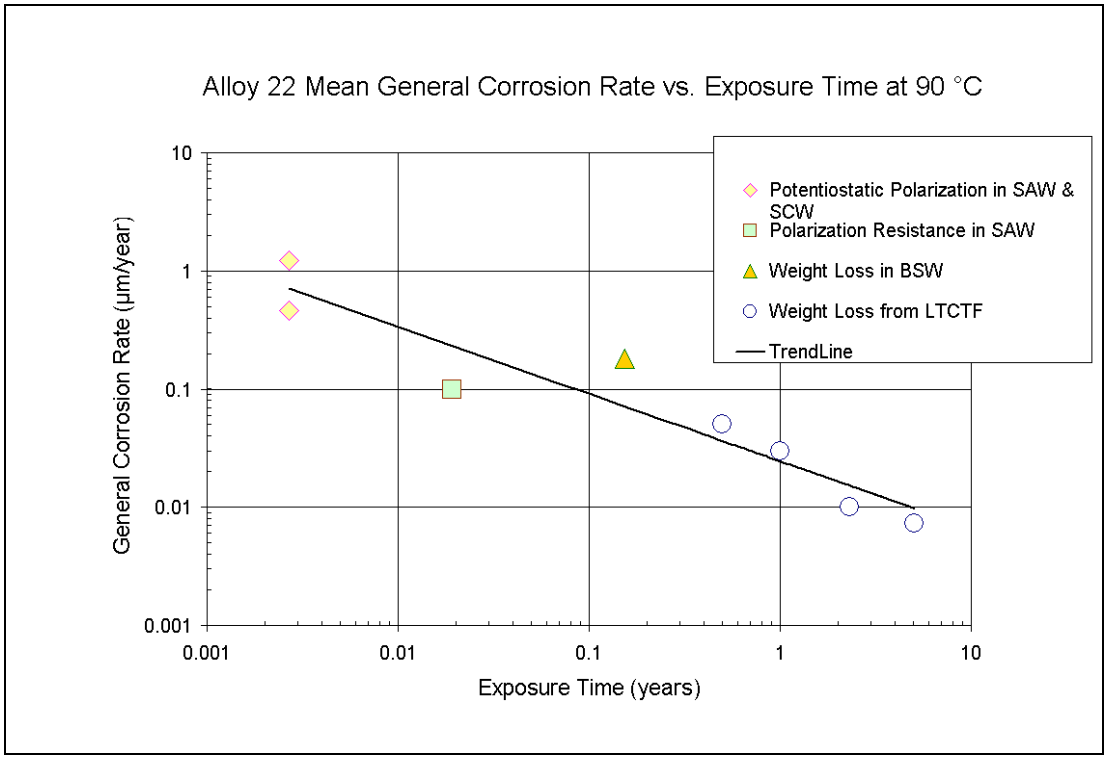

Figure 6-25. Time-Dependent General Corrosion Rate of Alloy 22 Measured by Different Techniques.

6.4.3.5.2 Alternative Conservative Interpretation of Long-Term General Corrosion Rates of Crevice Samples

As shown in Figure 6-20, the general corrosion rates of the crevice samples are higher than those of the "plain" weight-loss samples. This may have been caused by different surface polishing treatments between the two sample groups. Another supposition is that there might have been more active corrosion in the crevice area under the crevice former. See Figure 6-26 for the crevice sample diagram. One major assumption to be made for the analysis for the latter case was that the corrosion rate of the boldly exposed (non-crevice) area of the crevice samples can be represented by the average corrosion rate of the "plain" weight-loss samples. Assuming this assumption is valid, the following data manipulations were made to estimate the corrosion rate of the crevice area under the crevice former.

- Calculated the average weight loss per unit area of the plain weight-loss samples.
- Estimated the "true" weight loss of the boldly exposed area of the crevice samples by multiplying the average weight loss per unit area (from the plain weight loss samples above) by the boldly exposed area of the crevice samples.
- Calculated the weight loss from the crevice area under the crevice former by subtracting the "true" weight loss of the boldly exposed area from the total weight loss measured for the crevice samples.
- Calculated the corrosion rate of the crevice-area-only under the crevice former using the calculated weight loss from the crevice area.

The empirical CDF of the estimated corrosion rates of the crevice-area-only under the crevice former is shown in Figure 6-27, along with the empirical CDFs of the weight-loss samples and crevice samples for comparison. The median corrosion rate (50^{th} percentile rate) of the crevice-area-only is 51 nm/year and is about 10 times of the mean of the crevice samples. The maximum rate (100^{th} percentile rate) of the crevice area only case is about 214 nm/year, which is also about 10 times of the maximum rate of the crevice samples. Because the calculated corrosion rates of the crevice area only under the crevice former are much higher than those of the boldly exposed area of the crevice samples, microscopic examinations would be able to show the differences in the corrosion fronts between the two areas (or at least at the edge of the area under the crevice former). However, examinations by optical microscopy and SEM did not reveal such differences.

As with the crevice sample case, it was decided to use a Weibull distribution for R_o. The method of Maximum Likelihood Estimator (MLE) was used to estimate the parameters of the Weibull distribution. Therefore a Weibull distribution, with scale factor s = 82.3, shape factor b = 1.36, and location factor l = 0, best fits the corrosion rate distribution for the crevice-area-only case. The cumulative distribution function of R_o for the crevice-area-only case is given in Figure 6-28.

The measurement error for the crevice-area-only case was taken to be the same as the crevice sample case given in Table 6-5. Using the same mean value of the same temperature-dependence term (C_1) (i.e., $N(\mu = -3116.47,\ \sigma = 296.47)$) and sampling for R_o from the entire

corrosion rate distribution for the conservative crevice-area-only case (Figure 6-28), the general corrosion rate distributions were calculated at 25, 50, 75, 100, 125 and 150 °C using the temperature dependent model in Equation (6-28). The results are shown in Figure 6-29. For the C_1 value sampled at the mean, the CDFs in the figure represent the range of the variable general corrosion rates of the WPOB at each exposure temperature of interest for the conservative crevice-area-only case. Because it is not known yet what has caused the higher corrosion rates for the crevice samples, it is recommended that the alternative conservative interpretation of the Alloy 22 general corrosion rate be not included in the waste package degradation analysis.

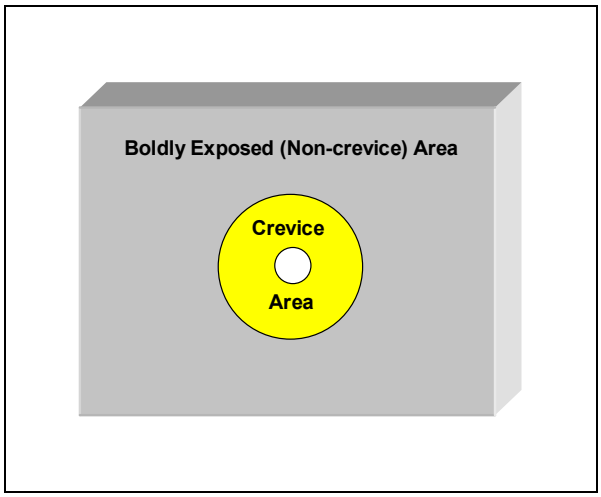

Note: Diameter of the crevice former (washer) is 0.75 inches (19.05 mm).

Figure 6-26. Schematic Showing the Boldly Exposed Area and the Crevice Area Under the Crevice Former of the Crevice Sample.

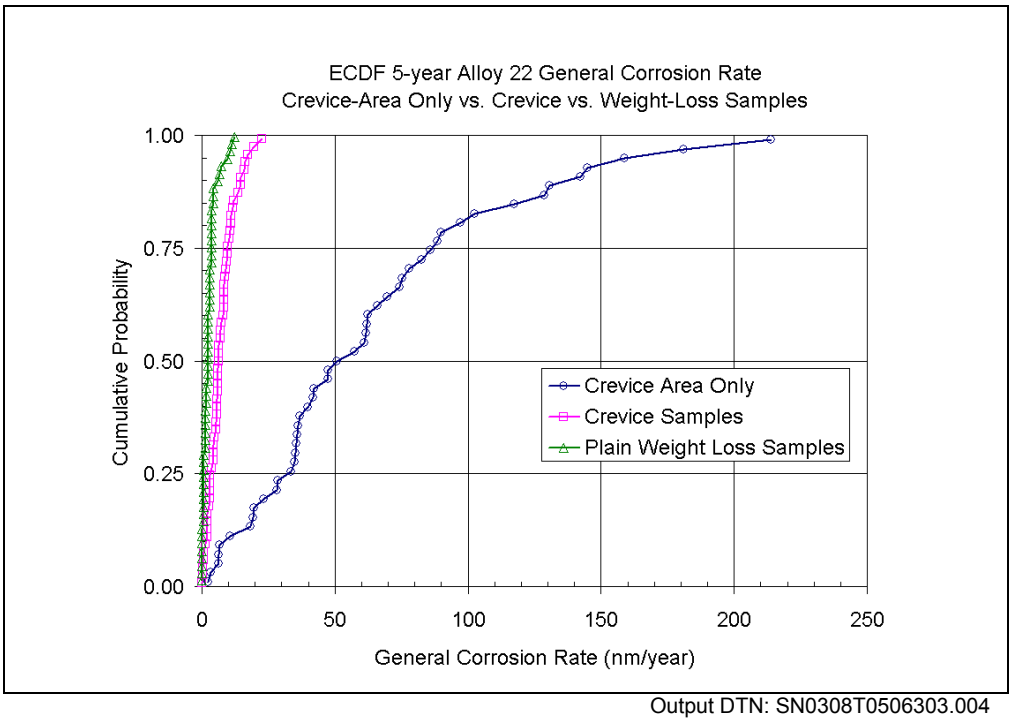

Output DTN: SN0308T0506303.004

Figure 6-27.Empirical CDFs for General Corrosion Rates of Crevice-Area Only, Crevice Samples, and Weight-Loss Samples After 5-Year Exposure in the LTCTF.

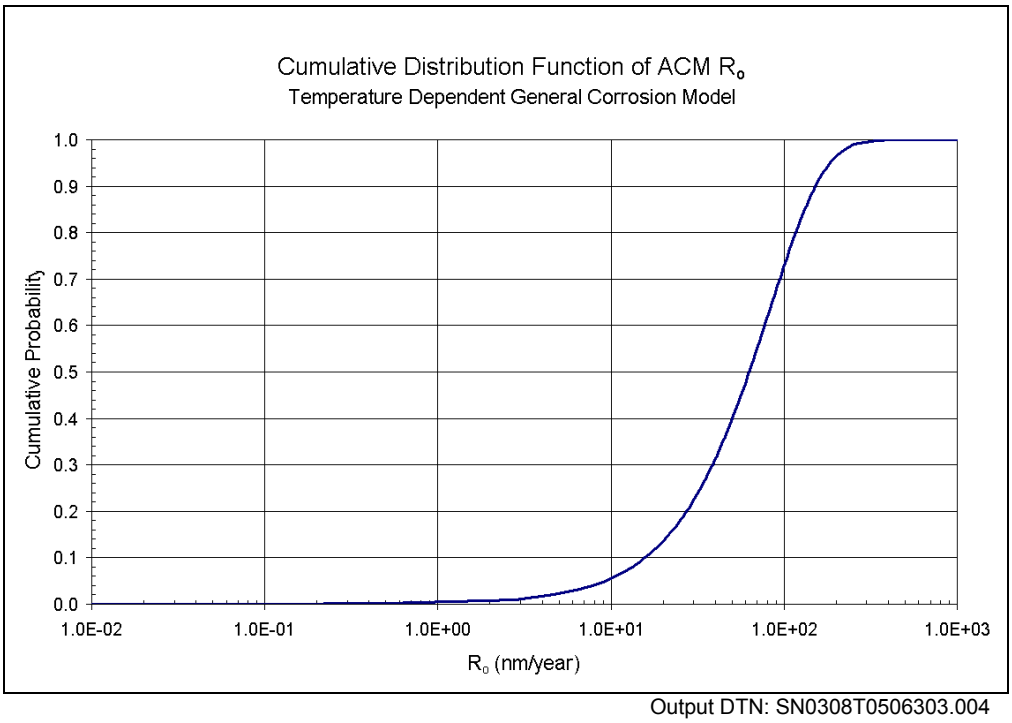

Output DTN: SN0308T0506303.004

Figure 6-28. Cumulative Distribution Function (CDF) of R_o of the Crevice-Area-Only Case Temperature Dependent General Corrosion Model of the WPOB.

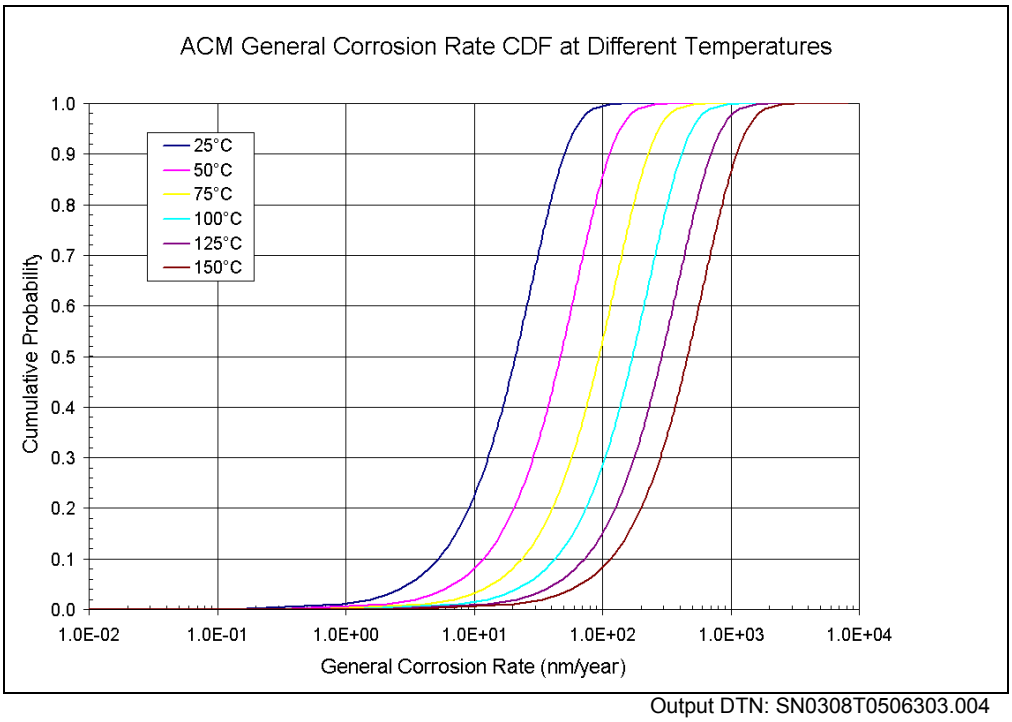

Output DTN: SN0308T0506303.004

Note: The calculation was performed using the mean value (-3116.47) of the temperature-dependency term (C_1), and the calculated general corrosion rate range represents the variability of the rate.

Figure 6-29. Calculated Model Outputs of the Temperature Dependent General Corrosion Model Based on the Crevice-Area-Only Case at Temperatures of 25, 50, 75, 100, 125 and 150 °C.

6.4.4 Localized Corrosion

Localized corrosion is a type of corrosion in which the attack progresses at discrete sites or in a non-uniform manner. The rate of localized corrosion is higher than the rate of general corrosion. The current analysis assumes that crevice corrosion is representative of localized corrosion of the WPOB under the exposure conditions expected in the post-closure repository (Assumption 5.3). This is a conservative bounding assumption because the initiation threshold for crevice corrosion in terms of water chemistry and temperature is lower than pitting corrosion, which is another form of localized corrosion attacking boldly exposed surfaces.

Localized corrosion of the WPOB is modeled with two model components: initiation model and propagation model. The initiation model considers that localized corrosion of the WPOB occurs when the open circuit potential, or corrosion potential (E_{corr}) is equal to or greater than a certain critical threshold potential ($E_{critical}$), that is, ΔE (= $E_{critical}$ - E_{corr}) ≤ 0. Also, the magnitude of this ΔE is an index of the localized corrosion resistance, that is, the larger the difference, the greater the localized corrosion resistance. This conceptual model of localized corrosion initiation is widely accepted by the corrosion community and has been published extensively (Bohni 2000, Section B; Dunn et al. 2000 and 2003; Frankel 1998; Frankel 2002; Frankel and Kelly 2002; Beavers et al. 2002, Section 8.3). The crevice corrosion initiation model components (i.e., E_{corr} and $E_{critical}$) could be affected by the sample configuration (crevice, disk or rod), metallurgical

conditions (mill annealed or welded), and exposure condition (temperature, pH, chloride ion concentration, nitrate ion concentration).

When localized corrosion occurs, the localized corrosion of the WPOB is assumed to propagate at a (time-independent) constant rate (Assumption 5.4). This assumption is highly conservative because it is known that the localized corrosion rate decreases with time and this is particularly more likely under a thin water film condition that is expected to form on the waste package surface in the post-closure repository. Also, in most cases, localized corrosion arrests or dies shortly after initiation. See Section 6.4.4.7 for additional discussions on this issue.

A series of the electrochemical corrosion tests were conducted to generate the data for the localized corrosion initiation model. The typical sequence for electrochemical testing is summarized in Attachment I. Further details of the tests are provided in the corresponding Scientific Notebooks cited in the Data Tracking Numbers (DTNs) of the input data documented in Section 4.1.1. As discussed in Section 6.4.4.4, a set of long-term open-circuit potential measurements have been underway to measure the long-term corrosion potentials (E_{corr}) of Alloy 22 in a wide range of exposure environments. Also a series of cyclic potentiodynamic polarization (CPP) tests were performed to measure the critical potentials ($E_{critical}$) of Alloy 22 for differing sample configurations and metallurgical conditions in a wide range of exposure environments.

6.4.4.1 Overview of Approaches to Selection of Critical Potential for Localized Corrosion Initiation

As discussed previously, localized corrosion of the WPOB is modeled with two model components: initiation model and propagation model. The initiation model considers that localized corrosion of the WPOB occurs when the long-term corrosion potential (E_{corr}) is equal to or greater than a certain critical potential ($E_{critical}$), that is, ΔE (= $E_{critical}$ - E_{corr}) ≤ 0. Note that initiation is a stable propagation stage of localized corrosion. The crevice corrosion initiation model components (i.e., E_{corr} and $E_{critical}$) could be affected by the sample configuration (crevice, disk or rod), metallurgical conditions (mill annealed, as-welded or as-welded plus thermally aged), and exposure condition (temperature, pH, chloride ion concentration, nitrate ion concentration).

$E_{critical}$ can be defined as a certain potential above which the current density or corrosion rate of Alloy 22 increases significantly and irreversibly above the general corrosion rate of the passive metal. This value represents local breakdown of the passive film. In environments that promote localized corrosion, $E_{critical}$ is the lowest potential that would trigger localized (e.g. crevice) corrosion. However the value of $E_{critical}$ cannot be measured as easily as the value of E_{corr} because the value of $E_{critical}$ is also affected by the method used for its measurement. In any case, the margin of safety against localized corrosion will always be given by the value of $\Delta E = E_{critical} - E_{corr}$.

The "true" value of $E_{critical}$ of a metal or alloy for a given set of conditions (including sample configuration, metallurgical condition, and exposure condition) would be the lowest potential at which the corrosion current (except the initial transients) does not decay with time and stay above the passive current density, when held potentiostatically. One of the approaches to

defining this $E_{critical}$ value with a high level of confidence is to conduct a series of potentiostatic polarization (PSP) tests at pre-determined potentials near the critical potentials initially measured by shorter term cyclic potentiodynamic polarization (CPP) tests. Because the CPP tests require much shorter test periods than the PSP tests, the CPP tests have been used widely to obtain the critical potential. Another approach is to use the CPP tests and employ a conservative criteria in selecting the $E_{critical}$ value from the polarization curve. The latter approach was used in the testing and analysis and model development for the critical potential for the WPOB.

In using the CPP technique to identify critical parameters for the initiation of localized corrosion, the potential-current curves are examined to look for values of the potential where there was a discernible, often abrupt, change of the current, much like a point of inflection on the potential-current curve. The advantage of this approach is that the current change can be related to physical/chemical events occurring on the metal surface over the course of the polarization cycle. Because the potential is scanned initially in the oxidizing or anodic direction, and then the potential is scanned in the reducing or cathodic direction, hysteresis of the curve is indicative of changes that have occurred on the metal surface during polarization, and the amount of this hysteresis is related to the localized corrosion susceptibility. Figure 6-30 shows a schematic of the CPP curves showing likely different behaviors of the curves during the potentiodynamic scanning of an alloy sample with high resistance to localized corrosion.

The electrochemical potential is continuously scanned from the open-circuit or corrosion potential following a relatively short period of exposure of the metal specimen to the environment. If the metal is passive (as in the case of Alloy 22), the current tends to have a low and nearly constant value for a wide range of potential, but eventually a potential is reached where there is a sharp increase in current. This change may simply be the beginning of oxygen evolution from water (if the applied potential is sufficient to electrolyze water). If this potential corresponds to oxygen evolution, one would not expect passive film breakdown and therefore no localized corrosion. This change may also indicate the breakdown of the passive film, which in itself could be a sequence of a number of electrochemical reactions.

After the "end point" of the polarization curve is reached, the potential scan is reversed. In some cases the hysteresis is nil or slightly negative, meaning that the reactions are reversible, and the current retraces the values from the forward scan. The current usually falls through zero, but almost always this new corrosion potential at the "zero" current is much more positive than the initial corrosion potential. If oxygen evolution has occurred, the solution has a higher oxygen content (it was likely de-aerated at the beginning of the test) and this would make the new corrosion potential more oxidizing. If some additional oxidation of the alloy has occurred, this would also make the corrosion potential more oxidizing on the reverse scan.

In cases where film breakdown due to localized corrosion has occurred, the metal surface is considerably altered from its initial state, and the current shows, on reverse scan, a prominent "positive" hysteresis. That is, compared to the forward scan, the current at a given potential is significantly higher on the reverse scan. However, eventually this reverse scan curve crosses over the curve generated on the forward scan. Where the reverse scan intersects the forward scan, the repassivation is considered to be complete, and the potential at the intersection is called the *repassivation potential* (e.g., the pit repassivation potential (E_{rp}) for a boldly exposed sample,

and the crevice repassivation potential (E_{rcrev}) for a creviced sample, depending on the sample geometry).

If transpassive dissolution is the dominant mechanism, the reverse scan does not cross the forward scan; it traces down the forward scan. In the transpassive region, the surface has been depassivated and has been chemically/structurally altered. Thus, the electrochemical characteristics of the alloy specimen are now that of the altered material. As the potential is scanned further in the reverse direction, this altered material becomes passivated.

However, the CPP technique was not always successful in evaluating more recent data obtained mostly on Alloy 22 in concentrated calcium chloride solutions, using a variety of different kinds of specimen geometry. Many of the cyclic polarization curves obtained in high calcium chloride-only solutions at elevated temperatures did not exhibit the same shapes as those observed in the mixed ionic environments. Quite often the shapes of polarization curves obtained in the current investigations differ significantly from the ideal curves, such as those illustrated in ASTM G 61 (ASTM G 61-86 1987) (i.e., Type 304 stainless steel and Ni-base Alloy C-276 in 3.5% NaCl at room temperature). In some of the $CaCl_2$ solutions, polarization curves of Alloy 22 did not appear to show a passive region. This may mean that the alloy is undergoing general corrosion, not localized corrosion.

Another complicating factor that was observed on many of the polarization curves obtained in the mixed ionic environments as well as the calcium chloride solutions was the appearance of one or more 'humps' in the passive region of the forward scan. These are believed due to additional oxidation of one or more of the metallic components in the passive film, and in some cases seem to indicate changes in the morphology and structure of the film, with possible implications on localized corrosion susceptibility. Usually, the hump was not observed in the reverse scan. For some test conditions in which no hump was present in the forward scan, humps were observed in the reverse scan.

There is not an agreement among researchers about the definition of the repassivation potential (E_{rp} or E_{rcrev}) from the CPP tests. Many researchers call the repassivation potential as the potential at which the reverse scan intersects the passive region of the forward scan (or potential at which the forward current density equals reverse current density). A critical potential is not measured for the conditions where there is no positive hysteresis, because no localized corrosion has occurred. However, for conditions where the passive region in the forward scan is not clearly defined, the reverse scan never intersects the forward scan, and/or the reverse scan crosses the forward scan more than once, this approach can be subjective to judgments of individual investigators and result in inconsistent selection of the critical potential values.

The above approach has been shown to produce over-conservative repassivation potential values for Type 304 stainless steel materials in chloride solutions (Akashi et al. 1998). In other studies using the Tsujikawa method (Akashi et al. 1998) and its variation (Jain et al. 2003) (also referred to as a potential step technique), which generally result in more reasonable values for the crevice repassivation potential than the CPP technique, Gruss et al. (1998) used a current density threshold of 1 $\mu A/cm^2$ in selecting the crevice repassivation potential. Later a current density threshold of 2 $\mu A/cm^2$ was used to define the crevice repassivation potential (Jain et al. 2003; Dunn and Brossia 2002; Brossia et al. 2001). However, comparison of the repassivation

potentials of Alloy 22 obtained with different test methods has shown that, when an appropriate criteria was employed in selecting the critical potential value, the repassivation potential obtained with the CPP method was similar to the repassivation potential obtained with the more time-consuming PSP method, the Tsujikawa method, or other similar methods (Jain et al. 2003).

As an alternative approach, a recent study for crevice corrosion behavior of Alloy 22 using the CPP technique and specimens containing multiple crevice assemblies (MCA) used three different current density thresholds to define critical potentials for crevice corrosion initiation and repassivation (Kehler et al. 1999; Scully et al. 1999; Kehler et al. 2001). The potential at which the current density permanently exceeded 1 $\mu A/cm^2$ in the forward scan was selected as a threshold potential to define the crevice corrosion initiation (or crevice stabilization). For the purpose of discussion in this section, this potential is referred to as E_{fl}. The study also used two current density thresholds in the reverse scan to define the repassivation potentials, 10 $\mu A/cm^2$ and 1 $\mu A/cm^2$, and for the purpose of discussion, the correspondingly selected potentials are referred to as E_{r10} and E_{r1} respectively (Kehler et al. 1999; Scully et al. 1999, Section 1.3; Kehler et al. 2001). It was shown that the crevice repassivation potentials were more stable and reproducible than the observed corrosion potential. The results for the crevice corrosion initiation potential were complex and sensitive to many experimental parameters. Especially, for many test conditions, the crevice corrosion initiation was associated with the transpassive dissolution and not associated with crevice corrosion. For the test conditions investigated in the study, the crevice repassivation potential at 1 $\mu A/cm^2$ was likely associated with deactivation of crevice corrosion that resulted from net cathodic electrochemical reactions in the crevice, and not necessarily associated with crevice repassivation. In addition, the crevice repassivation potential at 10 $\mu A/cm^2$ obtained at slow scan rate was more representative of crevice repassivation (Kehler et al. 1999; Kehler et al. 2001).

In most of the CPP scans of highly corrosion resistant alloys, the passive current is on the order of 1 to 10 $\mu A/cm^2$. It is noted that the passive current density is observed to be greater on the reverse scan compared to the initial (or forward) scan because the newly reformed oxides over the crevice site during the reverse scan is thin, defective and support charge transmission at higher rates. Moreover, the solution inside the crevice is acidified from hydrolysis of cations released into the crevice solution during the forward scan (Kehler et al. 1999; Kehler et al. 2001).

After detailed review of the different approaches to obtaining the critical potential for localized corrosion initiation, the repassivation potential approach from CPP tests was chosen for the localized corrosion analysis of the WPOB in this model report. For the data and information collected to date, this approach is most conservative and defensible for the prediction of long-term localized corrosion susceptibility of the WPOB in the proposed repository. As discussed in detail in the following section, only the repassivation potentials of the creviced samples (i.e., crevice repassivation potential, E_{rcrev}) were considered for the localized corrosion model analysis. The same approach (also using crevice samples) was also used by the investigators at the Center for Nuclear Waste Regulatory Analyses (CNWRA) for the Nuclear Regulatory Commission (NRC), and the data were documented in Brossia et al. (2001, Table A-1).

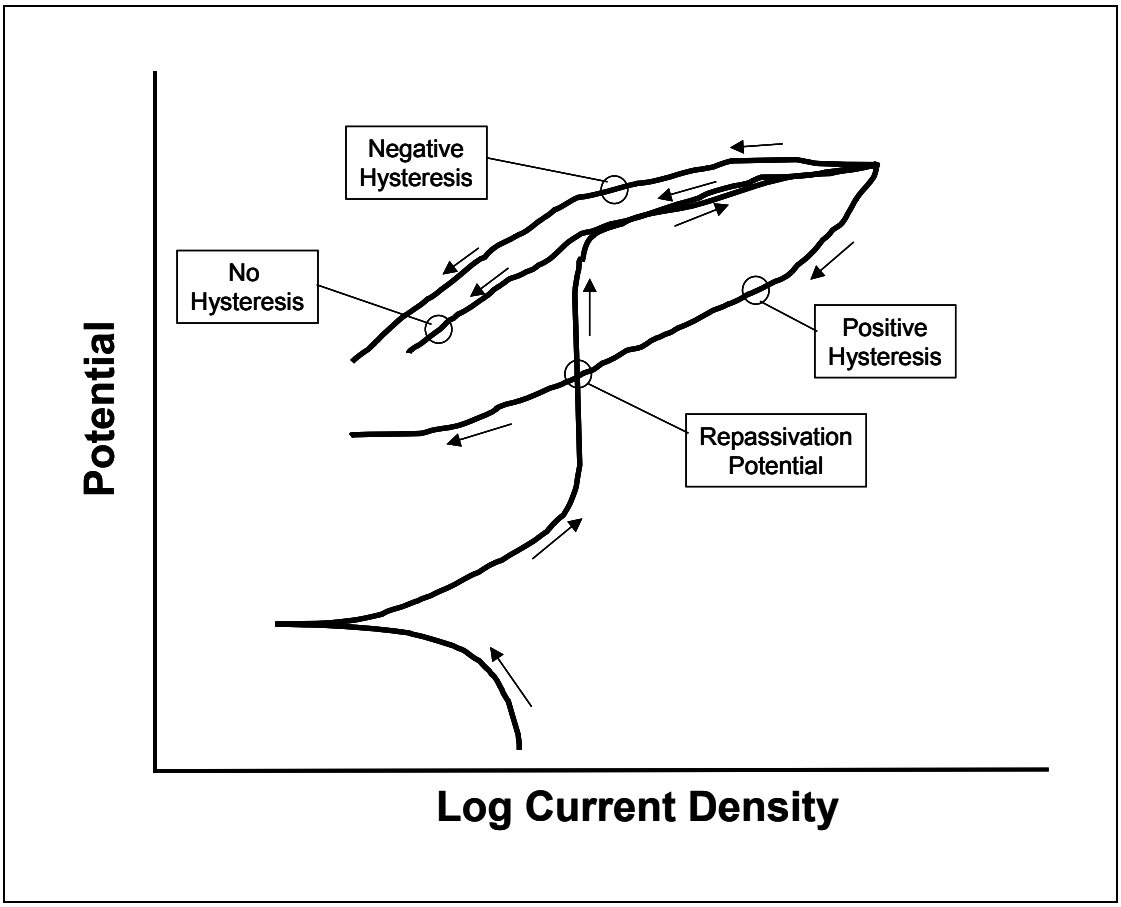

Figure 6-30. Schematic Potentiodynamic Polarization Curve Showing Likely Differing Behaviors of the Curves During Potentiodynamic Scanning of an Alloy with High Resistance to Localized Corrosion.

6.4.4.2 CPP Data Analysis for Crevice Repassivation Potential

A series of the CPP tests were performed for Alloy 22 samples over a wide range of exposure environments including electrolyte solution chemistry and temperature. Also included in the tests were a variety of sample geometries and configurations (i.e., multiple crevice assembly (MCA), rod and disc) and varying metallurgical conditions (i.e., mill annealed, as-welded, and as-welded plus thermally aged).

The CPP tests were performed for a set of simulated environments such as simulated dilute water (SDW), simulated concentrated water (SCW), and simulated acidic water (SAW) at 30, 60, and 90°C. The target compositions of those solutions are given in Table 6-2. The CPP tests also included simpler salt solutions such as NaCl, $CaCl_2$ and $CaCl_2$ + $Ca(NO_3)_2$ solutions and considered a wide range of their concentrations up to near saturation. Detailed descriptions of the electrochemical corrosion test procedures used to generate data for the analysis and model in this model report are provided in Attachment I. The CPP measurements were based on a procedure similar to ASTM G 5-94 (ASTM 1994). Necessary deviations have been noted in the

corresponding controlled SNs. Copies of these Scientific Notebooks (SNs) are available from the Project's database.

Detailed analyses of the CPP test data were performed to obtain the repassivation potentials. Detailed discussions on the data screening analysis and the results are documented in DTN LL030409512251.051. The repassivation potential data reported in DTN LL030409512251.051 were further screened as described below.

As discussed in Section 6.3, the conceptual model considers that contacts of the waste package with the structural components and other materials and mineral deposits from evaporative concentration of the solutions contacting the waste package could form crevices on the waste package surface. Therefore, only the crevice (MCA) sample data were considered for the repassivation potential analysis. The data for non-creviced samples (prisms and discs) were not included in the analysis. All the data included in the critical potential model analysis was crevice repassivation potential (E_{rcrev}). In addition, all the data tested in the LTCTF solutions (SDW, SAW, and SCW) were not included in the analysis as they did not show the occurrence of localized corrosion. The data that were tested in NaCl or $CaCl_2$ solutions but did not show the occurrence of localized corrosion were also not included in the analysis. As discussed in DTN LL030409512251.051, samples that showed abnormal behaviors were also excluded from the analysis. These excluded samples were those whose edges were contaminated and/or damaged during the sample fabrication process and were not subsequently polished so as to remove the affected surface layers.

The CPP test data for high chloride and high temperature conditions with and without nitrate ions in DTN LL030409812251.054 were not included in DTN LL030409512251.051. The missing data are those of Samples DEA598, DEA599, DEA600, DEA3125, and DEA3127. These additional data were analyzed following the same process as that used for the data in DTN LL030409512251.051. The results in terms of the crevice repassivation potential are given in Table 6-7. Because of the limited amount of MCA data for the high chloride and high temperature conditions with nitrate ions, the repassivation potential data for the disc samples (Samples DEA598, DEA599, and DEA600) were also included to improve the data population for the model analysis. Although the MCA and disc samples may have been subjected to different local passive film breakdown mechanisms, there are no significant differences in the repassivation potential between the two types of samples for these conditions. These additional data are included in the crevice repassivation potential database in Attachment VI.

For those salt solutions in Table 6-7, complete dissociation was considered for chloride and nitrate ion concentrations. As noted in Table 6-7 and Attachment VI, pH of the high chloride and high temperature solutions from DTN LL030409812251.054 was not reported. A pH of 4.14 for 5 M $CaCl_2$ solutions at 120 °C from DTN LL030400112251.043 was used for 7 M $CaCl_2$ solutions at 130 °C (Samples DEA3125 and DEA599). Also a measured pH of 5.34 for 5 M $CaCl_2$ plus 0.05 M $Ca(NO_3)_2$ solution at 120 °C from DTN LL030502212251.063 was used for $CaCl_2$ plus $Ca(NO_3)_2$ salt solutions (Samples DEA3127, DEA598 and DEA600). Because pH has a relatively smaller effect on the crevice repassivation potentials than temperature and chloride concentration (see Section 6.4.4.3), impact of the substitute pH values for the high chloride and high temperature solutions should be minor. In addition, Sample DEA3122 was

excluded from the analysis because the molal concentrations for chloride and nitrate ions and pH of the test solution (9 M $CaCl_2$ plus 0.9 M $Ca(NO_3)_2$ solution at 170 °C) were not available.

The crevice repassivation potential data, including those additional data from DTN LL030409812251.054, used for the critical potential model analysis are summarized in Attachment VI. The attachment also provides the test conditions including sample geometry/configuration, metallurgical condition, test temperature and electrolyte composition. For all the data in the attachment, complete dissociation was conservatively assumed for chloride and nitrate ion concentrations of the test solutions.

As discussed above, the investigators at the CNWRA used a similar approach to obtain the crevice repassivation potential data for Alloy 22, and the data were reported in Brossia et al. (2001, Table A-1). The test environments for the reported data are 0.005 M to 4 M chloride concentration and 80 to 150 °C. The data set for the mill annealed and as-welded conditions were used in the critical potential model analysis. The data set is summarized in Attachment VII, along with the test conditions including sample geometry/configuration, metallurgical condition, test temperature and electrolyte composition. For the test solutions, complete dissociation was assumed for the chloride ion concentrations.

Table 6-7 Crevice Repassivation Potentials Obtained from the Additional CPP Data in DTN LL030409812251.054.

Specimen ID	Sample Type	Material Condition	Electrolyte	Temp. (°C)	pH	[Cl] (moles/kg water)	[NO_3] (moles/kg water)	E_{rcrev} (mV, vs. SSC)
DEA598	Disc	MA	6 M $CaCl_2$ + 0.6 M $Ca(NO_3)_2$	120	5.34	16.323	1.640	37
DEA3125	MCA	MA	7 M $CaCl_2$	130	4.14	19.228	0.000	-197
DEA599	Disc	MA	7 M $CaCl_2$	130	4.14	19.228	0.000	-229
DEA3127	MCA	MA	7 M $CaCl_2$ + 0.7 M $Ca(NO_3)_2$	130	5.34	20.815	2.073	32
DEA600	Disc	MA	7 M $CaCl_2$ + 0.7 M $Ca(NO_3)_2$	130	5.34	20.815	2.073	24

Note: 1) MCA = multiple crevice assembly, MA = mill annealed, SSC = silver-silver chloride reference electrode.

2) A pH of 4.14 for 5 M $CaCl_2$ solutions at 120 °C from DTN LL030400112251.043 was used for 7 M $CaCl_2$ solutions at 130 °C (Samples DEA3125 and DEA599). Also a pH of 5.34 for 5 M $CaCl_2$ plus 0.05 M $Ca(NO_3)_2$ solution at 120 °C from DTN LL030502212251.063 was used for $CaCl_2$ plus $Ca(NO_3)_2$ salt solutions (Samples DEA3127, DEA598 and DEA600). All pH values were measured at room temperature.

3) Molal concentrations of chloride and nitrate ions of test solutions are from DTNs LL030703723121.031 and LL030706223121.032..

4) Complete dissociation was assumed for chloride and nitrate ion concentrations.

5) The E_{rcrev} values were obtained from the individual CPP curves following the same process as that used for the data in DTN LL030409512251.051

Source DTN: LL030409812251.054

6.4.4.3 Crevice Repassivation Potential Model for WPOB

As described in Section 6.4.4.1, the WPOB is considered to be subject to localized corrosion when the corrosion potential (E_{corr}) exceeds the crevice repassivation potential (E_{rcrev}), that is,

$$E_{corr} \geq E_{rcrev} \quad \text{(Equation 6-30)}$$

For the WPOB localized corrosion analysis in the post-closure repository environments, the crevice repassivation potential (E_{rcrev}) is expressed as follows.

$$E_{rcrev} = E^{o}_{rcrev} + \Delta E^{NO_3^-}_{rcrev} \quad \text{(Equation 6-31)}$$

where E^{o}_{rcrev} is the crevice repassivation potential in the absence of inhibitive nitrate ions, and $\Delta E^{NO_3^-}_{rcrev}$ is the crevice repassivation potential changes resulting from the inhibiting effect of nitrate ion in solution. Nitrate ion is considered to represent the effect of inhibiting ions present in the solution contacting the WP in the repository.

Development of the crevice repassivation potential model for the WPOB was performed considering a set of multiple regression models as a function of the major exposure environment variables such as temperature, pH, chloride ion concentration and nitrate ion concentration. The molal concentration unit (moles solute per kg water) was employed for the chloride and nitrate ion concentrations in the model development. This was to ensure an internal consistency with the total system performance assessment (TSPA), which also employs the molal concentration unit for the dissolved species. An advantage of using the molal concentrations is that the base of the concentration unit (i.e., mass of water), thus the concentration value, does not change with temperature over the temperature ranges expected in the proposed repository.

The crevice repassivation potential data for Alloy 22 from the Project and CNWRA are listed in Attachments VI and VII respectively. The CNWRA data are from the data compilation reported in Brossia et al. (2001, Table A-1). Because the crevice repassivation potential of both the mill annealed (MA) and as-welded (ASW) Alloy 22 samples behaved similarly, the data for two metallurgical conditions were combined for the model development. Such a negligible effect of welding on the crevice repassivation potential was also observed by the investigators at the CNWRA (Brossia et al. 2001, Section 3.2.2, Figure 3-19). The CNWRA data for the aged samples in the same data compilation table were not considered because of the high aging temperature (870 °C) employed for the sample preparation. The dominant secondary phase that forms at the above aging temperature, and is responsible for degradation of the corrosion resistance of the alloy, is σ phase, which is stable between 800 °C and 930 °C and forms rapidly (BSC 2003a, Section 6.6.1.1, Figures 76 and 77). The tetrahedrally closed-pack (TCP) phases that are more relevant to the repository conditions are P and μ phases, which are stable over a wider temperature range, (the lower bound down to a much lower temperature) than σ phase (BSC 2003a, Section 6.6.1.1, Figures 76 and 77). However, their formation kinetics are extremely slow at the temperatures that the waste packages are expected to experience in the proposed repository (BSC 2003a, Section 8.0).

6.4.4.3.1 Crevice Repassivation Potential Model in Absence of Inhibitive Nitrate Ions

Among the functional forms that were considered, the following empirical functional form was considered to adequately describe the relationship between the crevice repassivation potential of

the mill-annealed and as-welded Alloy 22 and the test environment parameters in the absence of inhibiting nitrate ions.

$$E^{o}_{rcrev} = a_o + a_1 T + a_2 pH + a_3 \log([Cl^-]) + a_4 T \times \log([Cl^-]) \qquad \text{(Equation 6-32)}$$

where E^{o}_{rcrev} is the crevice repassivation potential in the absence of inhibiting nitrate ions, a_o, a_1, a_2, a_3, and a_4 are constants, T is the temperature (°C), and $[Cl^-]$ is the chloride ion concentration in molality (m, moles/kg water).

The above functional form is similar to that for the crevice repassivation potential of Alloy 22 proposed by Brossia et al. (2001, Section 3.2.2). Dependence of the critical potential on a logarithmic form of chloride concentration and a linear form of temperature were also used to model the critical potential by other investigators (Brossia et al. 2001, Section 3.2.2; Frankel 1998; Frankel 2002; Kehler et al. 2001). The pH was not included in the functional forms from the above investigators because of a weak dependence of the critical potential on pH. Relatively narrow pH ranges of the data used by the investigators may have caused a problem in quantifying the pH effect. However, a reasonable pH range (pH 4.1 to 8, see Attachments VI and VII) of the database used in the current analysis allowed quantification of the pH effect. As will be discussed in Section 6.4.4.6, the crevice repassivation model results for the relatively weaker effect of pH than temperature and chloride concentration (see Figure 6-51 and Figure 6-52) are consistent with the observations by other investigators.

Using the method of least squares, the above functional form was fitted to the crevice repassivation potential data for the mill annealed and as-welded conditions in Attachments VI and VII. The model fitting was performed using Mathcad 2000 Professional, and the Mathcad worksheet for the model fitting is given in the output DTN SN0308T0506303.003 of this model report. The value of the coefficients and their uncertainty (±1 standard deviation) of the model parameters from the fitting were determined to be: $a_0 = 214.089 \pm 46.880$, $a_1 = -3.696 \pm 0.476$, $a_2 = 25.284 \pm 5.641$, $a_3 = -252.181 \pm 53.912$, and $a_4 = 1.414 \pm 0.547$. The covariance matrix resulting from the fitting procedure was determined to be:

$$CV = \begin{bmatrix} 2.198\times10^{3} & -1.516\times10^{1} & -8.325\times10^{1} & -1.805\times10^{3} & 1.590\times10^{1} \\ -1.516\times10^{1} & 2.267\times10^{-1} & -1.240\times10^{0} & 1.877\times10^{1} & -1.996\times10^{-1} \\ -8.325\times10^{1} & -1.240\times10^{0} & 3.183\times10^{1} & -3.237\times10^{1} & 7.425\times10^{-1} \\ -1.805\times10^{3} & 1.877\times10^{1} & -3.237\times10^{1} & 2.907\times10^{3} & -2.867\times10^{1} \\ 1.590\times10^{1} & -1.996\times10^{-1} & 7.425\times10^{-1} & -2.867\times10^{1} & 2.995\times10^{-1} \end{bmatrix}$$

(Equation 6-33)

The correlation coefficient R for the fit is 0.872, and the coefficient of determination R^2 is 0.760. R^2 is the ratio of the measures of variation explained by the regression model to the total

variation present in the output variable under consideration. Values of R^2 vary between 0 (no variation explained and a very poor regression model) to 1 (perfect explanation of the model variation by the regression model). With the measure of a R^2 value of 0.760, the regression model fits the experimental data reasonably well.

Spreads of the crevice repassivation potential data for a given test condition are due mostly to the uncertainties associated with the test procedures and selection criteria and process for the crevice repassivation potentials, in addition to some randomness in the localized corrosion process. Therefore the entire variance of the model is due to uncertainty. ASTM G 61 (ASTM G 61-86 1987) specifies that, *when the standard procedure for the CPP measurements is followed, an investigator's data should fall within the range of ±2 standard deviations of the mean because this includes 95 % of all data provided random variations are the only source of error*. Therefore it is recommended that the uncertainty of the parameter coefficients of the above model be limited to ±2 standard deviations. As discussed before, the approach and criteria for obtaining the crevice repassivation potentials from the CPP curves are already highly conservative, therefore bounding the uncertainty of the model parameters to ± 2 standard deviations is sufficient to capture the model uncertainty.

It is recommended that for the waste package degradation analysis, variability in the crevice repassivation potential among waste packages be represented by the temporally and spatially varying waste package temperature and chemistry of water contacting the waste package. In addition the chemistry of water contacting waste package may vary depending on the thermal and hydrologic condition on the waste package surface, for example, drip condition vs. no-drip condition. For no-drip condition, the chemistry of water film forming on the waste package surface would be determined by the interactions of the chemical constituents in the dust on the surface with the water vapor in the humid-air around the waste package.

The model results and the Project's data are shown as a function of temperature and chloride concentration in Figure 6-31 and Figure 6-32 respectively. Note the model results are for the average values of the test environment parameters (temperature, chloride concentration and pH) of the source data. The E_{rcrev} data for the test conditions that are off the average values are therefore not bound within ±2 standard deviations of the model mean.

As shown in Figure 6-31, the crevice repassivation potential is a strong function of temperature and a relativity weaker function of chloride concentration. This strong dependence of the crevice repassivation potential of Alloy 22 on temperature was also reported by others (Brossia et al. 2001, Section 3.2.2; Kehler et al. 2001). A logarithmic dependence of the crevice repassivation potential on chloride concentration (Figure 6-32) shows that the crevice repassivation potential decreases rapidly with chloride concentration for the low chloride concentration range, and the dependence becomes weaker as the chloride concentration increases. Although not shown here, it is seen from the value of the pH term coefficient that the crevice repassivation potential is a weak function of pH.

The model results and the CNWRA data are shown as a function of temperature and chloride concentration in Figure 6-33 and Figure 6-34 respectively. As for the Project's data discussion above, the model results are for the average values of the test environment parameters (temperature, chloride concentration and pH) of the source data. The E_{rcrev} data for the test

conditions that are off the average values are therefore not bound within ±2 standard deviations of the model mean. The behavior of the crevice repassivation potential data from CNWRA and their dependence on temperature and chloride concentration are consistent with the Project's data.

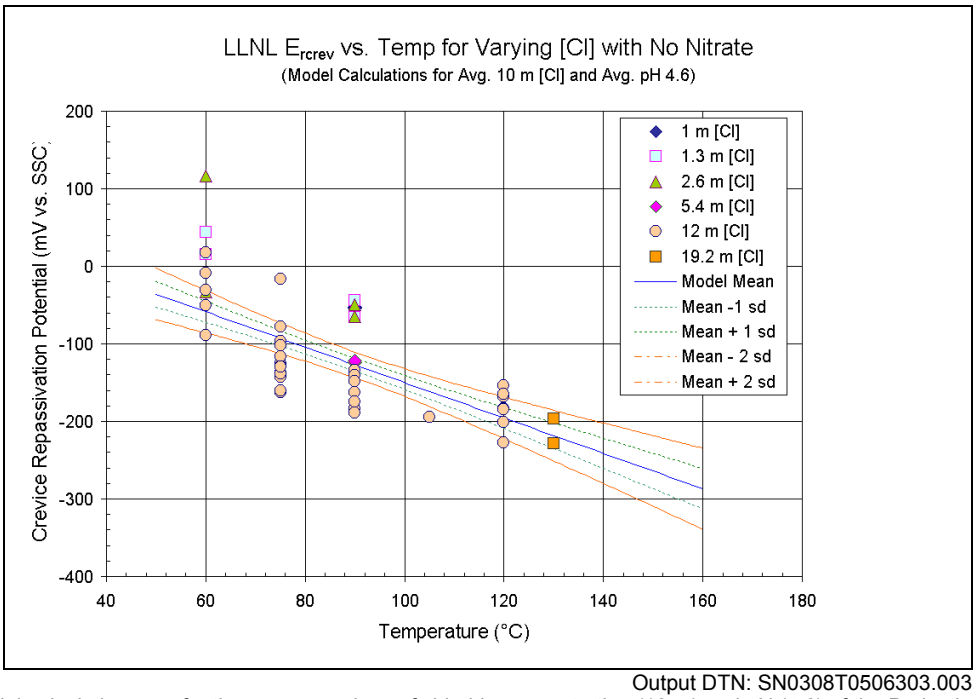

Output DTN: SN0308T0506303.003

Note: The model calculations are for the average values of chloride concentration (10 *m*) and pH (4.6) of the Project's crevice repassivation potential data used for the model development.

Figure 6-31. Model Results and Project's Experimental Data for the Crevice Repassivation Potential of the WPOB in Absence of Inhibiting Nitrate Ion As a Function of Temperature.

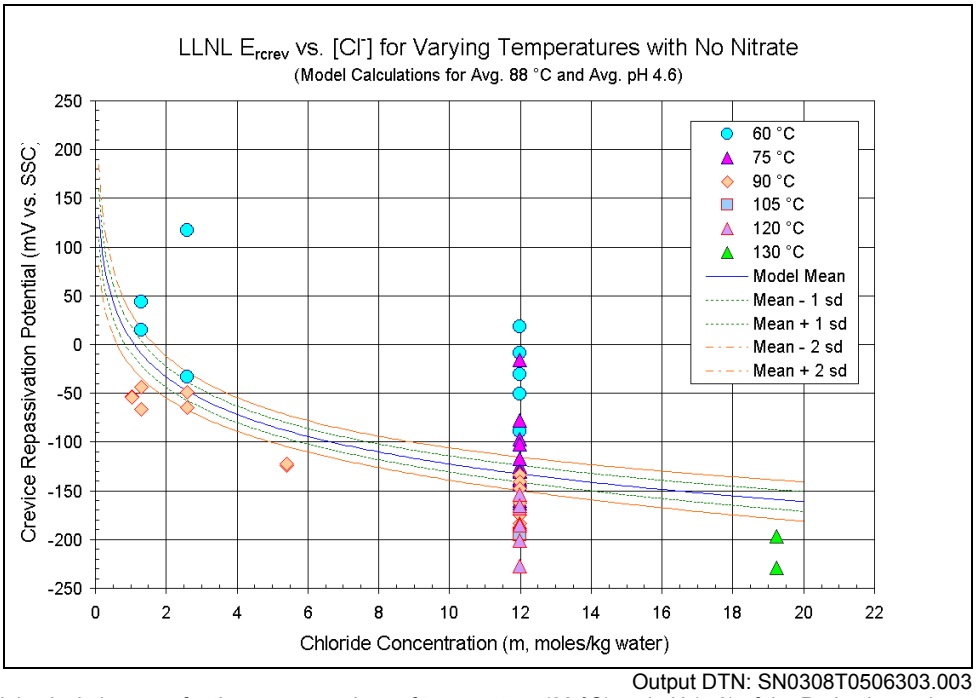

Output DTN: SN0308T0506303.003

Note: The model calculations are for the average values of temperature (88 °C) and pH (4.6) of the Project's crevice repassivation potential data used for the model development.

Figure 6-32 .Model Results and Project's Experimental Data for the Crevice Repassivation Potential of the WPOB in Absence of Inhibiting Nitrate Ion As a Function of Chloride Concentration.

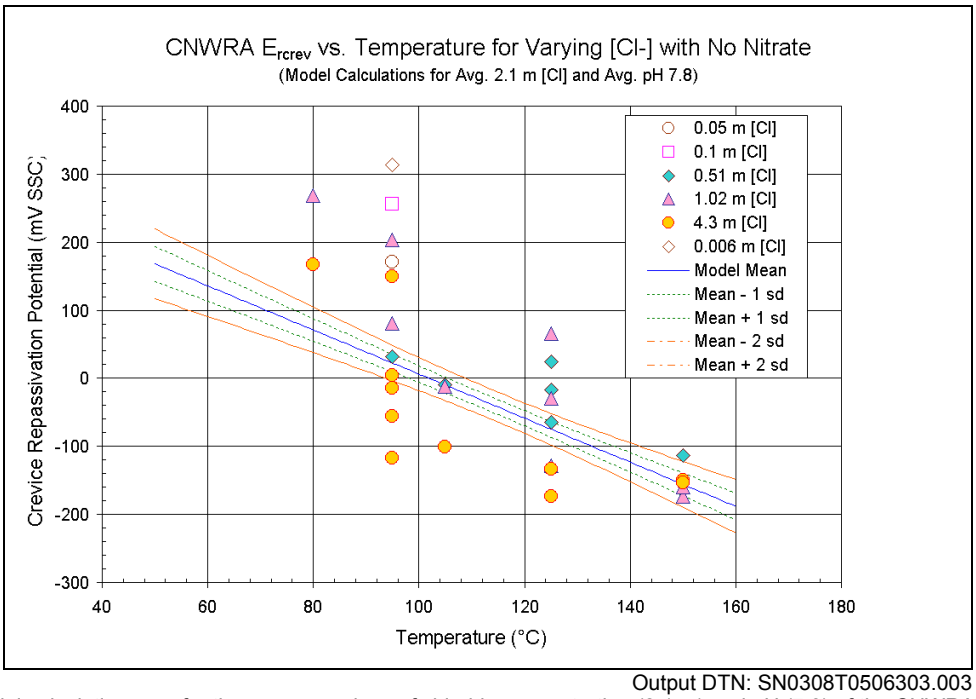

Output DTN: SN0308T0506303.003

Note: The model calculations are for the average values of chloride concentration (2.1 *m*) and pH (7.8) of the CNWRA's crevice repassivation potential data used for the model development.

Figure 6-33. Model Results and CNWRA's Experimental Data for the Crevice Repassivation Potential of the WPOB in Absence of Inhibiting Nitrate Ion As a Function of Temperature.

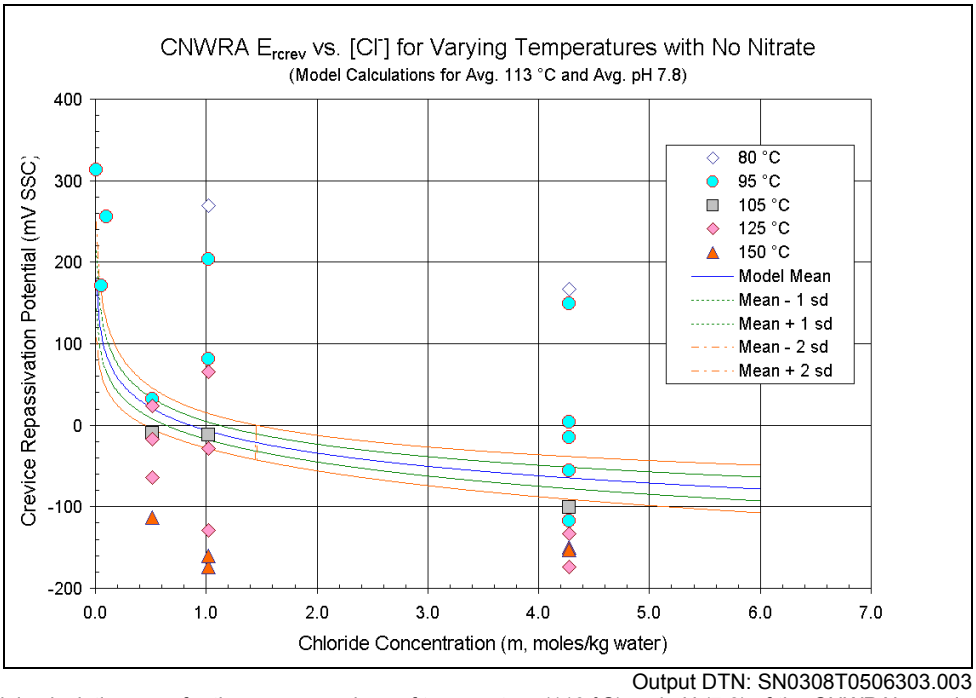

Output DTN: SN0308T0506303.003

Note: The model calculations are for the average values of temperature (113 °C) and pH (7.8) of the CNWRA's crevice repassivation potential data used for the model development.

Figure 6-34. Model Results and CNWRA's Experimental Data for the Crevice Repassivation Potential of the WPOB in Absence of Inhibiting Nitrate Ion As a Function of Chloride Concentration.

6.4.4.3.2 Crevice Repassivation Potential Changes in Presence of Inhibitive Nitrate Ions

The crevice repassivation potential data in Attachment VI clearly show that the presence of inhibitive nitrate ion raises the threshold potential, thus providing additional margin against localized corrosion susceptibility. The quantitative measure of the beneficial effect employed in the current model analysis is the difference ($\Delta E_{rcrev}^{NO_3^-}$) in the crevice repassivation potentials with and without the inhibitive nitrate ion for the same chloride concentration and temperature. The analysis steps and resulting values for $\Delta E_{rcrev}^{NO_3^-}$ are given in Table 6-8.

Among the functional forms that were considered, the following functional form was considered to adequately describe the effect of nitrate ion on the crevice repassivation potential.

$$\Delta E_{rcrev}^{NO_3^-} = b_o + b_1[NO_3^-] + b_2 \frac{[NO_3^-]}{[Cl^-]} \qquad \text{(Equation 6-34)}$$

where $\Delta E_{rcrev}^{NO_3^-}$ is the change of the crevice repassivation potential due to the inhibitive nitrate ion, $[Cl^-]$ is the chloride ion concentration in molality (m, moles/kg water), $[NO_3^-]$ is the nitrate ion concentration in molality (m, moles/kg water), and b_o, b_1 and b_2 are constant. Using the method of least squares, the above functional form was fitted to the $\Delta E_{rcrev}^{NO_3^-}$ data in Table 6-8. The model fitting was performed using Mathcad 2000 Professional, and the Mathcad worksheet for the model fitting is provided in the output DTN SN0308T0506303.003 of this model report.

The parameter coefficients and their uncertainty (±1 standard deviation) resulting from the fitting procedure were determined to be: $b_0 = $ -50.959 ± 78.168, $b_1 = 115.867 \pm 64.714$, and $b_2 = 1045 \pm 1320.076$. The covariance matrix resulting from the fitting procedure was determined to be:

$$CV = \begin{bmatrix} 6.110\times10^3 & 3.017\times10^2 & -6.712\times10^4 \\ 3.017\times10^2 & 4.188\times10^3 & -6.264\times10^4 \\ -6.712\times10^4 & -6.264\times10^4 & 1.743\times10^6 \end{bmatrix} \qquad \text{(Equation 6-35)}$$

The correlation coefficient R for the fit is 0.848, and the coefficient of determination R^2 is 0.719. With the measure of a R^2 value of 0.719, the regression model fits the experimental data fairly well.

In the above model, the effect of the interaction of the competing aggressive ion (chloride ion) and inhibitive nitrate ion on the crevice repassivation potential is represented with the ratio of the concentrations of the two competing ions and the concentration of nitrate ion. As discussed below, there is a linear relationship between $\Delta E_{rcrev}^{NO_3^-}$ and the concentration ratio. Therefore, in the current model analysis, the same linear relationship was considered for the conditions with the ratio greater than 0.1 and to be applicable to a maximum of 1.0. In addition, because the effect of the measurement uncertainty of the CPP tests has already been captured in the crevice

repassivation potential model with no nitrate ion present, it is recommended that the mean value of the $\Delta E_{rcrev}^{NO_3^-}$ model be used to determine the crevice repassivation potential (E_{rcrev}) using Equation (6-30).

It is recommended that for the waste package degradation analysis in the repository, variability in $\Delta E_{rcrev}^{NO_3^-}$ among waste packages be represented by the temporally and spatially varying nitrate and chloride ion concentrations of water contacting the waste package. In addition, the chemistry of water contacting the waste packages may vary depending on the thermal and hydrologic condition on the waste package surface. For example, drip condition vs. no-drip condition. For the no-drip condition, the chemistry of a water film forming on the waste package surface would be determined by the interactions of the chemical constituents in the dust on the surface with the water vapor in the humid-air around the waste package.

The model results and the $\Delta E_{rcrev}^{NO_3^-}$ data are shown in Figure 6-35. Note that the model results are for the average chloride concentration of 12.5 *m* of the source data. The $\Delta E_{rcrev}^{NO_3^-}$ data for the test conditions that are off the average values are therefore not bound within ± 2 standard deviations of the model mean.

Table 6-8. Analysis Summary for the Crevice Repassivation Potential Changes ($\Delta E_{rcrev}^{NO_3^-}$) Due to Inhibitive Nitrate Ions.

Specimen ID	Sample Type	Material Condition	Electrolyte	Temp (°C)	pH	[Cl] (moles/kg water)	[NO_3] (moles/kg water)	[NO_3]/[Cl] Ratio	E_{rcrev} (mV, vs. SSC)	Avg. E_{rcrev} w/o NO_3 (mV SSC)	$\Delta E_{rcrev}(NO_3)$ (mV SSC)
DEA3182	MCA	MA	1.25M CaCl2	60	5.83	2.582	0.000		117		
DEA3183	MCA	MA	1.25M CaCl2	60	5.83	2.582	0.000		-33	42	
DEA3105	MCA	MA	1.25 M CaCl2+ 0.0125 M Ca(NO3)2	60	6.47	2.570	0.026	0.010	61		**19**
DEA3184	MCA	MA	1.25M CaCl2	90	5.83	2.582	0.000		-65		
DEA3185	MCA	MA	1.25M CaCl2	90	5.83	2.582	0.000		-49	-57	
DEA3109	MCA	MA	1.25 M CaCl2+ 0.125 M Ca(NO3)2	90	6.41	2.612	0.263	0.101	-72		**-15**
DEA3167	MCA	MA	5 M CaCl2	105	4.45	11.988	0.000		-195		
DEA3168	MCA	MA	5 M CaCl2	105	4.45	11.988	0.000		-194	-195	
DEA3123	MCA	MA	5 M CaCl2 + 0.5 M Ca(NO3)2	105	4.86	12.593	1.264	0.100	108		**303**
DEA3124	MCA	MA	5 M CaCl2 + 0.5 M Ca(NO3)2	105	4.86	12.593	1.264	0.100	133		**328**
DEA3208	MCA	MA	5 M CaCl2	120	5.03	11.988	0.000		-168		
DEA3209	MCA	MA	5 M CaCl2	120	5.03	11.988	0.000		-154		
DEA3234	MCA	MA	5 M CaCl2	120	4.14	11.988	0.000		-168		
DEA3235	MCA	MA	5 M CaCl2	120	4.14	11.988	0.000		-227		

Specimen ID	Sample Type	Material Condition	Electrolyte	Temp (°C)	pH	[Cl] (moles/kg water)	[NO_3] (moles/kg water)	[NO_3]/[Cl] Ratio	E_{rcrev} (mV, vs. SSC)	Avg. E_{rcrev} w/o NO_3 (mV SSC)	$\Delta E_{rcrev}(NO_3)$ (mV SSC)
DEA3237	MCA	MA	5 M CaCl2	120	4.14	11.988	0.000		-201		
JE0022	MCA	ASW	5 M CaCl2	120	5.03	11.988	0.000		-184		
JE0034	MCA	ASW	5 M CaCl2	120	4.14	11.988	0.000		-165		
JE0035	MCA	ASW	5 M CaCl2	120	4.14	11.988	0.000		-184		
JE0036	MCA	ASW	5 M CaCl2	120	4.14	11.988	0.000		-185	-182	
JE0024	MCA	ASW	5 M CaCl2 + 0.05 M Ca(NO3)2	120	5.34	11.699	0.119	0.010	-264		**-82**
DEA598	Disc	MA	6 M CaCl2 + 0.6 M Ca(NO3)2	120	5.34	16.323	1.640	0.100	37		**219**
DEA3125	MCA	MA	7 M CaCl2	130	4.14	19.228	0.000		-197		
DEA599	Disc	MA	7 M CaCl2	130	4.14	19.228	0.000		-229	-213	
DEA3127	MCA	MA	7 M CaCl2 + 0.7 M Ca(NO3)2	130	5.34	20.815	2.073	0.100	32		**245**
DEA600	Disc	MA	7 M CaCl2 + 0.7 M Ca(NO3)2	130	5.34	20.815	2.073	0.100	24		**237**

Note: (a) MCA = multiple crevice assembly, MA = mill annealed, ASW = as-welded.

(b) avg. E_{rcrev} is the average of the crevice repassivation potentials with no nitrate ion present.

(c) ΔE_{rcrev} for a given chloride concentration and temperature was obtained by subtracting the average crevice repassivation potential with no nitrate ion present from the crevice repassivation potential with nitrate ion present.

Output DTN: SN0308T0506303.003

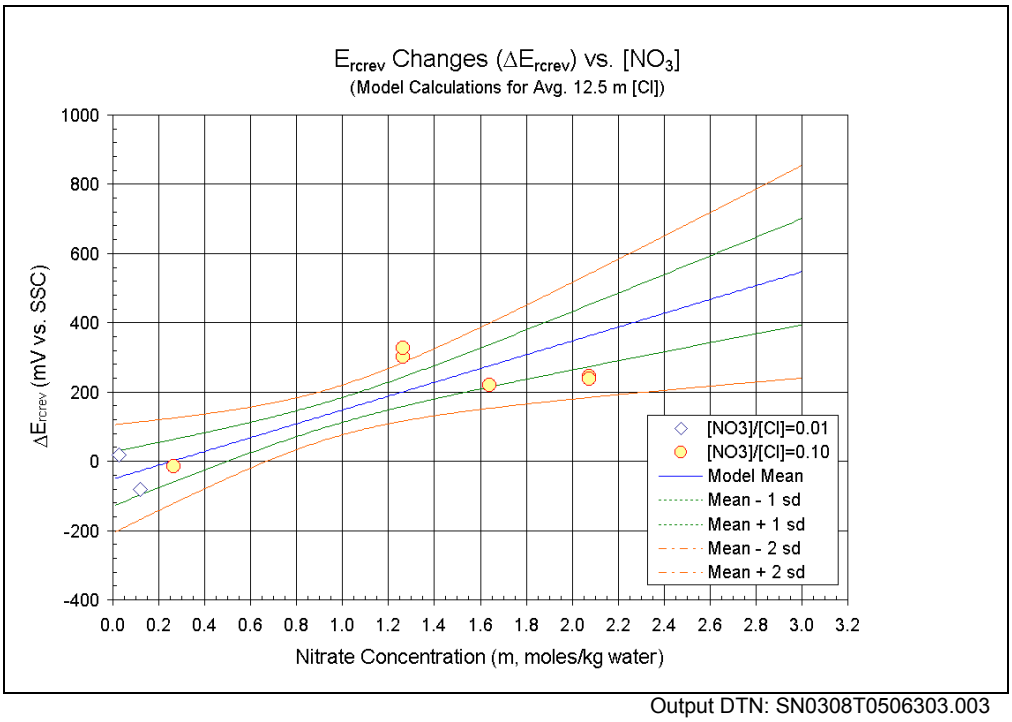

Output DTN: SN0308T0506303.003

Note: The model calculations are for the average values of chloride concentration (12.5 *m*) of the Project's crevice repassivation potential data used for the model development.

Figure 6-35. Model Results and Project's Experimental Data for the Crevice Repassivation Potential Changes of the WPOB in Presence of Inhibiting Nitrate Ions As a Function of Nitrate Ion Concentration.

6.4.4.4 Long-Term Open-Circuit Corrosion Potential Data Analysis

Because the corrosion potential of Alloy 22 may change over time, it is important to know the most probable value of long-term corrosion potential (E_{corr}) for Alloy 22 under different environmental conditions to evaluate the localized corrosion susceptability of the WPOB in the proposed repository. As discussed above, the localized corrosion initiation model of the WPOB considers that localized corrosion will only occur when E_{corr} is equal to or greater than a critical potential (crevice repassivation potential (E_{rcrev}) in the current model analysis). That is, if $E_{corr} < E_{rcrev}$, general or passive corrosion will occur. Passive corrosion rates are expected to be exceptionally low.

The specimens used to evaluate E_{corr} of Alloy 22 as a function of immersion time were machined from sheet and bar stock. There were two main groups of specimens, (1) Welded U-bend specimens and (2) Untested rod specimens. Approximately half of the U-bend specimens tested for long-term corrosion potential were from the Long Term Corrosion Test Facility (LTCTF), and the other half of the U-bend specimens were not previously exposed to any electrochemical test condition. The U-bend specimens from the LTCTF already had the passive film and other surface alterations from the exposure in the LTCTF. The U-bend specimens were tested in the as-received (AR) or as-machined conditions, which corresponded to a root mean square roughness of 32 µ-inch. The U-bend specimens were fabricated from ¾-inch (19.05 mm) wide and 1/16-inch (1.588 mm) thick metal strips according to ASTM G 30 (ASTM G 30-94 1994). The specimens were degreased in acetone and alcohol before testing. During the long-term open-

circuit corrosion potential monitoring, the U-bend specimens were fully immersed in the electrolyte of interest. The rod specimens were all previously untested. Rod specimens were ¼ inch (6.35 mm) in diameter and 12 inches (304.8 mm) long. They were polished with 600-grit paper and degreased with acetone and alcohol before testing. The data and test details reported in the source DTN LL020711612251.017 are summarized in Attachment V.

Alloy 22 specimens tested are listed in Attachment V. The samples are designated either DUB or DEA followed by three or four digits. The letter D stands for Alloy 22, the second letter stands for the type of sample, that is, U for U-bend specimen and E for electrochemical (or rod) specimen. The third letter could be either an A (mill annealed or not welded) or B (contains weld material).

Ten different electrolyte solutions were used in the tests (see Attachment V for the type of solutions tested). This included four multi-ionic solutions and six simpler salt solutions. The solutions from the LTCTF tanks (i.e., SDW, SAW and SCW) are referred to as "aged" solution (approximately 4.5-year old). The solutions that were freshly prepared (not from the LTCTF tanks) are referred to as "fresh" solution. In some solutions, more than one temperature was used for testing. The combination of tests totaled sixteen different conditions or cells (see Attachment V).

Chloride and nitrate ion concentrations of SAW, SCW, SDW and BSW solutions are the target values of the solutions from DTN LL000320405924.146 (see Table 6-2). That is, they are not measured compositions, and the actual compositions may vary significantly because of other experimental factors. For simpler salt solutions ($CaCl_2$ and $CaCl_2$-$Ca(NO_3)_2$ solutions), complete dissociation is assumed for chloride and nitrate ion concentrations. The pH of all the test solutions was measured at the room temperature and was documented in DTN LL030201212251.033.

The volume of the electrolyte solution in each cell was 2 liters. The electrolyte solutions were naturally aerated; that is, the solutions were not purged, but a stream of air was circulated above the level of the solution. This stream of air exited the vessel through a condenser to avoid evaporation of the electrolyte. The electrochemical potentials are reported in the saturated silver chloride scale (SSC). At ambient temperature, the SSC scale with the reference electrode in a saturated KCl solution is 199 mV more positive than the standard hydrogen electrode (SHE) (Sawyer and Roberts 1974, pages 39 to 45, Table 2-4).

Long-term corrosion potential behaviors of some selected Alloy 22 samples in the SDW, SAW and SCW solutions from the LTCTF tanks are shown in Figure 6-36. The figure shows that after initial changes, the corrosion potentials of the Alloy 22 samples become stable after about 100 days of testing. It is shown that the results of the welded U-bend samples (Samples DUB052 and DUB159) and (non-welded) rod samples (Samples DEA2850, DEA2851 and DEA2852) in aged SAW at 90 °C show no significant differences in their long-term open-circuit corrosion potential behaviors.

The values of E_{corr} of Alloy 22 in SAW (an acidic solution) are higher than those in other aged LTCTF solutions. The apparent steady state E_{corr} values of Alloy 22 in SAW at 60 and 90°C are in the order of 300 to 400 mV vs. SSC. Figure 6-37 compares the long-term corrosion potential

evolution of freshly polished Alloy 22 rods in freshly prepared SAW at 90 °C with the corrosion potential evolution of the welded U-bend and rod samples in aged SAW at 90 °C. Because of the long-term nature of the tests, the reference electrodes had to be replaced regularly during the tests due to their operations outside the specified accuracy range. The reference electrode replacements are indicated in the figure. Initially the Alloy 22 rods in the fresh SAW solution had the corrosion potential on the order of about –150 mV vs. SSC. However, over approximately 100 days of testing, the corrosion potential increased rapidly to a more noble potential value of approximately 330 mV vs. SSC. This apparent stable corrosion potential was maintained over the balance of the approximately 300-day test, slowly reaching a maximum value near 400 mV vs. SSC. This high value of E_{corr} is probably due to the formation of a more protective chromium rich oxide film on the Alloy 22 electrodes. The test results show that, regardless of the initial condition of the metal surface or the age of the electrolyte solution, eventually Alloy 22 undergoes ennoblement in SAW. This ennoblement is probably promoted by both the pH value and the presence of nitrate in the solution (Estill et al. 2003). Such an ennoblement of Alloy 22 with time has also been reported recently, and the ennoblement was more significant in acidic solutions (Jayaweera et al. 2003, Figures 9.12 and 9.13; Dunn et al. 2003, Figures 8 and 9).

In addition, the results in Figure 6-36 show that the E_{corr} values of Alloy 22 rods in SAW at 25 °C are lower than the values at 90 °C by about 150 mV. A similar trend is also observed for the welded U-bend samples in the SDW solutions. This effect could be attributed to kinetic mechanisms either in the behavior of the oxide film or on the redox reactions in solution. The temperature effect in the SCW solution was not evaluated because the tests at 60 °C were terminated early.

Figure 6-38 shows the test results for the E_{corr} behavior of Alloy 22 in $CaCl_2$ solutions with varying chloride concentrations and the effect of the addition of nitrate. The data show that E_{corr} of Alloy 22 in the $CaCl_2$ solutions is affected mostly by the chloride concentration, and addition of nitrate ions slows down the process to attain steady state. E_{corr} for Alloy 22 in 5 M $CaCl_2$ solution at 120 °C reached steady state in less than 50 days. The average values of E_{corr} after more than 300 days of testing were –129 mV vs. SSC (see Attachment V for the numerical values of the data). A sudden jump of the data at the beginning of the tests in 5 M $CaCl_2$ solution at 120 °C is probably due to the presence of gas bubbles inside the Luggin capillary probe connected to the reference electrode. The gas bubbles may have been trapped inside the probe during the elevated temperature tests and would have interrupted the electrical conductivity necessary for potential measurements.

After approximately 100 days of testing, the E_{corr} values for Alloy 22 in 5 M $CaCl_2$ solutions with nitrate added seemed to be approaching a steady state value. The average value of E_{corr} for Alloy 22 in 5 M $CaCl_2$ + 0.05 M $Ca(NO_3)_2$ solution at 90 °C was -39 mV vs. SSC after 100 days of testing. This solution represents a nitrate to chloride ratio of 0.01. A similar behavior was observed for Alloy 22 tested in 5 M $CaCl_2$ + 0.5 M $Ca(NO_3)_2$ solution (nitrate to chloride ratio of 0.1) at 90 °C, and the average E_{corr} value was –46 mV vs. SSC. For Alloy 22 electrodes immersed in 1 M $CaCl_2$ + 1 M $Ca(NO_3)_2$ solution (nitrate to chloride ratio of 1) at 90°C, it appears that, after 120 days of testing, the E_{corr} values had approached a steady state value, and the average E_{corr} value was 168 mV vs. SSC.

Figure 6-39 shows the steady state open-circuit potentials (or corrosion potentials) of all the Alloy 22 samples (those shown in the previous figures plus the rest of the data in the input DTN LL020711612251.017), as a function of chloride concentration. The figure shows that the sample geometry or configuration and the metallurgical condition have negligible effect on the long-term steady-state corrosion potential of Alloy 22. It is shown that the steady state corrosion potential decreases with chloride concentration, which is consistent with the fact that higher chloride concentration makes the metal more active. Also, part of the potential decrease with chloride concentration may be due to the 'salting out effect' because the dissolved oxygen decreases with increasing salt concentration.

As discussed later in the model analysis section, the steady-state corrosion potential is affected significantly by the solution pH.

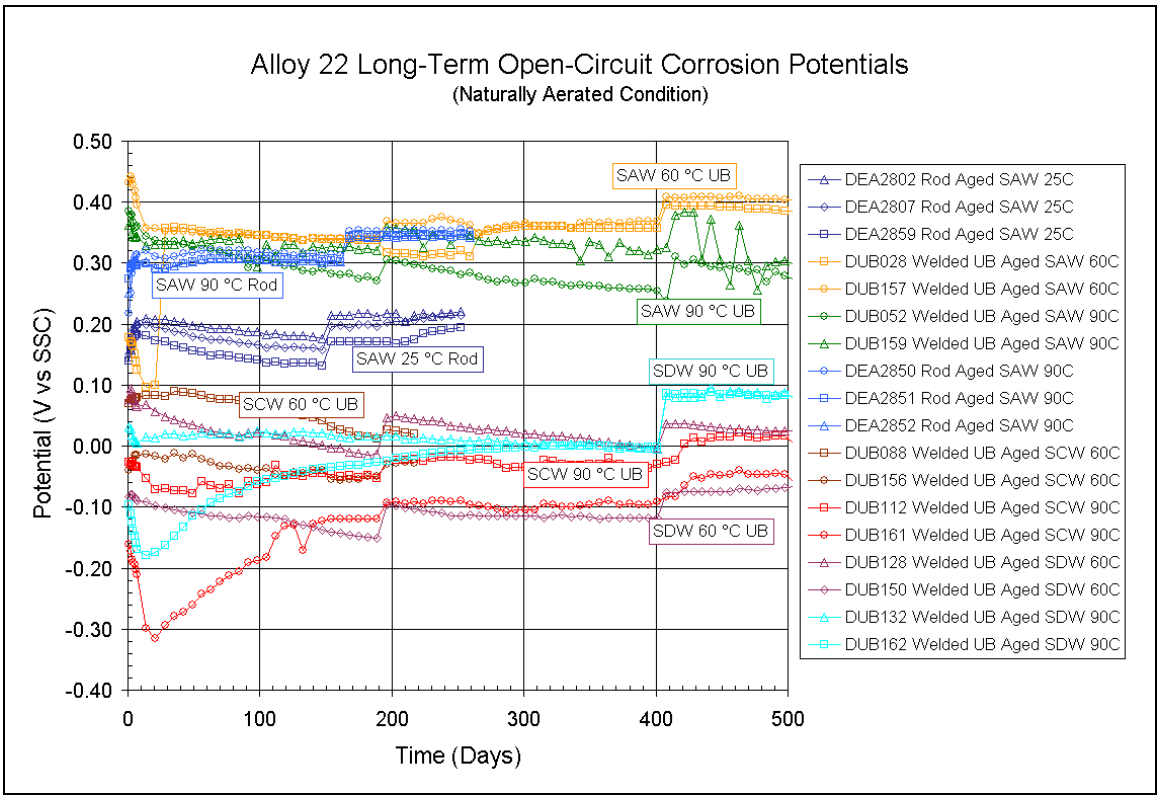

Output DTN: SN0308T0506303.003

Figure 6-36. Open-Circuit Corrosion Potential of Alloy 22 samples As a Function of Time in `Different Types of LTCTF Solutions.

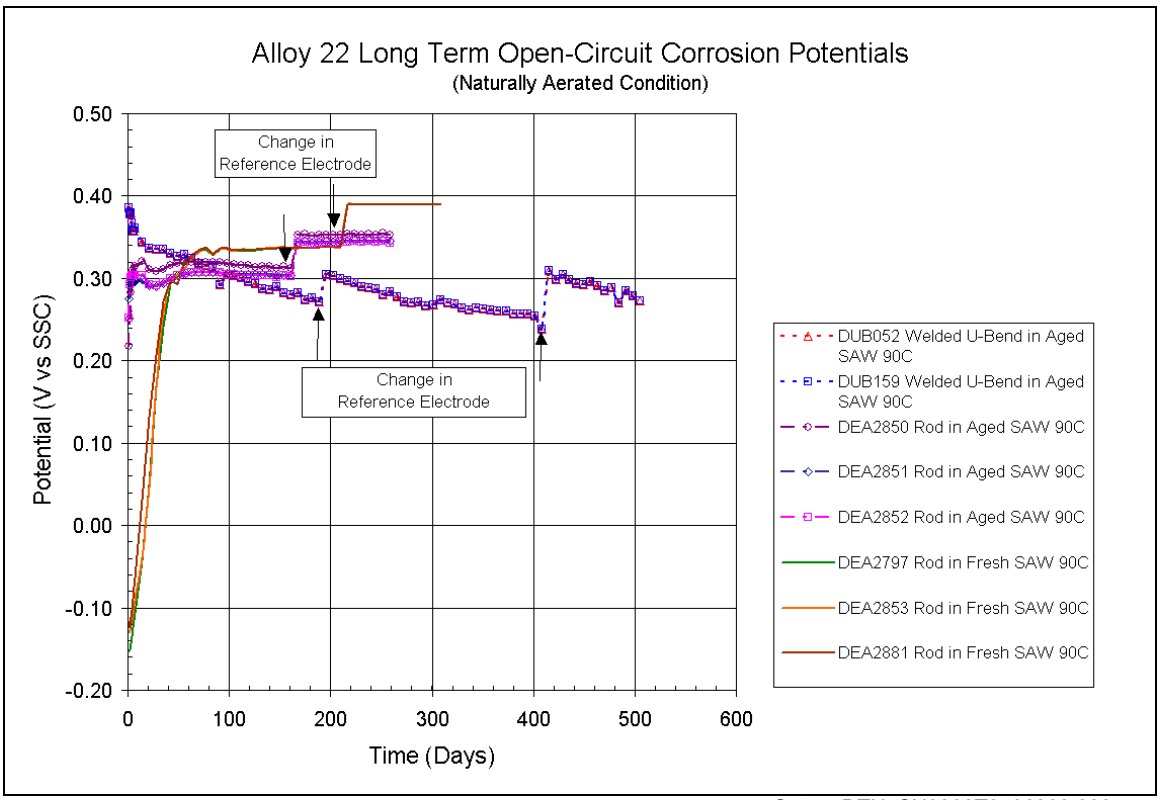

Output DTN: SN0308T0506303.003

Figure 6-37. Open-Circuit Corrosion Potential of Alloy 22 samples As a Function of Time in Differing Conditions of SAW Solutions.

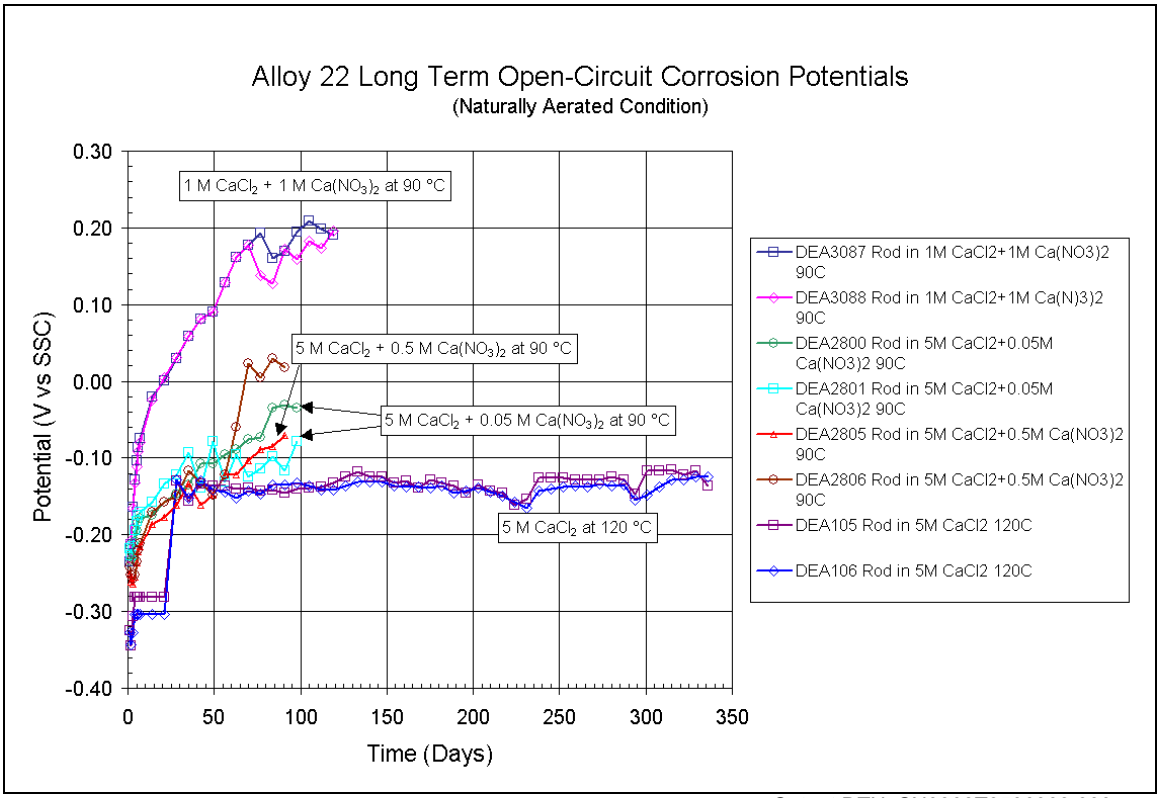

Output DTN: SN0308T0506303.003

Figure 6-38. Open-Circuit Corrosion Potential of Alloy 22 samples As a Function of Time in Differing Concentrations of $CaCl_2$ Solutions.

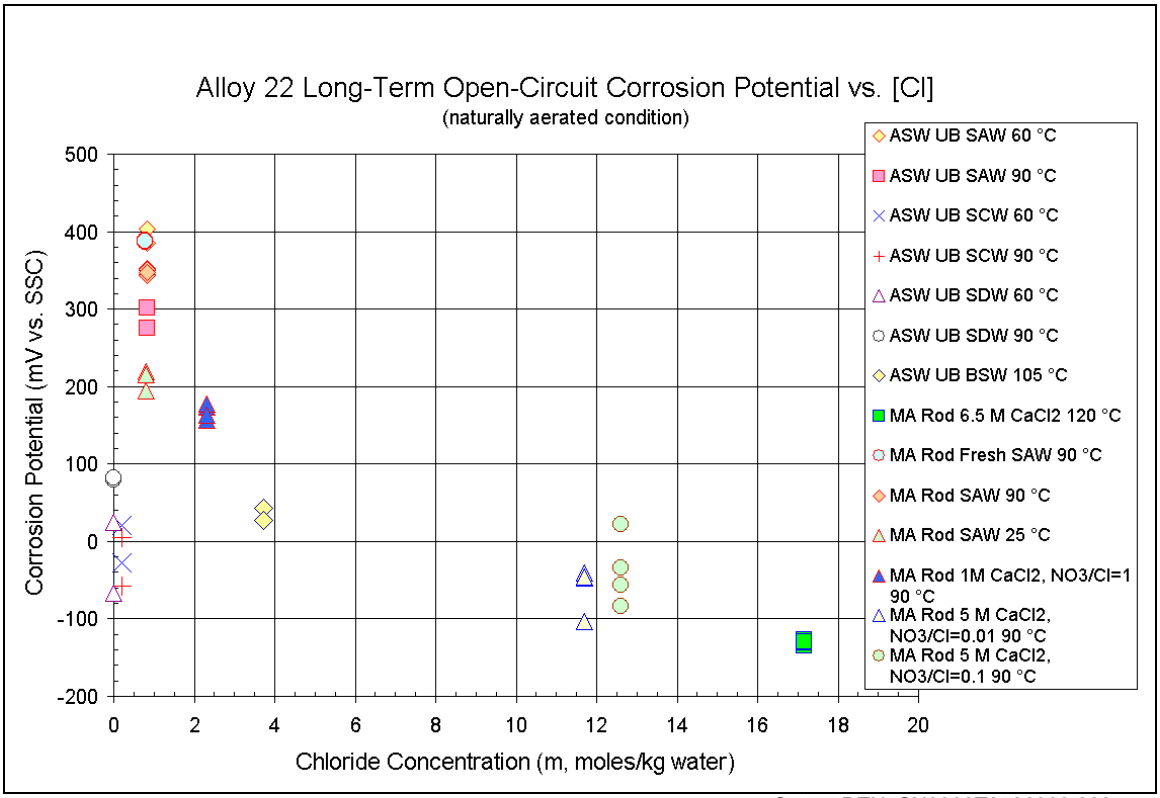

Output DTN: SN0308T0506303.003

Figure 6-39. Long-Term Open-Circuit Corrosion Potential vs. Chloride Ion Concentration of Alloy 22 Samples with Differing Sample Configurations and Metallurgical Conditions.

6.4.4.5 Long-Term Corrosion Potential Model

The long-term open circuit potential tests continue to obtain longer term behaviors of the corrosion potentials of Alloy 22. The data reported in DTN LL020711612251.017 capture the data that were available for this model report. Because of the measurement noises of the long-term corrosion potentials, an average of the readings for the final week of each sample was used as the steady state value for the model analysis. This was necessary to have representative values. The data that were obtained accordingly are listed in Attachment V. Development of the long-term corrosion potential model for the WPOB was performed considering a set of multiple regression models as a function of the test exposure environment parameters such as temperature, pH, chloride concentration and nitrate concentration. Chloride and nitrate ion concentrations of SAW, SCW, SDW and BSW solutions used in the model development are the target values of the solutions from DTN LL000320405924.146 (see Table 6-2). That is, they are not measured compositions, and the actual compositions may vary significantly because of other experimental factors. For simpler salt solutions ($CaCl_2$ and $CaCl_2$-$Ca(NO_3)_2$ solutions), complete dissociation was assumed for chloride and nitrate ion concentrations. The pH of all the test solutions was measured at the room temperature and was documented in DTN LL030201212251.033.

The initial models were fit to the long-term corrosion potential data (E_{corr}) listed in Attachment V, and evaluated for the goodness of their model fit using various statistical analysis techniques. Among the models that were considered, the following functional form was considered to adequately describe the relationship between E_{corr} and the test environment variables above.

$$E_{corr} = c_o + c_1 T + c_2 pH + c_3 [Cl^-] + c_4 \log(\frac{[NO_3^-]}{[Cl^-]}) \qquad \text{(Equation 6-36)}$$

where T is the temperature (°C), $[Cl^-]$ is the chloride ion concentration in molality (m, moles/kg water), $[NO_3^-]$ is the nitrate ion concentration in molality (m, moles/kg water), and c_o, c_1, c_2, c_3, *and* c_4 are coefficients of the model parameters. Using the method of least squares, the above model was fitted to the data in Attachment V. The model fitting was performed using Mathcad 2000 Professional, and the Mathcad worksheet for the model fitting is found in the output DTN SN0308T0506303.003 of this model report. For the data with the zero concentration of nitrate ion, a very small value of 1.0E-8 was used for the nitrate concentration in the regression analysis.

The estimated regression coefficients and their uncertainty (±1 standard deviation) are: $c_0 = 365.511 \pm 32.901$, $c_1 = 1.853 \pm 0.374$, $c_2 = -48.091 \pm 2.528$, $c_3 = -29.641 \pm 1.931$, and $c_4 = -4.263 \pm 4.326$. The covariance matrix resulting from the fitting procedure was determined to be:

$$CV = \begin{bmatrix} 1.083\times10^{3} & -1.082\times10^{1} & -3.149\times10^{1} & 7.753\times10^{0} & -3.717\times10^{1} \\ -1.082\times10^{1} & 1.398\times10^{-1} & -2.943\times10^{-2} & -1.269\times10^{-1} & 3.748\times10^{-1} \\ -3.149\times10^{1} & -2.943\times10^{-2} & 6.392\times10^{0} & 4.223\times10^{-1} & 5.973\times10^{-1} \\ 7.753\times10^{0} & -1.269\times10^{-1} & 4.223\times10^{-1} & 3.730\times10^{0} & 6.191\times10^{0} \\ -3.717\times10^{1} & 3.748\times10^{-1} & 5.973\times10^{-1} & 6.191\times10^{0} & 1.871\times10^{1} \end{bmatrix}$$

(Equation 6-37)

The correlation coefficient R for the fit is 0.974, and the coefficient of determination R^2 is 0.949. An R^2 value of 0.949 indicates that the regression model fits the experimental data very well.

As seen from the dependence of the corrosion potential on the logarithm of the nitrate to chloride ion concentration ratio, the model requires the nitrate concentration be greater than zero. Therefore, for a condition with no nitrate ion present, it is recommended that a small value (such as 0.001 m) be used for the nitrate ion concentration.

The entire variance of the model is due to the measurement uncertainty. The same logic as the crevice repassivation potential data (i.e., ASTM G 61 discussed in Section 6.4.4.3.1) was used to quantify the uncertainty of the long-term corrosion potential data. As with the crevice repassivation potential data, the steady-state corrosion potential data were considered to fall within the range of ±2 standard deviations of the mean—this includes 95 % of all data provided random variations are the only source of error. This uncertainty range appears to be sufficient as the data are highly reproducible (Estill et al. 2003). Therefore it is recommended that the

uncertainty of the parameter coefficients of the corrosion potential model be limited to ±2 standard deviations.

It is recommended that for the waste package degradation analysis in the repository, variability in the corrosion potential among waste packages be represented by the temporally and spatially varying waste package temperature and chemistry of water contacting the waste package. In addition, the chemistry of water contacting the waste package may vary depending on the thermal and hydrologic condition on the waste package surface, for example, drip condition vs. no-drip condition. For the no-drip condition, the chemistry of the water film forming on the waste package surface would be determined by the interactions of the chemical constituents in the dust on the surface with the water vapor in the humid-air around the waste package.

This corrosion potential model is to estimate the long-term steady-state open-circuit corrosion potential of Alloy 22 for a range of exposure conditions related to the proposed repository. The model is not intended for short-term transient conditions. This model is valid over the range of the input data for the model variables.

The model results and the steady-state corrosion potential data are shown in Figure 6-40 and Figure 6-41 as a function of pH and chloride concentration, respectively. Note the model results are for the average values of the test environment parameters (temperature, chloride concentration and pH) of the source data. The E_{corr} data for the test conditions that are off the average values are therefore not bound within ± 2 standard deviations of the model mean. The figures show that the steady-state corrosion potential is a strong function of both pH and chloride concentration.

Figure 6-40 shows a strong dependence of the steady-state corrosion potential on pH. The model predicts that the corrosion potential changes at a rate of about 45 mV per pH unit. This is reasonably consistent with the Nernst equation, which states that the corrosion potential changes by 59 mV per pH unit if the hydrogen reduction reaction is strongly contributing to the steady state mixed corrosion potential(Fontana 1986, pp. 451 to 452). This model behavior also represents the effect of a "marked" ennoblement of the alloy in acidic conditions as seen in the SAW solutions (see Figure 6-37). Such an ennoblement of Alloy 22 in acidic conditions was also reported by other investigators (Dunn et al. 2003, Figures 8 and 9; Jayaweera et al. 2003, Section 9.3.2, Figure 9.13). Corrosion potential of Alloy 22 is expected to drop sharply for very low pH conditions because the passive film on the alloy would become unstable in such extreme acidic conditions and the alloy would become more active. The current model does not represent this yet.

As shown in Figure 6-41, the corrosion potential is lowered as chloride concentration increases. This is because the alloy becomes more active as attack of the passive film by chloride ions would become more severe as chloride concentration increases. Also, lower oxygen solubility as chloride concentration increases could have contributed to lower open circuit corrosion potentials. It can be seen from the coefficient of the temperature term that the corrosion potential is a weak function of temperature and increases slightly with temperature. As shown in Figure 6-36, the corrosion potentials measured in the SAW solutions at different temperatures (25, 60 and 90 °C) more clearly show the temperature dependence trend, although the temperature dependence is somewhat mixed for the SCW and SDW solutions at 60 and 90 °C. This may

represent the effect that the passive film becomes more defect free at higher temperature as the defect repair processes in the passive film could become accelerated as temperature increases. The coefficient of the nitrate to chloride ion concentration ratio term shows that the corrosion potential is a weak function of the concentration ratio (i.e., nitrate ion concentration), and it increases slightly as the nitrate concentration increases.

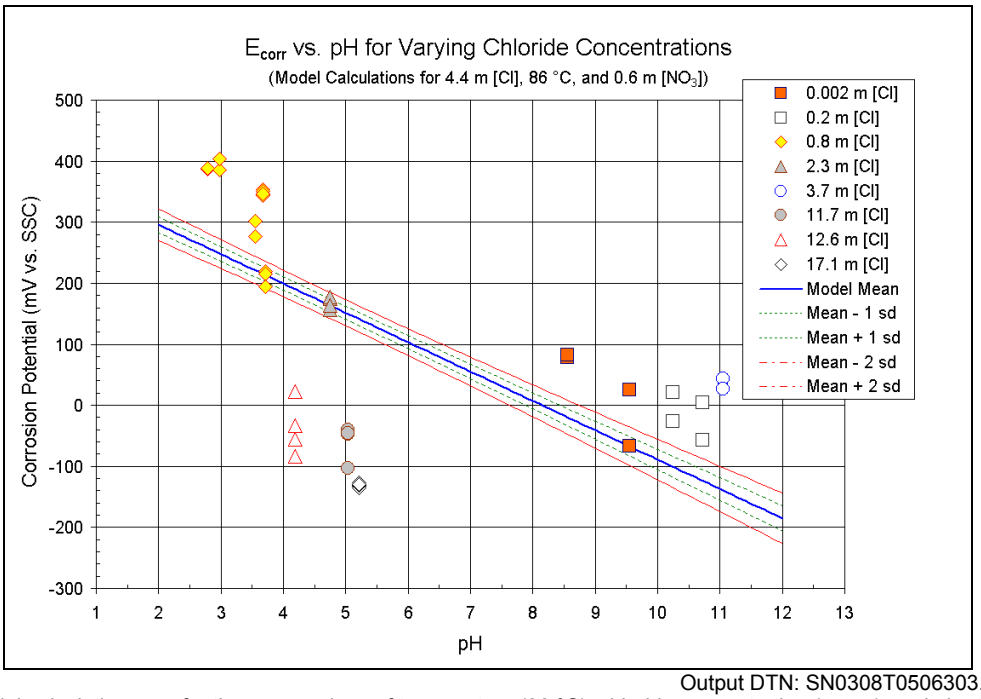

Output DTN: SN0308T0506303.003

Note: The model calculations are for the mean values of temperature (86 °C), chloride concentration (4.4 *m*), and nitrate concentration (0.6 m) of the long-term corrosion potential data of Alloy 22 used for the model development.

Figure 6-40. Model Results and Experimental Data for Long-Term E_{corr} of the WPOB As a Function of pH.

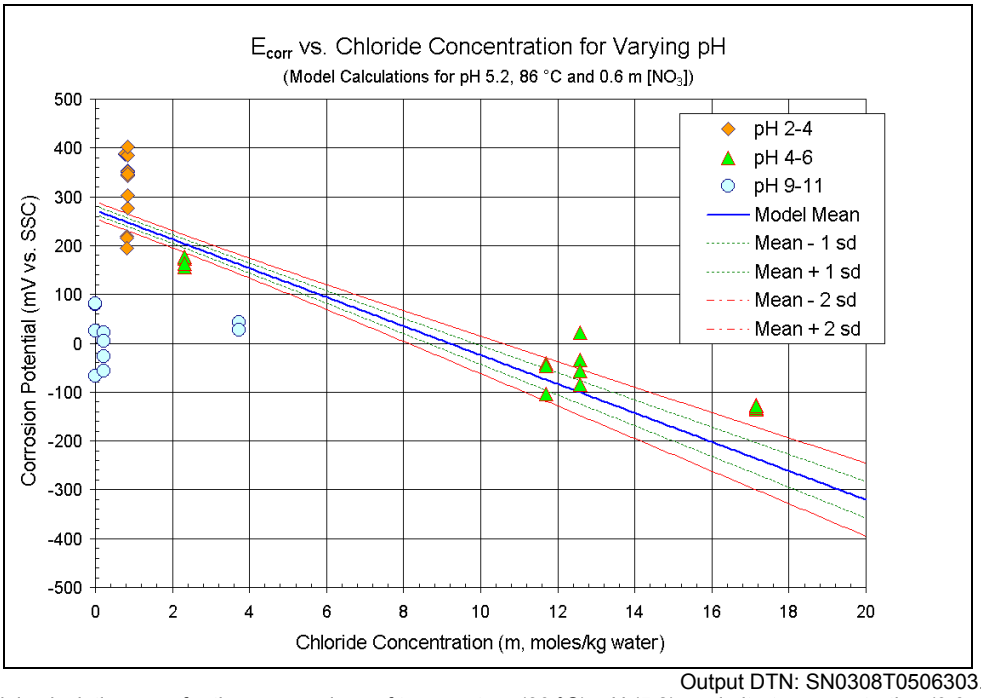

Output DTN: SN0308T0506303.003

Note: The model calculations are for the mean values of temperature (86 °C), pH (5.2), and nitrate concentration (0.6 *m*) of the long-term corrosion potential data of Alloy 22 used for the model development.

Figure 6-41. Model Results and Experimental Data for Long-Term E_{corr} of the WPOB As a Function of Chloride Concentration.

6.4.4.6 Analysis of Localized Corrosion Initiation Model

As discussed before, localized corrosion of the WPOB is modeled with two model components: an initiation model and a propagation model. The initiation model considers that localized corrosion of the WPOB occurs when the open circuit corrosion potential (E_{corr}) is equal to or greater than an appropriate critical potential (crevice repassivation potential (E_{rcrev}) in the current model analysis), that is, ΔE ($=E_{rcrev} - E_{corr}$) ≤ 0. This conceptual model of localized corrosion initiation is widely accepted by the corrosion community and has been published extensively (Bohni 2000, Section B; Dunn et al. 2000 and 2003; Frankel 1998; Frankel 2002; Frankel and Kelly 2002; Beavers et al. 2002, Section 8.3). For the current localized corrosion initiation model a conservative measure, the crevice repassivation potential (E_{rcrev}), was used for the critical potential. For the same or similar metallurgical conditions (mill annealed or welded), the crevice corrosion initiation model components (i.e., E_{corr} and E_{rcrev}) could be affected by the exposure condition (temperature, pH, chloride ion concentration, nitrate ion concentration).

This section documents the analysis of the localized corrosion initiation model for long-term localized corrosion susceptibility of the WPOB for a range of environmental conditions of interest. The analyses were performed by comparing the crevice repassivation potential model results with the long-term corrosion potential model results, as described above. The analyses were conducted with Mathcad 2000, and the Mathcad worksheet files are included in the output DTN SN0308T0506303.003 of this model report. Note that the localized corrosion initiation model, in conjunction with the long-term corrosion potential model, is to analyze the long-term localized corrosion susceptibility of the WPOB, not intended for short-term transient behavior.

6.4.4.6.1 Localized Corrosion Susceptibility vs. Temperature for 10 Molal Chloride and pH 7 Condition with Varying Nitrate Concentrations.

Figure 6-42 shows the model results for the localized corrosion susceptibility of the WPOB for a neutral pH concentrated chloride-containing brine (10 molal chloride) with a very low nitrate ion concentration (NO_3/Cl ratio = 0.001, or no nitrate present). The mean critical temperature for localized corrosion (crevice corrosion) for this condition is about 87 °C. The upper bound of the critical temperature, obtained from the intersection of the upper bound of the crevice repassivation potential and the lower bound of the corrosion potential, is about 103 °C. The lower bound of the critical temperature, obtained from the intersection of the lower bound of the crevice repassivation potential and the upper bound of the corrosion potential, is about 70 °C.

As shown in Figure 6-43, with an increase of nitrate concentration to 0.1 molal (NO_3/Cl ratio = 0.01), the mean critical temperature increases to about 92 °C, and the upper and lower bound critical temperatures are about 108 and 75 °C respectively.

With an additional increase of nitrate concentration to 1 molal (NO_3/Cl ratio = 0.1), the lower bound critical temperature is about 120 °C, which is likely above or close to the boiling temperature of 10 molal chloride-containing solution, and the mean critical temperature is about 140 °C. This is shown in Figure 6-44. Therefore, it is concluded that for the modeled corrosive neutral pH chloride-containing brines, the WPOB is exempt from localized corrosion susceptibility when the inhibitive nitrate ion concentration is 1 molal or higher.

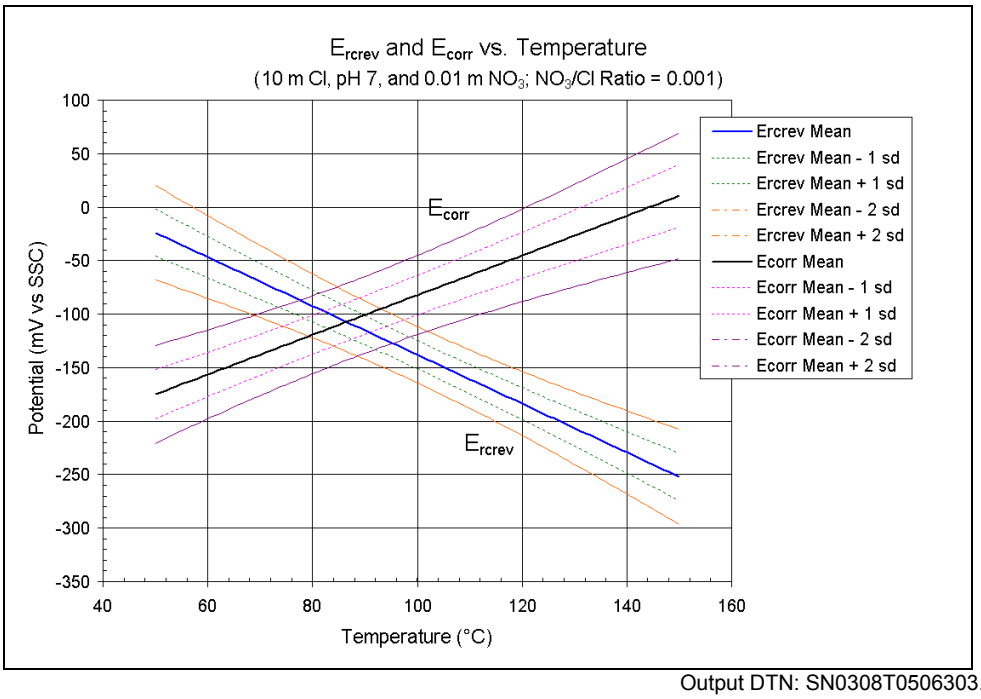

Output DTN: SN0308T0506303.003

Figure 6-42. Model Results for Crevice Corrosion Susceptibility of the WPOB As a Function of Temperature for 10 *m* Chloride, pH 7, and 0.01 *m* Nitrate (NO_3/Cl Ratio = 0.001).

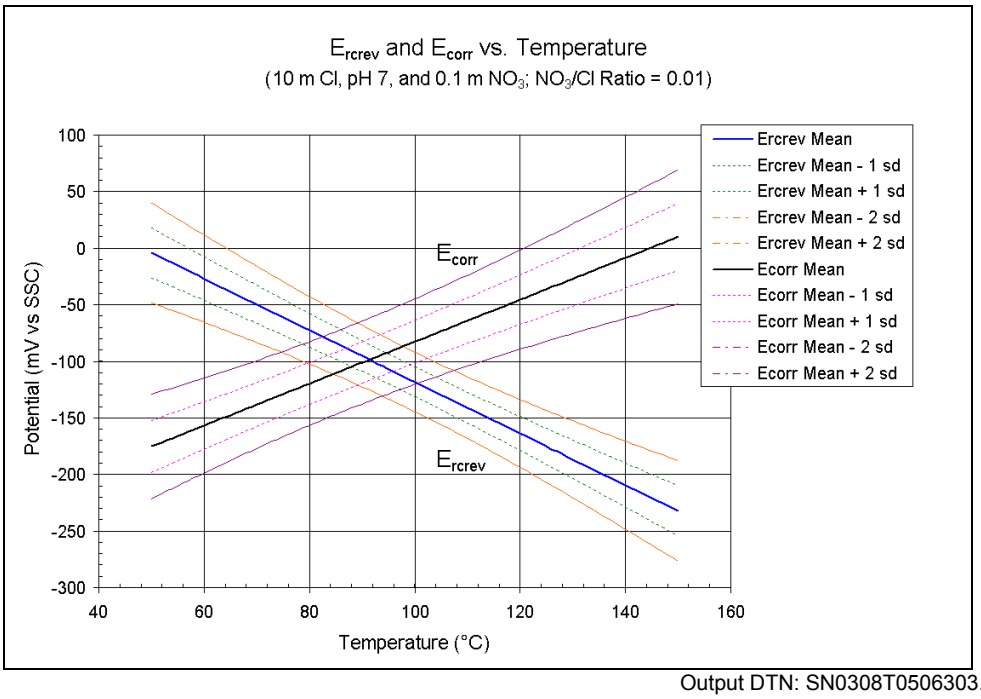

Output DTN: SN0308T0506303.003

Figure 6-43. Model Results for Crevice Corrosion Susceptibility of the WPOB As a Function of Temperature for 10 *m* Chloride, pH 7, And 0.1 *m* Nitrate (NO_3/Cl Ratio = 0.01).

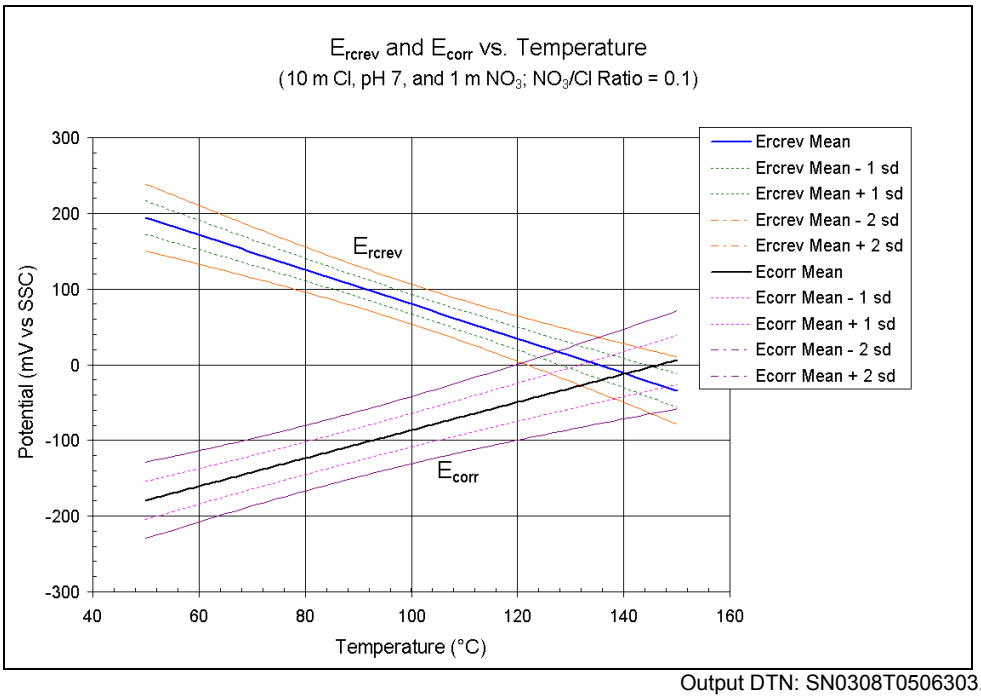

Output DTN: SN0308T0506303.003

Figure 6-44. Model Results for Crevice Corrosion Susceptibility of the WPOB As a Function of Temperature for 10 *M* Chloride, pH 7, and 1 *M* Nitrate (NO_3/Cl Ratio = 0.1).

6.4.4.6.2 Localized Corrosion Susceptibility vs. Temperature for 10 Molal Chloride and pH 3 (Acidic Condition) with Varying Nitrate Concentrations.

Concentrated chloride-containing hot brines become more corrosive as the pH is lowered to a more acidic condition. Although hot acidic chloride-dominant concentrated brines are not expected to form on the WP surface from the dust leachates under the DS, analyses were performed to identify potential exposure conditions in which localized corrosion of the WPOB is possible.

Figure 6-45 shows the model results, as a function of temperature, for acidic chloride-dominant concentrated brine (10 *m* chloride) conditions with a very low nitrate concentration (NO_3/Cl ratio = 0.001, or no nitrate present). As expected, the model predicts that the WPOB is subject to localized corrosion (crevice corrosion) for temperatures as low as 40 °C. However, an increase of nitrate concentration to 1 *m* (NO_3/Cl ratio = 0.1) increases the mean critical temperature to about 70 °C, and the upper and lower bound critical temperatures to about 90 and 50 °C respectively (Figure 6-46).

As shown in Figure 6-47, with an additional increase of nitrate concentration to 2 *m* (NO_3/Cl ratio = 0.2), the model predicts that the safety margin increases significantly and the susceptibility to localized corrosion becomes negligible even for the highly corrosive condition. The figure shows that the mean critical temperature is increased to above 125 °C (likely above the boiling temperature of 10 *m* chloride-dominant solutions), and the lower bound critical temperature is about 105 °C.

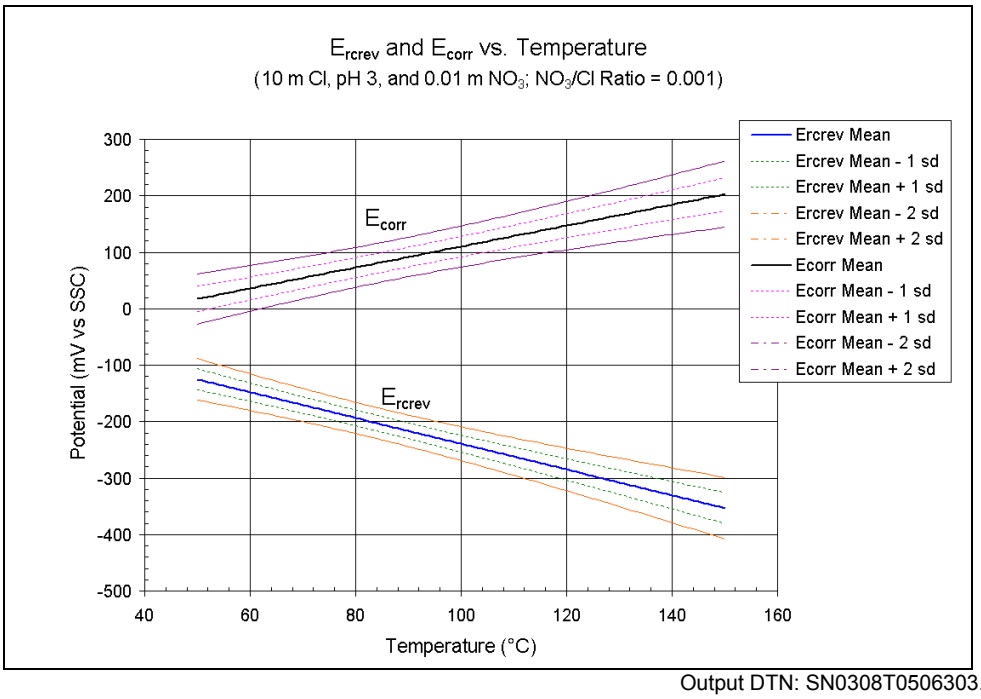

Output DTN: SN0308T0506303.003

Figure 6-45. Model Results for Crevice Corrosion Susceptibility of the WPOB As a Function of Temperature for 10 *m* Chloride, pH 3, and 0.01 *m* Nitrate (NO_3/Cl Ratio = 0.001).

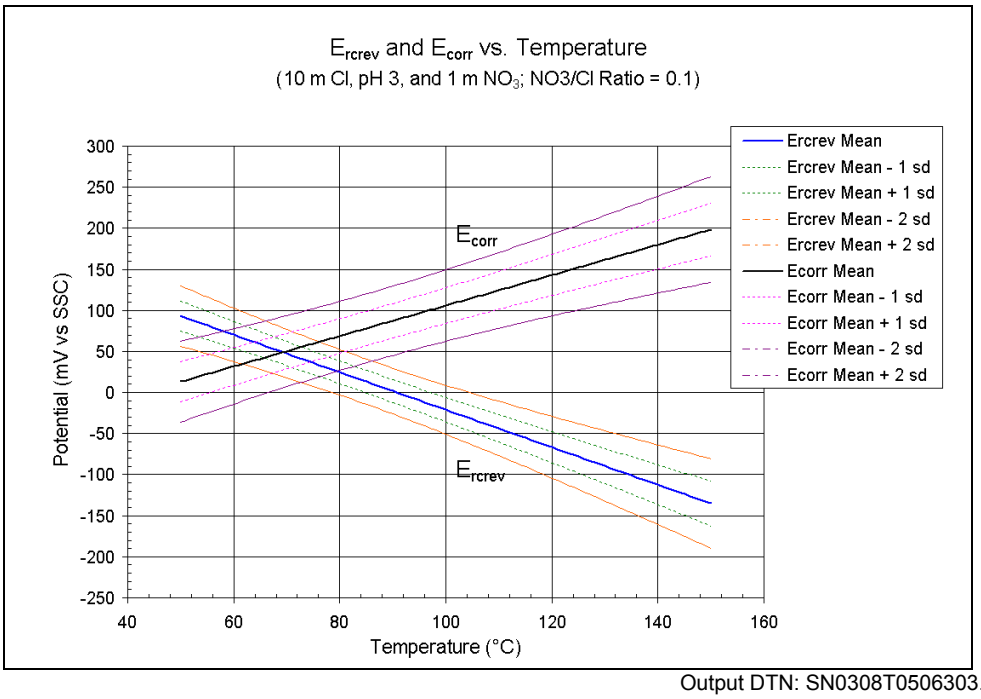

Output DTN: SN0308T0506303.003

Figure 6-46. Model Results for Crevice Corrosion Susceptibility of the WPOB As a Function of Temperature for 10 *m* Chloride, pH 3, and 1 *m* Nitrate (NO_3/Cl Ratio = 0.1).

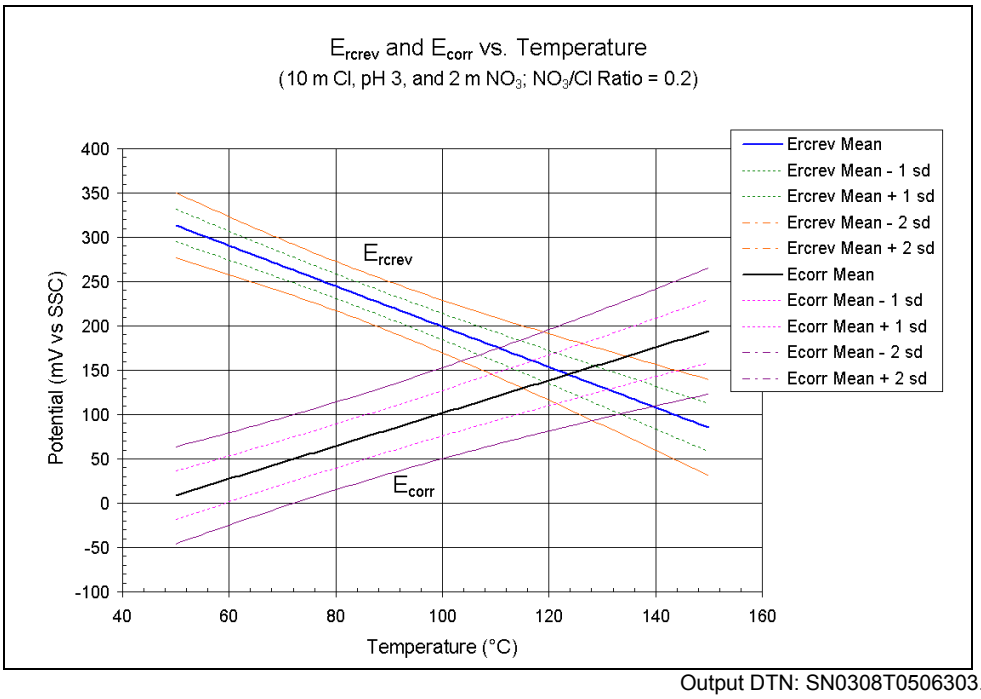

Output DTN: SN0308T0506303.003

Figure 6-47. Model Results for Crevice Corrosion Susceptibility of the WPOB As a Function of Temperature for 10 *m* Chloride, pH 3, and 2 *m* Nitrate (NO_3/Cl Ratio = 0.2).

6.4.4.6.3 Localized Corrosion Susceptibility vs. Chloride Concentration for 95 °C and pH 7 with Varying Nitrate Concentrations.

Analyses were performed to evaluate the model for the localized corrosion susceptibility of the WPOB as a function of chloride ion concentration. Because chloride-containing brines with neutral pH conditions are one of the likely water chemistries expected to contact the waste packages in the post-closure repository, analyses were performed for neutral pH chloride-containing brines at 95 °C.

Figure 6-48 shows the model results for neutral pH chloride-containing brines with a very low nitrate concentration (0.01 m) at 95 °C. The model predicts that, at 95 °C and with little or no nitrate ions present, the WPOB is subject to crevice corrosion for chloride concentrations from about 10 *m* (using the mean E_{rcrev} and E_{corr} values) down to very low concentrations. This model prediction for the crevice corrosion susceptibility in very low chloride concentrations is consistent with the CNWRA data, which reported the crevice repassivation potential (i.e., occurrence of crevice corrosion) in 0.005 and 0.05 M chloride at 95 °C (Brossia et al. 2001, Table A-1).

As shown in the figure, the model predicts no crevice corrosion for higher chloride concentrations (i.e., above 11 *m* from the mean estimation, above 9 *m* from the lower bound estimation, and above 15 *m* from the upper bound estimation). This model prediction results from a steeper dependence of the long-term corrosion potential on chloride concentration than the crevice repassivation potential.

Figure 6-49 shows that with an increase of nitrate concentration to 0.5 m, crevice corrosion of the WPOB is avoided over the modeled chloride ion concentration range in the 95 °C neutral chloride brines, except for an intermediate chloride concentration range (from 3 *m* to 9 *m*) in which a small chance of localized corrosion susceptibility is predicted to be possible. The model predicts that a further increase of nitrate concentration to 1 *m* eliminates the crevice corrosion susceptibility for the 95 °C neutral chloride brine condition (Figure 6-50).

6.4.4.6.4 Localized Corrosion Susceptibility vs. pH for 95 °C and 10 Molal Chloride with Varying Nitrate Concentrations.

Figure 6-51 shows the model results for the localized corrosion susceptibility as a function of pH for concentrated chloride-dominant brines (10 m) with a low nitrate concentration (or no nitrate) (0.01 m, NO_3/Cl ratio = 0.001) at 95 °C. The model predicts that crevice corrosion does not occur for neutral and alkaline conditions (pH above 7.5) from the mean-value estimation. The lower and upper bound pH values are about 6.5 and 8.5 respectively.

As shown in Figure 6-52, an increase of nitrate concentration to 1 *m* (NO_3/Cl ratio = 0.1) extends the pH bound for no crevice corrosion into acidic conditions for the modeled chloride brines: pH 4.5 from the mean estimation, pH 3.5 from the lower bound estimation, and pH 5.2 from the upper bound estimation.

6.4.4.6.5 Localized Corrosion Susceptibility vs. Nitrate Ion Concentration for 95 °C and 10 M Chloride for Neutral (pH 7) and Acidic (pH 3) Conditions.

Analyses were performed to evaluate the effect of inhibitive nitrate ion concentration on the localized corrosion susceptibility for neutral and acidic concentrated chloride-dominant brines at 95 °C. Figure 6-53 shows that, for the modeled 95 °C neutral chloride brines (10 *m* chloride and pH 7), only a moderate nitrate concentration (about 0.2 m, NO_3/Cl ratio = 0.02) is needed to avoid crevice corrosion. However, as shown in Figure 6-54, for acidic concentrated chloride brines (10 *m* chloride and pH 3) at 95 °, a significantly higher nitrate concentration is needed for the immunity from crevice corrosion: about 1.5 *m* nitrate from the mean estimation (NO_3/Cl ratio = 0.15), about 1.1 *m* nitrate from the lower bound estimation (NO_3/Cl ratio = 0.11), and about 1.7 *m* nitrate from the upper bound estimation (NO_3/Cl ratio = 0.17).

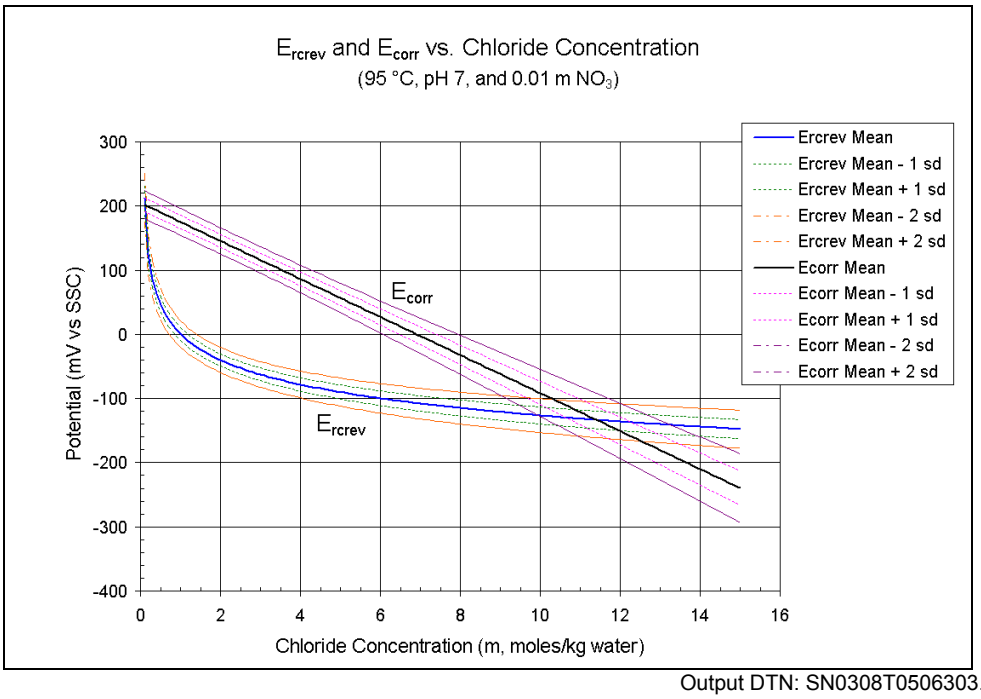

Output DTN: SN0308T0506303.003

Figure 6-48. Model Results for Crevice Corrosion Susceptibility of the WPOB As a Function of Chloride Concentration for 95 °C, pH 7, and 0.01 *m* Nitrate.

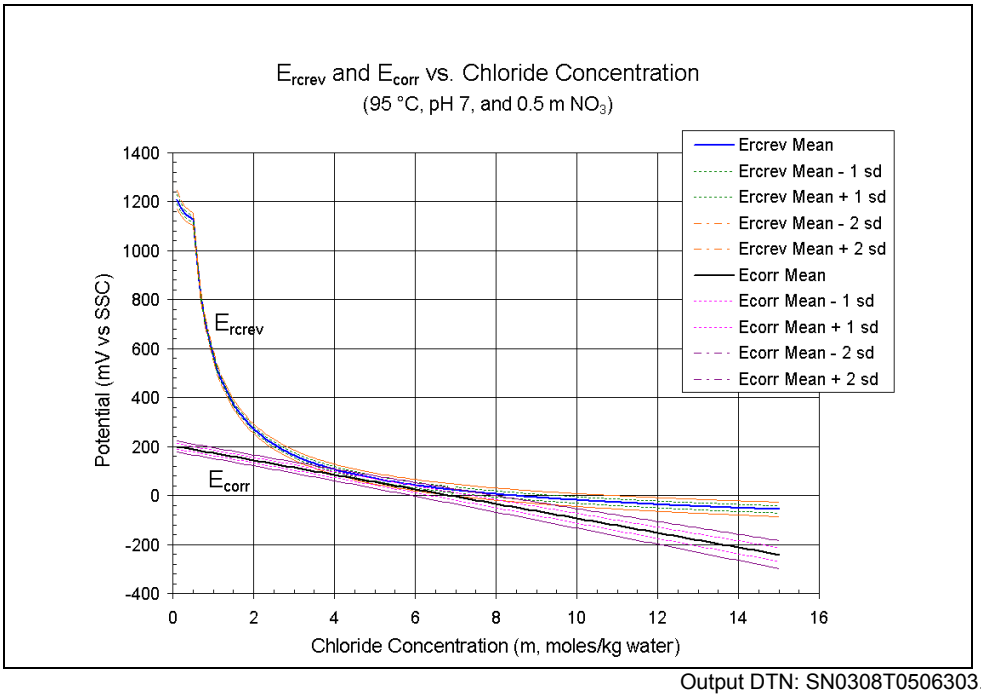

Output DTN: SN0308T0506303.003

Figure 6-49. Model Results for Crevice Corrosion Susceptibility of the WPOB As a Function of Chloride Concentration for 95 °C, pH 7, and 0.5 *m* Nitrate.

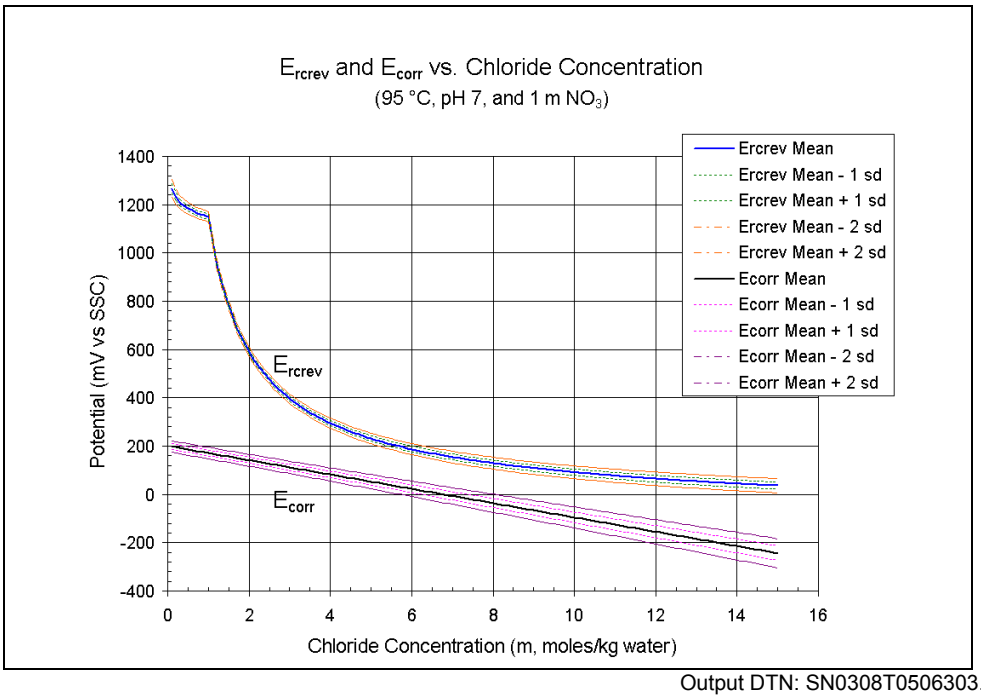

Output DTN: SN0308T0506303.003

Figure 6-50. Model Results for Crevice Corrosion Susceptibility of the WPOB As a Function of Chloride Concentration for 95 °C, pH 7, and 1 *m* Nitrate.

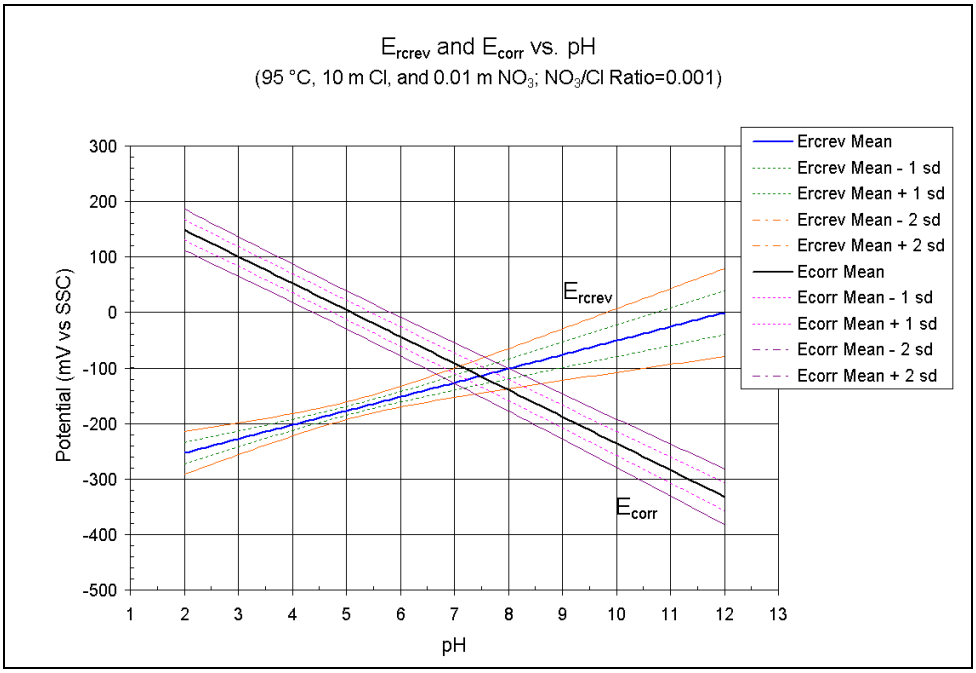

Output DTN: SN0308T0506303.003

Figure 6-51. Model Results for Crevice Corrosion Susceptibility of the WPOB As a Function of pH for 95 °C, 10 *m* Chloride, and 0.01 *m* Nitrate (NO_3/Cl Ratio = 0.001).

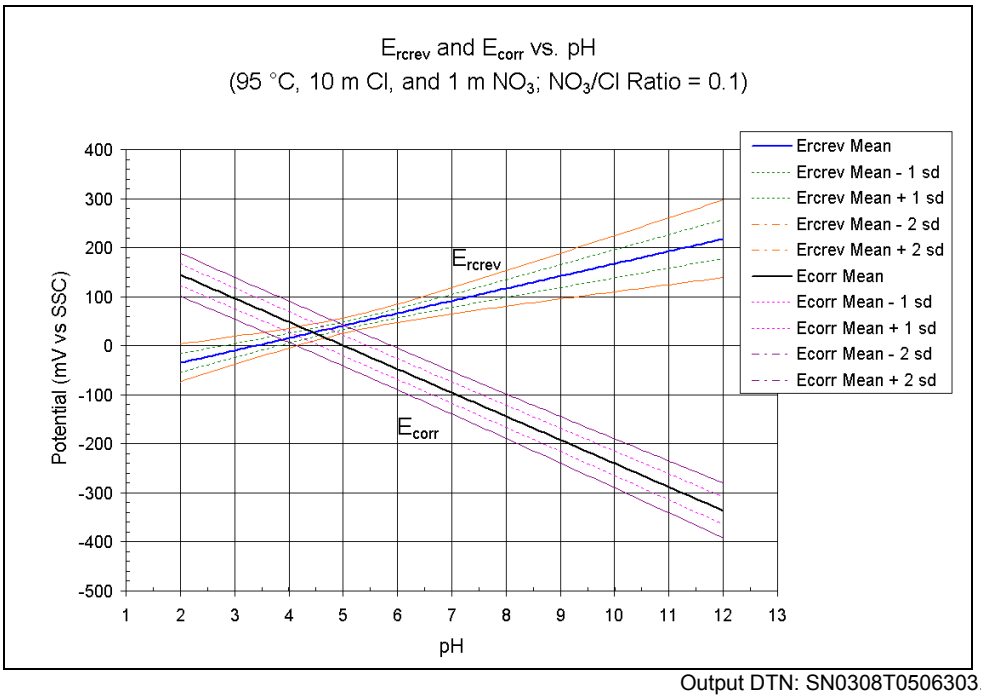

Output DTN: SN0308T0506303.003

Figure 6-52. Model Results for Crevice Corrosion Susceptibility of the WPOB As a Function of pH for 95 °C, 10 *m* Chloride, and 1 *m* Nitrate (NO_3/Cl Ratio = 0.1).

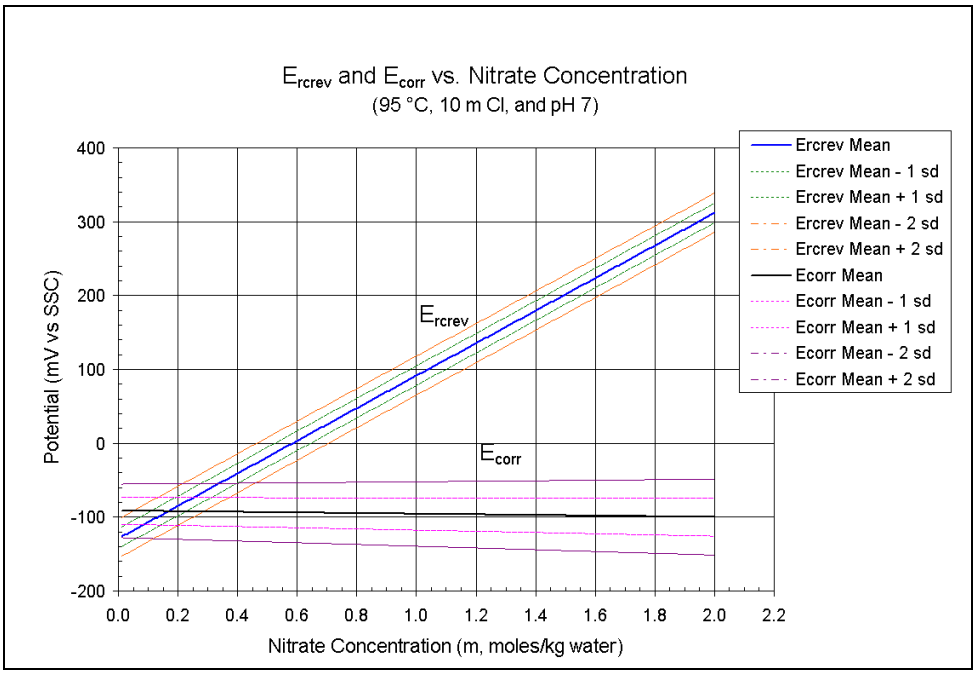

Output DTN: SN0308T0506303.003

Figure 6-53. Model Results for Crevice Corrosion Susceptibility of the WPOB As a Function of Nitrate Concentration for 95 °C, pH 7, and 10 *m* Chloride.

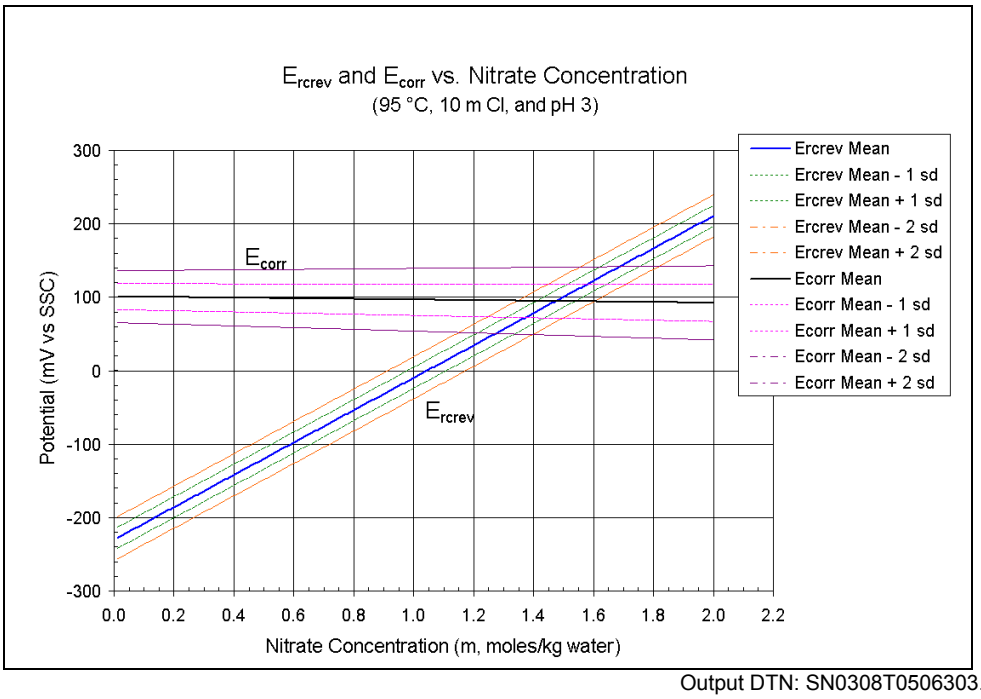

Output DTN: SN0308T0506303.003

Figure 6-54. Model Results for Crevice Corrosion Susceptibility of the WPOB As a Function of Nitrate Concentration for 95 °C, pH 3, and 10 *m* Chloride.

6.4.4.7 Localized Corrosion Penetration Rate Model

If the corrosion potential of the WPOB exceeds the critical potential, the WPOB is considered to be subject to localized corrosion, and penetration of the barrier by localized corrosion is modeled. Due to the outstanding corrosion resistance of Alloy 22, very little data exists for such localized corrosion under the conditions expected in the proposed repository. The literature data reviewed by Gdowski (1991, Table 22) indicate that the corrosion rate of Alloy 22 measured by weight loss in 10 weight percent $FeCl_3$ at 75°C might be as high as 12.7 µm/year. This rate is significantly higher than those measured by weight loss of the crevice specimens in the LTCTF and may be representative of the types of rates expected for localized corrosion, including crevice corrosion. In a solution composed of 7 volume percent H_2SO_4, 3 volume percent HCl, 1 weight percent $FeCl_3$, and 1 weight percent $CuCl_2$, a penetration rate of 610 µm/year measured by weight loss was observed for Alloy C-276 at 102 °C (Gdowski 1991, Table 23). The corrosion rate of Alloy C-276 in dilute HCl at the boiling point is somewhere between 5 and 50 mils per year (127 and 1270 µm/year) (Sedriks 1996, Figure 9.12; Haynes International 1997b, page 13). Comparable rates would be expected for Alloy 22. Note that the "true" localized corrosion rates in local areas may be higher than those measured by weight loss. However, the literature data mentioned above were from short-term tests, therefore are highly conservative for use in the long-term localized corrosion degradation analysis for the WPOB in the repository.

Based on these data, the localized corrosion penetration rates for the WPOB are modeled in a range from 12.7 to 1270 µm/year with the median value of 127 µm/year, as shown in Table 6-9. A log-uniform distribution between the bounds was chosen for the penetration rate. The basis for this selection is that the penetration rate values from the literature span three orders of

magnitude, and the percentiles provided are consistent with a log-uniform distribution. This distribution is based on data that bounds those extreme penetration rates found in the literature and are a highly conservative representation of localized corrosion rates of Alloy 22 for the exposure conditions expected in the post-closure repository. The entire variance in the penetration rate is due to uncertainty.

However, although localized corrosion rates are bounded by this distribution, the expected case is that once initiated, the crevice corrosion propagation rate would be expected to decrease with increasing depth if it were to initiate under realistic environmental conditions. More details of the time-dependent localized corrosion growth behavior are discussed in Section 6.4.4.8.2.

Table 6-9. Distribution of Localized Corrosion Rates for Alloy 22.

Percentile	Localized Corrosion Rate (μm/year)
0^{th}	12.7
50^{th}	127
100^{th}	1270

Output DTN: SN0308T0506303.003

6.4.4.8 Alternative Conceptual Models for Localized Corrosion

Alternative conceptual models (ACMs) are based on assumptions and simplifications that are different from those employed in the base-case model. An important reason for considering ACMs is to help build confidence that changes in modeling assumptions or simplifications will not change conclusions regarding subsystem and total system performance. Conceptual model uncertainty results from sparse observational data and a lack of available information to corroborate or refute plausible alternative interpretations of the subsystem and the processes occurring within the subsystem. This section discusses the ACMs for the localized corrosion models of the waste package outer barrier (WPOB).

6.4.4.8.1 Localized Corrosion Susceptibility of the WPOB

Localized corrosion of the WPOB is modeled with two model components: an initiation model and a propagation model. The base-case initiation model considers that localized corrosion of the WPOB occurs when the open circuit corrosion potential (E_{corr}) is equal to or greater than a certain critical potential (crevice repassivation potential (E_{rcrev}) in this model report), that is, ΔE ($=E_{rcrev} - E_{corr}$) ≤ 0. This conceptual model of localized corrosion initiation is widely accepted by the corrosion community and has been published extensively (Bohni 2000, Section B; Dunn et al. 2000 and 2003; Frankel 1998; Frankel 2002; Frankel and Kelly 2002; Beavers et al. 2002, Section 8.3). Exposure conditions in the proposed repository will evolve with time, making it necessary to know E_{corr} and E_{rcrev} as a function of this evolution. This requires that a database of E_{rcrev} values covering this range of conditions, plus a model for the evolution of E_{corr} with exposure time are required.

An alternative parameter that can be used to determine susceptibility to localized corrosion is temperature. The evolution of waste package temperature with time can be calculated with reasonable certainty. This evolution, coupled with a knowledge of the critical temperature for the initiation of localized corrosion (pitting/crevice corrosion) can then be used to determine when these processes may occur.

The use of critical temperatures in this manner was well documented (Frankel 1998), and values of critical pitting temperature (CPT) and critical crevice corrosion temperature (CCT) have been measured for a series of alloys, including Alloy 22, in relatively pure concentrated chloride solutions (i.e., high salinity, $[Cl^-]$ = 24,300 µg/g, and a high $[Cl^-]$ to $[SO_4^{2-}]$ ratio) (Haynes International Inc. 1997b; McGuire et al. 1998, Section 5.1.2). However the test conditions are not directly relevant to the potential environments on the waste package surface. Under these highly corrosive conditions, the CCT for Alloy 22 was measured to be 102 °C, and for Alloy 276 to be 80 °C. The CPT for Alloy 22 was greater than 150 °C, and that for Alloy 276 was 150 °C.

The critical temperature-based model is not considered in the TSPA because it does not account for the effects of electrochemical characteristics of the solution contacting the metal, particularly those of important corrosion inhibiting anions such as nitrate and sulfate ions present in the groundwater at the proposed repository.

6.4.4.8.2 Time-Dependent Growth Law for Localized Corrosion

The base case model assumes that, when localized corrosion of the WPOB occurs, it propagates at a (time-independent) constant rate (Assumption 5.4). This assumption is highly conservative because it is known that the localized corrosion rate decreases with time, and this is particularly more likely under discontinued tortuous thin water film conditions that are expected to form on the waste package surface in the post-closure repository. Also, in general, localized corrosion tends to arrest or die shortly after initiation.

An alternative conceptual model for the localized corrosion penetration is a time-dependent growth law. The growth law model can be developed based on a combination of electrochemical and corrosion exposure measurements. A simple pitting model based on hemispherical pit growth yields a penetration law of the form (CRWMS M&O 1998, Table 3-2; Hunkeler and Boehni 1983; McGuire et al. 1998, Section 5.2.8)

$$D = k \cdot t^n \qquad \text{(Equation 6-38)}$$

where D is the depth of penetration, t is time, and k is a growth constant. The growth constant will be dependent on the properties of the material, particularly its susceptibility to anodic dissolution in the acidic environment prevailing in a propagating localized corrosion site. The time exponent, n, would be about 0.5 for both diffusion-controlled (i.e., diffusion of metal ions out of the pit) and ohmically-controlled (i.e., rate determined by the ohmic potential drop which develops in the electrolyte in the pit) pit growth (McGuire et al. 1998, Section 5.2.8; Vetter and Strehblow 1974). The above model was used in a separate analysis for the proposed repository by the Electric Power Research Institute (EPRI) (EPRI 2002, Section 5.3.1).

The significance of this pit penetration law has been discussed by Frankel (1998) and leads to a pit growth current density (i) proportional to the inverse square root of time (i.e., $i \propto t^{-1/2}$) in potentiostatic electrochemical experiments. Hunkeler and Boehni (1983) have shown that this growth law is obeyed for both the pitting and crevice corrosion of stainless steels. Newman and Franz (1984) have also observed a similar relationship on stainless steel.

When trying to adapt such a law for practical applications, two main problems arise: (1) insufficient penetration rate data are available, especially for relatively new materials such as Alloy 22, to determine values of k and n; and (2) the factors that control the form of this apparently simple growth law are complex and, at best, only qualitatively understood. In order to determine values of k and n, it is necessary to employ short term experiments in which the pit growth process is accelerated electrochemically. In these experiments those features of the propagation process which enhance growth (the development of critical chemistry; the evolution of pit geometry) are dominant. However, it is necessary to predict penetration behavior after long periods of exposure, when those factors that limit growth (IR drop, loss of critical chemistry, evolution of metallurgical factors, polarization of cathodic processes) are more important.

The literature data available for less corrosion resistant materials (Hunkeler and Bohni 1983; Marsh et al. 1991; Mughabghab and Sullivan 1989; Sharland et al. 1991; and Ishikawa et al. 1991) clearly show that a penetration growth law of the form of Equation (6-38) is appropriate, and that a value of $n = 0.5$, the theoretically predicted value, is justifiable. A key point with the materials discussed above (e.g., iron, carbon steel, copper and Titanium Grade 2) is that they are materials which would be expected to undergo rapid propagation. Providing it is not stifled by the accumulation of corrosion product deposits or slow cathodic kinetics, propagation would be limited only by diffusive or ohmic effects, leading to a value of n approaching 0.5.

By contrast, for highly corrosion resistant materials such as Alloy 22 that are designed and fabricated to resist localized corrosion, additional metallurgical features will be important in determining the value of n. One example of such a metallurgical influence that is pertinent to the case of Alloy 22 is the ability of Mo to decrease the pitting current densities in stainless steels, possibly by reducing the active dissolution rate within the pit (Frankel 1998; and Newman 1985). This prevents the maintenance of the critical pit or crevice chemistry to sustain propagation, leading to repassivation. Again, the n value in the growth law in Equation (6-38) would effectively tend to zero. This is supported by the observation of Kehler et al. (2001), who showed that the depth of crevice penetration for Alloy 22 electrochemically driven in extremely saline (5 mol/L LiCl) solutions at 85 °C was limited to less than 100 μm. The adoption of such a value considers that metallurgical features, such as the influence of Mo on pit/crevice propagation will suppress penetration.

Localized corrosion rate data are needed to obtain a value for k. The only presently available source of crevice corrosion rate data is that published by Haynes (1997b) and summarized in Table 22 of Gdowski (1991). These data were recorded in 10 weight percent $FeCl_3$, i.e. under extremely aggressive oxidizing conditions.

The localized corrosion growth law model of the form of Equation (6-38) is not used in the TSPA because of lack of data to obtain the values of the model parameters, n and k for Alloy 22 for the exposure conditions relevant to the proposed repository. The base-case model (time-

independent constant penetration rate model) is much more conservative than the growth law model. The base-case model should bound the penetration rate range by localized corrosion of the WPOB when it occurs.

6.4.5 Effect of Microbial Activity on Corrosion

Microbially influenced corrosion (MIC) is the contribution to the corrosion of a metal or alloy due to the presence or activity, or both, of microorganisms. MIC most often occurs due to the increase in anodic or cathodic reactions due to the direct impact of microorganisms on the alloy or by indirect chemical effects on the surrounding solution. Microorganisms can affect the corrosion behavior of an alloy either by acting directly on the metal or through their metabolic products. For example, some types of aerobic bacteria may produce sulfuric acid by oxidizing reduced forms of sulfur (elemental, sulfide, sulfite), and certain fungi transform organic matter into organic acids (Fontana 1986, Section 8-10). H^+ is known to be generated by bacterial isolates from Yucca Mountain. Furthermore, *thiobaccilus ferro-oxidans* oxidize Fe^{2+}, while *geobacter metallireducens* reduce Fe^{3+}. Other microbes can reduce SO_4^{2-} and produce S^{2-}.

It has been observed that nickel-based alloys such as Alloy 22 are relatively resistant to microbially influenced corrosion (Lian et al. 1999). Furthermore, it is believed that microbial growth in the repository will be limited by the availability of nutrients (CRWMS M&O 2000b, Section 6.6.2). There are no standard tests designed specifically to investigate the susceptibility of an engineering alloy to MIC (Stoecker 1987). One commonly used type of evaluation to determine the MIC factor is to test the alloy of interest in-situ (in the field) using the same variables as for the intended application. However, testing in the laboratory with live organisms can provide more controlled conditions of various environmental variables, and sterile controls can be incorporated to better assess MIC-specific effects (Horn and Jones 2002). This approach was used to evaluate the microbiological processes on general corrosion of the WPOB. For general corrosion of the WPOB, the effect of MIC can be described as follows;

$$CR_{MIC} = CR_{st} \cdot f_{MIC} \qquad \text{(Equation 6-39)}$$

where CR_{MIC} is the general corrosion rate in the presence of microorganisms, CR_{st} is the general corrosion rate of the alloy in the absence of MIC, and f_{MIC} is the MIC factor. If f_{MIC} is greater than one, there is an enhancement of the corrosion rate of the alloy as a consequence of the presence or activity of microorganisms.

Lian et al. (1999)has shown that MIC can enhance corrosion rates of Alloy 22 by a factor of two. Measurements for Alloy 22 and other similar materials are shown in Table 6-10. The MIC factor f_{MIC} is calculated as the ratio of corrosion rates (microbes to sterile) from the table. The value of f_{MIC} for Alloy 22 in sterile media is one (f_{MIC} = 1), whereas the value of f_{MIC} for Alloy 22 in inoculated media is larger (f_{MIC} = 2). MIC factor f_{MIC} is uniformly distributed between 1 and 2, and that this distribution is all due to uncertainty. The MIC factor is applied to the WPOB general corrosion rate when the relative humidity at the WPOB surface is above 90 %. This MIC initiation threshold RH is based on the analysis documented in the model report titled *In-Drift Microbial Communities* (CRWMS M&O 2000b, Sections 6.3.1.6 and 6.5.2, Table 23).

MIC is defined as a local area effect; thus, not all areas are equivalent on any given waste package with respect to bacterial colonization. It is well documented that bacteria preferentially colonize on weldments, and heat-affected zones (Borenstein and White 1989; Walsh 1999; Enos and Taylor 1996). However, the current model is based on data collected using un-welded specimens. In order to account for preferential areas of colonization in the model, it is recommended that the MIC factor f_{MIC} be uniformly distributed with respect to area distribution.

The principal nutrient-limiting factor to microbial growth *in situ* at Yucca Mountain has been determined to be low levels of phosphate (CRWMS M&O 2000b, Section 6.6.2). There is virtually no phosphate contained in J-13 groundwater. Yucca Mountain bacteria grown in the presence of Yucca Mountain tuff are apparently able to solubilize phosphate contained in the tuff to support growth to levels of 10^6 cells/ml of groundwater. When exogenous phosphate is added (10 mM), the levels of bacterial growth increase to 10^7 to 10^8 cells/ml (CRWMS M&O 2000b, Figures 20 and 21, Table 85). The one to two orders-of-magnitude difference in bacterial growth with and without the presence of exogenous phosphate is almost certainly not significant with respect to effects on corrosion rates because the microbe concentrations are already high enough. Therefore, nutrient limitation, at least as a first approximation, was not factored into the overall MIC model. It may be noted, however, that the maximum two-fold f_{MIC} included in the model was in the presence of sufficient phosphate to sustain higher levels of bacterial growth (in an effort to achieve accelerated conditions).

Other environmental factors that could affect levels of bacterial growth include temperature and radiation. These factors, however, are closely coupled to RH; as temperature and radiation decrease in the repository, RH is predicted to increase. At the same time, while there are some types of microorganisms that can survive elevated temperatures (≤ 120 °C) and high radiation doses if there is no available water, then bacterial activity is completely prevented. Thus, because water availability is the primary limiting factor and this factor is coupled to other less critical limiting factors, water availability (as expressed by RH) was used as the primary gauge of microbial activity.

Determination of a critical mass of *total* bacteria required to cause MIC is not an issue that needs to be addressed in the MIC model. Bacterial densities in Yucca Mountain rock have been determined to be on the order of 10^4 to 10^5 cells/gm of rock (CRWMS M&O 2000b, Figures 20 and 21, Table 85). In absolute terms, this is almost certainly above the threshold required to cause MIC. Further, bacterial densities were shown to increase one to two orders-of-magnitude when water is available (above). A more germane concern is the *types* of bacteria present, their abundance, and how their relative numbers are affected when water is available for growth. Corrosion rates will be affected (at least on some WP materials) for example, if organic acid producers out-compete sulfate reducers or inorganic acid producers for available nutrients when water is sufficient to support growth. No data are currently available regarding the composition of the bacterial community over the changing environmental conditions anticipated during repository evolution. Instead, this issue has been addressed in the current model by determining overall corrosion rates under a standardized set of conditions, in the presence and absence of a defined set of characterized Yucca Mountain bacteria.

Table 6-10. Alterations in Corrosion Potentials Associated with Microbial Degradation

Tested Sample Initial Condition	Average Corrosion Rate (μm/year)	Corrosion Potential E_{corr} (V vs. SCE)	
		Initial	Endpoint
CS1020 + YM Microbes	8.80	-0.660	-0.685
Sterile CS 1020	1.40	-0.500	-0.550
M400 + YM Microbes	1.02	-0.415	-0.315
Sterile M400	0.005	-0.135	-0.070
C-22 + YM Microbes	**0.022**	**-0.440**	**-0.252**
Sterile C-22	**0.011**	**-0.260**	**-0.200**
I625 + YM Microbes	0.013	-0.440	-0.285
Sterile I625	0.003	-0.160	-0.130
304SS + YM Microbes	0.035	-0.540	-0.280
Sterile 304SS	0.003	-0.145	-0.065

Input DTN: LL991203505924.094

6.4.6 Effect of Aging and Phase Stability on Corrosion

As specified in the waste package design and fabrication specification (Plinski 2001, Section 8.1), the WPOB base metal and all fabrication welds (not including the welds for the closure lids) are fully annealed before the waste packages are loaded with waste. In addition, for a range of thermal loading designs of the proposed repository, the waste package surface temperature will be always kept below 200 °C (BSC 2001, Section 5.4.1, Figures 5.4.1-2 and 5.4.1-6). With this constraint, the effect of aging and phase instability on the corrosion of the WPOB will be insignificant in the repository. The analysis documented in the model report titled *Aging and Phase Stability of Waste Package Outer Barrier* (BSC 2003a, Sections 6.6.5.3 and 8.0) has shown that phase instabilities are not expected in Alloy 22 base metal and welded material so long as the temperature remains below about 200°C. Non-thermal stress mitigation processes, currently planned for the closure weld, however, may introduce cold work into the material. Although this cold work might accelerated phase transformation kinetics, it would have to do so by at least a couple of orders of magnitude before it would be expected to be observed at low temperatures in 10,000 years.

Comparison of the anodic passive current densities of the as-welded Alloy 22 samples to those of the base metal samples showed no significant effect of the welds on the passive corrosion behavior of the alloy (Brossia et al. 2001, Section 3.2.1.3, Figure 3-13). Rebak et al. (2002) have investigated the effects of high-temperature aging on the corrosion resistance of Alloy 22 in concentrated hydrochloric acid. However, due to the temperature used to age the samples (922-1033 K) and the extreme test media used (boiling 2.5% HCl and 1 M HCl at 339 K), these data are considered not relevant to performance assessment for the repository.

The fabrication welds including the closure welds of the WPOB can be subject to long-term thermal aging and phase instability under the repository thermal conditions. For the analysis of

the thermal aging effect on corrosion of Alloy 22, three metallurgical conditions of Alloy 22 were studied using the multiple crevice assembly (MCA) samples: mill annealed, as-welded, and as-welded plus thermally aged (at 700 °C for 173 hours). The samples were tested in 5 M $CaCl_2$ and 5 M $CaCl_2$ + 0.5 M $Ca(NO_3)_2$ solutions with the test temperatures up to 120 °C. As described in Attachment I, after being immersed in the test solution in an open circuit condition for 24 hours, the polarization resistance of the samples was measured.

Comparison of the calculated corrosion rates of the mill annealed (MA), as-welded (ASW), and as-welded plus thermally aged samples are shown in Figure 6-55 for 5 M $CaCl_2$ solutions and Figure 6-56 for 5 M $CaCl_2$ + 0.5 M $Ca(NO_3)_2$ solutions. The corrosion rate data are listed in Attachment IV. As discussed earlier (see Sections 4.1.1.4 and 6.4.3.4), the corrosion rates from the polarization resistance measurements were only for a comparative analysis for the thermal aging and phase stability effect; *the tests were not intended to obtain the absolute values of the corrosion rate*. The mill annealed MCA samples in 5 M $CaCl_2$ solutions at differing temperatures were considered as the baseline condition for the analysis. The baseline condition rates were compared with those of the ASW and ASW plus thermally aged MCA samples tested in the same electrolyte solution condition. A data trend-line was drawn for the baseline condition data for an easier comparison with the ASW and ASW plus thermally aged sample data. The comparison shown in Figure 6-55 clearly shows that there is no apparent enhancement of the corrosion rate due to welding or thermal aging of the welded samples for the tested conditions.

A similar comparison is made for the corrosion rates measured in 5 M $CaCl_2$ + 0.5 M $Ca(NO_3)_2$ solutions, as shown in Figure 6-56. As for the 5 M $CaCl_2$ solution case, the MA MCA samples at differing temperatures were considered as the baseline condition, and a data trend-line was drawn for the baseline condition data for an easier comparison. The comparison in Figure 6-56 again clearly shows no apparent enhancement of the corrosion rate due to welding or thermal aging of the welded samples. It is also noted that the corrosion rates of all three type samples (MA, ASW, and ASW plus thermally aged) were reduced by a factor of 3 to 4 in the nitrate containing solutions, compared to those in 5 M $CaCl_2$ solutions. The beneficial effects of inhibiting nitrate ions are clearly demonstrated.

The above analyses are consistent with the results by Rebak et al. (2002). Based on the above analysis and insignificant aging and phase stability processes under the thermal conditions expected in the repository (BSC 2003a, Sections 6.6.5.3 and 8.0), the corrosion performance of the WPOB is not expected to be affected by the aging and phase stability in the repository. Hence thermal aging and phase instability of the WPOB was not included in TSPA.

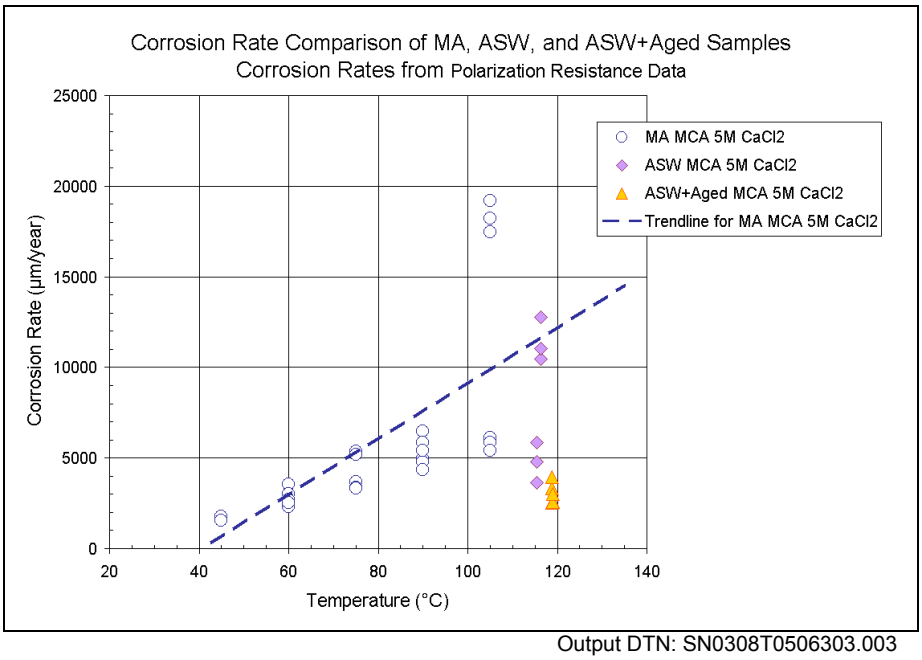

Output DTN: SN0308T0506303.003

Figure 6-55. Comparison of Corrosion Rates from Polarization Resistance Measurements of Mill Annealed (MA), As-Welded (ASW), and As-Welded Plus Aged Alloy 22 MCA Samples in 5 M $CaCl_2$ Brines at Varying Temperatures.

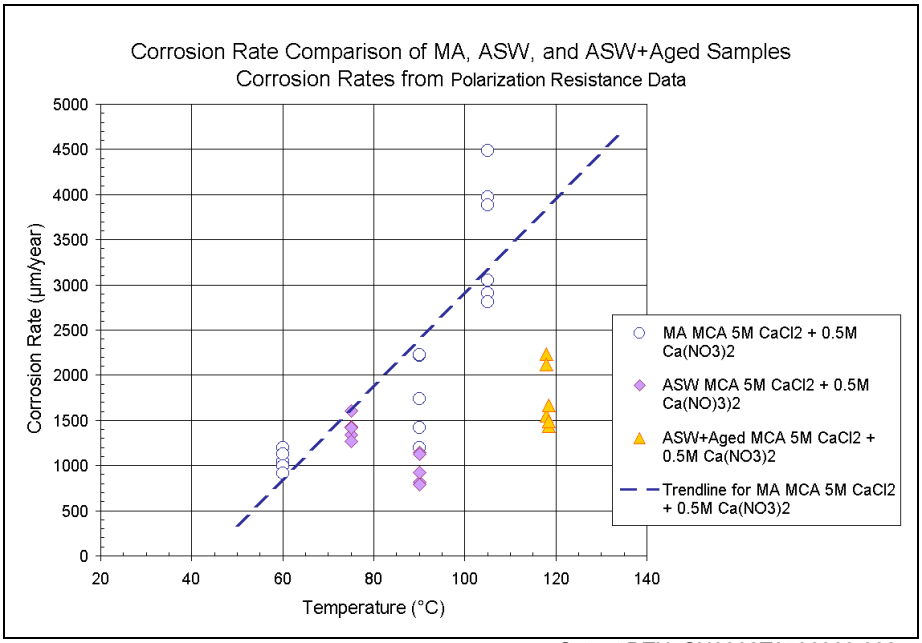

Output DTN: SN0308T0506303.003

Figure 6-56. Comparison of Corrosion Rates from Polarization Resistance Measurements of Mill Annealed (MA), As-Welded (ASW), and As-Welded Plus Aged Alloy 22 MCA Samples in 5 M $CaCl_2$ + 0.5 M $Ca(NO_3)_2$ Brines at Varying Temperatures.

7 MODEL VALIDATION

Models described in this model report are expected to predict accurately general and localized corrosion processes of the WPOB under the exposure conditions expected in the proposed repository for a period of at least 10,000 years. This extraordinarily long time factor makes it extremely difficult to validate these models in the usual way, i.e., by comparison of model predicted values with those observed experimentally for the whole range of time (ASTM C 1174, Sections 19.3 and 20.4). Consequently, a different approach was adopted in the TWP (BSC 2002a) for the validation of these models. According to this approach, these models were validated by validating the input parameter values used and comparing these parameters and model predictions to available peer reviewed and qualified project data. The high level of confidence in the WPOB general and localized corrosion models, as mentioned in the TWP, will be obtained by corroborating and/or validating the model output values with those available in the peer reviewed scientific literature. The corroborating/supporting data and information used to complete the model validation activities can be found in the DIRS report of this model report. Those are identified in the report as "reference only" and listed as used in Section 7. The model validation activities presented in this section also address the items of the Technical Error Report (TER) TER-02-0022 and TER-02-0072.

Four criteria were developed and documented in the TWP (BSC 2002a) to ensure that the required level of confidence in these models for the models' stated purposes has been achieved. These are:

Criterion One: The rate (or a range of the rates) of the general corrosion model of WP is reasonable and consistent with the rate measured by alternative techniques for the conditions expected in the repository.

Criterion Two: The response of the correlation for E_{corr} of WP is reasonable and consistent with the literature data on relevant corrosion resistant alloys and available analogues for the conditions expected in the repository.

Criterion Three: The response of the correlation for $E_{critical}$ of WP is reasonable and consistent with the literature data on relevant corrosion resistant alloys and available analogues for the conditions expected in the repository.

Criterion Four: The propagation rate (or a range of the rates) of the localized corrosion model of WP is reasonable and consistent with the literature data on relevant corrosion resistant alloys for the conditions expected in the repository.

A detailed description of the validation of the WPOB general and localized corrosion models in light of these criteria is given below.

7.1 GENERAL CORROSION MODEL OF THE WPOB

Validation of the general corrosion model of the WPOB requires meeting Criterion One.

Criterion One: *Is the rate (or a range of the rates) of the general corrosion model of WP reasonable and consistent with the rate measured by alternative techniques for the conditions expected in the repository?*

As described in Section 6.4.3.4, the base-case general corrosion model for the WPOB is based on a temperature dependence of the corrosion process, represented by an activation energy using the natural logarithmic form of a modified Arrhenius relation. The model is expressed as follows:

$$\ln(R_T) = \ln(R_o) + C_1\left(\frac{1}{T} - \frac{1}{333.15}\right) \qquad \text{(Equation 7-1)}$$

R_T is temperature-dependent general corrosion rate in nm/year, T is temperature in Kelvin, and R_o and C_1 are constants. The temperature dependence term (C_1) was obtained from short-term polarization resistance data for Alloy 22 specimens tested for a range of sample configurations, metallurgical conditions, and exposure conditions. See Section 6.4.3.4 for details of the model derivation and parameter evaluation. Normal distribution was used for the temperature dependence term, and it was determined to have a mean of -3116.47 and a standard deviation of 296.47. The activation energy was estimated to be 25.9 ± 2.5 kJ/mol. R_o is a Weibull distribution (α = 8.88, β = 1.62, and θ = 0) fitted to the general corrosion rate distribution derived from the weight loss data of the 5-year crevice specimens, considering it represents the distribution of long-term general corrosion rate of the WPOB at 60 °C. The median (50th percentile) rate of R_o is 7.08 nm/year, and the 99.999th percentile rate is 40.1 nm/year.

Temperature dependence of the passive corrosion rate of Alloy 22 was also reported by other investigators. Dunn et al. (2002) found a temperature dependence of the passive corrosion rate of Alloy 22 in low salinity solutions (0.028 *M* [Cl^-]), but no temperature dependence at higher salinities (4.0 *M* [Cl^-]). Based on the passive current densities of Alloy 22 measured in 5 M LiCl solutions with small amounts of [SO_4^-] and [NO_3^-] added (Scully et al. 2001, Table 4, Section 1.4), an activation energy of 36 kJ/mol was estimated (BSC 2001, Section 7.3.5.3). The same analysis also estimated an activation energy of 32 kJ/mol from the measured passive current densities of Alloy 22 in the solutions of 1 *M* NaCl at pH 1 (Lloyd et al. 2001). EPRI (2002, Section 5.3.2) estimated an activation energy of 19 kJ/mol for Alloy C-4 from the corrosion rates from weight loss measurements of the alloy measured over a period of 3 to 5 years at temperatures in the range of 90 to 200 °C in saturated Mg^{2+}-dominated brines (Smailos et al. 1987). A recent study sponsored by the Project estimated activation energies of 26.8 kJ/mol and 24.9 kJ/mol for annealed Alloy 22 and welded Alloy 22 respectively. The activation energies were from the corrosion rates based on the weight loss measurements in BSW solutions at temperatures from 60 to 105 °C over a period of 8 weeks (Hua 2002, page 90, Table 8-2).

As indicated by the literature data cited above, the temperature dependence of general corrosion of Alloy 22 and other similar corrosion resistant Ni-Cr-Mo alloys is about the same considering differing test conditions (especially solution chemistry and sample condition) employed in the tests. Also, as shown for the 5-year weight loss data (Section 6.4.3.2, and Attachments II and III) and the corrosion rates from the polarization resistance measurements (Section 6.4.3.4, and Attachment IV), there is no significant dependence of the general corrosion rate of Alloy 22 on the metallurgical conditions and sample geometry. In addition, the activation energy of the

general corrosion rate of Alloy 22 obtained in this model report is similar to the results from other investigators cited above. It is noted that the activation energies of general corrosion rate of highly corrosion resistant Ni-Cr-Mo alloys are similar regardless of the exposure time in the test environments. That is, the temperature dependence of general corrosion rate of Alloy 22 does not change significantly as the general corrosion rate decreases with the exposure time.

Because of extremely slow corrosion rates of Alloy 22, there are little data for Alloy 22 in the scientific literature that could be used to evaluate the general corrosion model. However, similar passive corrosion behavior has also been observed for nickel-chromium-molybdenum type corrosion-resistant alloys. For example, Alloy C is found to retain a very thin passive film, indicated by the retained mirror-like finish after 44 years of exposure at Kure Beach to a marine environment (i.e., salt air with alternate wetting and drying as well as the presence of surface deposits) (Baker 1988, p. 134 and Table 6). More recent examination of specimens from this alloy after more than 50 years of exposure indicates that the samples continue to maintain a mirror-like finish and passive film behavior (McCright 1998, Figure ES-1). Under these same conditions, the less corrosion-resistant Alloy 600 exhibited a corrosion rate of 8 nm/yr after 36 years of exposure. This long-term corrosion rate is consistent with the model prediction. The 50^{th}, 95^{th} and 100^{th} (theoretical maximum) percentile rates at 25 °C predicted by the base-case model are 2.4, 5.8 and 26.4 nm/year respectively (see the 25 °C CDF of the general corrosion rates calculated with the model shown in Figure 6-24). As discussed above, general corrosion behavior of corrosion resistant Ni-Cr-Mo alloys are similar. These long-term results provide corroborative support for the expected excellent long-term passive corrosion behavior of Alloy 22 under chloride-containing aqueous environments that are relevant to repository exposure conditions.

In addition, the general corrosion model implemented in the TSPA assumes that general corrosion of the WPOB progresses uniformly over a large surface (Assumption 5.2). The general corrosion rate is temperature dependent, and for a given temperature, it is assumed to be constant (i.e., time-independent) (Assumption 5.2). Therefore, for a given temperature, the depth of penetration or thinning of the WPOB by general corrosion is equal to the general corrosion rate at that temperature, multiplied by the time duration that the waste package surface is at that temperature. However, general corrosion rates of metals and alloys tend to decrease with time. The dependence of the general corrosion rate of Alloy 22 on the exposure time is shown in Figure 7-1 for the mean general corrosion rates of Alloy 22 measured with different test techniques for exposure time up to 5 years. A trendline was drawn for the data for a better visualization of the data trend. See Table 6-6 for the summary of the data shown in the figure. It is noted that the corrosion rates measured by short term electrochemical techniques provide corroboration of the rates from weight loss method.

The mean general corrosion rate of the crevice samples after 5-year exposure at the LTCTF was 0.0072 μm/year, and the standard deviation was 0.005 μm/year. Each data point for up to 2 years is the mean of the measurements on at least 144 samples, and the data point for 5-year is the mean of 59 samples. The trend of decreasing general corrosion rate with time is consistent with the expected corrosion behavior of passive alloys such as Alloy 22 under repository-type aqueous conditions. The current conservative approach for the constant (time-independent) general corrosion rate at a given temperature in the waste package degradation analysis provides an additional confidence for the general corrosion model.

A comparison of the rates obtained from the temperature-dependent general corrosion model with the rates from alternative techniques from the scientific literature shows that Criterion One has been met. In addition, the conservative approach used in calculating the penetration depth by general corrosion over time would provide an additional confidence to the model and the modeling approach.

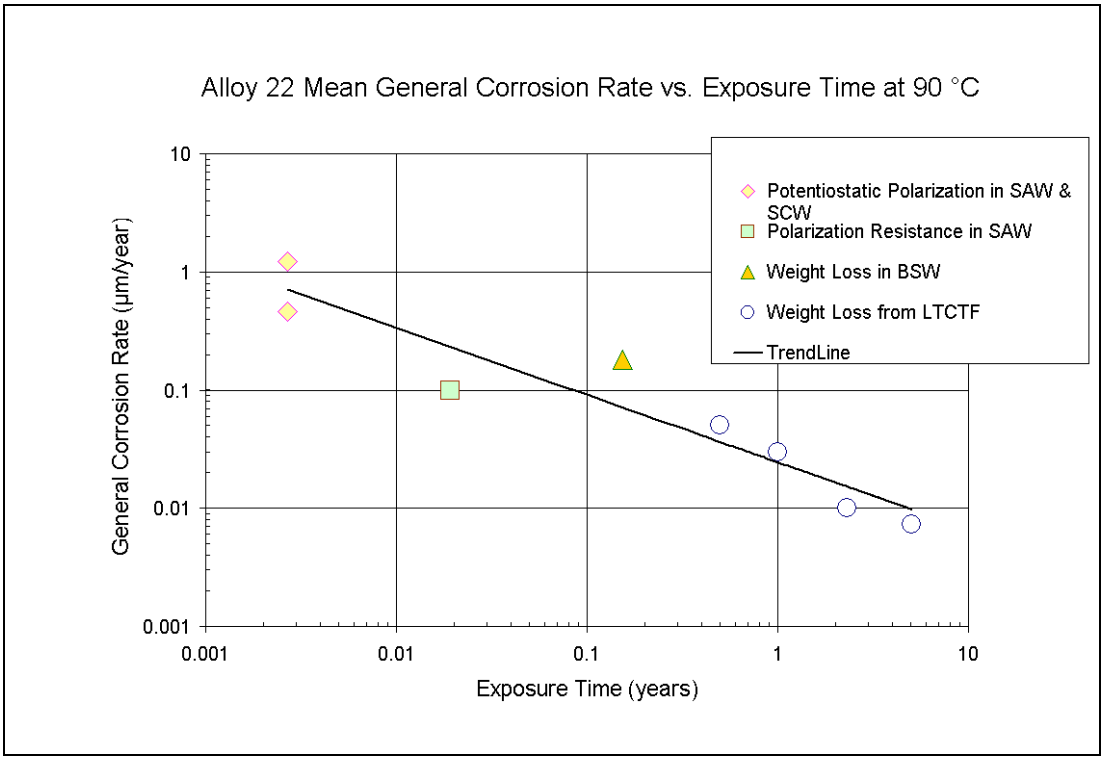

Figure 7-1. Decrease of the Mean General Corrosion Rate of Alloy 22 with Time.

7.2 CORROSION POTENTIAL MODEL OF THE WPOB

Validation of the corrosion potential model of the WPOB requires meeting Criterion Two.

Criterion Two: *Is the response of the correlation for E_{corr} of WP reasonable and consistent with the literature data on relevant corrosion resistant alloys and available analogues for the conditions expected in the repository?*

The long-term corrosion potential model developed to analyze the localized corrosion behavior of the WPOB under the conditions expected in the proposed repository is expressed as follows:

$$E_{corr} = c_o + c_1 T + c_2 pH + c_3 [Cl] + c_4 \log\left(\frac{[NO_3]}{[Cl]}\right) \qquad \text{(Equation 7-2)}$$

where E_{corr} is the long-term corrosion potential in mV vs. SSC, T is the temperature (°C), $[Cl]$ is the chloride ion concentration in moles per kg water, $[NO_3]$ is the nitrate ion concentration in moles per kg water, and c_o, c_1, c_2, c_3, and c_4 are coefficients of the model parameters. The model parameters were evaluated by fitting the model to the long-term corrosion potential data. The estimated regression coefficients and their uncertainty (± 1 standard deviation) are: $c_0 = 365.511 \pm 32.901$, $c_1 = 1.853 \pm 0.374$, $c_2 = -48.091 \pm 2.528$, $c_3 = -29.641 \pm 1.931$, and $c_4 = -4.263 \pm 4.326$. This model is to estimate the long-term steady-state open-circuit corrosion potential of Alloy 22 for a range of exposure conditions related to the proposed repository. The model is not intended to predict short-term corrosion potential because the corrosion potential of Alloy 22 evolves with time under the conditions relevant to the proposed repository.

Few data exist for the steady-state corrosion potential of Alloy 22 for conditions related to the proposed repository that can be used to evaluate the corrosion potential model. A very recent study sponsored by the DOE Nuclear Energy Research Initiative published the measurements of open-circuit corrosion potential of Alloy 22 under air-saturated conditions in a saturated NaCl solution (pH = 3) at 80 °C for a period of 200 days (Jayaweera et al. 2003, pages 9-18 to 9-22, Figure 9.13). At the end of the testing, the corrosion potentials appeared to be approaching steady state values. Chloride ion concentration of the solution was about 6.2 *M*. The measured corrosion potential at the end of the testing (200 days) ranges from 160 to 250 mV vs. SHE.

Because the corrosion potential model is based on the molal concentration (*m*, moles per kg water) for chloride and nitrate ions, the molar chloride concentration (6.2 *M*) for the NaCl solution was approximately converted to 6.5 *m*, conservatively assuming complete dissociation. For the same exposure condition (6.5 *m* [Cl], pH 3 and 80 °C) with a very low nitrate ion concentration of 0.001 *m*, the mean value of the corrosion potential from the corrosion potential model is 177 mV vs. SSC, and ± 2 standard deviation values are 202 and 152 mV vs. SSC respectively. At 25 °C the SSC scale with the reference electrode in saturated KCl solution is more noble than the SHE scale by 199 mV (Sawyer and Roberts 1974, pages 39 to 45, Table 2-4), therefore the model predicted corrosion potentials in the SHE scale are 376 mV (mean), 401 mV (+2 standard deviation), and 351 mV (-2 standard deviation). Although the lower bound of the model predicted corrosion potentials is still higher by about 100 mV, this is considered a reasonably good match with the independently measured data for the alloy. In addition over-estimates of the corrosion potential by the model are conservative because, for a given condition, this would result in narrower margins between the critical potential and corrosion potential.

A comparison of the long-term corrosion potential obtained from the corrosion potential model with the long-term corrosion potential data of Alloy 22 measured independently has shown that Criterion Two has been met.

7.3 CRITICAL POTENTIAL MODEL OF THE WPOB

Validation of the critical potential model of the WPOB requires meeting Criterion Three.

Criterion Three: *Is the response of the correlation for $E_{critical}$ of WP reasonable and consistent with the literature data on relevant corrosion resistant alloys and available analogues for the conditions expected in the repository?*

$E_{critical}$ can be defined as a certain potential above which the current density or corrosion rate of Alloy 22 increases significantly and irreversibly above the general corrosion rate of the passive metal. As a conservative measure, the base-case localized corrosion model uses the crevice repassivation potential (E_{rcrev}) as the critical potential for the localized corrosion initiation analysis. The crevice repassivation potential (E_{rcrev}) is expressed as follows.

$$E_{rcrev} = E^{o}_{rcrev} + \Delta E^{NO_3^-}_{rcrev} \qquad \text{(Equation 7-3)}$$

where E^{o}_{rcrev} is the crevice repassivation potential in the absence of inhibitive nitrate ions, and $\Delta E^{NO_3^-}_{rcrev}$ is the crevice repassivation potential changes resulted from the inhibiting effect of nitrate ion in solution. The crevice repassivation potential of Alloy 22 in the absence of inhibitive nitrate ion is expressed as follows.

$$E^{o}_{rcrev} = a_o + a_1 T + a_2 pH + a_3 \log([Cl]) + a_4 T \times \log([Cl]) \qquad \text{(Equation 7-4)}$$

where a_o, a_1, a_2, a_3, and a_4 are constants, T is the temperature (°C), and $[Cl]$ is the chloride ion concentration in moles per kg water. The value of the coefficients and their uncertainty (±1 standard deviation) of the model parameters from the least square fitting were determined to be: $a_0 = 214.089 \pm 46.880$, $a_1 = -3.696 \pm 0.476$, $a_2 = 25.284 \pm 5.641$, $a_3 = -252.181 \pm 53.912$, and $a_4 = 1.414 \pm 0.547$.

The effect of nitrate ion on the crevice repassivation potential is represented by the following functional form:

$$\Delta E^{NO_3^-}_{rp} = b_o + b_1[NO_3] + b_2 \frac{[NO_3]}{[Cl]} \qquad \text{(Equation 7-5)}$$

where $[Cl]$ is the chloride ion concentration in moles per kg water, $[NO_3]$ is the nitrate ion concentration in moles per kg water, and b_o, b_1 and b_2 are constant. The parameter coefficients and their uncertainty (±1 standard deviation) resulting from the fitting procedure were determined to be: $b_0 = -50.959 \pm 78.168$, $b_1 = 115.867 \pm 64.714$, and $b_2 = 1045 \pm 1320.076$.

There are limited data in the scientific literature for the crevice repassivation potential of Alloy 22 for the conditions relevant to the proposed repository. Even for those literature data that may be applicable, it is difficult to use those data to evaluate the critical potential model because they were obtained using different criteria and/or approaches.

There are three crevice repassivation potential data points for Alloy 22 previously reported by the investigators at the CNWRA for the NRC (Dunn et al. 1999, Figures 3-6 and 3-9). These data were not included in Brossia et al. (2001) and not included in the crevice repassivation model development. These data are summarized in Table 7-1. The data were generated under the CNWRA QA procedures. The crevice repassivation potentials were read directly from the

figures. As shown in the table, the model predicted crevice repassivation potentials of Alloy 22 are all consistent with the measured data.

Table 7-1 Summary of Model Validation Analysis for Crevice Repassivation Potential Model.

Exposure Environment and Data Source	Measured E_{rcrev} (mV SCE)	Measured E_{rcrev} (mV SSC)	Environmental Condition Inputs to Model Calculation	E_{rcrev}, Mean Model Prediction (mV vs. SSC)	E_{rcrev}, ±2 s.d. Model Prediction (mV vs. SSC)
0.5 M NaCl, 10 ppm NO3, pH 8, 175 °C (Dunn et al. 1999, Figure 3-9)	-275	-233	0.51 *m* [Cl], 0.00016 *m* [NO_3], pH 8, 175 °C	-280	-193 (+2 s.d.) -366 (-2 s.d.)
9 M LiCl, 10 ppm NO3, pH 5.6, 95 °C (Dunn et al. 1999, Figure 3-7)	-230	-188	11 *m* [Cl] (assumed), 0.00016 *m* [NO_3], pH 5.6, 95 °C	-169	-152 (+2 s.d.) -186 (-2 s.d.)
11 M LiCl, 10 ppm NO3, pH 5.6, 95 °C (Dunn et al. 1999, Figure 3-7)	-260	-218	13 *m* [Cl] (assumed), 0.00016 *m* [NO_3], pH 5.6, 95 °C	-178	-159 (+2 s.d.) -196 (-2 s.d.)
Note: At 25 °C the saturated calomel reference electrode (SCE) is 42 mV more noble than the silver-silver chloride reference electrode (SSC). The SCE scale potentials were converted to the SSC scale potentials by adding 42 mV.					

Additional model validation was performed by comparing the model prediction for localized corrosion susceptibility (in conjunction with the corrosion potential model validated in Section 7.2) with relevant observations. As discussed in Section 6.4.3 for the WPOB general corrosion model analysis, Alloy 22 crevice samples were tested for over 5 years in three different solutions (SDW, SCW and SAW) in the long-term corrosion testing facility (LTCTF). Because none of the crevice samples have suffered localized corrosion attack after being tested for over 5 years, there are no crevice repassivation potentials to be assigned to those samples. These observations are used just for model validation of the crevice corrosion initiation model (i.e., crevice repassivation potential model in conjunction with the corrosion potential model), assuming as if the crevice samples *were* subject to crevice corrosion. The chloride and nitrate ion moal concentrations of the solutions are target compositions from DTNs LL030703723121.031 and LL030706223121.032. The pHs of the solutions are measured values of the aged solutions from the LTCTF documented in DTN LL030201212251.033.

The analysis results are summarized in Table 7-2. As indicated by the results in the table, the model predicts no localized corrosion occurrence for the exposure conditions, which is consistent with the experimental observations for the 5-year crevice samples. This demonstrates that the crevice corrosion initiation model (crevice repassivation potential model, in conjunction with the corrosion potential model) correctly predicts the crevice corrosion susceptibility of Alloy 22.

The model validation documented in this section has shown that Criterion Three has been met.

Table 7-2 Comparison of Model Prediction for Localized Corrosion Susceptibility with Experimental Observations of Alloy 22 Crevice Samples Tested for Over 5 Years in LTCTF.

Exposure Environment	Crevice Corrosion Observation	pH	[Cl] (m, moles/kg water)	[NO_3] (m, moles/kg water)	Mean E_{corr} (mV vs. SSC)	Mean E_{rcrev} (mV vs. SSC)	Mean ΔE ($E_{rcrev} - E_{corr}$) (mV vs. SSC)
SDW, 90 °C	No	8.55	0.002	0.001	121	906	785
SCW, 90 °C	No	10.72	0.211	0.111	10	748	738
SAW, 90 °C	No	3.55, 3.67 (Avg. 3.61)	0.838	0.426	332	512	180
Note:	1) SDW = simulated dilute water, SCW = simulated concentrated water, SAW = simulated acidified water. 2) The pH values of the aged SDW, SAW and SCW solutions are from DTN LL030201212251.033. 3)) Molal concentrations of chloride and nitrate ions of aged SAW and SCW solutions are from DTNs LL030703723121.031 and LL030706223121.032. Complete dissociation is assumed for chloride and nitrate ion concentrations. 4) Molal concentrations of chloride and nitrate ions of aged SDW solutions were assumed to be same as the target molar concentrations of the species from DTN LL000320405924.146. 4) E_{corr} was calculated using Eqn. (7-2), and E_{rcrev} using Eqn. (7-3).						

7.4 LOCALIZED CORROSION PENETRATION MODEL OF THE WPOB

Validation of the localized corrosion penetration model of the WPOB requires meeting Criterion Four.

Criterion Four: *Is the propagation rate (or a range of the rates) of the localized corrosion model of WP reasonable and consistent with the literature data on relevant corrosion resistant alloys for the conditions expected in the repository?*

Due to the outstanding corrosion resistance of Alloy 22, very little data exist for such localized corrosion under the conditions expected in the proposed repository. The literature data for localized corrosion of relevant alloys that were considered for the current localized penetration rate model are for extremely corrosive conditions that are not expected in the proposed repository. Those extreme penetration rates found in the literature were used to bound localized corrosion rates of Alloy 22 under repository conditions.

In addition, the localized corrosion penetration model assumes that, when it occurs, localized corrosion of the WPOB propagates at a (time-independent) constant rate (Assumption 5.4). This assumption is highly conservative because it is known that the localized corrosion rate decreases with time, and this is particularly more likely under discontinued tortuous thin water film conditions that are expected on the waste package surface in the post-closure repository. See Section 6.4.4.8 for detailed discussion on the above issues.

Because of the conservative approaches that were already embedded in the penetration rate model, further validation of the localized corrosion penetration is not necessary, and Criterion Four has been met.

7.5 SUMMARY OF MODEL VALIDATION

In light of the above discussion, it may be concluded that the general and localized corrosion models for the WPOB and their output corroborate well with those reported in the scientific literature. It is also clear from the above discussion that the validation activities performed for building confidence in the model have sufficiently strong scientific bases, and that all of the four criteria used to determine that the required level of confidence in the model has been achieved have been met.

In order to provide further confidence, post-development validation of the general corrosion and localized corrosion models will continue. Post-development validation for the general corrosion model will include comparison of the model against any additional applicable data in the corrosion literature and any long-term corrosion data from the LTCTF that is obtained or processed after the development of this report. Post-development validation for the localized corrosion model will include comparison of the correlations of the crevice repassivation potential (E_{rcrev}) and the long-term steady state corrosion potential (E_{corr}) of Alloy 22 against any additional applicable literature data and additional data from the Project's on-going waste package materials testing programs. Also included in the post-development validation activities is publication of the model and analysis and the supporting data in peer-reviewed professional journals.

8 CONCLUSIONS

8.1 BASE CASE MODEL SUMMARY

This model report documents the analyses and models for general and localized corrosion of the waste package outer barrier (WPOB). The purpose of the general and localized corrosion models are to analyze degradation of the Alloy 22 outer barrier by general and localized corrosion processes under the expected repository environmental conditions over the repository performance period. The general and localized corrosion models include several sub-models, which account for dry oxidation, aqueous general corrosion, microbially influenced corrosion (MIC), crevice corrosion initiation, and crevice corrosion growth. The model overview is presented in Figure 8-1.

Corrosion performance of the WPOB depends on the integrity of the thin, compact, adherent passive film formed on the alloy surface in contact with the exposure environments in the repository. The extremely low general corrosion rates and excellent resistance to localized corrosion of the WPOB in the repository intimately depend on the long-term stability of the passive film on the surface of the barrier. The passivity of Alloy 22 was evaluated by examining the oxide layers formed in a mixed-salt environment at 95 °C. The surface analysis data indicated that the oxide layers responsible for passivity of Alloy 22 consist of chromium oxide (Cr_2O_3) containing Ni. The collected data indicated that (1) the passive films become very protective and stable, (2) contributions from metal corrosion become extremely small, and (3) redox reactions from the species in solution are stable.

Dry oxidation is not a performance limiting process of the WPOB under the exposure conditions expected in the repository and is not considered for the waste package performance analysis. Aging and phase stability of Alloy 22 is not expected to significantly impact the WPOB corrosion performance under the thermal conditions expected in the repository, therefore this process is not considered in the waste package performance analysis.

General corrosion of the WPOB occurs when the RH at the waste package surface is equal to or greater than the RH threshold ($RH_{threshold}$) for corrosion initiation. The general corrosion rate of the WPOB is a function of temperature, expressed with an activation energy using a modified Arrhenius relation. Because of very low general corrosion rates of the WPOB for the conditions expected in the repository, waste package performance is not limited by general corrosion during the regulatory time period. As a bounding conservative analysis, for a constant waste package surface temperature of 150 ºC, the median penetration depth by general corrosion over 10,000 years, using the median general corrosion rate of 51.8 nm/year, is about 518 µm, which is less than 3 percent of the total thickness of the WPOB (20 mm). For the upper bound value of the general corrosion rate of 256 nm/year (99.99^{th} percentile rate at 150 °C), the total penetration depth by general corrosion is about 2560 µm, which is less than 13 percent of the total thickness of the WPOB. This bounding analysis demonstrates that the waste package performance in the repository is not limited by general corrosion.

The WPOB is subject to MIC when the relative humidity at the waste package surface is equal to or greater than 90 %. The MIC effect is represented by an enhancement to the abiotic general corrosion rate of the WPOB.

Crevice corrosion of the WPOB is modeled with a crevice corrosion initiation model and a propagation model. The initiation model considers that crevice corrosion of the WPOB occurs when the steady-state corrosion potential (E_{corr}) is equal to or greater than the crevice repassivation potential (E_{rcrev}), that is, ΔE (= E_{rcrev} - E_{corr}) ≤ 0. The WPOB is not subject to crevice corrosion if the solution contacting the waste package has a neutral to alkaline pH or contains significant concentrations of inhibitive ions such as nitrate. The WPOB is potentially susceptible to crevice corrosion if an acidic chloride-containing solution with relatively lower concentrations of inhibitive ions contacts the waste package while it is at elevated temperatures. However, once the waste package cools to temperatures that are lower than a minimum temperature for crevice corrosion initiation in such chloride-containing solutions, the waste packages are completely immune to crevice corrosion. Such threshold temperatures depend on pH, chloride concentration and nitrate concentration of the contacting solutions.

Additional details of the model summary are given in the following subsections.

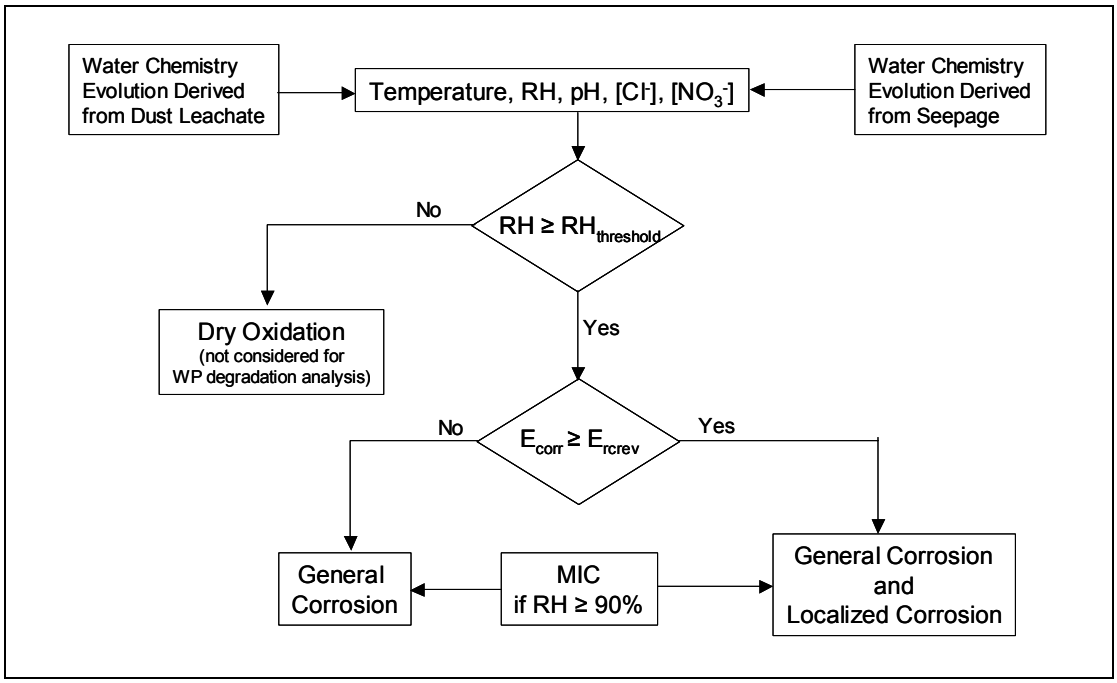

Figure 8-1. Schematic Representation of General Corrosion and Localized Corrosion Model of the WPOB.

8.2 GENERAL CORROSION MODEL

General corrosion of the WPOB occurs when the RH at the waste package surface is equal to or greater than the RH threshold for corrosion initiation ($RH_{threshold}$). The base-case general corrosion model for the WPOB is based on a temperature dependence of the corrosion process, represented by an activation energy using a modified Arrhenius relation. The model is expressed as follows:

$$\ln(R_T) = \ln(R_o) + C_1\left(\frac{1}{T} - \frac{1}{333.15}\right) \quad \text{(Equation 8-1)}$$

R_T is the temperature-dependent general corrosion rate in nm/year, T is temperature in Kelvin, and R_o and C_1 are constants. The activation energy term (C_1) was obtained from short-term polarization resistance data for Alloy 22 specimens tested for a range of sample configurations, metallurgical conditions, and exposure conditions. The activation energy term is normally distributed with a mean of -3116.47 and a standard deviation of 296.47. The activation energy was estimated to be 25.9 ± 2.5 kJ/mol. R_o is a Weibull distribution (α = 8.88, β = 1.62, and θ = 0) fitted to the general corrosion rate distribution derived from the weight loss data of the 5-year crevice specimens. The 5-year data were considered to represent the distribution of long-term general corrosion rates of the WPOB at 60 °C.

The entire variance in R_o represents the variability of the general corrosion process. It is recommended that the general corrosion rate variability represented by the parameter be applied to among the waste packages to be modeled and also the local areas on an individual waste package. The entire variance in the temperature dependence term (C_1) is due to uncertainty, and the uncertainty is limited to ± 3 standard deviations.

The WPOB is considered to be subject to MIC when the relative humidity at the WPOB surface is equal to or greater than 90 %. The effect of MIC on general corrosion of the WPOB is represented by an enhancement factor (or MIC factor) to the general corrosion rate in the absence of MIC. The MIC factor is uniformly distributed between 1 and 2, and the entire variance of the distribution is due to uncertainty.

The general corrosion model is applied to the conditions in which a stable aqueous water film can exist on the waste package surface. The MIC model is applied when the relative humidity at the waste package surface is greater than 90 %.

The technical product outputs of the general corrosion model analysis are documented in the output DTN SN0308T0506303.004 and summarized in Table 8-1.

8.3 LOCALIZED CORROSION INITIATION MODEL

Localized corrosion of the WPOB is modeled with two model components: an initiation model and a propagation model. The initiation model considers that localized corrosion of the WPOB occurs when the steady-state corrosion potential (E_{corr}) is equal to or greater than a certain critical potential ($E_{critical}$), that is, ΔE (= $E_{critical}$ - E_{corr}) ≤ 0. As a conservative measure, the localized corrosion initiation model uses the crevice repassivation potential (E_{rcrev}) as the critical potential. The crevice repassivation potential (E_{rcrev}) is expressed as follows.

$$E_{rcrev} = E^{o}_{rcrev} + \Delta E^{NO_3^-}_{rcrev} \quad \text{(Equation 8-2)}$$

where E^{o}_{rcrev} is the crevice repassivation potential in the absence of inhibitive nitrate ions, and $\Delta E^{NO_3^-}_{rcrev}$ is the crevice repassivation potential changes resulting from the inhibiting effect of nitrate ion in solution. The potentials are in mV vs. SSC.

Table 8-1. Summary of General Corrosion Model Output for WPOB

Output Name	Output Description	DTN	Output Uncertainty		
			Source of Uncertainty	Uncertainty Distribution (if applicable)	Characteristic Values (if applicable)
Parameter R_o of temperature dependent general corrosion model, Equation 8-1.	Weibull distribution (scale factor α = 8.88, shape factor β = 1.62, and location factor θ = 0). (Section 6.4.3.4)	SN0308T0506303.004	Measurement	No uncertainty (entire variance due to variability)	N/A
Parameter C_1 of temperature dependent general corrosion model, Equation 8-1.	Normal distribution (mean –3116.47, s.d. 296.47). Limited to ± 3 standard deviations. (Section 6.4.3.4)	SN0308T0506303.004	Measurement	Entire distribution	N/A
MIC enhancement factor	Uniform distribution (1, 2). (Section 6.4.5)	SN0308T0506303.004	Measurement	Entire distribution	N/A
MIC initiation threshold	Relative humidity threshold for MIC initiation. (see Section 6.4.5)	SN0308T0506303.004	N/A	N/A	90 %
Error analysis	Summary of error analysis for corrosion rates based on 5-year weight loss measurements. (Tables 6-4 and 6-5)	SN0308T0506303.004	Measurement	N/A	N/A

The crevice repassivation potential of the WPOB in the absence of inhibitive nitrate ion is expressed as follows.

$$E^{o}_{rcrev} = a_o + a_1 T + a_2 pH + a_3 \log([Cl^-]) + a_4 T \times \log([Cl^-]) \qquad \text{(Equation 8-3)}$$

where a_o, a_1, a_2, a_3, and a_4 are constants, T is the temperature (°C), and $[Cl^-]$ is the chloride ion concentration in molal (moles/kg water). The value of the coefficients and their uncertainty (±1

standard deviation) of the model parameters are $a_0 = 214.089 \pm 46.880$, $a_1 = -3.696 \pm 0.476$, $a_2 = 25.284 \pm 5.641$, $a_3 = -252.181 \pm 53.912$, and $a_4 = 1.414 \pm 0.547$. The variance of the model is calculated via the covariance matrix (see Section 6.4.4.3), and the entire variance is due to uncertainty. It is recommended that the uncertainty of the coefficients be limited to ±2 standard deviations.

The effect of nitrate ion on the crevice repassivation potential is represented as follows.

$$\Delta E_{rcrev}^{NO_3^-} = b_o + b_1[NO_3^-] + b_2 \frac{[NO_3^-]}{[Cl^-]} \qquad \text{(Equation 8-4)}$$

where b_o, b_1 and b_2 are constants, $[NO_3^-]$ is the nitrate ion concentration in molal (moles/kg water), and other parameters are defined as before. The parameter coefficients and their uncertainty (±1 standard deviation) are: $b_0 = -50.959 \pm 78.168$, $b_1 = 115.867 \pm 64.714$, and $b_2 = 1045 \pm 1320.076$. The effect of the interaction of the competing aggressive ion (chloride ion) and inhibitive nitrate ion on the crevice repassivation potential is represented with the ratio of the concentrations of the two competing ions and the concentration of nitrate ion. The maximum value of the ratio term is limited to 1.0. Because the effect of the measurement uncertainty of the CPP tests has already been captured in the crevice repassivation potential model with no nitrate ion present (E_{rcrev}^{o}), it is recommended that the mean value of the $\Delta E_{rcrev}^{NO_3^-}$ model be used to determine the crevice repassivation potential ($E_{rcrev.}$).

The long-term steady-state corrosion potential model for the WPOB is expressed as follows:

$$E_{corr} = c_o + c_1 T + c_2 pH + c_3[Cl^-] + c_4 \log(\frac{[NO_3^-]}{[Cl^-]}) \qquad \text{(Equation 8-5)}$$

where E_{corr} is the long-term steady-state corrosion potential in mV vs. SSC, c_o, c_1, c_2, c_3, *and* c_4 are coefficients of the model parameters, and other parameters are defined as before. The model was evaluated by fitting it to the long-term corrosion potential data. The estimated regression coefficients and their uncertainty (± 1 standard deviation) are: $c_0 = 365.511 \pm 32.901$, $c_1 = 1.853 \pm 0.374$, $c_2 = -48.091 \pm 2.528$, $c_3 = -29.641 \pm 1.931$, and $c_4 = -4.263 \pm 4.326$. The variance of the model is calculated via the covariance matrix (see Section 6.4.4.5), and the entire variance is due to uncertainty. As with the crevice repassivation potential model, it is recommended that the uncertainty of the parameter coefficients of the corrosion potential model be limited to ±2 standard deviations.

This corrosion potential model is *to estimate the long-term steady-state open-circuit corrosion potential of Alloy 22* for a range of exposure conditions related to the proposed repository. The model *is not intended for short-term transient conditions*. As seen from the dependence of the corrosion potential on the logarithm of the nitrate to chloride ion concentration ratio, the model

requires the nitrate concentration be greater than zero. Therefore, for a condition with no nitrate ion present, it is recommended that a small value be used for the nitrate ion concentration.

The localized corrosion model is applied for the following conditions.

- Temperature from 20 °C up to boiling temperature of $CaCl_2$–containing brines.
- Solution pH from 2 to 12.
- Chloride concentration from a very low non-zero value to 25 molal (*m*, moles/kg water). A value of 0.001 *m* is recommended for the chloride concentration for solutions with no chloride.
- Nitrate concentration from a very low non-zero value to 6 molal (*m*, moles/kg water). A value of 0.001 *m* is recommended for the nitrate concentration for solutions with no nitrate.
- The nitrate to chloride concentration ratio from zero to 1.0 for the crevice repassivation potential model. For solutions with the ratio greater than 1.0, the ratio is limited to 1.0. This ratio range is not applied to the corrosion potential model.

The entire variance of the crevice corrosion initiation model (i.e., crevice repassivation potential model and corrosion potential model) is due to uncertainty. Variability in the crevice repassivation potential and corrosion potential among the waste packages to be modeled is represented with the temporally and spatially varying waste package temperature and water chemistry contacting the waste packages.

Note that the crevice corrosion initiation model is used for evaluating *the long-term localized corrosion susceptibility of the WPOB* and is not intended for short-term transient behavior. Because only nitrate ions are accounted for in the crevice corrosion initiation model for the inhibitive effect, the model results for solutions with significant amounts of other potentially inhibitive ions such as carbonate and sulfate (in addition to nitrate ions) are highly conservative. The model results for the beneficial effects of the inhibitive ions combined with the alkaline pH conditions of the typical carbonate waters in the repository are consistent with the experimental observations of no localized corrosion susceptibility of Alloy 22 in those waters (see Section 7.3).

The technical product outputs of the crevice corrosion initiation model analysis are documented in the output DTN SN0308T0506303.003 and summarized in Table 8-2.

8.4 LOCALIZED CORROSION PROPAGATION MODEL

The localized corrosion penetration model assumes that, when it occurs, localized corrosion propagates in the WPOB at a (time-independent) constant rate (Assumption 5.4). This is a highly conservative assumption because it is known that the localized corrosion rate decreases with time, and this is particularly more likely under discontinued tortuous thin water film conditions that are expected to form on the waste package surface in the post-closure repository. Also, in general, localized corrosion tends to arrest or die shortly after initiation.

Due to the outstanding corrosion resistance of Alloy 22, very little data exist for such localized corrosion under the conditions expected in the proposed repository. The literature data for

localized corrosion of relevant alloys that were considered for the current localized penetration rate model are for extremely corrosive conditions that are not expected in the proposed repository. Those extreme penetration rates found in the literature were used to bound localized corrosion rates of Alloy 22 under repository conditions.

The technical product outputs of the crevice corrosion propagation model analysis are documented in the output DTN SN0308T0506303.003 and summarized in Table 8-2.

Table 8-2. Summary of Localized Corrosion Model Output for WPOB

Output Name	Output Description	DTN	Output Uncertainty		
			Source of Uncertainty	Uncertainty Distribution (if applicable)	Characteristic Values (if applicable)
5 coefficients of crevice repassivation potential model without nitrate, Equation 8-3	a_o = normal distribution, N(mean = 214.089, s.d. = 46.880) a_1 = N(mean = -3.696, s.d. = 0.476) a_2 = N(mean = 25.284, s.d. = 5.641) a_3 = N(mean = -252.181, s.d. = 53.912) a_4 = N(mean = 1.414, s.d. = 0.547) All distributions are limited to 2 standard deviations.	SN0308T0506303.003	Measurement	Entire distribution	N/A
3 coefficients of crevice repassivation potential change model due to nitrate, Equation 8-4	b_o = -50.959 b_1 = 115.867 b_2 = 1045.0	SN0308T0506303.003	N/A	N/A	N/A
5 coefficients of corrosion potential model, Equation 8-5	c_o = normal distribution, N(mean = 365.511, s.d. = 32.901) c_1 = N(mean = 1.853, s.d. = 0.374) c_2 = N(mean = -48.091, s.d. =	SN0308T0506303.003	Measurement	Entire distribution	N/A

Output Name	Output Description	DTN	Output Uncertainty		
			Source of Uncertainty	Uncertainty Distribution (if applicable)	Characteristic Values (if applicable)
	2.528) c_3 = N(mean = -29.641, s.d. = 1.931) c_4 = N(mean = -4.263, s.d. = 4.326) All distributions are limited to 2 standard deviations.				
Crevice corrosion propagation rate (Table 6-8)	Log-uniform distribution, 0^{th} percentile = 12.7 μm/year 50^{th} percentile = 127 μm/year 100^{th} percentile = 1270 μm/year	SN0308T0506303.003	Conceptual model, data	Entire distribution	N/A

8.5 ACCEPTANCE CRITERIA

1. System Description and Demonstration of Multiple Barriers

   - AC1: Identification of Barriers is Adequate (Sections 1.3 and 6.3)
   - AC2: Description of the Capability of Identified Barriers is Acceptable (Section 6.3)
   - AC3: Technical Basis for Barrier Capability is Adequately Presented (Sections 6.4.3, 6.4.4, 6.4.5, and 6.4.6)

The system that this model report addresses is the engineering barrier system (EBS), and the barrier that this model report addresses is the waste package outer barrier (WPOB). This is described in Sections 1.3 and 6.3. The capability of the WPOB is to contain the waste in the waste package and prevent water from contacting the waste, which is described in Section 6.3 as part of the conceptual model discussion for general and localized corrosion of the WPOB. The technical basis for the barrier capability is documented in detail in Sections 6.4.2, 6.4.3, 6.4.4, 6.4.5, and 6.4.6. Section 6.4.3 documents the technical basis for the general corrosion model, Section 6.4.4 for the localized corrosion model, and Section 6.4.5 for the microbially influenced corrosion (MIC) model. Section 6.4.2 documents the technical basis that the degradation of the WPOB by dry oxidation is negligible under the repository thermal conditions, therefore not included in the waste package degradation analysis. Section 6.4.6 documents the technical basis that aging and phase stability of Alloy 22 is not expected to significantly affect the corrosion performance of the WPOB in the repository, therefore not included in the waste package degradation analysis.

2. Degradation of Engineered Barriers

- AC1: System Description and Model Integration are Adequate (Section 6.3)
- AC2: Data are Sufficient for Model Justification (Sections 4.1.1 and 7)
- AC3: Data Uncertainty is Characterized and Propagated Through the Model Abstraction (Sections 6.4.3, 6.4.4 and 6.4.5)
- AC4: Model Uncertainty is Characterized and Propagated Through the Model Abstraction (Sections 6.4.3, 6.4.4 and 6.4.5)
- AC5: Model Abstraction Output is Supported by Objective Comparisons (Section 7)

The waste package system and the WPOB that this model report addresses are described in detail in Section 6.3 as part of the conceptual model discussion for general and localized corrosion of the WPOB. Integration of the sub-models for the WPOB corrosion degradation analysis (aqueous general corrosion model, MIC model, crevice repassivation potential model, corrosion potential model, and localized corrosion penetration model) is also described in Section 6.3. Section 4.1.1 documents in detail the input data and their use for the model analysis. Attachments II to VII document the numerical values of the data used in the model development and analysis.

Uncertainties in the data used for the general corrosion model analysis (5-year weight loss measurements and short-term linear polarization resistance measurements) were characterized and quantified, and propagated through the general corrosion model abstraction (Section 6.4.3). Uncertainties in the data used for the localized corrosion model analysis (crevice repassivation potentials, and long-term steady-state corrosion potentials) were characterized and quantified, and propagated through the localized corrosion model abstraction (Section 6.4.4). A conservative bounding approach, based on the literature data for similar alloys in highly corrosive environments, was used to capture the uncertainty in the localized corrosion rate of Alloy 22 (Section 6.4.4). The MIC data uncertainty was quantified and propagated through the MIC model abstraction (Section 6.4.5).

The uncertainties in the general corrosion and localized corrosion models were addressed through the qualitative assessment of a number of alternative conceptual models (Sections 6.4.3 and 6.4.4). The general corrosion and localized corrosion models were validated by comparing the model outputs with independent data from the literature (Section 7).

9 INPUTS AND REFERENCES

9.1 DOCUMENTS CITED

Agarwal, D.C. 2000. "Nickel and Nickel Alloys." Chapter 45 of *Uhlig's Corrosion Handbook.* 2nd Edition. Revie, R.W., ed. New York, New York: John Wiley & Sons. TIC: 248360.

Akashi, M.; Nakayama, G.; and Fukuda, T. 1998. "Initiation Criteria for Crevice Corrosion of Titanium Alloys Used for HLW Disposal Overpack." *[Corrosion in Advanced Materials and Systems, Proceedings of] Corrosion/98 [Research Topical Symposium].* Paper No. 158. Houston, Texas: NACE International. TIC: 254584.

Andresen, P.L.; Young, L.M.; Kim, Y.J.; Emigh, P.W.; Catlin, G.M.; and Martiniano, P.J. 2002. *Stress Corrosion Crack Initiation & Growth Measurements in Environments Relevant to High Level Nuclear Waste Packages.* [Schenectady, New York]: GE Global Research Center. ACC: MOL.20020614.0298.

ASM International. 1987. *Corrosion.* Volume 13 of *ASM Handbook.* Formerly 9th Edition, Metals Handbook. [Materials Park, Ohio]: ASM International. TIC: 240704.

Baker, E.A. 1988. “Long-Term Corrosion Behavior of Materials in the Marine Atmosphere.” Degradation of Metals in the Atmosphere, [Proceedings of the Symposium on Corrosion of Metals, Philadelphia, Pennsylvania, 12-13 May 1986]. Dean, S.W. and Lee, T.S., eds. ASTM STP 965. Pages 125-144. Philadelphia, Pennsylvania: American Society for Testing and Materials. TIC: 224019.

Beavers, J.A.; Devine, T.M., Jr.; Frankel, G.S.; Jones, R.H.; Kelly, R.G.; Latanision, R.M.; and Payer, J.H. 2002. *Final Report, Waste Package Materials Performance Peer Review Panel, February 28, 2002.* [Las Vegas, Nevada]: Waste Package Materials Performance Peer Review Panel. ACC: MOL.20020614.0035.

Böhni, H. 2000. "Localized Corrosion of Passive Metals." Chapter 10 of *Uhlig's Corrosion Handbook.* Revie, R.W., ed. 2nd Edition. New York, New York: John Wiley & Sons. TIC: 248360.

Borenstein, S.W. and White, D.C. 1989. “Influence of Welding Variables on Microbiologically Influenced Corrosion of Austenitic Stainless Steel Weldments.” *Corrosion 89 April-17-21, 1989 New Orleans Convention Center, New Orleans, Louisiana, Paper Number 183,* 183/1 - 183/13. Houston, Texas: National Association of Corrosion Engineers. TIC: 246583.

Brossia, C.S.; Browning, L.; Dunn, D.S.; Moghissi, O.C.; Pensado, O.; and Yang, L. 2001. *Effect of Environment on the Corrosion of Waste Package and Drip Shield Materials.* CNWRA 2001-003. San Antonio, Texas: Center for Nuclear Waste Regulatory Analyses. TIC: 252324.

BSC (Bechtel SAIC Company) 2001. *FY 01 Supplemental Science and Performance Analyses, Volume 1: Scientific Bases and Analyses.* TDR-MGR-MD-000007 REV 00 ICN 01. Las Vegas, Nevada: Bechtel SAIC Company. ACC: MOL.20010801.0404; MOL.20010712.0062; MOL.20010815.0001.

BSC (Bechtel SAIC Company) 2002a. *Technical Work Plan for: Waste Package Materials Data Analyses and Modeling.* TWP-EBS-MD-000005 REV 05. Las Vegas, Nevada: Bechtel SAIC Company. ACC: MOL.20021218.0029.

BSC (Bechtel SAIC Company) 2002b. *The Enhanced Plan for Features, Events, and Processes (FEPs) at Yucca Mountain.* TDR-WIS-PA-000005 REV 00. Las Vegas, Nevada: Bechtel SAIC Company. ACC: MOL.20020417.0385.

BSC (Bechtel SAIC Company) 2002c. *Repository Design Project, Repository/PA IED Emplacement Drift Configuration.* 800-IED-EBS0-00200-000-00A. Las Vegas, Nevada: Bechtel SAIC Company. ACC: MOL.20021031.0104.

BSC (Bechtel SAIC Company) 2003a. *Aging and Phase Stability of Waste Package Outer Barrier.* ANL-EBS-MD-000002 REV 01 ICN 0. Las Vegas, Nevada: Bechtel SAIC Company. ACC: DOC.20030807.0004.

BSC (Bechtel SAIC Company) 2003b. *Repository Design Project, RDP/PA IED Typical Waste Package Components Assembly 1 of 9.* 800-IED-WIS0-00201-000-00B. Las Vegas, Nevada: Bechtel SAIC Company. ACC: ENG.20030808.0004.

Canori, G.F. and Leitner, M.M. 2003. *Project Requirements Document.* TER-MGR-MD-000001 REV 01. Las Vegas, Nevada: Bechtel SAIC Company. ACC: DOC.20030404.0003.

Cleveland, W.S. 1993. *Visualizing Data.* Summit, New Jersey: Hobart Press. TIC: 254702.

CRWMS M&O 1998. *Waste Package Degradation Expert Elicitation Project.* Rev. 1. Las Vegas, Nevada: CRWMS M&O. ACC: MOL.19980727.0002.

CRWMS M&O 1999a. *Waste Package Material Properties.* BBA000000-01717-0210-00017 REV 00. Las Vegas, Nevada: CRWMS M&O. ACC: MOL.19990407.0172.

CRWMS M&O 1999b. *Classification of the MGR Uncanistered Spent Nuclear Fuel Disposal Container System.* ANL-UDC-SE-000001 REV 00. Las Vegas, Nevada: CRWMS M&O. ACC: MOL.19990928.0216.

CRWMS M&O 2000a. *Total System Performance Assessment for the Site Recommendation.* TDR-WIS-PA-000001 REV 00 ICN 01. Las Vegas, Nevada: CRWMS M&O. ACC: MOL.20001220.0045.

CRWMS M&O 2000b. *In-Drift Microbial Communities.* ANL-EBS-MD-000038 REV 00 ICN 01. Las Vegas, Nevada: CRWMS M&O. ACC: MOL.20001213.0066.

CRWMS M&O 2000c. *Waste Package Degradation Process Model Report.* TDR-WIS-MD-000002 REV 00 ICN 02. Las Vegas, Nevada: CRWMS M&O. ACC: MOL.20001228.0229.

CRWMS M&O 2001. *FEPs Screening of Processes and Issues in Drip Shield and Waste Package Degradation.* ANL-EBS-PA-000002 REV 01. Las Vegas, Nevada: CRWMS M&O. ACC: MOL.20010216.0004.

DOE (U.S. Department of Energy) 2003. *Quality Assurance Requirements and Description.* DOE/RW-0333P, Rev. 13. Washington, D.C.: U.S. Department of Energy, Office of Civilian Radioactive Waste Management. ACC: DOC.20030422.0003.

Dunn, D.S.; Pan, Y-M.; and Cragnolino, G.A. 1999. *Effects of Environmental Factors on the Aqueous Corrosion of High-Level Radioactive Waste Containers—Experimental Results and Models.* CNWRA 99-004. San Antonio, Texas: Center for Nuclear Waste Regulatory Analyses. TIC: 246615.

Dunn, D.S.; Cragnolino, G.A.; and Sridhar, N. 2000. "An Electrochemical Approach to Predicting Long-Term Localized Corrosion of Corrosion-Resistant High-Level Waste Container Materials." *Corrosion, 56,* (1), 90-104. Houston, Texas: National Association of Corrosion Engineers. TIC: 254836.

Dunn, D.S. and Brossia, C.S. 2002. "Assessment of Passive and Localized Corrosion Processes for Alloy 22 as a High-Level Nuclear Waste Container Material." *Corrosion/2002, [57th Annual Conference & Exposition, April 7-11, 2002, Denver, Colorado].* Paper No. 02548. Houston, Texas: NACE International. TIC: 254579.

Dunn, D.S.; Yang, L.; Pan, Y.-M.; and Cragnolino, G.A. 2003. "Localized Corrosion Susceptibility of Alloy 22." *Corrosion/2003, [58th Annual Conference & Exposition, March 16-20, 2003, San Diego, California].* Paper No. 03697. Houston, Texas: NACE International. TIC: 254387.

Enos, D.G. and Taylor, S.R. 1996. "Influence of Sulfate-Reducing Bacteria on Alloy 625 and Austenitic Stainless Steel Weldments." Corrosion *Science, 52,* (11), 831-843. Houston, Texas: National Association of Corrosion Engineers International. TIC: 246554.

EPRI (Electric Power Research Institute) 2002. Evaluation of the Proposed High-Level Radioactive Waste Repository at Yucca Mountain Using Total System Performance Assessment, Phase 6. EPRI TR-1003031. Palo Alto, California: Electric Power Research Institute. TIC: 252239.

Estill, J.C.; Hust, G.A.; and Rebak, R.B. 2003. "Long Term Corrosion Potential Behavior of Alloy 22." *Corrosion/2003, [58th Annual Conference & Exposition, March 16-20, 2003, San Diego, California].* Paper No. 03688. Houston, Texas: NACE International. TIC: 254387.

Estill, J.C. 1998. *"Long-Term Corrosion Studies." Engineered Materials Characterization Report.* UCRL-ID-119564. Vol. 3. Livermore, California: Lawrence Livermore National Laboratory. ACC: MOL.19981222.0137.

Evans, M.; Hastings, N.; and Peacock, B. 1993. *Statistical Distributions.* 2nd Edition. New York, New York: John Wiley & Sons. TIC: 246114.

Evans, K.J. and Rebak, R.B. 2002. "Passivity of Alloy 22 in Concentrated Electrolytes Effect of Temperature and Solution Composition." *Corrosion Science, A Retrospective and Current Status in Honor of Robert P. Frankenthal, Proceedings of the International Symposium.* Frankel, G.S.; Isaacs, H.S.; Scully, J.R.; and Sinclair, J.D., eds. Proceedings Volume 2002-13. 344-354. Pennington, New Jersey: Electrochemical Society. TIC: 254801.

Fontana, M.G. 1986. *Corrosion Engineering.* 3rd Edition. New York, New York: McGraw-Hill. TIC: 240700.

Frankel, G.S. 1998. "Pitting Corrosion of Metals, A Review of the Critical Factors." *Journal of the Electrochemical Society, 145,* (6), 2186-2198. Pennington, New Jersey: Electrochemical Society. TIC: 254587.

Frankel, G.S. 2002. "Localized Corrosion Phenomenology and Controlling Parameters." Section 6 of *Waste Package Materials Performance Peer Review, A Compilation of Special Topic Reports.* Wong, F.M.G. and Payer, J.H., eds. Las Vegas, Nevada: Waste Package Materials Performance Peer Review Panel. ACC: MOL.20020731.0138.

Frankel, G.S. and Kelly, R.G. 2002. "Passivity-Induced Ennoblement." Section 11 of *Waste Package Materials Performance Peer Review, A Compilation of Special Topic Reports.* Wong, F.M.G. and Payer, J.H., eds. Las Vegas, Nevada: Waste Package Materials Performance Peer Review Panel. ACC: MOL.20020731.0138.

Freeze, G.A.; Brodsky, N.S.; Swift, P.N 2001. *The Development of Information Catalogued in REV00 of the YMP FEP Database*. TDR-WIS-MD-000003 REV 00 ICN 01. Las Vegas, Nevada: Bechtel SAIC Company. ACC: MOL.20010301.0237.

Gdowski, GE 1991. *Survey of Degradation Modes of Four Nickel-Chromium-Molybdenum Alloys.* UCRL-ID-108330. Livermore, California: Lawrence Livermore National Laboratory. ACC: NNA.19910521.0010.

Gruss, K.A.; Cragnolino, G.A.; Dunn, D.S.; and Sridhar, N. 1998. "Repassivation Potential for Localized Corrosion of Alloys 625 and C22 in Simulated Repository Environments." *Proceedings of Corrosion 98, March 22-27, 1998, San Diego, California,* 149/1 to 149/15. Houston, Texas: NACE International. TIC: 237149.

Hack, H.P. 1983. "Crevice Corrosion Behavior of Molybdenum-Containing Stainless Steels in Seawater." *Materials Performance, 22,* (6), 24-30. Houston, Texas: NACE International. TIC: 245826.

Haynes International. 1997a. *Hastelloy C-22 Alloy*. Kokomo, Indiana: Haynes International. TIC: 238121.

Haynes International 1997b. *Hastelloy Alloy C-276. Haynes International Product Brochure.* Kokomo, Indiana: Haynes International. TIC: 238832.

Horn, J. and Jones, D. 2002. "Microbiologically Influenced Corrosion: Perspectives and Approaches." *Manual of Environmental Microbiology.* 2nd Edition. Hurst, C.J., ed. Pages 1072-1083. Washington, D.C.: ASM Press. TIC: 254738.

Hua, F.H. 2002. *Testing of Candidate Container Materials to Resolve Post-VA Waste Package Materials Issues, DE-AC08-01RW12101, Final Report.* RDD:02:43761-301-000:02. Alliance, Ohio: McDermott Technology. ACC: MOL.20030709.0142.

Hunkeler, F. and Boehni, H. 1983. "Pit Growth Measurments on Stainless Steels." Passivity of Metals and Semiconductors, [Proceedings of the Fifth International Symposium on Passivity, Bombannes, France, May 30-June 3, 1983]. Froment, M., ed. Pages 655-660. New York, New York: Elsevier. TIC: 236283.

Ishikawa, H.; Honda, A.; and Sasaki, N. 1994. "Long Life Prediction of Carbon Steel Overpacks for Geological Isolation of High-Level Radioactive Waste." *Life Prediction of Corrodible Structures.* Parkins, R.N.; ed. Volume 1. 454-483. Houston, Texas: NACE International. TIC: 254834.

Jain, V.; Dunn, D.; Sridhar, N.; and Yang, L. 2003. "Effect of Measurement Methods and Solution Chemistry on the Evaluation of the Localized Corrosion of Candidate High-Level Waste Container Materials." *Corrosion/2003, [58th Annual Conference & Exposition, March 16-20, 2003, San Diego, California].* Paper No. 03690. Houston, Texas: NACE International. TIC: 254387.

Jayaweera, P.; Macdonald, D.D.; Engelhard, G.; and Davydov, A., 2003. Deterministic Prediction of Localized Corrosion Damage to Alloy C-22 HLNW Canisters. SRI International Report, Menlo Park, CA. TIC: 253900.

Jones, D.A. 1996. *Principles and Prevention of Corrosion.* 2nd Edition. Upper Saddle River, New Jersey: Prentice Hall. TIC: 241233.

Kehler, B.A.; Ilevbare, G.O.; and Scully, J.R. 1999. "Comparison of the Crevice Corrosion Resistance of Alloys 625 and C22." *Passivity and Localized Corrosion, An International Symposium in Honor of Professor Norio Sato.* Seo, M.; MacDougall, B.; Takahashi, H.; and Kelly, R.G., eds. *99-27,* 644-654. Pennington, New Jersey: Elecetrochemical Society. TIC: 254581.

Kehler, B.A.; Ilevbare, G.O.; and Scully, J.R. 2001. "Crevice Corrosion Stabilization and Repassivation Behavior of Alloy 625 and Alloy 22." *Corrosion, 57,* (12), 1042-1065. [Houston, Texas]: NACE International. TIC: 254305.

Lian, T.; Martin, S.; Jones, D.; Rivera, A.; and Horn, J. 1999. “Corrosion of Candidate Container Materials by Yucca Mountain Bacteria.” *Corrosion 99, Paper No. 476,* Houston, Texas: NACE International. TIC: 245833.

Lian, T.; Estill, J.C.; Hust, G.A.; Fix, D.V.; and Rebak, R.B. 2002. "Passive Corrosion Behavior of Alloy 22 in Multi-Ionic Aqueous Environments." *Transportation, Storage, and Disposal of Radioactive Materials –2002– presented at the 2002 ASME Pressure Vessels and Piping Conference, Vancouver, British Columbia, Canada, August 5-9, 2002.* Hafner, R.S.; Farmer, J.C.; Hensel, S.J.; Lake, W.H., Jr. and Smith, A.C., eds. *PVP-Vol. 449,* 67-74. New York, New York: American Society of Mechanical Engineers. TIC: 254800.

Lide, D.R., ed. 1991. *CRC Handbook of Chemistry and Physics.* 72nd Edition. Boca Raton, Florida: CRC Press. TIC: 3595.

Lloyd, A.C.; Shoesmith, D.W.; McIntyre, N.S.; and Noël, J.J. 2001. "Investigating the Localized Corrosion Properties of Ni-Cr-Mo Alloys for Their Use in Nuclear Waste Disposal Systems." *Stainless Steel World, 13,* (4), 29-30, 33. [Zutphen, The Netherlands]: KCI Publishing. TIC: 249982.

Lorang, G.; Jallerat, N.; Quang, K.V.; and Langeron, J.-P. 1990. "AES Depth Profiling of Passive Overlayers Formed on Nickel Alloys." *Surface and Interface Analysis, 16,* 325-330. [New York, New York]: John Wiley & Sons. TIC: 249830.

Macdonald, D.D. 1992. "The Point Defect Model for the Passive State." *Journal of the Electrochemical Society, 139, (12), 3434-3449. Manchester, New Hampshire:* Electrochemical Society. TIC: 249804.

Macdonald, D.D. 1999. "Passivity–the Key to Our Metals-Based Civilization." *Pure and Applied Chemistry, 71,* (6), 951-978. Oxford, England: Blackwell Scientific Publishers. TIC: 249795.

Manahan, M.P., Sr.; Macdonald, D.D.; and Peterson, A.J., Jr. 1995. "Determination of the Fate of the Current in the Stress Corrosion Cracking of Sensitized Type 304SS in High Temperature Aqueous Systems." *Corrosion Science, 37,* (1), 189-208. [New York, New York]: Pergamon. TIC: 254586.

Marcus, P. and Maurice, V. 2000. "Passivity of Metals and Alloys." Chapter 3 of Corrosion and Environmental Degradation Vol. I. Schutze, M., Volume Editor. Materials Science and Technology, A Comprehensive Treatment. New York, New York: Wiley-VCH. TIC: 249831.

Marsh, G.P.; Taylor, K.J.; and Harker, A.H. 1991. *The Kinetices of Pitting Corrosion of Carbon Steel Applied to Evaluating Containers for Nuclear Waste Disposal.* SKB TR-91-62. Stockholm, Sweden: Svensk Kärnbränsleförsörjning AB. TIC: 206582.

McCright, R.D. 1998. *Corrosion Data and Modeling Update for Viability Assessment.* Volume 3 of *Engineered Materials Characterization Report.* UCRL-ID-119564, Rev. 1.1. Livermore, California: Lawrence Livermore National Laboratory. ACC: MOL.19981222.0137.

McGuire, R.; Vlasity, J.; Kessler, J.; Long, A.; Childs, S.; Ross, B.; Schwartz, F.; Shoesmith, D.; Kolar, M.; Apted, M.; Zhou, W.; Sudicky, E.; Smith, G.; Kozak, M.; Salter, P.; Klos, R.; Venter, A.; Stenhouse, M.; Watkins, B.; and Little, R. 1998. *Alternative Approaches to Assessing the Performance and Suitability of Yucca Mountain for Spent Fuel Disposal.* EPRI TR-108732. Palo Alto, California: Electric Power Research Institute. TIC: 248813.

Mughabghab, S.F. and Sullivan, T.M. 1989. "Evaluation of the Pitting Corrosion of Carbon Steels and Other Ferrous Metals in Soil Systems." *Waste Management, 9,* (4), 239-251. Elmsford, New York: Pergamon Press. TIC: 254591.

Newman, R.C. and Franz, E.M. 1984. "Growth and Repassivation of Single Corrosion Pits in Stainless Steel." *Corrosion, 40,* (7), 325-330. [Houston, Texas]: National Associaition of Corrosion Engineers. TIC: 254580.

Newman, R.C. 1985. "The Dissolution and Passivation Kinetics of Stainless Alloys Containing Molybdenum—I. Coulometric Studies of Fe–Cr and Fe–Cr–Mo Alloys." *Corrosion Science, 25,* (5), 331-339. [New York, New York]: Elsevier. TIC: 254590.

NRC (U.S. Nuclear Regulatory Commission) 2003. *Yucca Mountain Review Plan, Final Report.* NUREG-1804, Rev. 2. Washington, D.C.: U.S. Nuclear Regulatory Commission, Office of Nuclear Material Safety and Safeguards. TIC: 254568.

Papoulis, A. 1965. *Probability, Random Variables, and Stochastic Processes.* New York, New York: McGraw-Hill Book Company. TIC: 254701.

Plinski, M.J. 2001. *Waste Package Operations Fabrication Process Report.* TDR-EBS-ND-000003 REV 02. Las Vegas, Nevada: Bechtel SAIC Company. ACC: MOL.20011003.0025.

Pourbaix, M. 1974. *Atlas of Electrochemical Equilibria in Aqueous Solutions.* Houston, Texas: National Association of Corrosion Engineers. TIC: 208955.

Rebak, R.B.; Edgecumbe Summers, T.S.; Lian, T.; Carranza, R.M.; Dillman, J.R.; Corbin, T.; and Crook, P. 2002. "Effect of Thermal Aging on the Corrosion Behavior of Wrought and Welded Alloy 22." *Corrosion/2002, [57th Annual Conference & Exposition, April 7-11, 2002, Denver, Colorado]*. Paper No. 02542. Houston, Texas: NACE International. TIC: 254582.

Sawyer, D.T. and Roberts, J.L., Jr. 1974. "II. Reference Electrodes." *Experimental Electrochemistry for Chemists.* Pages 34-60. New York, New York: John Wiley & Sons. TIC: 254739.

Scully, J.R.; Hudson, J.L.; Lunt, T.; Ilevbare, G.; and Kehler, B. 1999. *Localized Corrosion Initiation and Transition to Stabilization in Alloys 625 and C-22.* 1-27. Charlottesville, Virginia: University of Virginia. TIC: 246630.

Scully, J.R.; Ilevbare, G.; and Marks, C. 2001. *Passivity and Passive Corrosion of Alloys 625 and 22.* SEAS Report No. UVA/527653/MSE01/103. Charlottesville, Virginia: University of Virginia, School of Engineering & Applied Science. TIC: 248056.

Sedriks, A.J. 1996. *Corrosion of Stainless Steels.* 2nd Edition. 179, 377. New York, New York: John Wiley & Sons. TIC: 245121.

Sharland, S.M.; Naish, C.C.; Taylor, K.J.; and Marsh, G.P. 1994. "An Experimental and Modelling Study of the Localized Corrosion of Carbon Steel Overpacks for the Geological Disposal of Radioactive Waste." *Life Prediction of Corrodible Structures.* Parkins, R.N.; ed. Volume 1. 402-418. Houston, Texas: NACE International. TIC: 254835.

Smailos, E. and Köster, R. 1987. "Corrosion Studies on Selected Packaging Materials for Disposal of High Level Wastes." Materials Reliabity in the Back End of the Nuclear Fuel Cycle, Proceedings of a Technical Committee Meeting, Vienna, 2-5 September 1986. IAEA TECHDOC-421, 7-24. Vienna, Austria: International Atomic Energy Agency. TIC: 252877.

Stedinger, J.R.; Vogel, R.M.; and Foufoula-Georgiou, E. 1993. "Frequency Analysis of Extreme Events." Chapter 18 of *Handbook of Hydrology.* Maidment, D.R., ed. New York, New York: McGraw-Hill. TIC: 236568.

Stoecker, J.G., II. 1987. "Evaluation of Microbiological Corrosion." In *Corrosion,* Volume 13, Pages 314-315 of *Metals Handbook.* 9th Edition. Metals Park, Ohio: ASM International. TIC: 209807.

Taylor, B.N. and Kuyatt, C.E. 1994. *Guidelines for Evaluating and Expressing the Uncertainty of NIST Measurement Results.* NIST Technical Note 1297. 1994 Edition. Gaithersburg, Maryland: National Institute of Standards and Technology, Physics Laboratory. TIC: 254588.

Treseder, R.S.; Baboian, R.; and Munger, C.G. 1991. *NACE Corrosion Engineer's Reference Book.* 156-181. Houston, Texas: NACE International. TIC: 245834.

Urquidi, M. and Macdonald, D.D. 1985. "Solute-Vacancy Interaction Model and the Effect of Minor Alloying Elements on the Initiation of Pitting Corrosion." *Journal of the Electrochemical Society, 132,* (3), 555-558. [New York, New York]: Electrochemical Society. TIC: 249843.

Vetter, K.J. and Strehblow, H.H. 1974. "Pitting Corrosion in an Early Stage and its Theoretical Implications." *Localized Corrosion, [U.R. Evans Conference on Localized Corrosion], December 6-10, 1971, Williamsburg, Virginia.* International Corrosion Conference Series, NACE-3. Pages 240-251. Houston, Texas: Natioanl Asscociation of Corrosion Engineers. TIC: 254803.

Walsh, D.W. 1999. "The Effects of Microstructure on MIC Susceptibility in High Strength Aluminum Alloys." *Corrosion 99, Paper 187,* 1-13. Houston, Texas: National Association of Corrosion Engineers. TIC: 246549.

Welsch, G.; Smialek, J.L.; Doychak, J.; Waldman, J.; and Jacobson, N.S. 1996. "High Temperature Oxidation and Properties." Chapter 2 of *Oxidation and Corrosion of Intermetallic Alloys.* Welsch, G. and Desai, P.D.; eds. West Lafayette, Indiana: Purdue University. TIC: 245280.

Zhang, L. and Macdonald, D.D. 1998a. "Segregation of Alloying Elements in Passive Systems—I. XPS Studies on the Ni–W System." *Electrochimica Acta, 43,* (18), 2661-2671. [New York, New York]: Pergamon Press. TIC: 249845.

Zhang, L. and Macdonald, D.D. 1998b. "Segregation of Alloying Elements in Passive Systems—II. Numerical Simulation." *Electrochimica Acta, 43,* (18), 2673-2685. [New York, New York]: Pergamon Press. TIC: 249846.

Zhou, X.; Balachov, I.; and Macdonald, D.D. 1998. "The Effect of Dielectric Coatings on IGSCC in Sensitized Type 304 SS in High Temperature Dilute Sodium Sulfate Solution." *Corrosion Science, 40,* (8), 1349-1362. [New York, New York]: Pergamon. TIC: 254585.

9.2 CODES, STANDARDS, REGULATIONS, AND PROCEDURES

10 CFR 63. Energy: Disposal of High-Level Radioactive Wastes in a Geologic Repository at Yucca Mountain, Nevada. Readily available.

AP-2.14Q, Rev. 2, ICN 2. *Review of Technical Products and Data.* Washington, D.C.: U.S. Department of Energy, Office of Civilian Radioactive Waste Management. ACC: DOC.20030206.0001.

AP-2.27Q, Rev. 0, ICN 0. *Planning for Science Activities.* Washington, D.C.: U.S. Department of Energy, Office of Civilian Radioactive Waste Management. ACC: MOL.20020701.0184.

AP-3.15Q, Rev. 4, ICN 2. *Managing Technical Product Inputs.* Washington, D.C.: U.S. Department of Energy, Office of Civilian Radioactive Waste Management. ACC: DOC.20030627.0002.

AP-SIII.10Q, Rev. 1, ICN 2. *Models.* Washington, D.C.: U.S. Department of Energy, Office of Civilian Radioactive Waste Management. ACC: DOC.20030627.0003.

AP-SV.1Q, Rev. 0, ICN 3. *Control of the Electronic Management of Information.* Washington, D.C.: U.S. Department of Energy, Office of Civilian Radioactive Waste Management. ACC: MOL.20020917.0133.

AP-SI.1Q, Rev. 5, ICN 2. *Software Management.* Washington, D.C.: U.S. Department of Energy, Office of Civilian Radioactive Waste Management. ACC: DOC.20030902.0003.

ASTM B 575-94. 1994. *Standard Specification for Low-Carbon Nickel-Molybdenum-Chromium and Low-Carbon Nickel-Chromium-Molybdenum Steel Alloy Plate, Sheet, and Strip*. Philadelphia, Pennsylvania: American Society for Testing and Materials. TIC: 237683.

ASTM C 1174-97. 1998. *Standard Practice for Prediction of the Long-Term Behavior of Materials, Including Waste Forms, Used in Engineered Barrier Systems (EBS) for Geological Disposal of High-Level Radioactive Waste*. West Conshohocken, Pennsylvania: American Society for Testing and Materials. TIC: 246015.

ASTM G 1-90 (Reapproved 1999). 1990. *Standard Practice for Preparing, Cleaning, and Evaluating Corrosion Test Specimens*. West Conshohocken, Pennsylvania: American Society for Testing and Materials. TIC: 238771.

ASTM G 3-89 (Reapproved 1999). 1989. *Standard Practice for Conventions Applicable to Electrochemical Measurements in Corrosion Testing*. West Conshohocken, Pennsylvania: American Society for Testing and Materials. TIC: 247076.

ASTM G 5 - 94. *Standard Reference Test Method for Making Potentiostatic and Potentiodynamic Anodic Polarization Measurements*. Philadelphia, Pennsylvania: American Society for Testing and Materials. TIC: 231902.

ASTM G 30-94. 1994. *Standard Practice for Making and Using U-Bend Stress-Corrosion Test Specimens*. Philadelphia, Pennsylvania: American Society for Testing and Materials. TIC: 246890.

ASTM G 59-97. 1998. *Standard Test Method for Conducting Potentiodynamic Polarization Resistance Measurements*. West Conshohocken, Pennsylvania: American Society for Testing and Materials. TIC: 249897.

ASTM G 61-86 (Reapproved 1998). 1987. Standard Test Method for Conducting Cyclic Potentiodynamic Polarization Measurements for Localized Corrosion Susceptibility of Iron-, Nickel-, or Cobalt-Based Alloys. West Conshohocken, Pennsylvania: American Society for Testing and Materials. TIC: 246716.

ASTM G 102-89 (Reapproved 1999). 1989. *Standard Practice for Calculation of Corrosion Rates and Related Information from Electrochemical Measurements*. West Conshohocken, Pennsylvania: American Society for Testing and Materials. TIC: 249897.

9.3 INPUT SOURCE DATA

LL991203505924.094. Approach and Supporting Data for MIC Modeling. Submittal date: 12/13/1999.

LL000320405924.146. Target Compositions of Aqueous Solutions Used for Corrosion Testing. Submittal date: 03/22/2000.

LL020711612251.017. Open Circuit Potential Tests. Submittal date: 10/11/2002.

LL021105112251.022. Electrochemical Behavior of Alloy 22 in Simulated Acidic Concentrated Water (SAW), Simulated Concentrated Water (SCW) and 5 M CaCl2 Solutions. Submittal date: 12/11/2002.

LL021105312251.023. Stress Corrosion Crack Growth and Initiation Measurements for C-22 and Ti-7, General Electric Global Research Center (GEGRC) 121202. Submittal date: 01/08/2003.

LL030201212251.033. Chemical Analysis and Thermodynamic Calculations of Solutions Used to Monitor Corrosion Potentials of Alloy C22. Submittal date: 02/25/2003.

LL030309512251.042. Low Temperature Operating Mode Electrochemical Test Data: Corrosion Potential, Linear Polarization, and Cyclic Polarization Tests of Alloy 22 in Oxalic Acid, NaF, NaCl, NaF+NaCl, and CaCl{subscript 2} Solutions Recorded at 30, 45, 60, 75, 90 and 105°C. Submittal date: 05/22/2003.

LL030400112251.043. Electrochemical Behavior of Multiple Crevice Assembly (MCA) Alloy 22 Specimens in 5M CaCl2. Submittal date: 04/07/2003.

LL030406212251.044. Alloy 22 in 5M CaCl2 at 75C - Supplemental. Submittal date: 04/08/2003.

LL030406412251.045. Transmission Electron Microscopy (TEM) Images of Oxide Film on Air-Oxidized Alloy22 (UNS N06022) Samples Aged at 550C. Submittal date: 04/11/2003.

LL030409512251.051. Electrochemical Analysis of Alloy 22 - CaCl2 Data at Various Temperatures, Surface Conditions, and Electrolyte Solutions.. Submittal date: 05/23/2003.

LL030409812251.054. Electrochemical Data of Alloy 22 in CaCl2 Solutions-Effect of Nitrate.. Submittal date: 06/26/2003.

LL030412512251.057. LTCTF Corrosion Rate Calculations for Five-Year Exposed Alloy C22 Specimens Cleaned under TIP-CM-51.. Submittal date: 05/28/2003.

LL030502212251.063. Corrosion Potential, Polarization Resistance, and Cyclic Polarization in Several Environments at Several Temperatures for Alloy 22.. Submittal date: 05/20/2003.

LL030703723121.031. Conversion of Corrosion Testing Solutions from Molar to Molal Concentration Units.. Submittal date: 07/10/2003.

LL030706223121.032. Conversion of Corrosion Testing Solutions from Molar to Molal Concentration Units (II). Submittal date: 07/17/2003.

LL030709812251.067. Basic Saturated Water (BSW) Test Solution Composition.. Submittal date: 07/25/2003.

MO0003RIB00071.000. Physical and Chemical Characteristics of Alloy 22. Submittal date: 03/13/2000.

MO0306SEPFEPS3.000. LA FEP List. Submittal date: 06/03/2003.

9.4 OUTPUT DATA

SN0308T0506303.003. Updated Localized Corrosion Model and Analyses of Waste Package Outer Barrier. Submittal date: 08/20/2003.

SN0308T0506303.004. Updated General Corrosion Model and Analyses of Waste Package Outer Barrier. Submittal date: 08/20/2003.

10 ATTACHMENTS

Attachment I: Summary of the Electrochemical Corrosion Test Procedures to Generate Input Data for Analyses and Models in This Model Report.

Attachment II: General Corrosion Rate of Alloy 22 Crevice Samples Based on the Weight Loss Measurement After 5-Year Exposure in the Long-Term Corrosion Testing Facility.

Attachment III: General Corrosion Rate of Alloy 22 Weight-Loss Samples Based on the Weight Loss Measurement After 5-Year Exposure in the Long-Term Corrosion Testing Facility.

Attachment IV: Corrosion Rate of Alloy 22 as a Function of Temperature Calculated from the Polarization Resistance Measurement.

Attachment V: Long-Term Steady-State Corrosion Potential Measurement of Alloy 22 Samples Used in the Corrosion Potential Model and Analysis.

Attachment VI: Project's Crevice Repassivation Potential Data of Alloy 22 Samples Used in the Critical Potential Model and Analysis.

Attachment VII: CNWRA Crevice Repassivation Potential Data of Alloy 22 Samples Used in the Critical Potential Model and Analysis.

ATTACHMENT I

Summary of the Electrochemical Corrosion Test Procedures to Generate Input Data for Analyses and Models in This model report

This attachment summarizes the electrochemical corrosion tests that were employed to generate the input data for the analyses and models for the WPOB documented in this model report. The typical sequence for electrochemical testing was as follows:

- Grind and polish the testing specimen to eliminate residual effects of fabrication. The surface finishing of the test specimens corresponded to abrasive paper grit 600. This grinding was done within one hour prior of immersing the test specimen in the electrolyte solution. The testing cell is standard and is described in ASTM standard G 5-94 (ASTM 1994).

- After immersion of the specimen in the electrolyte solution of interest, the free corrosion potential of the specimen was monitored for 24 hour. The value of potential at the end of this 24-hour period was called the corrosion potential (E_{corr}). In a few cases the corrosion potential was monitored for shorter times (1 or 2 hours).

- After this 24-hour period, at least three polarization resistance (PR) tests were carried out according to ASTM G 59 (ASTM G 59-97 1997). The value of the slope of the resistance to polarization (R_p) was used to calculate the general corrosion rate (ASTM G 59 and G 102) (ASTM G 102-89 1989).

- After the polarization resistance tests, one cyclic polarization (CP) test was carried out according to ASTM G 61(ASTM G 61-86 1987). The cyclic polarization curve yielded the value of the critical potential for localized corrosion of the WPOB.

Details of the tests are provided in the corresponding Scientific Notebooks cited in the Data Tracking Numbers (DTNs) of the input data documented in Section 4.1.1.

I.1 Determination of Corrosion Rates from Polarization Resistance Tests

The polarization resistance test was carried out following the default of the set-up from the manufacturer of the potentiostat and the software that runs the potentiostat. The test consists of ramping the potential at a rate of 0.167 mV/sec (0.6 V/hr) while recording the current applied to the specimen. The potential scan was started 20 mV below E_{corr} and finished 20 mV above E_{corr}. The value of E_{corr} chosen by the instrument for this scan is the E_{corr} value 10 seconds before the scan was started (default set up). The resulting data consists of applied values of potential (E) and applied values of current (I). If these data are plotted E vs. I on a linear scale, a more or less straight line is obtained. The slope of this line is called the resistance to polarization or R_p. ASTM standards G 59 (ASTM G 59-97 1997) and G 102 (ASTM G 102-89 1989) explains the reasoning behind the use of this slope in calculating instantaneous corrosion rates. To calculate the corrosion rates, besides the slope R_p, several other data are needed. These data include, (1) the exposed area of the specimen, (2) the values of the Tafel slopes, (3) the Faraday constant (charge passed by one mole of electrons), (4) the value of the equivalent weight of the tested

alloy and (5) the density of the tested alloy. The last two data are needed to use the Faraday conversion of current to penetration rate.

The calculation performed in the current report was done considering the following.

- The exposed area of the specimens: For multiple crevice assembly (MCA) samples, the area changed according to the length of the immersed specimen in the electrolyte solution. The exposed area of samples with other geometries (e.g., prism, rod and disc) also varies from sample to sample.

- The cathodic and anodic Tafel slopes are both equal to 0.12 V/decade. That is, it is considered that it takes 0.12 V to change the current on the specimen by one order of magnitude. This is a default setting of the Gamry software.

- The charge passed by one mole of electrons is 96,486 C (Lide 1991, Table 1, page I-1).

- The equivalent weight (EW) for Alloy 22 (N06022) is calculated considering that the alloy dissolves stoichiometrically, and it depends on the valence for the dissolved elements. The value used was taken from Table 1 of ASTM G 102, third oxidation state. That is EW = 23.28.

- The density of Alloy 22 (N06022) is 8.69 g/cm³ (Haynes International 1997a).

The value of R_p in V/A can be calculated by plotting the curve and estimating the slope. This can be done manually. The Gamry software has a program to calculate the corrosion rate directly from the acquired data. The calculation of Rp (corrosion rate) can be done by choosing the entire range of potentials (40 mV) or a specific predetermined range around the potential for zero applied current (E_{corr}). Since in most environments the plots of potential vs. current in the linear scale were not straight (linear), a smaller range of potential around E_{corr} was chosen (see ASTM G 3 (ASTM G 3-89 1989)). The range chosen in our calculations was 10 mV below E_{corr} and 10 mV above E_{corr}. To perform the calculation, the E_{corr} at 10 seconds before the test was selected and from this value 10 mV were subtracted (E_s = E_{corr} in mV – 10). This potential was the starting potential for the calculation range (E_s). Similarly the finish potential point (E_f) was chosen as E_f = E_{corr} in mV + 10.

$$i_{corr} = 10^6 \frac{B}{R_p} \qquad \text{(Equation I-1)}$$

where i_{corr} is the corrosion current density in µA/cm², and R_p is the slope in Ohm-cm². B is the Stern-Geary coefficient and is related to the anodic and cathodic Tafel slopes as follows (ASTM G-59-97 1997).

$$B = \frac{b_a \cdot b_c}{2.303(b_a + b_c)} \qquad \text{(Equation I-2)}$$

where b_a and b_c are the anodic and cathodic Tafel slopes respectively, which are both considered to be 0.12 V. The corrosion rate is then calculated as

$$CR(\mu m / year) = 3.27 \frac{i_{corr} \cdot EW}{\rho} \qquad \text{(Equation I-3)}$$

where EW is the equivalent weight of the alloy (23.28 for N06022) (ASTM G 102, Table 1), and ρ is the density of the alloy (8.69 g/cm³ for N06022).

I.2 Determination of the Critical Potential or Repassivation Potential from the Cyclic Polarization Tests

In the cyclic polarization tests, the specimen was polarized at a constant scan rate, while the applied current was recorded. The potential scan rate was 0.167 mV/sec or 0.6 V/hr starting at a potential of 150 mV below E_{corr} and continuing until the current density reached a value of 5 mA/cm² (ASTM G 61 1987). At this point the scan rate was reversed, and the test was terminated at the original E_{corr} or before. It may also be terminated manually after the reversing curve intersects the forward curve.

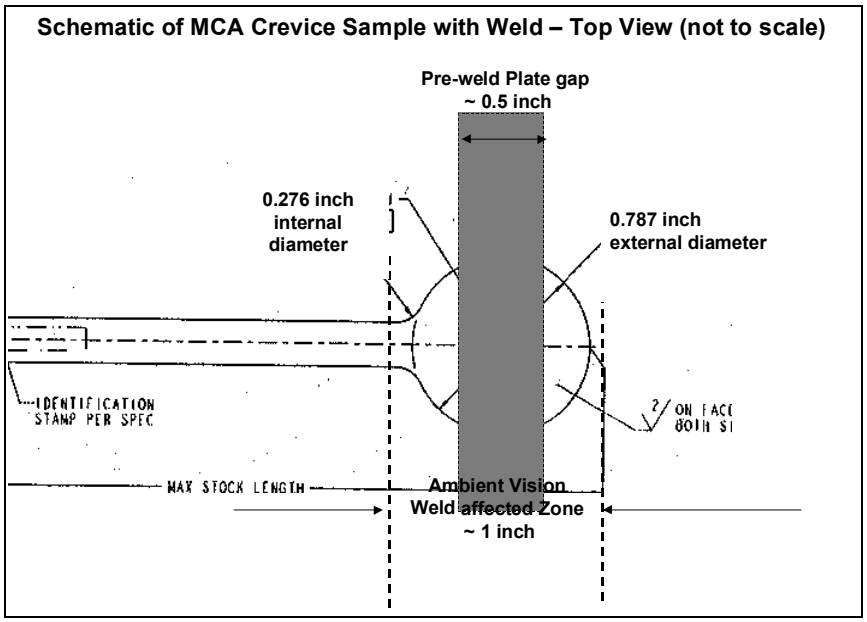

Figure I-1. Schematic of An As-Welded Multiple Crevice Assembly (MCA) Sample.

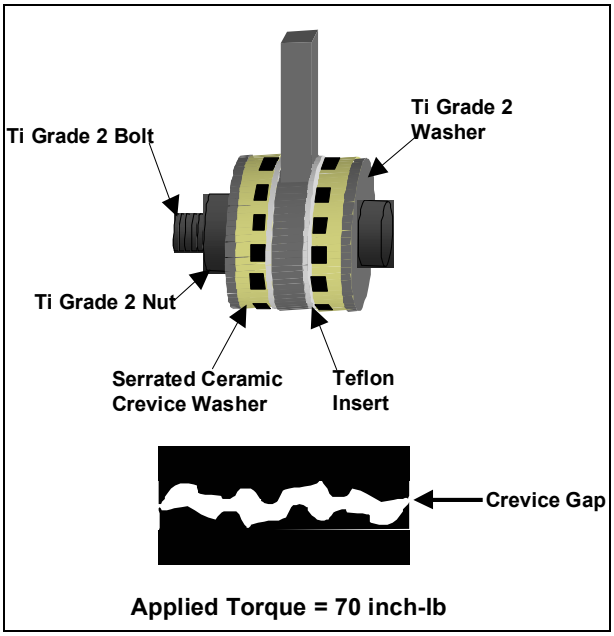

Source: Kehler et al. (2001).

Figure I-2. Schematic of a Multiple Crevice Assembly (MCA) Sample.

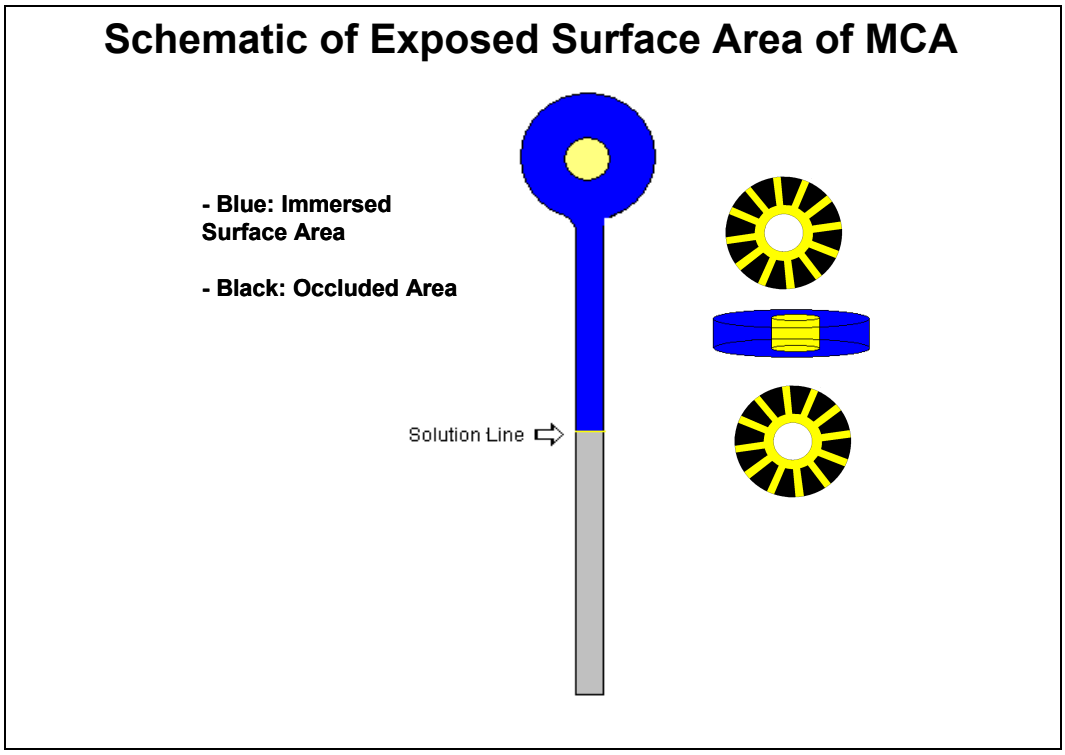

Figure I-3. Schematic Showing the Exposed Surface Area of a Multiple Crevice Assembly (MCA) Sample During Electrochemical Testing.

ATTACHMENT II

General Corrosion Rate of Alloy 22 Crevice Samples Based on the Weight Loss Measurement After 5-Year Exposure in the Long-Term Corrosion Testing Facility.

Sample ID	Length (in)	Width (in)	Thickness (in)	Initial Weight (g)	Sample Condition [1)]	Exposure Environment	Final Weight (g)	Weight Loss (g)	Exposed Time (hours)	Surface Area (cm^2)	Corrosion Rate (nm/year) [3)]
DCA019	2.0120	2.0120	0.1145	64.6723	MA Crevice	SAW Vapor Phase 60 C	64.6698	0.0025	46296	57.917	9.41
DCA020	2.0155	2.0150	0.1175	66.3190	MA Crevice	SAW Vapor Phase 60 C	66.3168	0.0022	46296	58.270	8.23
DCA021	2.0105	2.0125	0.1165	65.4770	MA Crevice	SAW Vapor Phase 60 C	65.4747	0.0023	46296	58.006	8.64
DCA022	2.0135	2.0135	0.1175	65.8096	MA Crevice	SAW Aqueous Phase 60 C	65.8079	0.0017	46296	58.174	6.37
DCA023	2.0135	2.0115	0.1165	65.5176	MA Crevice	SAW Aqueous Phase 60 C	65.5150	0.0026	46296	58.061	9.76
DCA024	2.0125	2.0110	0.1165	64.9706	MA Crevice	SAW Aqueous Phase 60 C	64.9646	0.0060	46296	58.020	22.52
DCA049	2.0175	2.0120	0.1180	66.0889	MA Crevice	SAW Vapor Phase 90 C	66.0857	0.0032	45960	58.272	12.05
DCA050	2.0170	2.0160	0.1175	66.1281	MA Crevice	SAW Vapor Phase 90 C	66.1235	0.0046	45960	58.339	17.30
DCA051	2.0160	2.0155	0.1205	67.2585	MA Crevice	SAW Vapor Phase 90 C	67.2543	0.0042	45960	58.473	15.76
DCA052	2.0135	2.0090	0.1015	57.4226	MA Crevice	SAW Aqueous Phase 90 C	57.4211	0.0015	45960	57.119	5.77
DCA053	2.0140	2.0140	0.1160	65.4009	MA Crevice	SAW Aqueous Phase 90 C	65.3987	0.0022	45960	58.114	8.31
DCA054	2.0160	2.0140	0.1170	65.8061	MA Crevice	SAW Aqueous Phase 90 C	65.8044	0.0017	45960	58.227	6.41
DCA079	2.0135	2.0120	0.1160	65.3198	MA Crevice	SCW Vapor Phase 60 C	65.3190	0.0008	45456	58.045	3.06
DCA080	2.0160	2.0155	0.1000	57.5590	MA Crevice	SCW Vapor Phase 60 C	57.5582	0.0008	45456	57.277	3.11
DCA081	2.0155	2.0155	0.1160	65.5190	MA Crevice	SCW Vapor Phase 60 C	65.5179	0.0011	45456	58.197	4.20
DCA082	2.0160	2.0145	0.1170	65.7599	MA Crevice	SCW Aqueous Phase 60 C	65.7574	0.0025	45456	58.241	9.53

Sample ID	Length (in)	Width (in)	Thickness (in)	Initial Weight (g)	Sample Condition [1]	Exposure Environment	Final Weight (g)	Weight Loss (g)	Exposed Time (hours)	Surface Area (cm^2)	Corrosion Rate (nm/year) [3]
DCA083	2.0190	2.0145	0.1160	65.2679	MA Crevice	SCW Aqueous Phase 60 C	65.2660	0.0019	45456	58.265	7.24
DCA084	2.0150	2.0100	0.1030	59.6044	MA Crevice	SCW Aqueous Phase 60 C	59.6006	0.0038	45456	57.274	14.72
DCA109	2.0110	2.0155	0.1160	65.2077	MA Crevice	SCW Vapor Phase 90 C	65.2062	0.0015	44832	58.073	5.82
DCA110	2.0130	2.0145	0.1165	65.2979	MA Crevice	SCW Vapor Phase 90 C	65.2949	0.0030	44832	58.129	11.61
DCA111	2.0165	2.0165	0.1190	66.6259	MA Crevice	SCW Vapor Phase 90 C	66.6244	0.0015	44832	58.427	5.78
DCA112	2.0150	2.0115	0.1120	63.2332	MA Crevice	SCW Aqueous Phase 90 C	63.2324	0.0008	44832	57.840	3.12
DCA113	2.0105	2.0150	0.1065	60.1129	MA Crevice	SCW Aqueous Phase 90 C	60.1102	0.0027	44832	57.492	10.57
DCA114	2.0175	2.0125	0.1080	60.9881	MA Crevice	SCW Aqueous Phase 90 C	60.9853	0.0028	44832	57.702	10.92
DCA139	2.0170	2.0105	0.1110	62.0138	MA Crevice	SDW Vapor Phase 60 C	62.0126	0.0012	44448	57.809	4.72
DCA140	2.0140	2.0120	0.1100	61.6079	MA Crevice	SDW Vapor Phase 60 C	61.6070	0.0009	44448	57.709	3.54
DCA141	2.0180	2.0160	0.1110	62.3601	MA Crevice	SDW Vapor Phase 60 C	62.3594	0.0007	44448	57.987	2.75
DCA142	2.0150	2.0115	0.1120	62.7895	MA Crevice	SDW Aqueous Phase 60 C	62.7879	0.0016	44448	57.840	6.28
DCA143	2.0120	2.0120	0.1115	62.4663	MA Crevice	SDW Aqueous Phase 60 C	62.4648	0.0015	44448	57.742	5.90
DCA144	2.0100	2.0125	0.1100	61.4272	MA Crevice	SDW Aqueous Phase 60 C	61.4251	0.0021	44448	57.614	8.27
DCA175	2.0170	2.0120	0.0900	49.9140	MA Crevice	SDW Vapor Phase 90 C	49.9138	0.0002	43488	56.625	0.83
DCA176	2.0075	2.0090	0.1045	58.6401	MA Crevice	SDW Vapor Phase 90 C	58.6399	0.0002	43488	57.130	0.82
DCA177 [2]	2.0125	2.0100	0.1100	61.7156	MA Crevice	SDW Vapor Phase 90 C	61.7040	0.0116	43488	57.614	46.68
DCA178	2.0145	2.0120	0.1140	63.9838	MA Crevice	SDW Aqueous Phase 90 C	63.9817	0.0021	43488	57.956	8.41
DCA179	2.0125	2.0100	0.1075	60.3046	MA Crevice	SDW Aqueous Phase 90 C	60.3033	0.0013	43488	57.468	5.25
DCA180	2.0135	2.0065	0.1020	57.4820	MA Crevice	SDW Aqueous Phase 90 C	57.4807	0.0013	43488	57.080	5.29
DCB019	2.0010	1.9975	0.0810	45.0056	ASW Crevice	SAW Vapor Phase 60 C	45.0030	0.0026	46296	55.279	10.25
DCB020	1.9945	2.0010	0.1035	55.5235	ASW Crevice	SAW Vapor Phase 60 C	55.5217	0.0018	46296	56.501	6.94

Sample ID	Length (in)	Width (in)	Thickness (in)	Initial Weight (g)	Sample Condition [1]	Exposure Environment	Final Weight (g)	Weight Loss (g)	Exposed Time (hours)	Surface Area (cm^2)	Corrosion Rate (nm/year) [3]
DCB022	2.0030	2.0000	0.0900	49.1369	ASW Crevice	SAW Aqueous Phase 60 C	49.1354	0.0015	46296	55.922	5.85
DCB023	2.0050	2.0110	0.1010	56.3136	ASW Crevice	SAW Aqueous Phase 60 C	56.3118	0.0018	46296	56.912	6.89
DCB049	2.0045	2.0070	0.0865	46.3703	ASW Crevice	SAW Vapor Phase 90 C	46.3662	0.0041	45960	55.948	16.08
DCB050	2.0050	2.0115	0.0840	44.8726	ASW Crevice	SAW Vapor Phase 90 C	44.8689	0.0037	45960	55.938	14.52
DCB052	2.0040	2.0040	0.0925	50.3147	ASW Crevice	SAW Aqueous Phase 90 C	50.3136	0.0011	45960	56.202	4.30
DCB053	2.0000	2.0065	0.0830	45.6403	ASW Crevice	SAW Aqueous Phase 90 C	45.6388	0.0015	45960	55.610	5.92
DCB079	2.0010	2.0030	0.0835	45.7966	ASW Crevice	SCW Vapor Phase 60 C	45.7961	0.0005	45456	55.572	2.00
DCB080	2.0130	2.0000	0.0920	52.2193	ASW Crevice	SCW Vapor Phase 60 C	52.2173	0.0020	45456	56.307	7.88
DCB082	2.0010	1.9990	0.0840	46.2660	ASW Crevice	SCW Aqueous Phase 60 C	46.2611	0.0049	45456	55.493	19.59
DCB083	1.9970	1.9965	0.0855	48.1762	ASW Crevice	SCW Aqueous Phase 60 C	48.1728	0.0034	45456	55.405	13.62
DCB109	2.0060	2.0150	0.1040	57.7242	ASW Crevice	SCW Vapor Phase 90 C	57.7231	0.0011	44832	57.223	4.33
DCB110	1.9940	1.9990	0.0950	51.1169	ASW Crevice	SCW Vapor Phase 90 C	51.1164	0.0005	44832	55.941	2.02
DCB112	2.0105	2.0095	0.1035	56.9739	ASW Crevice	SCW Aqueous Phase 90 C	56.9716	0.0023	44832	57.167	9.05
DCB113	2.0055	2.0040	0.0870	48.0842	ASW Crevice	SCW Aqueous Phase 90 C	48.0815	0.0027	44832	55.923	10.86
DCB139	1.9805	1.9860	0.1045	56.1890	ASW Crevice	SDW Vapor Phase 60 C	56.1890	0.0000	44448	55.775	0.01
DCB140	1.9965	1.9975	0.0920	48.7987	ASW Crevice	SDW Vapor Phase 60 C	48.7980	0.0007	44448	55.795	2.85
DCB142	2.0015	2.0025	0.0900	49.2450	ASW Crevice	SDW Aqueous Phase 60 C	49.2445	0.0005	44448	55.949	2.03
DCB143	1.9985	1.9985	0.0900	49.7742	ASW Crevice	SDW Aqueous Phase 60 C	49.7728	0.0014	44448	55.760	5.70
DCB175	1.9990	2.0060	0.1090	59.1477	ASW Crevice	SDW Vapor Phase 90 C	59.1476	0.0001	43488	57.077	0.41
DCB176	2.0050	2.0030	0.0825	45.3890	ASW Crevice	SDW Vapor Phase 90 C	45.3885	0.0005	43488	55.621	2.09
DCB178	2.0015	2.0035	0.0865	47.7164	ASW Crevice	SDW Aqueous Phase 90 C	47.7161	0.0003	43488	55.773	1.26
DCB179	2.0040	2.0120	0.0845	47.0565	ASW Crevice	SDW Aqueous Phase 90 C	47.0564	0.0001	43488	55.953	0.42

Note: 1) MA = mill annealed, ASW = as-welded.

Sample ID	Length (in)	Width (in)	Thickness (in)	Initial Weight (g)	Sample Condition [1]	Exposure Environment	Final Weight (g)	Weight Loss (g)	Exposed Time (hours)	Surface Area (cm^2)	Corrosion Rate (nm/year) [3]

2) Outlier not included in the analysis.

3) The input data from DTN LL030412512251.057 are the initial and final weight measurements, sample dimensions, and exposure conditions and time. The sample surface areas and corrosion rates were calculated in this model report. The calculated corrosion rates in this table are slightly different from those in DTN LL030412512251.057 due to the round-off errors.

Source DTN: LL030412512251.057

ATTACHMENT III

General Corrosion Rate of Alloy 22 Weight-Loss Samples Based on the Weight Loss Measurement After 5-Year Exposure in the Long-Term Corrosion Testing Facility.

Sample ID	Length (in)	Width (in)	Thickness (in)	Initial Weight (g)	Sample Condition [1]	Exposure Environment	Final Weight (g)	Weight Loss (g)	Exposed Time (hours)	Surface Area (cm^2)	Corrosion Rate (nm/year) [4]
DWA019	2.0135	1.0100	0.1120	30.3252	MA WL	SAW Vapor Phase 60 °C	30.3246	0.0006	46296	30.3317	4.32
DWA020	2.0135	1.0085	0.1130	30.9953	MA WL	SAW Vapor Phase 60 °C	30.9950	0.0003	46296	30.3359	2.17
DWA021	2.0145	1.0095	0.1140	31.0549	MA WL	SAW Vapor Phase 60 °C	31.0544	0.0005	46296	30.4231	3.59
DWA022	2.0120	1.0115	0.1140	31.0362	MA WL	SAW Aqueous Phase 60 °C	31.0361	0.0001	46296	30.4417	0.73
DWA023	2.0110	1.0095	0.1125	30.2366	MA WL	SAW Aqueous Phase 60 °C	30.2361	0.0005	46296	30.3044	3.61
DWA024	2.0095	1.0085	0.0945	25.6040	MA WL	SAW Aqueous Phase 60 °C	25.6035	0.0005	46296	29.4406	3.71
DWA034	2.0145	1.0105	0.1125	30.5218	MA WL	SAW Waterline 60 °C [3]	30.5213	0.0005	46296	30.3826	3.60
DWA039	2.0155	1.0120	0.1145	31.2482	MA WL	SAW Waterline 60 °C [(d)]	31.2476	0.0006	45960	30.5290	4.33
DWA059	2.0100	1.0110	0.1130	30.5308	MA WL	SAW Vapor Phase 90 °C	30.5304	0.0004	45960	30.3537	2.90
DWA060	2.0135	1.0095	0.1130	30.9395	MA WL	SAW Vapor Phase 90 °C	30.9391	0.0004	45960	30.3633	2.90
DWA061	2.0170	1.0120	0.1105	29.9892	MA WL	SAW Vapor Phase 90 °C	29.9891	0.0001	45960	30.3692	0.74
DWA062	2.0120	1.0090	0.1120	30.0884	MA WL	SAW Aqueous Phase 90 °C	30.0882	0.0002	45960	30.2826	1.46
DWA063	2.0145	1.0100	0.1145	31.0229	MA WL	SAW Aqueous Phase 90 °C	31.0225	0.0004	45960	30.4595	2.89
DWA064	2.0080	1.0100	0.1150	30.5525	MA WL	SAW Aqueous Phase 90 °C	30.5521	0.0004	45960	30.3879	2.90
DWA089 [2]	2.0145	1.0120	0.1160	31.0278	MA WL	SCW Vapor Phase 60 °C	31.0280	-0.0002	45456	30.5825	-1.44
DWA090	2.0175	1.0105	0.1145	30.7848	MA WL	SCW Vapor Phase 60 °C	30.7848	0.0000	45456	30.5168	0.01
DWA091	2.0150	1.0070	0.1160	30.8690	MA WL	SCW Vapor Phase 60 °C	30.8687	0.0003	45456	30.4523	2.20

Sample ID	Length (in)	Width (in)	Thickness (in)	Initial Weight (g)	Sample Condition [1)]	Exposure Environment	Final Weight (g)	Weight Loss (g)	Exposed Time (hours)	Surface Area (cm^2)	Corrosion Rate (nm/year) [4)]
DWA092	2.0100	1.0095	0.1065	29.9109	MA WL	SCW Aqueous Phase 60 °C	29.9106	0.0003	45456	30.0183	2.23
DWA093	2.0090	1.0095	0.1100	29.7822	MA WL	SCW Aqueous Phase 60 °C	29.7820	0.0002	45456	30.1623	1.49
DWA094	2.0155	1.0115	0.1165	30.8081	MA WL	SCW Aqueous Phase 60 °C	30.8077	0.0004	45456	30.6060	2.91
DWA104	2.0140	1.0100	0.1120	30.6273	MA WL	SCW Waterline 60 °C [(d)]	30.6270	0.0003	45456	30.3389	2.21
DWA109	2.0160	1.0110	0.1100	30.0620	MA WL	SCW Waterline 60 °C [(d)]	30.0620	0.0000	45984	30.3046	0.01
DWA129	2.0155	1.0090	0.1005	27.1346	MA WL	SCW Vapor Phase 90 °C	27.1343	0.0003	44832	29.8117	2.28
DWA130	2.0105	1.0125	0.1160	31.3506	MA WL	SCW Vapor Phase 90 °C	31.3501	0.0005	44832	30.5380	3.70
DWA131	2.0190	1.0115	0.1130	30.7217	MA WL	SCW Vapor Phase 90 °C	30.7215	0.0002	44832	30.4980	1.49
DWA132	2.0135	1.0095	0.1090	29.0636	MA WL	SCW Aqueous Phase 90 °C	29.0623	0.0013	44832	30.1820	9.70
DWA133	2.0160	1.0100	0.1115	30.2796	MA WL	SCW Aqueous Phase 90 °C	30.2786	0.0010	44832	30.3452	7.42
DWA134	2.0155	1.0100	0.1150	30.8393	MA WL	SCW Aqueous Phase 90 °C	30.8385	0.0008	44832	30.4967	5.91
DWA147	2.0135	1.0090	0.1155	31.2833	MA WL	SDW Vapor Phase 60 °C	31.2833	0.0000	44448	30.4629	0.01
DWA148	2.0130	1.0100	0.1050	28.2562	MA WL	SDW Aqueous Phase 60 °C	28.2561	0.0001	44448	30.0071	0.77
DWA154	2.0185	1.0100	0.1140	30.7483	MA WL	SDW Waterline 60 °C [(d)]	30.7479	0.0004	44448	30.4949	2.99
DWA167	2.0010	1.0030	0.1255	33.5921	MA WL	SDW Waterline 90 °C [(d)]	33.5918	0.0003	43488	30.5685	2.29
DWA174	2.0015	1.0025	0.1250	33.6543	MA WL	SDW Vapor Phase 90 °C	33.6542	0.0001	43488	30.5395	0.77
DWA175	2.0020	0.9960	0.1245	33.2710	MA WL	SDW Aqueous Phase 90 °C	33.2710	0.0000	43488	30.3459	0.02
DWB019	2.0000	1.0055	0.1005	27.1924	ASW WL	SAW Vapor Phase 60 °C	27.1922	0.0002	46296	29.4949	1.49
DWB020	1.9990	1.0030	0.1000	27.0152	ASW WL	SAW Vapor Phase 60 °C	27.0152	0.0000	46296	29.3904	0.01
DWB021	1.9995	1.0050	0.1000	27.2070	ASW WL	SAW Vapor Phase 60 °C	27.2070	0.0000	46296	29.4517	0.01
DWB022	1.9995	1.0035	0.0980	26.6246	ASW WL	SAW Aqueous Phase 60 °C	26.6241	0.0005	46296	29.3209	3.73
DWB023	2.0045	1.0070	0.0940	25.5992	ASW WL	SAW Aqueous Phase 60 °C	25.5990	0.0002	46296	29.3062	1.50

Sample ID	Length (in)	Width (in)	Thickness (in)	Initial Weight (g)	Sample Condition [1]	Exposure Environment	Final Weight (g)	Weight Loss (g)	Exposed Time (hours)	Surface Area (cm^2)	Corrosion Rate (nm/year) [4]
DWB024	1.9920	1.0010	0.1045	28.0650	ASW WL	SAW Aqueous Phase 60 °C	28.0645	0.0005	46296	29.4390	3.71
DWB059	1.9990	1.0060	0.1095	29.6327	ASW WL	SAW Vapor Phase 90 °C	29.6327	0.0000	45960	29.9001	0.01
DWB060	2.0020	1.0065	0.1120	30.1549	ASW WL	SAW Vapor Phase 90 °C	30.1548	0.0001	45960	30.0697	0.74
DWB061	1.9960	1.0065	0.1075	28.9565	ASW WL	SAW Vapor Phase 90 °C	28.9563	0.0002	45960	29.7803	1.49
DWB062	2.0000	1.0050	0.1080	29.1079	ASW WL	SAW Aqueous Phase 90 °C	29.1073	0.0006	45960	29.8196	4.43
DWB063	1.9985	1.0050	0.1075	29.0647	ASW WL	SAW Aqueous Phase 90 °C	29.0646	0.0001	45960	29.7755	0.75
DWB064	1.9955	1.0025	0.1105	29.2528	ASW WL	SAW Aqueous Phase 90 °C	29.2526	0.0002	45960	29.7996	1.49
DWB089	2.0000	1.0045	0.1130	30.0101	ASW WL	SCW Vapor Phase 60 °C	30.0100	0.0001	45456	30.0314	0.75
DWB090	2.0015	1.0045	0.0995	27.0584	ASW WL	SCW Vapor Phase 60 °C	27.0583	0.0001	45456	29.4441	0.77
DWB091	1.9950	1.0020	0.0980	26.6267	ASW WL	SCW Vapor Phase 60 °C	26.6267	0.0000	45456	29.2164	0.02
DWB092	1.9970	1.0005	0.0960	26.1388	ASW WL	SCW Aqueous Phase 60 °C	26.1385	0.0003	45456	29.1143	2.30
DWB093	1.9950	1.0050	0.1090	29.3467	ASW WL	SCW Aqueous Phase 60 °C	29.3462	0.0005	45456	29.7928	3.74
DWB094	1.9910	0.9995	0.1075	28.8795	ASW WL	SCW Aqueous Phase 60 °C	28.8786	0.0009	45456	29.5189	6.78
DWB129	1.9780	1.0055	0.1075	29.1972	ASW WL	SCW Vapor Phase 90 °C	29.1971	0.0001	44832	29.4947	0.78
DWB130	1.9955	1.0020	0.1065	28.6787	ASW WL	SCW Vapor Phase 90 °C	28.6784	0.0003	44832	29.6060	2.29
DWB131	2.0040	1.0050	0.1070	29.2996	ASW WL	SCW Vapor Phase 90 °C	29.2993	0.0003	44832	29.8319	2.28
DWB132	2.0000	1.0025	0.1065	28.7651	ASW WL	SCW Aqueous Phase 90 °C	28.7637	0.0014	44832	29.6840	10.62
DWB133	2.0000	1.0015	0.1105	29.7020	ASW WL	SCW Aqueous Phase 90 °C	29.7005	0.0015	44832	29.8370	11.32
DWB134	1.9960	1.0040	0.1075	29.2460	ASW WL	SCW Aqueous Phase 90 °C	29.2444	0.0016	44832	29.7125	12.12
DWB147	1.9955	1.0025	0.1060	28.6604	ASW WL	SDW Vapor Phase 60 °C	28.6603	0.0001	44448	29.5971	0.78
DWB148	1.9955	1.0045	0.1085	29.4282	ASW WL	SDW Aqueous Phase 60 °C	29.4280	0.0002	44448	29.7639	1.54
DWB 174	1.9960	0.9960	0.1180	30.5213	ASW WL	SDW Vapor Phase 90 °C	30.5210	0.0003	43488	29.9671	2.34

Sample ID	Length (in)	Width (in)	Thickness (in)	Initial Weight (g)	Sample Condition [1]	Exposure Environment	Final Weight (g)	Weight Loss (g)	Exposed Time (hours)	Surface Area (cm^2)	Corrosion Rate (nm/year) [4]
DWB175	2.0000	0.9995	0.1110	28.4575	ASW WL	SDW Aqueous Phase 90 °C	28.4573	0.0002	43488	29.8051	1.57

Note: 1) MA = mill annealed, WL = weight loss.
2) Outlier not included in the analysis.
3) The waterline data are treated as the aqueous phase data in the analysis.
4) The input data from DTN LL030412512251.057 are the initial and final weight measurements, sample dimensions, and exposure conditions and time. The sample surface areas and corrosion rates were calculated in this model report. The calculated corrosion rates in this table are slightly different from those in DTN LL030412512251.057 due to the round-off errors.

Source DTN: LL030412512251.057

ATTACHMENT IV

Corrosion Rate of Alloy 22 as a Function of Temperature Calculated from the Polarization Resistance Measurement

Note: The corrosion rates from the polarization resistance measurements in this table are for a comparative analysis for the temperature dependence of the corrosion rate. The measurements are not intended for obtaining the absolute values of the corrosion rate.

Source DTN	Sample ID	Sample Type	Material Condition	Environment	Temp (°C)	1/(T+273.15) (1/K)	pH	Corrosion Rate (nm/yr)
LL030309512251.042	DEA3264	MCA	MA	1M NaCl	60	0.00300	7.50	266
LL030309512251.042	DEA3264	MCA	MA	1M NaCl	60	0.00300	7.50	335
LL030309512251.042	DEA3264	MCA	MA	1M NaCl	60	0.00300	7.50	313
LL030309512251.042	DEA3265	MCA	MA	1M NaCl	60	0.00300	7.68	1553
LL030309512251.042	DEA3265	MCA	MA	1M NaCl	60	0.00300	7.68	1166
LL030309512251.042	DEA3265	MCA	MA	1M NaCl	60	0.00300	7.68	1265
LL030309512251.042	DEA3262	MCA	MA	1M NaCl	90	0.00275	7.63	1927
LL030309512251.042	DEA3262	MCA	MA	1M NaCl	90	0.00275	7.63	1660
LL030309512251.042	DEA3262	MCA	MA	1M NaCl	90	0.00275	7.63	1361
LL030309512251.042	DEA3263	MCA	MA	1M NaCl	90	0.00275	7.68	2554
LL030309512251.042	DEA3263	MCA	MA	1M NaCl	90	0.00275	7.68	2401
LL030309512251.042	DEA3263	MCA	MA	1M NaCl	90	0.00275	7.68	1286
LL030309512251.042	DEA3147	MCA	MA	1.25M NaCl	60	0.00300	6.99	774
LL030309512251.042	DEA3147	MCA	MA	1.25M NaCl	60	0.00300	6.99	700
LL030309512251.042	DEA3147	MCA	MA	1.25M NaCl	60	0.00300	6.99	580
LL030309512251.042	DEA3148	MCA	MA	1.25M NaCl	60	0.00300	6.49	754
LL030309512251.042	DEA3148	MCA	MA	1.25M NaCl	60	0.00300	6.49	866

Source DTN	Sample ID	Sample Type	Material Condition	Environment	Temp (°C)	1/(T+273.15) (1/K)	pH	Corrosion Rate (nm/yr)
LL030309512251.042	DEA3148	MCA	MA	1.25M NaCl	60	0.00300	6.49	835
LL030309512251.042	DEA3267	MCA	MA	1.25M NaCl	60	0.00300	7.95	139
LL030309512251.042	DEA3267	MCA	MA	1.25M NaCl	60	0.00300	7.95	146
LL030309512251.042	DEA3267	MCA	MA	1.25M NaCl	60	0.00300	7.95	166
LL030309512251.042	DEA3268	MCA	MA	1.25M NaCl	60	0.00300	7.61	525
LL030309512251.042	DEA3268	MCA	MA	1.25M NaCl	60	0.00300	7.61	584
LL030309512251.042	DEA3268	MCA	MA	1.25M NaCl	60	0.00300	7.61	669
LL030309512251.042	DEA3273	MCA	MA	1.25M NaCl	60	0.00300	7.06	133
LL030309512251.042	DEA3273	MCA	MA	1.25M NaCl	60	0.00300	7.06	51
LL030309512251.042	DEA3273	MCA	MA	1.25M NaCl	60	0.00300	7.06	151
LL030309512251.042	DEA3269	MCA	MA	1.25M NaCl	90	0.00275	7.09	1205
LL030309512251.042	DEA3269	MCA	MA	1.25M NaCl	90	0.00275	7.09	1036
LL030309512251.042	DEA3269	MCA	MA	1.25M NaCl	90	0.00275	7.09	612
LL030309512251.042	DEA3271	MCA	MA	1.25M NaCl	90	0.00275	7.32	407
LL030309512251.042	DEA3271	MCA	MA	1.25M NaCl	90	0.00275	7.32	509
LL030309512251.042	DEA3271	MCA	MA	1.25M NaCl	90	0.00275	7.32	226
LL030309512251.042	DEA3182	MCA	MA	1.25M $CaCl_2$	60	0.00300	6.78	164
LL030309512251.042	DEA3182	MCA	MA	1.25M $CaCl_2$	60	0.00300	6.78	260
LL030309512251.042	DEA3182	MCA	MA	1.25M $CaCl_2$	60	0.00300	6.78	231
LL030309512251.042	DEA3183	MCA	MA	1.25M $CaCl_2$	60	0.00300	6.77	198
LL030309512251.042	DEA3183	MCA	MA	1.25M $CaCl_2$	60	0.00300	6.77	92
LL030309512251.042	DEA3184	MCA	MA	1.25M $CaCl_2$	90	0.00275	6.78	2323

Source DTN	Sample ID	Sample Type	Material Condition	Environment	Temp (°C)	1/(T+273.15) (1/K)	pH	Corrosion Rate (nm/yr)
LL030309512251.042	DEA3184	MCA	MA	1.25M $CaCl_2$	90	0.00275	6.78	1698
LL030309512251.042	DEA3184	MCA	MA	1.25M $CaCl_2$	90	0.00275	6.78	1778
LL030309512251.042	DEA3185	MCA	MA	1.25M $CaCl_2$	90	0.00275	7.39	3553
LL030309512251.042	DEA3185	MCA	MA	1.25M $CaCl_2$	90	0.00275	7.39	2420
LL030309512251.042	DEA3185	MCA	MA	1.25M $CaCl_2$	90	0.00275	7.39	3095
LL030309512251.042	DEA3274	MCA	MA	2.5M $CaCl_2$	60	0.00300	7.05	255
LL030309512251.042	DEA3274	MCA	MA	2.5M $CaCl_2$	60	0.00300	7.05	1162
LL030309512251.042	DEA3274	MCA	MA	2.5M $CaCl_2$	60	0.00300	7.05	946
LL030309512251.042	DEA3275	MCA	MA	2.5M $CaCl_2$	60	0.00300	7.04	1212
LL030309512251.042	DEA3275	MCA	MA	2.5M $CaCl_2$	60	0.00300	7.04	304
LL030309512251.042	DEA3275	MCA	MA	2.5M $CaCl_2$	60	0.00300	7.04	327
LL030309512251.042	DEA3189	MCA	MA	2.5M $CaCl_2$	90	0.00275	6.32	6866
LL030309512251.042	DEA3189	MCA	MA	2.5M $CaCl_2$	90	0.00275	6.32	6627
LL030309512251.042	DEA3189	MCA	MA	2.5M $CaCl_2$	90	0.00275	6.32	6529
LL030309512251.042	DEA3190	MCA	MA	2.5M $CaCl_2$	90	0.00275	6.98	5232
LL030309512251.042	DEA3190	MCA	MA	2.5M $CaCl_2$	90	0.00275	6.98	5559
LL030309512251.042	DEA3190	MCA	MA	2.5M $CaCl_2$	90	0.00275	6.98	5861
LL030309512251.042	DEA3186	MCA	MA	5M $CaCl_2$	45	0.00314	5.42	1703
LL030309512251.042	DEA3186	MCA	MA	5M $CaCl_2$	45	0.00314	5.42	1684
LL030309512251.042	DEA3186	MCA	MA	5M $CaCl_2$	45	0.00314	5.42	1749
LL030309512251.042	DEA3187	MCA	MA	5M $CaCl_2$	45	0.00314	5.53	1756
LL030309512251.042	DEA3187	MCA	MA	5M $CaCl_2$	45	0.00314	5.53	1539

Source DTN	Sample ID	Sample Type	Material Condition	Environment	Temp (°C)	1/(T+273.15) (1/K)	pH	Corrosion Rate (nm/yr)
LL030309512251.042	DEA3187	MCA	MA	5M $CaCl_2$	45	0.00314	5.53	1573
LL030309512251.042	DEA3180	MCA	MA	5M $CaCl_2$	60	0.00300	6.06	3554
LL030309512251.042	DEA3180	MCA	MA	5M $CaCl_2$	60	0.00300	6.06	3017
LL030309512251.042	DEA3180	MCA	MA	5M $CaCl_2$	60	0.00300	6.06	2998
LL030309512251.042	DEA3181	MCA	MA	5M $CaCl_2$	60	0.00300	5.95	2294
LL030309512251.042	DEA3181	MCA	MA	5M $CaCl_2$	60	0.00300	5.95	2698
LL030309512251.042	DEA3181	MCA	MA	5M $CaCl_2$	60	0.00300	5.95	2542
LL030309512251.042	DEA3260	MCA	MA	5M $CaCl_2$	75	0.00287	5.73	5334
LL030309512251.042	DEA3260	MCA	MA	5M $CaCl_2$	75	0.00287	5.73	5366
LL030309512251.042	DEA3260	MCA	MA	5M $CaCl_2$	75	0.00287	5.73	5174
LL030309512251.042	DEA3261	MCA	MA	5M $CaCl_2$	75	0.00287	6.07	3678
LL030309512251.042	DEA3261	MCA	MA	5M $CaCl_2$	75	0.00287	6.07	3386
LL030309512251.042	DEA3261	MCA	MA	5M $CaCl_2$	75	0.00287	6.07	3323
LL030309512251.042	DEA3176	MCA	MA	5M $CaCl_2$	90	0.00275	5.58	4947
LL030309512251.042	DEA3176	MCA	MA	5M $CaCl_2$	90	0.00275	5.58	4798
LL030309512251.042	DEA3176	MCA	MA	5M $CaCl_2$	90	0.00275	5.58	4344
LL030309512251.042	DEA3177	MCA	MA	5M $CaCl_2$	90	0.00275	5.74	6487
LL030309512251.042	DEA3177	MCA	MA	5M $CaCl_2$	90	0.00275	5.74	5863
LL030309512251.042	DEA3177	MCA	MA	5M $CaCl_2$	90	0.00275	5.74	5398
LL030309512251.042	DEA3167	MCA	MA	5M $CaCl_2$	105	0.00264	6.14	19210
LL030309512251.042	DEA3167	MCA	MA	5M $CaCl_2$	105	0.00264	6.14	18240
LL030309512251.042	DEA3167	MCA	MA	5M $CaCl_2$	105	0.00264	6.14	17450

Source DTN	Sample ID	Sample Type	Material Condition	Environment	Temp (°C)	1/(T+273.15) (1/K)	pH	Corrosion Rate (nm/yr)
LL030309512251.042	DEA3168	MCA	MA	5M $CaCl_2$	105	0.00264	6.12	6101
LL030309512251.042	DEA3168	MCA	MA	5M $CaCl_2$	105	0.00264	6.12	5850
LL030309512251.042	DEA3168	MCA	MA	5M $CaCl_2$	105	0.00264	6.12	5428
LL030409812251.054	DEA3125	MCA	MA	7M $CaCl_2$	130	0.00248	**4.14**	7505
LL030409812251.054	DEA3125	MCA	MA	7M $CaCl_2$	130	0.00248	**4.14**	5711
LL030409812251.054	DEA3125	MCA	MA	7M $CaCl_2$	130	0.00248	**4.14**	6572
LL030409812251.054	DEA599	Disc	MA	7M $CaCl_2$	130	0.00248	**4.14**	6803
LL030409812251.054	DEA599	Disc	MA	7M $CaCl_2$	130	0.00248	**4.14**	6344
LL030409812251.054	DEA599	Disc	MA	7M $CaCl_2$	130	0.00248	**4.14**	6551
LL030409812251.054	DEA595	Disc	MA	8M $CaCl_2$	100	0.00268	**4.14**	2212
LL030409812251.054	DEA595	Disc	MA	8M $CaCl_2$	100	0.00268	**4.14**	2118
LL030409812251.054	DEA595	Disc	MA	8M $CaCl_2$	100	0.00268	**4.14**	1763
LL030409812251.054	DEA595	Disc	MA	8M $CaCl_2$	100	0.00268	**4.14**	2005
LL030409812251.054	DEA596	Disc	MA	9M $CaCl_2$	150	0.00236	**4.14**	20270
LL030409812251.054	DEA596	Disc	MA	9M $CaCl_2$	150	0.00236	**4.14**	18820
LL030409812251.054	DEA596	Disc	MA	9M $CaCl_2$	150	0.00236	**4.14**	18760
LL030409812251.054	DEA3105	MCA	MA	1.25M $CaCl_2$ + 0.0125M $Ca(NO_3)_2$	60	0.00300	6.47	1618
LL030409812251.054	DEA3105	MCA	MA	1.25M $CaCl_2$ + 0.0125M $Ca(NO_3)_2$	60	0.00300	6.47	1990
LL030409812251.054	DEA3105	MCA	MA	1.25M $CaCl_2$ + 0.0125M $Ca(NO_3)_2$	60	0.00300	6.47	981
LL030409812251.054	DEA3108	MCA	MA	1.25M $CaCl_2$ + 0.125M $Ca(NO_3)_2$	60	0.00300	6.41	211
LL030409812251.054	DEA3108	MCA	MA	1.25M $CaCl_2$ + 0.125M $Ca(NO_3)_2$	60	0.00300	6.41	154
LL030409812251.054	DEA3108	MCA	MA	1.25M $CaCl_2$ + 0.125M $Ca(NO_3)_2$	60	0.00300	6.41	160

Source DTN	Sample ID	Sample Type	Material Condition	Environment	Temp (°C)	1/(T+273.15) (1/K)	pH	Corrosion Rate (nm/yr)
LL030409812251.054	DEA3109	MCA	MA	1.25M $CaCl_2$ + 0.125M $Ca(NO_3)_2$	90	0.00275	6.41	654
LL030409812251.054	DEA3109	MCA	MA	1.25M $CaCl_2$ + 0.125M $Ca(NO_3)_2$	90	0.00275	6.41	1821
LL030409812251.054	DEA3109	MCA	MA	1.25M $CaCl_2$ + 0.125M $Ca(NO_3)_2$	90	0.00275	6.41	1333
LL030409812251.054	DEA3101	MCA	MA	5M $CaCl_2$ + 0.5M $Ca(NO_3)_2$	60	0.00300	5.78	1043
LL030409812251.054	DEA3101	MCA	MA	5M $CaCl_2$ + 0.5M $Ca(NO_3)_2$	60	0.00300	5.78	994
LL030409812251.054	DEA3101	MCA	MA	5M $CaCl_2$ + 0.5M $Ca(NO_3)_2$	60	0.00300	5.78	912
LL030409812251.054	DEA3103	MCA	MA	5M $CaCl_2$ + 0.5M $Ca(NO_3)_2$	60	0.00300	5.78	1193
LL030409812251.054	DEA3103	MCA	MA	5M $CaCl_2$ + 0.5M $Ca(NO_3)_2$	60	0.00300	5.78	916
LL030409812251.054	DEA3103	MCA	MA	5M $CaCl_2$ + 0.5M $Ca(NO_3)_2$	60	0.00300	5.78	1130
LL030409812251.054	DEA3102	MCA	MA	5M $CaCl_2$ + 0.5M $Ca(NO_3)_2$	90	0.00275	5.78	1418
LL030409812251.054	DEA3102	MCA	MA	5M $CaCl_2$ + 0.5M $Ca(NO_3)_2$	90	0.00275	5.78	1196
LL030409812251.054	DEA3104	MCA	MA	5M $CaCl_2$ + 0.5M $Ca(NO_3)_2$	90	0.00275	5.78	1739
LL030409812251.054	DEA3104	MCA	MA	5M $CaCl_2$ + 0.5M $Ca(NO_3)_2$	90	0.00275	5.78	2215
LL030409812251.054	DEA3104	MCA	MA	5M $CaCl_2$ + 0.5M $Ca(NO_3)_2$	90	0.00275	5.78	2221
LL030409812251.054	DEA3123	MCA	MA	5M $CaCl_2$ + 0.5M $Ca(NO_3)_2$	105	0.00264	4.86	3052
LL030409812251.054	DEA3123	MCA	MA	5M $CaCl_2$ + 0.5M $Ca(NO_3)_2$	105	0.00264	4.86	2906
LL030409812251.054	DEA3123	MCA	MA	5M $CaCl_2$ + 0.5M $Ca(NO_3)_2$	105	0.00264	4.86	2810
LL030409812251.054	DEA3124	MCA	MA	5M $CaCl_2$ + 0.5M $Ca(NO_3)_2$	105	0.00264	4.86	4488
LL030409812251.054	DEA3124	MCA	MA	5M $CaCl_2$ + 0.5M $Ca(NO_3)_2$	105	0.00264	4.86	3971
LL030409812251.054	DEA3124	MCA	MA	5M $CaCl_2$ + 0.5M $Ca(NO_3)_2$	105	0.00264	4.86	3887
LL030409812251.054	DEA598	Disc	MA	6M $CaCl_2$ + 0.6M $Ca(NO_3)_2$	120	0.00254	**5.34**	2647
LL030409812251.054	DEA598	Disc	MA	6M $CaCl_2$ + 0.6M $Ca(NO_3)_2$	120	0.00254	**5.34**	2244

Source DTN	Sample ID	Sample Type	Material Condition	Environment	Temp (°C)	1/(T+273.15) (1/K)	pH	Corrosion Rate (nm/yr)
LL030409812251.054	DEA598	Disc	MA	6M $CaCl_2$ + 0.6M $Ca(NO_3)_2$	120	0.00254	**5.34**	2523
LL030409812251.054	DEA3127	MCA	MA	7M $CaCl_2$ + 0.7M $Ca(NO_3)_2$	130	0.00248	**5.34**	3117
LL030409812251.054	DEA3127	MCA	MA	7M $CaCl_2$ + 0.7M $Ca(NO_3)_2$	130	0.00248	**5.34**	2445
LL030409812251.054	DEA3127	MCA	MA	7M $CaCl_2$ + 0.7M $Ca(NO_3)_2$	130	0.00248	**5.34**	2638
LL030409812251.054	DEA600	Disc	MA	7M $CaCl_2$ + 0.7M $Ca(NO_3)_2$	130	0.00248	**5.34**	1946
LL030409812251.054	DEA600	Disc	MA	7M $CaCl_2$ + 0.7M $Ca(NO_3)_2$	130	0.00248	**5.34**	1304
LL030409812251.054	DEA600	Disc	MA	7M $CaCl_2$ + 0.7M $Ca(NO_3)_2$	130	0.00248	**5.34**	1812
LL030409812251.054	DEA3118	MCA	MA	8M $CaCl_2$ + 0.8M $Ca(NO_3)_2$	140	0.00242	**5.34**	1775
LL030409812251.054	DEA3118	MCA	MA	8M $CaCl_2$ + 0.8M $Ca(NO_3)_2$	140	0.00242	**5.34**	3659
LL030409812251.054	DEA3118	MCA	MA	8M $CaCl_2$ + 0.8M $Ca(NO_3)_2$	140	0.00242	**5.34**	6509
LL030409812251.054	DEA3119	MCA	MA	8M $CaCl_2$ + 0.8M $Ca(NO_3)_2$	140	0.00242	**5.34**	1147
LL030409812251.054	DEA3119	MCA	MA	8M $CaCl_2$ + 0.8M $Ca(NO_3)_2$	140	0.00242	**5.34**	1202
LL030409812251.054	DEA3119	MCA	MA	8M $CaCl_2$ + 0.8M $Ca(NO_3)_2$	140	0.00242	**5.34**	896
LL030409812251.054	DEA597	Disc	MA	9M $CaCl_2$ + 0.9M $Ca(NO_3)_2$	150	0.00236	**5.34**	5602
LL030409812251.054	DEA597	Disc	MA	9M $CaCl_2$ + 0.9M $Ca(NO_3)_2$	150	0.00236	**5.34**	4817
LL030409812251.054	DEA597	Disc	MA	9M $CaCl_2$ + 0.9M $Ca(NO_3)_2$	150	0.00236	**5.34**	5139
LL030409812251.054	DEA3120	MCA	MA	9M $CaCl_2$ + 0.9M $Ca(NO_3)_2$	160	0.00231	**5.34**	5041
LL030409812251.054	DEA3120	MCA	MA	9M $CaCl_2$ + 0.9M $Ca(NO_3)_2$	160	0.00231	**5.34**	4710
LL030409812251.054	DEA3120	MCA	MA	9M $CaCl_2$ + 0.9M $Ca(NO_3)_2$	160	0.00231	**5.34**	6839
LL030409812251.054	DEA3122	MCA	MA	9M $CaCl_2$ + 0.9M $Ca(NO_3)_2$	170	0.00226	**5.34**	2692
LL030409812251.054	DEA3122	MCA	MA	9M $CaCl_2$ + 0.9M $Ca(NO_3)_2$	170	0.00226	**5.34**	7070
LL030409812251.054	DEA3122	MCA	MA	9M $CaCl_2$ + 0.9M $Ca(NO_3)_2$	170	0.00226	**5.34**	2729

Source DTN	Sample ID	Sample Type	Material Condition	Environment	Temp (°C)	1/(T+273.15) (1/K)	pH	Corrosion Rate (nm/yr)
LL030309512251.042	KK006	Prism	ASW	1M NaCl	90	0.00275	6.70	157
LL030309512251.042	KK006	Prism	ASW	1M NaCl	90	0.00275	6.70	211
LL030502212251.063	JE 0022	MCA	ASW	5M CaCl2	115.5	0.00257	5.95	3613
LL030502212251.063	JE 0022	MCA	ASW	5M CaCl2	115.5	0.00257	5.95	5848
LL030502212251.063	JE 0022	MCA	ASW	5M CaCl2	115.5	0.00257	5.95	4770
LL030502212251.063	JE 0023	MCA	ASW	5M CaCl2	116.4	0.00257	5.96	10470
LL030502212251.063	JE 0023	MCA	ASW	5M CaCl2	116.4	0.00257	5.96	11040
LL030502212251.063	JE 0023	MCA	ASW	5M CaCl2	116.4	0.00257	5.96	12770
LL030502212251.063	JE 0032	MCA	ASW	1M CaCl2+1M Ca(NO3)2	104.8	0.00265	6.73	1649
LL030502212251.063	JE 0032	MCA	ASW	1M CaCl2+1M Ca(NO3)2	104.8	0.00265	6.73	1590
LL030502212251.063	JE 0032	MCA	ASW	1M CaCl2+1M Ca(NO3)2	104.8	0.00265	6.73	972
LL030502212251.063	JE 0033	MCA	ASW	1M CaCl2+1M Ca(NO3)2	104.8	0.00265	6.85	1696
LL030502212251.063	JE 0033	MCA	ASW	1M CaCl2+1M Ca(NO3)2	104.8	0.00265	6.85	2347
LL030502212251.063	JE 0033	MCA	ASW	1M CaCl2+1M Ca(NO3)2	104.8	0.00265	6.85	1047
LL030502212251.063	JE 0024	MCA	ASW	5M CaCl2+0.05M Ca(NO3)2	118.4	0.00255	5.89	9428
LL030502212251.063	JE 0024	MCA	ASW	5M CaCl2+0.05M Ca(NO3)2	118.4	0.00255	5.89	9360
LL030502212251.063	JE 0024	MCA	ASW	5M CaCl2+0.05M Ca(NO3)2	118.4	0.00255	5.89	8894
LL030502212251.063	JE 0025	MCA	ASW	5M CaCl2+0.05M Ca(NO3)2	118.6	0.00255	5.94	8081
LL030502212251.063	JE 0025	MCA	ASW	5M CaCl2+0.05M Ca(NO3)2	118.6	0.00255	5.94	7893
LL030502212251.063	JE 0025	MCA	ASW	5M CaCl2+0.05M Ca(NO3)2	118.6	0.00255	5.94	8218
LL030409812251.054	KK001	Prism	ASW	5M $CaCl_2$ + 0.5M $Ca(NO_3)_2$	75	0.00287	5.78	1609
LL030409812251.054	KK001	Prism	ASW	5M $CaCl_2$ + 0.5M $Ca(NO_3)_2$	75	0.00287	5.78	1431

Source DTN	Sample ID	Sample Type	Material Condition	Environment	Temp (°C)	1/(T+273.15) (1/K)	pH	Corrosion Rate (nm/yr)
LL030409812251.054	KK001	Prism	ASW	5M $CaCl_2$ + 0.5M $Ca(NO_3)_2$	75	0.00287	5.78	1337
LL030409812251.054	KK004	Prism	ASW	5M $CaCl_2$ + 0.5M $Ca(NO_3)_2$	75	0.00287	5.78	1602
LL030409812251.054	KK004	Prism	ASW	5M $CaCl_2$ + 0.5M $Ca(NO_3)_2$	75	0.00287	5.78	1415
LL030409812251.054	KK004	Prism	ASW	5M $CaCl_2$ + 0.5M $Ca(NO_3)_2$	75	0.00287	5.78	1265
LL030409812251.054	KK002	Prism	ASW	5M $CaCl_2$ + 0.5M $Ca(NO_3)_2$	90	0.00275	5.78	1147
LL030409812251.054	KK002	Prism	ASW	5M $CaCl_2$ + 0.5M $Ca(NO_3)_2$	90	0.00275	5.78	920
LL030409812251.054	KK002	Prism	ASW	5M $CaCl_2$ + 0.5M $Ca(NO_3)_2$	90	0.00275	5.78	820
LL030409812251.054	KK003	Prism	ASW	5M $CaCl_2$ + 0.5M $Ca(NO_3)_2$	90	0.00275	5.78	1125
LL030409812251.054	KK003	Prism	ASW	5M $CaCl_2$ + 0.5M $Ca(NO_3)_2$	90	0.00275	5.78	919
LL030409812251.054	KK003	Prism	ASW	5M $CaCl_2$ + 0.5M $Ca(NO_3)_2$	90	0.00275	5.78	788
LL030502212251.063	JE 0027	MCA	ASW	5M CaCl2+1M Ca(NO3)2	121.8	0.00253	5.95	1925
LL030502212251.063	JE 0027	MCA	ASW	5M CaCl2+1M Ca(NO3)2	121.8	0.00253	5.95	2182
LL030502212251.063	JE 0027	MCA	ASW	5M CaCl2+1M Ca(NO3)2	121.8	0.00253	5.95	1870
LL030502212251.063	JE 0027	MCA	ASW	5M CaCl2+1M Ca(NO3)2	121.8	0.00253	5.95	2221
LL030502212251.063	JE 0026	MCA	ASW	5M CaCl2+1M Ca(NO3)2	123.7	0.00252	5.72	6419
LL030502212251.063	JE 0026	MCA	ASW	5M CaCl2+1M Ca(NO3)2	123.7	0.00252	5.72	6060
LL030502212251.063	JE 0026	MCA	ASW	5M CaCl2+1M Ca(NO3)2	123.7	0.00252	5.72	6089
LL030502212251.063	JE 0011	MCA	ASW + Aged, 173 hrs at 700 °C	5M CaCl2	118.8	0.00255	6.58	3333
LL030502212251.063	JE 0011	MCA	ASW + Aged, 173 hrs at 700 °C	5M CaCl2	118.8	0.00255	6.58	2544
LL030502212251.063	JE 0011	MCA	ASW + Aged, 173 hrs at 700 °C	5M CaCl2	118.8	0.00255	6.58	3929
LL030502212251.063	JE 0012	MCA	ASW + Aged, 173 hrs at 700 °C	5M CaCl2	119.0	0.00255	6.62	2616
LL030502212251.063	JE 0012	MCA	ASW + Aged, 173 hrs at 700 °C	5M CaCl2	119.0	0.00255	6.62	2561

Source DTN	Sample ID	Sample Type	Material Condition	Environment	Temp (°C)	1/(T+273.15) (1/K)	pH	Corrosion Rate (nm/yr)
LL030502212251.063	JE 0012	MCA	ASW + Aged, 173 hrs at 700 °C	5M CaCl2	119.0	0.00255	6.62	3005
LL030502212251.063	JE 0009	MCA	ASW + Aged, 173 hrs at 700 °C	1M CaCl2+1M Ca(NO3)2	104.8	0.00265	6.69	947
LL030502212251.063	JE 0009	MCA	ASW + Aged, 173 hrs at 700 °C	1M CaCl2+1M Ca(NO3)2	104.8	0.00265	6.69	879
LL030502212251.063	JE 0009	MCA	ASW + Aged, 173 hrs at 700 °C	1M CaCl2+1M Ca(NO3)2	104.8	0.00265	6.69	584
LL030502212251.063	JE 0010	MCA	ASW + Aged, 173 hrs at 700 °C	1M CaCl2+1M Ca(NO3)2	104.8	0.00265	6.73	1289
LL030502212251.063	JE 0010	MCA	ASW + Aged, 173 hrs at 700 °C	1M CaCl2+1M Ca(NO3)2	104.8	0.00265	6.73	1628
LL030502212251.063	JE 0010	MCA	ASW + Aged, 173 hrs at 700 °C	1M CaCl2+1M Ca(NO3)2	104.8	0.00265	6.73	1019
LL030502212251.063	JE 0016	MCA	ASW + Aged, 173 hrs at 700 °C	5M CaCl2+0.05M Ca(NO3)2	119.2	0.00255	6.07	7786
LL030502212251.063	JE 0016	MCA	ASW + Aged, 173 hrs at 700 °C	5M CaCl2+0.05M Ca(NO3)2	119.2	0.00255	6.07	7538
LL030502212251.063	JE 0016	MCA	ASW + Aged, 173 hrs at 700 °C	5M CaCl2+0.05M Ca(NO3)2	119.2	0.00255	6.07	6334
LL030502212251.063	JE 0015	MCA	ASW + Aged, 173 hrs at 700 °C	5M CaCl2+0.05M Ca(NO3)2	119.8	0.00254	6.15	4396
LL030502212251.063	JE 0015	MCA	ASW + Aged, 173 hrs at 700 °C	5M CaCl2+0.05M Ca(NO3)2	119.8	0.00254	6.15	4752
LL030502212251.063	JE 0015	MCA	ASW + Aged, 173 hrs at 700 °C	5M CaCl2+0.05M Ca(NO3)2	119.8	0.00254	6.15	4669
LL030502212251.063	JE 0018	MCA	ASW + Aged, 173 hrs at 700 °C	5M CaCl2+0.5M Ca(NO3)2	118.0	0.00256	6.54	2237
LL030502212251.063	JE 0018	MCA	ASW + Aged, 173 hrs at 700 °C	5M CaCl2+0.5M Ca(NO3)2	118.0	0.00256	6.54	2119
LL030502212251.063	JE 0018	MCA	ASW + Aged, 173 hrs at 700 °C	5M CaCl2+0.5M Ca(NO3)2	118.0	0.00256	6.54	1547
LL030502212251.063	JE 0017	MCA	ASW + Aged, 173 hrs at 700 °C	5M CaCl2+0.5M Ca(NO3)2	118.5	0.00255	6.51	1438
LL030502212251.063	JE 0017	MCA	ASW + Aged, 173 hrs at 700 °C	5M CaCl2+0.5M Ca(NO3)2	118.5	0.00255	6.51	1487
LL030502212251.063	JE 0017	MCA	ASW + Aged, 173 hrs at 700 °C	5M CaCl2+0.5M Ca(NO3)2	118.5	0.00255	6.51	1670

Note: A pH of 4.14 for 5 M CaCl2 solutions at 120 °C from DTN LL030400112251.043 was used for high temperature and high CaCl2 solutions (Samples DEA595, DEA596, DEA599, and DEA3125). Also a measured pH of 5.34 for 5 M CaCl2 plus 0.05 M Ca(NO3)2 solution at 120 °C from DTN LL030502212251.063 was used for CaCl2 plus Ca(NO3)2 salt solutions (Samples DEA597, DEA598, DEA600, DEA3118, DEA3119, DEA3120, DEA3122, and DEA3127).

Source DTNs: LL030309512251.042, LL030502212251.063, LL030409812251.054

ATTACHMENT V

Long-Term Steady-State Corrosion Potential Measurement of Alloy 22 Samples Used in the Corrosion Potential Model and Analysis.

Cell Number	Sample ID	Sample Type	Sample Initial Condition	Environment	Temp (°C)	pH	[Cl] (m,)	[NO3] (m)	Ecorr (mV SSC)
1	DUB028	Welded Alloy 22 U-Bend	1527 days (4+ Years) in LTCTF	Aged LTCTF SAW	60	2.98	0.838	0.426	385
1	DUB157	Welded Alloy 22 U-Bend	Untested, 600 grit surface polish	Aged LTCTF SAW	60	2.98	0.838	0.426	403
2	DUB052	Welded Alloy 22 U-Bend	1512 days (4+ Years) in LTCTF	Aged LTCTF SAW	90	3.55	0.838	0.426	276
2	DUB159	Welded Alloy 22 U-Bend	Untested, 600 grit surface polish	Aged LTCTF SAW	90	3.55	0.838	0.426	302
3	DUB112	Welded Alloy 22 U-Bend	1464 days (4+ Years) in LTCTF	Aged LTCTF SCW	90	10.72	0.211	0.111	5
3	DUB161	Welded Alloy 22 U-Bend	Untested, 600 grit surface polish	Aged LTCTF SCW	90	10.72	0.211	0.111	-57
4	ARC22 U20A & ARC22 U20B	Wrought Alloy 22 Double U-Bend	407 days (1+ year) in Bench Top	Fresh BSW	105	11.05	3.722	2.364	43
4	DUB163	Welded Alloy 22 U-Bend	Untested, 600 grit surface polish	Fresh BSW	105	11.05	3.722	2.364	27
5	DUB128	Welded Alloy 22 U-Bend	1460 days (4+ Years) in LTCTF	Aged LTCTF SDW	60	9.55	0.002	0.001	25
5	DUB150	Welded Alloy 22 U-Bend	Untested, 600 grit surface polish	Aged LTCTF SDW	60	9.55	0.002	0.001	-67
6	DUB132	Welded Alloy 22 U-Bend	1457 days (4+ Years) in LTCTF	Aged LTCTF SDW	90	8.55	0.002	0.001	79
6	DUB162	Welded Alloy 22 U-Bend	Untested, 600 grit surface polish	Aged LTCTF SDW	90	8.55	0.002	0.001	82
7	DUB088	Welded Alloy 22 U-Bend	1495 days (4+ Years) in LTCTF	Aged LTCTF SCW	60	10.24	0.211	0.111	21
7	DUB156	Welded Alloy 22 U-Bend	Untested, 600 grit surface polish	Aged LTCTF SCW	60	10.24	0.211	0.111	-27
7N	DEA2802	Wrought Alloy 22 Rod	Untested, 600 grit surface polish	Aged LTCTF SAW	25	3.72	0.806	0.407	219
7N	DEA2807	Wrought Alloy 22 Rod	Untested, 600 grit surface polish	Aged LTCTF SAW	25	3.72	0.806	0.407	215

Cell Number	Sample ID	Sample Type	Sample Initial Condition	Environment	Temp (°C)	pH	[Cl] (m,)	[NO3] (m)	Ecorr (mV SSC)
7N	DEA2859	Wrought Alloy 22 Rod	Untested, 600 grit surface polish	Aged LTCTF SAW	25	3.72	0.806	0.407	194
8	DEA105	Wrought Alloy 22 Rod	Untested, 600 grit surface polish	6.5 M CaCl2	120	5.21	17.145	0.000	-133
8	DEA106	Wrought Alloy 22 Rod	Untested, 600 grit surface polish	6.5 M CaCl2	120	5.21	17.145	0.000	-127
8	DEA107	Wrought Alloy 22 Rod	Untested, 600 grit surface polish	6.5 M CaCl2	120	5.21	17.145	0.000	-135
8	DEA108	Wrought Alloy 22 Rod	Untested, 600 grit surface polish	6.5 M CaCl2	120	5.21	17.145	0.000	-131
8	DEA109	Wrought Alloy 22 Rod	Untested, 600 grit surface polish	6.5 M CaCl2	120	5.21	17.145	0.000	-129
9	DEA2797	Wrought Alloy 22 Rod	Untested, 600 grit surface polish	Fresh SAW	90	2.78	0.781	0.399	389
9	DEA2853	Wrought Alloy 22 Rod	Untested, 600 grit surface polish	Fresh SAW	90	2.78	0.781	0.399	389
9	DEA2881	Wrought Alloy 22 Rod	Untested, 600 grit surface polish	Fresh SAW	90	2.78	0.781	0.399	389
9	DEA2928	Wrought Alloy 22 Rod	Untested, 600 grit surface polish	Fresh SAW	90	2.78	0.781	0.399	389
9	DEA2940	Wrought Alloy 22 Rod	Untested, 600 grit surface polish	Fresh SAW	90	2.78	0.781	0.399	388
9	DEA3010	Wrought Alloy 22 Rod	Untested, 600 grit surface polish	Fresh SAW	90	2.78	0.781	0.399	388
9	DEA3014	Wrought Alloy 22 Rod	Untested, 600 grit surface polish	Fresh SAW	90	2.78	0.781	0.399	387
9	DEA3082	Wrought Alloy 22 Rod	Untested, 600 grit surface polish	Fresh SAW	90	2.78	0.781	0.399	388
10	DEA2850	Wrought Alloy 22 Rod	Untested, 600 grit surface polish	Aged LTCTF SAW	90	3.67	0.838	0.426	353
10	DEA2851	Wrought Alloy 22 Rod	Untested, 600 grit surface polish	Aged LTCTF SAW	90	3.67	0.838	0.426	345
10	DEA2852	Wrought Alloy 22 Rod	Untested, 600 grit surface polish	Aged LTCTF SAW	90	3.67	0.838	0.426	344
10	DEA2854	Wrought Alloy 22 Rod	Untested, 600 grit surface polish	Aged LTCTF SAW	90	3.67	0.838	0.426	350
10	DEA2855	Wrought Alloy 22 Rod	Untested, 600 grit surface polish	Aged LTCTF SAW	90	3.67	0.838	0.426	351
10	DEA2856	Wrought Alloy 22 Rod	Untested, 600 grit surface polish	Aged LTCTF SAW	90	3.67	0.838	0.426	343
10	DEA2857	Wrought Alloy 22 Rod	Untested, 600 grit surface polish	Aged LTCTF SAW	90	3.67	0.838	0.426	347

Cell Number	Sample ID	Sample Type	Sample Initial Condition	Environment	Temp (°C)	pH	[Cl] (m,)	[NO3] (m)	Ecorr (mV SSC)
10	DEA2858	Wrought Alloy 22 Rod	Untested, 600 grit surface polish	Aged LTCTF SAW	90	3.67	0.838	0.426	347
13	DEA3087	Wrought Alloy 22 Rod	Untested, 600 grit surface polish	1 M CaCl2 + 1 M Ca(NO3)2	90	4.75	2.311	2.232	174
13	DEA3088	Wrought Alloy 22 Rod	Untested, 600 grit surface polish	1 M CaCl2 + 1 M Ca(NO3)2	90	4.75	2.311	2.232	157
13	DEA3089	Wrought Alloy 22 Rod	Untested, 600 grit surface polish	1 M CaCl2 + 1 M Ca(NO3)2	90	4.75	2.311	2.232	177
13	DEA3090	Wrought Alloy 22 Rod	Untested, 600 grit surface polish	1 M CaCl2 + 1 M Ca(NO3)2	90	4.75	2.311	2.232	163
14	DEA2800	Wrought Alloy 22 Rod	Untested, 600 grit surface polish	5 M CaCl2 + 0.05 M Ca(NO3)2	90	5.04	11.699	0.119	-41
14	DEA2801	Wrought Alloy 22 Rod	Untested, 600 grit surface polish	5 M CaCl2 + 0.05 M Ca(NO3)2	90	5.04	11.699	0.119	-103
14	DEA2803	Wrought Alloy 22 Rod	Untested, 600 grit surface polish	5 M CaCl2 + 0.05 M Ca(NO3)2	90	5.04	11.699	0.119	-47
14	DEA2804	Wrought Alloy 22 Rod	Untested, 600 grit surface polish	5 M CaCl2 + 0.05 M Ca(NO3)2	90	5.04	11.699	0.119	-46
15	DEA2805	Wrought Alloy 22 Rod	Untested, 600 grit surface polish	5 M CaCl2 + 0.5 M Ca(NO3)2	90	4.19	12.593	1.264	-84
15	DEA2806	Wrought Alloy 22 Rod	Untested, 600 grit surface polish	5 M CaCl2 + 0.5 M Ca(NO3)2	90	4.19	12.593	1.264	22
15	DEA2808	Wrought Alloy 22 Rod	Untested, 600 grit surface polish	5 M CaCl2 + 0.5 M Ca(NO3)2	90	4.19	12.593	1.264	-34
15	DEA2809	Wrought Alloy 22 Rod	Untested, 600 grit surface polish	5 M CaCl2 + 0.5 M Ca(NO3)2	90	4.19	12.593	1.264	-56

Note: 1. Long-term corrosion potential data, sample characteristics, and test environments and temperature were from DTN LL020711612251.017.

2. pH values of the test solutions were from DTN LL030201212251.033.

3. Molal concentrations of chloride and nitrate ions of test solutions in Cell Numbers 1, 2, 3, 7, 7N, 9, 10 and 13 were from DTN LL030706223121.032.

4. Molal concentrations of chloride and nitrate ions of test solutions in Cell Numbers 8, 14 and 15 were from DTN LL030703723121.031.

5. Molal concentrations of chloride and nitrate ions of fresh BSW solution (Cell Number 4) were from DTN LL030709812251.067.

6. Molal concentrations of chloride and nitrate ions of aged SDW solutions (Cell Numbers 5 and 6) were assumed to be same as the molar concentrations of the species from DTN LL000320405924.146.

Source DTN LL020711612251.017

ATTACHMENT VI

Project's Crevice Repassivation Potential Data of Alloy 22 Samples Used in the Critical Potential Model and Analysis.

Source DTN [a]	Specimen ID	Sample Type [b]	Material Condition [b]	Electrolyte	Temperature (°C)	pH	[Cl] (moles/kg water)	[NO_3] (moles/kg water)	E_{rcrev} (mV_1 vs. SSC) [c]
LL030309512251.042	DEA3262	MCA	MA	1M NaCl	90	5.97	1.023	0.000	-53
LL030309512251.042	DEA3263	MCA	MA	1M NaCl	90	5.97	1.023	0.000	-54
LL030309512251.042	DEA3267	MCA	MA	1.25M NaCl	60	4.41	1.289	0.000	44
LL030309512251.042	DEA3268	MCA	MA	1.25M NaCl	60	4.41	1.289	0.000	15
LL030309512251.042	DEA3269	MCA	MA	1.25M NaCl	90	4.41	1.289	0.000	-66
LL030309512251.042	DEA3271	MCA	MA	1.25M NaCl	90	4.41	1.289	0.000	-44
LL030309512251.042	DEA3182	MCA	MA	1.25M CaCl2	60	5.83	2.582	0.000	117
LL030309512251.042	DEA3183	MCA	MA	1.25M CaCl2	60	5.83	2.582	0.000	-33
LL030309512251.042	DEA3184	MCA	MA	1.25M CaCl2	90	5.83	2.582	0.000	-65
LL030309512251.042	DEA3185	MCA	MA	1.25M CaCl2	90	5.83	2.582	0.000	-49
LL030309512251.042	DEA3189	MCA	MA	2.5M CaCl2	90	5.75	5.401	0.000	-124
LL030309512251.042	DEA3190	MCA	MA	2.5M CaCl2	90	5.75	5.401	0.000	-122
LL030400112251.043	DEA3224	MCA	MA	5 M CaCl2	60	4.33	11.988	0.000	-9
LL030400112251.043	DEA3225	MCA	MA	5 M CaCl2	60	4.33	11.988	0.000	18
LL030400112251.043	DEA3226	MCA	MA	5 M CaCl2	60	4.33	11.988	0.000	-31
LL030400112251.043	DEA3220	MCA	MA	5 M CaCl2	75	4.33	11.988	0.000	-97
LL030400112251.043	DEA3223	MCA	MA	5 M CaCl2	75	4.33	11.988	0.000	-78
LL030400112251.043	DEA3228	MCA	MA	5 M CaCl2	75	4.33	11.988	0.000	-143
LL030400112251.043	DEA3233	MCA	MA	5 M CaCl2	75	4.33	11.988	0.000	-137
LL030400112251.043	DEA3238	MCA	MA	5 M CaCl2	75	4.14	11.988	0.000	-117

Source DTN [a]	Specimen ID	Sample Type [b]	Material Condition [b]	Electrolyte	Temperature (°C)	pH	[Cl] (moles/kg water)	[NO_3] (moles/kg water)	E_{rcrev} (mV_1 vs. SSC) [c]
LL030406212251.044	DEA3278	MCA	MA	5 M CaCl2	75	4.29	11.988	0.000	-139
LL030406212251.044	DEA3279	MCA	MA	5 M CaCl2	75	4.29	11.988	0.000	-102
LL030406212251.044	DEA3280	MCA	MA	5 M CaCl2	75	4.29	11.988	0.000	-16
LL030406212251.044	DEA3281	MCA	MA	5 M CaCl2	75	4.29	11.988	0.000	-125
LL030400112251.043	DEA3216	MCA	MA	5 M CaCl2	90	4.33	11.988	0.000	-184
LL030400112251.043	DEA3217	MCA	MA	5 M CaCl2	90	4.33	11.988	0.000	-134
LL030400112251.043	DEA3218	MCA	MA	5 M CaCl2	90	4.33	11.988	0.000	-141
LL030400112251.043	DEA3219	MCA	MA	5 M CaCl2	90	4.33	11.988	0.000	-148
LL030309512251.042	DEA3167	MCA	MA	5 M CaCl2	105	4.45	11.988	0.000	-195
LL030309512251.042	DEA3168	MCA	MA	5 M CaCl2	105	4.45	11.988	0.000	-194
LL021105112251.022	DEA3208	MCA	MA	5 M CaCl2	120	5.03	11.988	0.000	-168
LL021105112251.022	DEA3209	MCA	MA	5 M CaCl2	120	5.03	11.988	0.000	-154
LL030400112251.043	DEA3234	MCA	MA	5 M CaCl2	120	4.14	11.988	0.000	-168
LL030400112251.043	DEA3235	MCA	MA	5 M CaCl2	120	4.14	11.988	0.000	-227
LL030400112251.043	DEA3237	MCA	MA	5 M CaCl2	120	4.14	11.988	0.000	-201
LL030409812251.054	DEA3125	MCA	MA	7 M CaCl2	130	**4.14** [d]	19.228	0.000	-197
LL030409812251.054	DEA599	Disc	MA	7 M CaCl2	130	**4.14** [d]	19.228	0.000	-229
LL030400112251.043	JE0111	MCA	ASW	5 M CaCl2	60	4.14	11.988	0.000	-51
LL030400112251.043	JE0112	MCA	ASW	5 M CaCl2	60	4.14	11.988	0.000	-89
LL030400112251.043	JE0113	MCA	ASW	5 M CaCl2	60	4.14	11.988	0.000	-51
LL021105112251.022	JE0106	MCA	ASW	5 M CaCl2	75	5.10	11.988	0.000	-163
LL021105112251.022	JE0107	MCA	ASW	5 M CaCl2	75	5.10	11.988	0.000	-160
LL030400112251.043	JE0040	MCA	ASW	5 M CaCl2	75	4.14	11.988	0.000	-129

Source DTN [a]	Specimen ID	Sample Type [b]	Material Condition [b]	Electrolyte	Temperature (°C)	pH	[Cl] (moles/kg water)	[NO_3] (moles/kg water)	E_{rcrev} ($mV_{}$ vs. SSC) [c]
LL030400112251.043	JE0041	MCA	ASW	5 M CaCl2	75	4.14	11.988	0.000	-117
LL030400112251.043	JE0042	MCA	ASW	5 M CaCl2	75	4.14	11.988	0.000	-130
LL030400112251.043	JE0037	MCA	ASW	5 M CaCl2	90	4.14	11.988	0.000	-189
LL030400112251.043	JE0038	MCA	ASW	5 M CaCl2	90	4.14	11.988	0.000	-163
LL030400112251.043	JE0039	MCA	ASW	5 M CaCl2	90	4.14	11.988	0.000	-175
LL030502212251.063	JE0022	MCA	ASW	5 M CaCl2	120	5.03	11.988	0.000	-184
LL030400112251.043	JE0034	MCA	ASW	5 M CaCl2	120	4.14	11.988	0.000	-165
LL030400112251.043	JE0035	MCA	ASW	5 M CaCl2	120	4.14	11.988	0.000	-184
LL030400112251.043	JE0036	MCA	ASW	5 M CaCl2	120	4.14	11.988	0.000	-185
LL030409812251.054	DEA3105	MCA	MA	1.25 M CaCl2+ 0.0125 M Ca(NO3)2	60	6.47	2.570	0.026	61
LL030502212251.063	JE0024	MCA	ASW	5 M CaCl2 + 0.05 M Ca(NO3)2	120	5.34	11.699	0.119	-264
LL030409812251.054	DEA3109	MCA	MA	1.25 M CaCl2+ 0.125 M Ca(NO3)2	90	6.41	2.612	0.263	-72
LL030409812251.054	DEA3123	MCA	MA	5 M CaCl2 + 0.5 M Ca(NO3)2	105	4.86	12.593	1.264	108
LL030409812251.054	DEA3124	MCA	MA	5 M CaCl2 + 0.5 M Ca(NO3)2	105	4.86	12.593	1.264	133
LL030409812251.054	DEA598	Disc	MA	6 M CaCl2 + 0.6 M Ca(NO3)2	120	**5.34** [d]	16.323	1.640	37
LL030409812251.054	DEA3127	MCA	MA	7 M CaCl2 + 0.7 M Ca(NO3)2	130	**5.34** [d]	20.815	2.073	32
LL030409812251.054	DEA600	Disc	MA	7 M CaCl2 + 0.7 M Ca(NO3)2	130	**5.34** [d]	20.815	2.073	24
LL030409812251.054	DEA3122	MCA	MA	9 M CaCl2 + 0.9 M Ca(NO3)2	170	**5.34** [d]	N/A [e]	N/A [e]	264

Note:

a) The sample characteristics and test environments are from the original source DTNs.

b) MCA = multiple crevice assembly, MA = mill annealed, ASW = as-welded, Aged = aging for 173 hours at 700 °C.

c) The crevice repassivation potentials (E_{rcrev}) are from DTN LL030409512251.051.

d) pH of the high chloride and high temperature solutions of DTN LL030409812251.054 was not reported. A pH of 4.14 for 5 M CaCl2 solutions at 120 °C from DTN LL030400112251.043 was used for 7 M CaCl2 solutions at 130 °C (Samples DEA3125 and DEA599). Also, the measured pH of 5.34 for 5 M CaCl2 plus 0.05 M Ca(NO3)2 solution at 120 °C from DTN LL030502212251.063 was used for CaCl2 plus Ca(NO3)2 salt solutions (Samples DEA3127, DEA598 and DEA600).

e) The molal concentrations (moles/kg water) of chloride and nitrate ions were not measured.

Source DTN [a]	Specimen ID	Sample Type [b]	Material Condition [b]	Electrolyte	Temperature (°C)	pH	[Cl] (moles/kg water)	[NO_3] (moles/kg water)	E_{rcrev} (mV_1 vs. SSC) [c]
	f) Molal concentrations of chloride and nitrate ions of test solutions are from DTNs LL030703723121.031 and LL030706223121.032. Complete dissociation is assumed for chloride and nitrate ion concentrations.								
	g) The pH values of all test solutions were measured at room temperature.								

Source DTN LL030409512251.051

ATTACHMENT VII

CNWRA Crevice Repassivation Potential Data of Alloy 22 Samples Used in the Critical Potential Model and Analysis.

Specimen ID	Sample Type	Material Condition	Electrolyte	Temperature (°C)	pH	[Cl] (moles/kg water)	[NO_3] (moles/kg water)	Ercrev (mV, vs. SCE)	Ercrev (mV, vs. SSC)
CNWRA	MCA	MA	0.5 M NaCl	105	8.00	0.510	0.000	-52	-10
CNWRA	MCA	MA	0.5 M NaCl	125	8.00	0.510	0.000	-106	-64
CNWRA	MCA	MA	0.5 M NaCl	125	8.00	0.510	0.000	-18	24
CNWRA	MCA	MA	0.5 M NaCl	150	8.00	0.510	0.000	-155	-113
CNWRA	MCA	MA	1.0 M NaCl	80	8.00	1.023	0.000	227	269
CNWRA	MCA	MA	1.0 M NaCl	95	8.00	1.023	0.000	161	203
CNWRA	MCA	MA	1.0 M NaCl	95	8.00	1.023	0.000	39	81
CNWRA	MCA	MA	1.0 M NaCl	105	8.00	1.023	0.000	-54	-12
CNWRA	MCA	MA	1.0 M NaCl	125	8.00	1.023	0.000	-171	-129
CNWRA	MCA	MA	1.0 M NaCl	125	8.00	1.023	0.000	24	66
CNWRA	MCA	MA	1.0 M NaCl	150	8.00	1.023	0.000	-216	-174
CNWRA	MCA	MA	1.0 M NaCl	150	8.00	1.023	0.000	-202	-160
CNWRA	MCA	MA	4.0 M NaCl	80	8.00	4.278	0.000	125	167
CNWRA	MCA	MA	4.0 M NaCl	95	8.00	4.278	0.000	-57	-15
CNWRA	MCA	MA	4.0 M NaCl	95	8.00	4.278	0.000	107	149
CNWRA	MCA	MA	4.0 M NaCl	95	8.00	4.278	0.000	-98	-56
CNWRA	MCA	MA	4.0 M NaCl	105	8.00	4.278	0.000	-143	-101
CNWRA	MCA	MA	4.0 M NaCl	125	8.00	4.278	0.000	-175	-133
CNWRA	MCA	MA	4.0 M NaCl	150	8.00	4.278	0.000	-192	-150

Specimen ID	Sample Type	Material Condition	Electrolyte	Temperature (°C)	pH	[Cl] (moles/kg water)	[NO_3] (moles/kg water)	Ercrev (mV, vs. SCE)	Ercrev (mV, vs. SSC)
CNWRA	MCA	ASW	0.005 M NaCl	95	6.00	0.006	0.000	271	313
CNWRA	MCA	ASW	0.05 M NaCl	95	6.00	0.050	0.000	129	171
CNWRA	MCA	ASW	0.1 M NaCl	95	6.00	0.100	0.000	214	256
CNWRA	MCA	ASW	0.5 M NaCl	95	8.00	0.510	0.000	-10	32
CNWRA	MCA	ASW	0.5 M NaCl	125	8.00	0.510	0.000	-59	-17
CNWRA	MCA	ASW	1.0 M NaCl	125	8.00	1.023	0.000	-71	-29
CNWRA	MCA	ASW	4.0 M NaCl	95	8.00	4.278	0.000	-38	4
CNWRA	MCA	ASW	4.0 M NaCl	95	8.00	4.278	0.000	-159	-117
CNWRA	MCA	ASW	4.0 M NaCl	125	8.00	4.278	0.000	-216	-174
CNWRA	MCA	ASW	4.0 M NaCl	150	8.00	4.278	0.000	-195	-153

Note:

a) The pH of test solutions was measured at the room temperature.

b) For NaCl test solutions, complete dissociation was assumed for [Cl^-] ion concentration.

c) The crevice repassivation potentials reported are with respect to the saturated calomel reference electrode (SCE). The Project's crevice repassivation potentials were reported with respect to the Ag/AgCl (SSC) reference electrode in saturated KCl solution. At 25 °C the SSC reference electrode is 199 mV more noble than the standard hydrogen electrode (SHE), and 42 mV less noble than the SCE. The SCE scale potentials were converted to the SSC scale potentials by adding 42 mV.

d) MA = mill annealed, ASW = as-welded, MCA = multiple crevice assembly.

e) Molal concentrations of chloride and nitrate ions of test solutions are from DTNs LL030703723121.031 and LL030706223121.032. Complete dissociation is assumed for chloride and nitrate ion concentrations.

Source: Brossia et al. (2001, Table A-1)